KAUNAS UNIVERSITY OF TECHNOLOGY

AUDRIUS BUČINSKAS

INVESTIGATION OF STRUCTURE-PROPERTIES RELATIONSHIP OF ORGANIC CARBAZOLYL-CONTAINING SEMICONDUCTORS

Doctoral dissertation
Technological Sciences, Chemical Engineering (05T)

2015, Kaunas

UDK 547.759 + 621.315.59 + 547.672 + 66.095.14] (043.3)

The research was carried out at Kaunas University of Technology, Faculty of Chemical Technology, Department of Polymer Chemistry and Technology in the period of 2011–2015. Research was supported by the Research Council of Lithuania.

Scientific supervisor:

Prof. habil. dr. Juozas Vidas GRAŽULEVIČIUS (Kaunas University of Technology, Technological sciences, Chemical engineering – 05T).

Scientific advisor:

Dr. Aušra TOMKEVIČIENĖ (Kaunas University of Technology, Physical Sciences, Chemistry – 03P).

Editor: Tony BEXON

ISBN

KAUNO TECHNOLOGIJOS UNIVERSITETAS

AUDRIUS BUČINSKAS

KARBAZOLILFRAGMENTĄ TURINČIŲ ORGANINIŲ PUSLAIDININKIŲ STRUKTŪROS IR SAVYBIŲ TARPUSAVIO PRIKLAUSOMYBĖS TYRIMAS

Daktaro disertacija
Technologiniai mokslai, Chemijos inžinerija (05T)

2015, Kaunas

UDK 547.759 + 621.315.59 + 547.672 + 66.095.14] (043.3)

Disertacija parengta 2011–2015 metais Kauno technologijos universiteto Cheminės technologijos fakultete, Polimerų chemijos ir technologijos katedroje. Mokslinius tyrimus rėmė Lietuvos mokslo taryba.

Mokslinis vadovas:

Prof. habil. dr. Juozas Vidas GRAŽULEVIČIUS (Kauno technologijos universitetas, technologijos mokslai, chemijos inžinerija – 05T).

Mokslinė konsultantė:

Dr. Aušra TOMKEVIČIENĖ (Kauno technologijos universitetas, fiziniai mokslai, chemija – 03P).

ISBN

LIST OF ABBREVATIONS

α – Pool-Frenkel parameter
ε – extinction
η_p – power efficiency
$\lambda^{abs}{}_{max}$ – absorption maximum
$\lambda^{em}{}_{max}$ – emission maximum
λ_e– electron reorganization energy
λ_h– hole reorganization energy
μ – charge carrier mobility
μ_o – zero field mobility
μ_h– hole mobility
μ_e – electron mobility
χ^2_{sol} – chi-square values from solution
χ^2_{film} – chi-square values from film
^{1}HNMR – proton magnetic resonance
^{13}CNMR – carbon-13 nuclear magnetic resonance
AIE – aggregation induced emission
Ar – aromatic(s), aryl
CD - circular dichroism
CIE – International Commission on Illumination
CIL – cathode interfacial layer
CV – cyclic voltammetry
d – doublet
dd – double doublet
DFT – density functional theory
DSC – differential scanning calorimetry
E_g– energy band-gap
$E_{ox1/2}$– electrochemical half-wave oxidation potential
$E_{oxonset}$– electrochemical onset oxidation potential
E_{oxpa} – electrochemical oxidation anodic potential
E_{oxpc} – electrochemical oxidation cathodic potential
E_{redpa} – electrochemical reduction anodic potential
E_{redpc} – electrochemical reduction cathodic potential
EBL – electron blocking layer
EL – electroluminescence
EQE – external quantum efficiency
ETL – electron transporting layer
HIL – hole injection layer
HOMO – highest occupied molecular orbital
HRMS – high resolution mass spectrometry
HTL– hole transporting layer
IP – ionization potential

IR – infrared
k_r – radiative decay rate constant
k_{nr}– non-radiative decay rate constant
L – brightness
LE – current efficiency
LEL – light emitting layer
LUMO – lowest unoccupied molecular orbital
m – multiplet
m.p. – melting point
MS – mass spectrometry
m/z – mass-to-charge ratio
OLED – organic light emitting diode
ORTEP –oak ridge thermal ellipsoid plot
OTFT – organic thin film transistor
PHOLED – phosphorescent organic light-emitting diode
PL – photoluminescence
ppm – parts per million
S – singlet state
s – singlet
T – triplet state
t – triplet
T_d – destruction temperature
T_g– glass-transition temperature
T_m– melting temperature (also melting point)
TD-DFT – time-dependent density functional theory
TLC – thin layer chromatography
TOF –time-of-flight
XTOF – xerographic time-of-flight
WF – work function
V_{on} – turn-on voltage
XRD – X-ray diffraction

3,7-DBTOF – 3,7-bis(9-methyl-9H-carbazol-2-yl)dibenzo[b,d]thiophene 5,5-dioxide
2,8-DBTOF – 2,8-bis(9-methyl-9H-carbazol-3-yl)dibenzo[b,d]thiophene 5,5-dioxide
2Cz-PBI – 9,9'-(5-(1-phenyl-1H-benzo[d]imidazol-2-yl)-1,3-phenylene)bis(3,6-di-tert-butyl-9H-carbazole)
4Cz-PBI – 3,6-bis(3,6-di-tert-butyl-9H-carbazole-9-yl)-9-(3-(1-phenyl-1H-benzo[d]imidazol-2-yl)phenyl)-9H-carbazole
6Cz-PBI – 9,9'-(5-(1-phenyl-1H-benzo[d]imidazol-2-yl)-1,3-phenylene)bis(3,6-bis(3,6-di-tert-butyl-9H-carbazole-9yl)-9H-carbazole)
2CzPN – 4,5-di(9H-carbazol-9-yl)phthalonitrile
4CzIPN – 2,4,5,6-tetra(9H-carbazol-9-yl)isophthalonitrile
4CzTPN-Ph – 2,3,5,6-tetrakis(3,6-diphenyl-9H-carbazol-9-yl)terephthalonitrile
26DCzPPy – 2,6-bis(3-(carbazol-9-yl)phenyl)pyridine

35DCzPPy – 3,5-bis(3-(carbazol-9-yl)phenyl)pyridine
26PyzCz – 2,6-bis(9-phenyl-9H-carbazol-3-yl) pyrazine
ACBP – 10-(4'-(9H-carbazol-9-yl)biphenyl-4-yl)acridin-9(10H)-one
Alq_3 –tris-(8-hydroxyquinoline)aluminum
BBTC – 3,6-Bis-biphenyl-4-yl-9-[1,1',4',1"]terphenyl-4-yl-9H-carbazole
BCBP – 10-(4-(9H-carbazol-9-yl)phenyl)-8,8-di-p-tolyl-8H-indolo[3,2,1-de]acridine
BCP – 2,9-dimethyl-4,7 diphenyl-1,10-phenanthroline
BCPCB – 1,3-bis(3-(diphenylphosphoryl)-9H-carbazole-9-yl)benzene
BCzSi – 9-phenyl-9'-(triphenylsilyl)-3,3'-bicarbazole
BCzPh – 9,9'-diphenyl-9H,9'H-3,3'-bicarbazole
BCzPO – (9H,9'H-[3,3'-bicarbazole]-9,9'-diylbis(4,1-phenylene))bis(diphenylphosphine oxide)
BCzPPh – 1,3-bis(3-(3,6-di-n-butylcarbazol-9-yl)phenyl)benzene
BCzPPm – 4,6-bis(3-(3,6-di-n-butylcarbazol-9-yl)phenyl)pyrimidine
BCzTPA – 4,4'-(9H,9'H-[3,3'-bicarbazole]-9,9'-diyl)bis(N,N-diphenylaniline)
BCzTPM – 9,9'-bis(4-tritylphenyl)-9H,9'H-3,3'-bicarbazole
BF4 – 7,7′-bis(N-hexylcarbazol-3-yl-ethenyl)-9,9,9′,9′-tetrahexyl-[2,2′]-bifluorene
BIMCzNPh_3b – 9-(Naphthyl-2-yl)-3-(4-(1-phenyl-1 H-benzo[d]imidazol-2-yl)phenyl)-9H-carbazole
BIMCzPh_3a – 9-Phenyl-3-(4-(1-phenyl-1 H-benzo[d]imidazol-2-yl)phenyl)-9 H-carbazole
BIQMCz – (6,6'-(9-p-tolyl-9H-carbazole-3,6-diyl)bis(6H-indolo[2,3-b]quinoxaline))
bis-CMPC – 9-(4-(bis(9-ethyl-9H-carbazol-3-yl)methyl)phenyl)-9H-carbazole
BPTRZ - 3-(carbazol-9-yl)-3′-(4,6-(dicarbazol-9-yl)-1,3,5-triazin-2-yl)-1,1′-biphenyl
BSB-Cz – 4,4'-bis[(N-carbazole)styryl]biphenyl
BT-mCP – 9,9'-(5-(triphenylen-2-yl)-1,3-phenylene)bis(9Hcarbazole)
BT-PC – 9-(4-(2,3-diphenylbenzo[b]thiophen-5-yl)phenyl)-9H-carbazole
CBP – N,N'-dicarbazolyl-4,4'-biphenyl
CBP-CN – 4,4'-bis((9H-carbazol-9-yl)-3,3'-dicyano)biphenyl
CBZ1-F2 – 9-phenyl-3,6-bis(9-phenylfluoren-9-yl)carbazole
CBZDPA – 9,10-bis(4-carbazole)phenylene-2-(1,3,5-trimethylphenyl)anthracene
CC2BP_2 – bis(4-(9H-[3,9'-bicarbazol]-9-yl)phenyl)methanone
$CDCl_3$ – deuterated chloroform
CFL – 4,4'-bis(N-carbazolyl)-9,9'-spirobifluorene
CFP – 2-(3,6-di-tert-butylcarbazol-N-yl)-7-pyrenyl-9,9-dihexylfluorene
CFTP – 2-(3,6-di-tert-butylcarbazol-N-yl)-7-(5-pyrenylthiophen-2-yl)-9,9-dihexylfluorene
CFT2P – 2-(3,6-di-tert-butylcarbazol-N-yl)-7-(5'-pyrenyl-2,2'-bithiophen-5-yl)-9,9-dihexylfluorene
CFT3P – 2-(3,6-di-tert-butylcarbazol-N-yl)-7-(5"-pyrenyl-2,2':5',2"-terthiophen-5-yl)-9,9-dihexylfluorene

CFT4P – 2-(3,6-di-tert-butylcarbazol-N-yl)-7-(5’”-pyrenyl-2,2’:5’,2”:5“,2’”-quaterthiophen-5-yl)-9,9-dihexylfluorene
CMP – 9’,9’”-(2,2’-dimethyl-[1,1’-biphenyl]-4,4’-diyl)bis(3,3”,6,6”-tetra-tert-butyl-9’H-9,3’:6’,9”-tercarbazole)
CPMP – 9’-(4’-(3-(1H-pyrazol-1-yl)-9H-carbazol-9-yl)-2,2’-dimethyl-[1,1’-biphenyl]-4-yl)-3,3”,6,6”-tetra-tert-butyl-9’H-9,3’:6’,9”-terbenzo[b]indole
Cz-2 – 3,3’-bis(9-octylcarbazole)
Cz-3 – 3,6-bis[9’-octylcarbazol-3’-yl]-9-octylcarbazole
Cz-4 – 1,3,6-tri(9’-octylcarbazol-3’-yl)-9-octylcarbazole
Cz-5 – 1,3,6,8-tetra(9’-octylcarbazol-3’-yl)-9-octylcarbazole
Cz-2PBI – 3-(3,5-bis(1-phenyl-1H-benzo[d]imidazol-2-yl)phenyl)-9-phenyl-9H-carbazole
Cz-4PBI – 3,6-bis(3,5-bis(1-phenyl-1H-benzo[d]imidazol-2-yl)phenyl)-9-phenyl-9H-carbazole
Cz-6PBI – 9-(3’,5’-bis(1-phenyl-1H-benzo[d]imidazol-2-yl)biphenyl-4-yl)-3,6-bis(3,5-bis(1-phenyl-1H-benzo[d]imidazol-2-yl)phenyl)-9H-carbazole
Cz-1TPE – 9-octyl-3-(4-(1,2,2-triphenylvinyl)phenyl)-9H-carbazole
Cz-2TPE(2,7) – 9-octyl-3-(4-(1,2,2-triphenylvinyl)phenyl)-9H-carbazole
Cz-2TPE(3,6) – 9-octyl-3,6-bis(4-(1,2,2-triphenylvinyl)phenyl)-9H-carbazole
Cz-3TPE – 9-octyl-1,3,8-tris(4-(1,2,2-triphenylvinyl)phenyl)-9H-carbazole
Cz-4TPE – 9-octyl-1,3,6,8-tetrakis(4-(1,2,2-triphenylvinyl)phenyl)-9H-carbazole
Cz-NPh – {4-[2-(9-Ethyl-9H-carbazol-3-yl)-vinyl]-phenyl}-naphthalen-2-yl-phenyl-amine
Cz-Ph3 – 3-(2-anthracen-9-yl-vinyl)-9-ethyl-9H-carbazole
Cz-PhI_6 – 1-[6-(9-carbazolyl)hexyl]-2-phenylindole
Cz-SiPh – 9-ethyl-3-{(E)-2-[4-(1,1,1-triphenylsilyl) phenyl]-1-ethenyl}-9H-carbazole
Cz2BP_1 – bis(4-(9H-carbazol-9-yl)phenyl)methanone
Cz3An – 9,10-bis(9-ethyl-9H-carbazol-3-yl)anthracene
Cz3Ant – 2-tert-Butyl-9,10-bis(9-ethyl-9H-carbazol-3-yl)anthracene
Cz3PhAn – 9,10-Bis[4-(9-ethyl-9H-carbazol-3-yl)phenyl]anthracene
Cz3PhAnt – 2-tert-Butyl-9,10-bis[4-(9-ethyl-9H-carbazol-3-yl)phenyl]anthracene
CzBPCb – 9-(3′-(9H-carbazol-9-yl)-[1,1′-biphenyl]-3-yl)-9H-pyrido[2,3-b]indole
CzDPhI_8 – 9,9’-bis[6-(2-phenylindol-1-yl)hexyl][3,3’]bicarbazole
CzF1 – 2-(9H-carbazole-9-yl)-7-(4-cyanophenyl)-9,9-dihexylfluorene
CzF2 – 7-(9H-carbazol-9-yl)-7’-(4-cyanophenyl)-2,2’-bi(9,9-dihexylfluorene)
CzF3 – 7-(9H-carbazole-9-yl)-7”-(4-cyanophenyl)-2,2’:7’,2”–ter(9,9-dihexyl-fluorene)
CzF4 – 7-(9H-carbazole-9-yl)-7’”-(4-cyanophenyl)-2,2’:7’,2”:7”,2’”-quarter(9,9-dihexylfluorene)
Cz(MP)2 – 9,9’-diisobutyl-9H,9’H-3,3’-bicarbazole
CzPAPCz – 2,6-bis(4-(3,6-di-tert-butyl-9H-carbazol-9-yl)phenyl)anthracene-9,10-dione

CPBDC – 9-(3-(9H-carbazole-9-yl)phenyl-3,6-bis(diphenylphosphoryl)-9H-carbazole
CPF - 9,9-bis[4-(9-carbazolyl)phenyl]fluorene
CPTBF – 9,9-bis[4-(carbazol-9-yl)phenyl]-2,7-di-tert-butylfluorene
Cz-G1 – 4,4’-bis(3,6-di-tert-butyl-9H-carbazol-9-yl)-1,1'-biphenyl
Cz-G2 – 4,4’-bis(3,3”,6,6”-tetra-tert-butyl-9’H-[9,3’:6’,9”-tercarbazol]-9’-yl)-1,1’-biphenyl
Cz-G3 – 4,4'-bis(3,3””,6,6””-tetra-tert-butyl-6’,6’”-bis(3,6-di-tert-butyl-9H-carbazol-9-yl)-9”H-[9,3’:9’,3”:6”,9””:3’”,9””-quinquecarbazol]-9"-yl)-1,1'-biphenyl
CzDBF – 9-(3-(dibenzo[b,d]furan-2-yl)phenyl)-9H-carbazole
CzDPOTA – (((4-(9H-Carbazol-9-yl)phenyl)azanediyl)bis(1,4-phenylene))-bis(diphenylphosphine oxide)
CzIM_M1 – (2-(4-(9H-carbazol-9-yl)phenyl)-1-phenyl-1H-phenanthro[9,10-d]imidazole
CzIM_M2 - 1-phenyl-2-(4-(3-(1-phenyl-1H-phenanthro[9,10-d]imidazol-2-yl)-9H-carbazol-9-yl)phenyl)-1H-phenanthro[9,10-d]imidazole
CzIM_M3 – 1-phenyl-2-(9-phenyl-9H-carbazol-3-yl)-1H-phenanthro[9,10-d]imidazole
CzIM_M4 – 2,2’-(9-phenyl-9H-carbazole-3,6-diyl)bis(1-phenyl-1H-phenanthro[9,10-d]imidazole)
CzIM_M5 – 2-(4’-(9H-carbazol-9-yl)-[1,1’-biphenyl]-4-yl)-1-phenyl-1H-phenanthro[9,10-d]imidazole
CzOXD – 2,5-bis(4-(9-(2-ethylhexyl)-9H-carbazol-3-yl)phenyl)-1,3,4-oxadiazole
CzPAMe – N,N-bis-[3,5-di(9H-carbazol-9-yl)phenyl]methylamine
CzPAPm – N,N-bis-[3,5-di(9H-carbazol-9-yl)phenyl]pyrimidin-2-amine
CzPPCzQ – 9,9’-(quinoline-2,4-diylbis(4,1-phenylene))-bis(9 H-carbazole)
CzPPQ – 9-(4-(4-phenylquinolin-2-yl)phenyl)-9H-carbazole
CzPPQCz – 9-(4-(6-(9 H-carbazol-9-yl)-4-phenylquinolin-2-yl)phenyl)-9 H-carbazole
CzPhB – 3-{4-(1,1- dimesitylboryl)-phenyl}-9-ethyl-9H-carbazole
CPhBzIm – 9-phenyl-3,6-bis(4-(1-phenyl-1H-benzo[d]imidazol-2-yl)phenyl)-9H-carbazole
CzPhCN_3 – 4,4’-(9-hexyl-9H-carbazole-3,6-diyl)dibenzonitrile
CzPhCOMe_4 – 1,1’-((9-hexyl-9H-carbazole-3,6-diyl)bis(4,1-phenylene))diethanone
CzPhO – 5-[4-(carbazo-9-yl)phenyl]diphosphole-5-oxide
CzPhOMe_2 – 9-hexyl-3,6-bis(4-methoxyphenyl)-9H-carbazole
CzPhONI – 6-{3,5-bis-[9-(4-t-butylphenyl)-9H-carbazol-3-yl]-phenoxy}-2-(4-t-butylphenyl)-benzo[de]isoquinoline-1,3-dione
CzPhTr_4 – 9-hexyl-3-(4-(2-(4-(9-hexyl-9H-carbazol-3-yl)phenyl)ethynyl)phenyl)-9H-carbazole
CzPO1 – 9,9’-(5-(diphenylphosphoryl)-1,3-phenylene)bis(9H-carbazole)
CzPO2 – 9-(3,5-bis(diphenylphosphoryl)phenyl)-9Hcarbazole
CzPPO – tetrakis-[3,3’,5,5’-(9H-carbazol-9-yl)]triphenylphosphine oxide

CZPT – 3,8-bis[4-(9H-carbazol-9-yl)-phenyl]-1,10-phenanthroline
CzPyr_5 – 3,6-bis(8,10-dihydropyren-1-yl)-9-hexyl-9H-carbazole
CzPySiSF – 9-(4-((4-(9,9'-spirobi[fluoren]-2-yl)phenyl)(phenyl)(4-(pyridin-4-yl)phenyl)silyl)phenyl)-9H-carbazole
CzSiSF – 9-(4-((4-(9,9'-spirobi[fluoren]-2-yl)phenyl)diphenylsilyl)phenyl)-9H-carbazole
CzT – 9-(4,6-diphenyl-1,3,5-triazin-2-yl)-9'-phenyl-3,3'-bicarbazole
CzT1 – 9-(4,6-diphenyl-1,3,5-triazin-2-yl)-9'-phenyl-3,3'-bicarbazole
CzT_7 – 9,9'-Bis[6-(carbazol-9-yl)hexyl][3,3']bicarbazole
CzThB – 3-(5-(1,1-dimesitylboryl)-thiophen-2-yl)-9-ethyl-9H-carbazole
CzTPN – 2,5-di(9H-carbazol-9-yl)terephthalonitrile
CzTrDPh_1 – 3,6-di-tert-butyl-9-(4-(phenylethynyl)phenyl)-9H-carbazole
DBFDPOCz – 2-carbazolyl-4,6-bis-(diphenylphosphinoyl)dibenzofuran
DBFDPOCz2 – 2,8-dicarbazolyl-4,6-bis-(diphenylphosphinoyl)dibenzofuran
DBFSPOCz – 2-carbazolyl-6-(diphenylphosphinoyl)dibenzofuran
DBFSPOCz2 – 2,8-dicarbazolyl-4-(diphenylphosphinoyl)dibenzofuran
DCzGe – bis(4-(9H-carbazol-9-yl)phenyl)diphenylgermane
DCzP – 3,8-di(9H-carbazol-9-yl)-6-phenylphenanthridine
DCzPOTA – (4-(bis(4-(9H-carbazol-9-yl)phenyl)amino)phenyl)diphenylphosphine oxide
DDPFTBC – 3,6-di[8-(7,10-diphenylfluoranthenyl)]-9-[4'-tert-butylphenyl]carbazole
DEC – N-ethylcarbazole(N, N'-diethyl-3,3'-bicarbazyl)
DFBC – 3,3'-(2,7-di(quinolin-8-yl)-9H-fluorene-9,9-diyl)bis(9-phenyl-9H-carbazole)
DMOC – bis[4-(3,6-dimethoxycarbazole)phenyl]sulfone
DPEC – 3,6-dipyrenyl-9-ethylcarbazole
DPEPO – bis[2-(diphenylphosphino)phenyl]ether oxide
DTCPFB – 1,4-bis(9-(4-(3,6-di-tert-butyl-9H -carbazol-9-yl)phenyl)-9H-fluoren-9-yl)benzene
DTP-mCP – 9-(3,5-di(triphenylen-2-yl)phenyl)-9H-carbazole
DTPCZ – 3-dimesityboron-9-(4-(1,2,2-triphenylvinyl)phenyl)-9H-carbazole
EBCz-ThX - 9,9-bis(9-ethyl-9H-carbazol-3-yl)-9H-thioxanthene-10,10-dioxide
fac-Ir(mpim)$_3$– fac -tris(mesityl-2-phenyl-1H-imidazole)iridium(III)
FCNIr – tris[(3,5-difluoro-4-cyanophenyl)pyridine]iridium(III)
FCNIrpic – bis((3,5-difluoro-4-cyanophenyl)pyridine) iridium picolinate
FIrpic – bis[2-(4,6-difluorophenyl)pyridinato-C2,N](picolinato)iridium(III)
G2-PTP-G2 – 5,5"-bis{3,6-bis[4-(diphenylamino)-1-phenyl]carbazol-9-yl}-2,2':5',2"-terthiophene
GITO – gallium-indium-tin-oxide
Ir(2-phq)$_3$– tris(2-phenylquinoline)iridium(III)
Ir(dbi)$_3$– tris[1-(2,4-diisopropyldibenzo[b,d]furan-3-yl)-2-phenylimidazole] iridium(III)
Ir(mppy)$_3$ – tris[2-(p-tolyl)pyridine]iridium(III)

$Ir(piq)_3$ – tris[1-phenylisoquinoline]iridium(III)
$Ir(piq)_3(acac)$ – bis[1-phenyl-isoquinoline](acetylacetonato)iridium(III)
$Ir(pq)_3$ – tris[2-phenylquinoline]iridium(III)
$Ir(ppy)_3$ – tris[2-phenylpyridine]iridium(III)
ITO – indium-tin oxide (n In_2O_3 × m SnO_2)
m-ATP-CDP – 9,9'-(dibenzo[f,h]quinoxaline-7,10-diyl)bis(N,N-diphenyl-9H-carbazol-3-amine)
m-CBP – 9,9'-biphenyl-3,3'-diylbis-9H-carbazole
m-CzCzCN – 6-(3-(9H-carbazol-9-yl)phenyl)-9-ethyl-9H-carbazole-3-carbonitrile
m-CzOCN – 8-(3-(9H-carbazol-9-yl)phenyl)dibenzo[b, d]furan-2-carbonitrile
m-CzSCN – 8-(3-(9H-carbazol-9-yl)phenyl)dibenzo[b, d]thiophene-2-carbonitrile
MBPTRZ – 3-(carbazol-9-yl)-6,6'-dimethyl-3'-(4,6-(dicarbazol-9-yl)-1,3,5-triazin-2-yl)-1,1'-biphenyl
mCP - N,N'-dicarbazolyl-3,5-benzene
mCP2PI – 1,3-bis(3-(9-pyrido[2,3-b]indol-9-yl)-9-carbazol-9-yl)benzene
mCPCzCN – 6-(3,5-di(9H-carbazol-9-yl)phenyl)-9-ethyl-9H-carbazole-3-carbonitrile
mCPPI – 9-(9-(3-(9-carbazol-9-yl)phenyl)-9-carbazol-3-yl)-9-pyrido[2,3-b]indole
mCPPO1 – 9-(3-(9H -carbazole-9-yl)phenyl)-3-(dibromophenylphosphoryl)-9H -carbazole
meta_CBP_1 – 3,3'-bis(carbazolyl)biphenyl
meta_CBP_2 – 3,3'-bis(3,6-dimethylcarbazolyl)biphenyl
meta_CBP_3 – 3,3'-bis(carbazolyl)-6,6'-dimethylbiphenyl
meta_CBP_4 – 3,3'-bis(3,6-dimethylcarbazolyl)-6,6'-dimethylbiphenyl
mOXDDSiCz – 9,9'-{1,3,4-oxadiazole-2,5-diylbis[3,1-phenylene-(diphenylsilanediyl)-3,1-phenylene]} bis(3,6-di-tert-butyl-9H-carbazole)
MTDATA – 4,4',4"-tris(N-3-methylphenyl-N-phenylamino)triphenylamine
MTPC-Et – 9-ethyl-1,3,6,8-tetraphenyl-9H-carbazole
MTPC-Me – 9-methyl-1,3,6,8-tetraphenyl-9H-carbazole
MTXSFCZ – 3-methyl-2-(9-phenyl-9-(9-phenyl-9H-carbazol-3-yl)-9H-fluoren-2-yl)-9H-thioxanthen-9-one
NFBC – 3,3'-(2,7-di(naphthaline-2-yl)-9H-fluorene-9,9-diyl)bis(9-phenyl-9H-carbazole)
NPB – N,N'-di(1-naphthyl)-N,N'-diphenyl-(1,1'-biphenyl)-4,4'-diamine
o-CBP – 9,9'-biphenyl-2,2'-diylbis-9H-carbazole
o-CzCzCN – 6-(2-(9H-carbazol-9-yl)phenyl)-9-ethyl-9H-carbazole-3-carbonitrile
OFC-G2 – 9',9"-(9,9-dioctyl-9H-fluorene-2,7-diyl)bis-9' H-9,3' :6',9" -tercarbazole
OFCT-G2 – 9,9' -(9,9-dioctyl-9H-fluorene-2,7-diyl)bis(3,6-di-2-thienyl-9H-carbazole)
OxCz_1 – 2-(4-(7-(9H-carbazol-9-yl)-9,9-dihexyl-9H-fluoren-2-yl)phenyl)-5-(4-(tert-butyl)phenyl)-1,3,4-oxadiazole
OxCz_2 – 2-(6-(7-(9H-carbazol-9-yl)-9,9-dihexyl-9H-fluoren-2-yl)pyridin-3-yl)-5-(4-(tert-butyl)phenyl)-1,3,4-oxadiazole

OxCz_3 – 2-(5-(7-(9H-carbazol-9-yl)-9,9-dihexyl-9H-fluoren-2-yl)thiophen-2-yl)-5-(4-(tert-butyl)phenyl)-1,3,4-oxadiazole
OxCz_4 – 2-(4-(tert-butyl)phenyl)-5-(4-(7-(3,6-dimethoxy-9H-carbazol-9-yl)-9,9-dihexyl-9H-fluoren-2-yl)phenyl)-1,3,4-oxadiazole
OxCz_5 – 2-(4-(tert-butyl)phenyl)-5-(4-(7-(3,6-di-tert-butyl-9H-carbazol-9-yl)-9,9-dihexyl-9H-fluoren-2-yl)phenyl)-1,3,4-oxadiazole
OxCz_6 – 2-(4-(7'-(9H-carbazol-9-yl)-9,9,9',9'-tetrahexyl-9H,9'H-[2,2'-bifluoren]-7-yl)phenyl)-5-(4-(tert-butyl)phenyl)-1,3,4-oxadiazole
OxCz_7 – 2-(4-(tert-butyl)phenyl)-5-(4-(3,6-di-tert-butyl-9H-carbazol-9-yl)phenyl)-1,3,4-oxadiazole
OXD-7 – 1,3-bis[2-(4-tert-butylphenyl)-1,3,4-oxadiazo-5-yl]benzene
PC – N-phenylcarbazole
PC-Z – bisphenol-Z polycarbonate
PCz-BFP – 3-(3-(carbazole-9-yl)phenyl)benzofuro[2,3-b]pyridine
PEDOT–PSS – poly(3,4-ethylenedioxythiophene)-poly(styrenesulfonate)
Ph – phenyl
PHI_M1 – (2-(4-(9H-carbazol-9-yl)phenyl)-1-phenyl-1H-phenanthro[9,10-d]imidazole
PHI_M2 – 1-phenyl-2-(4-(3-(1-phenyl-1H-phenanthro[9,10-d]imidazol-2-yl)-9H-carbazol-9-yl)phenyl)-1H-phenanthro[9,10-d]imidazole
PHI_M3 – 1-phenyl-2-(9-phenyl-9H-carbazol-3-yl)-1H-phenanthro[9,10-d]imidazole
PhosCz_3 – hexa-(3-carbazole-phenyoxy)cyclotriphosphazene
PhosCz_5 – hexa-(2-carbazole-5-pyridin-ox y)cyclotriphosphazene
PO-01 – bis(4-phenylthieno 3,2– c]pyridinato-N,C 2')acetylacetonate
pOXDDSiCz – 9,9'-{1,3,4-oxadiazole-2,5-diylbis[4,1-phenylene-(diphenylsilanediyl)-4,1-phenylene]} bis(3,6-di-tert-butyl-9H-carbazole)
PPO1 – 3-(diphenylphosphoryl)-9-phenyl-9H-carbazole
PPO2 – 3,6-bis(diphenylphosphoryl)-9-phenyl-9H-carbazole
PPO27 – 2,7-bis(diphenylphosphoryl)-9-phenyl-9H-carbazole
PPO36 – 3,6-bis(diphenylphosphoryl)-9-phenyl-9H-carbazole
PPO21 – 3-(diphenylphosphoryl)-9-(4-(diphenylphosphoryl)phenyl)-9-carbazole
PPS21 – 3-(diphenylphosphorothioyl)-9-(4-(diphenylphosphorothioyl)-phenyl)-9H-carbazole
PPV – poly(p-phenylene vinylene)
PVK – poly(N-vinylcarbazole)
PzCz – hexakis(9H-carbazol-9-yl)cyclotriphosphazene
SBFC-G2 – 9',9" -(9,9' -spirobi[fluorene]-2,7-diyl)bis-9'H-9,3':6',9" -tercarbazole
SBFCT-G2 – 9,9' -(9,9' -spirobi[fluorene]-2,7-diyl)bis(3,6-di-2-thienyl-9H-carbazole)
SFC-G2 – 9',9"-spiro[cyclododecane-1,9' -fluorene]-2',7' -diylbis-9' H-9,3' :6' ,9" -tercarbazole
SFCT-G2 – 9,9' -spiro[cyclododecane-1,9' -fluorene]-2' ,7'-diylbis(3,6-di-2-thienyl-9H-carbazole)

SiDCz_2b – bis(4-(N-carbazolyl)phenyl)dimethylsilane
SiDCz_3b – bis(4-(N-carbazolyl)phenyl)diphenylsilane
SimCP – 3,5-bis(9-carbazolyl)tetraphenylsilane
SimCP2 – 3,5-di(9H-carbazol-9-yl)tetraphenylsilane
SitCz – 9'-triphenylsilanyl-9'H-[9,3',6',9"]tercarbazole
SiTCz_2c – tris(4-(N-carbazolyl)phenyl)methylsilane
SiTCz_3c – tris(4-(N-carbazolyl)phenyl)phenylsilane
SPhCz_3 – bis[4-(3,6-di-tert-butylcarbazole)phenyl]sulfone
Spiro-2CBP – 2,7-bis(carbazo-9-yl)-9,9-ditolyfluorene
StiCz1 – (E)-1,2-Bis(9-ethyl-9 H-carbazol-3-yl)ethane
StiCz2 – (E)-1,2-Bis(9-ethyl-3,9 0-bi(9 H-carbazol)-6-yl)-ethene
StiCz3 – (E)-6,6'-(Ethene-1,2-diyl)bis(9-ethyl- N, Ndiphenyl-9 H-carbazol-3-amine)
(t-bt)2Ir(acac) – bis[2-(4-tertbutylphenyl)benzothiazolato-N,$C^{2'}$]iridium (acetylacetonate)
t-CmOxa – 9-{4-[5-(4-tert-butylphenyl)-[1,3,4] oxadiazol-2-yl]-benzyl}-9H-carbazole
TAPC – 4,4"-cyclohexylidenebis[N,N-bis(4-methylphenyl)benzenamine]
TBCPF – 9,9-bis[4-(3,6-di-tert-butylcarbazol-9-yl)phenyl]fluorine
TCPC-6 – 2",7"-bis(9,9-bis(6-(9H-carbazol-9-yl)hexyl)-9H-fluoren-2-yl)-9,9"-spirobi[fluorene]
TCTA – tris(4-carbazoyl-9-ylphenyl)amine
TCTP - 4,4',4"-tri(N-carbazolyl)triphenylphosphine oxide
TCzMe – 3,6-di(dicarbazolyl)-9(4-methylphenyl)-carbazole
THF – tetrahydrofuran
TP-mCP – 9,9'-(5-(triphenylen-2-yl)-1,3-phenylene)bis(9H-carbazole)
TPA – triphenylamine
TPBI – 1,3,5-tris(N-phenylbenzimidizol-2-yl)benzene
TPCz – 3,6-bis(diphenylphosphoryl)-9-(4'-(diphenylphosphoryl)phenyl)carbazole
TRCz_6 – 3,5-bis-(3-(9-carbazoyl)-phenyl)-4-(4-butyl-phenyl)-4H-[1,2,4]triazole
TPD – N,N′-bis(3-methylphenyl)-N,N′-diphenylbenzidine
TRZ-1Cz(MP)2 – 6-(3-(4-(4,6-diphenyl-1,3,5-triazin-2-yl)phenyl)propyl)-9,9'-diisobutyl-9H,9'H-3,3'-bicarbazole
TRZ-3Cz(MP)2 – 6,6"-(((6-(3-(3-(9,9'-diisobutyl-9H,9'H-[3,3'-bicarbazol]-6-yl)propyl)phenyl)-1,3,5-triazine-2,4-diyl)bis(4,1-phenylene))bis(propane-3,1-diyl))bis(9,9'-diisobutyl-9H,9'H-3,3'-bicarbazole)
TrzCz_1 – 9,9'-(4',4"-(4-Phenyl-4H-1,2,4-triazole-3,5-diyl)bis(biphenyl-4',4-diyl))bis(9H-carbazole)
TrzCz_2 – 9,9'-(4',4"-(4-Phenyl-4H-1,2,4-triazole-3,5-diyl)bis(biphenyl-4',3-diyl))bis(9H-carbazole)
TrzCz_3 – 9,9'-(3',3"-(4-Phenyl-4H-1,2,4-triazole-3,5-diyl)bis(biphenyl-4,3'-diyl))bis(9H-carbazole)
TrzCz_4 – 9,9'-(3',3"-(4-Phenyl-4H-1,2,4-triazole-3,5-diyl)bis(biphenyl-3',3-diyl))bis(9H-carbazole)

TRZ-Cz_1a – 12,12’-(6-([1,1’-biphenyl]-4-yl)-1,3,5-triazine-2,4-diyl)bis(11-phenyl-11,12-dihydroindolo[2,3-a]carbazole)
TRZ-Cz_2a – 9’-(4-(4,6-diphenyl-1,3,5-triazin-2-yl)phenyl)-3,3”,6,6”-tetraphenyl-9’H-9,3’:6’,9”-terbenzo[b]indole
TRZ-Cz_2b – 9’-(4-(4,6-diphenyl-1,3,5-triazin-2-yl)phenyl)-9’H-9,3’:6’,9”-terbenzo[b]indole
TRZ-Cz_2c – 9-(4-(4,6-diphenyl-1,3,5-triazin-2-yl)phenyl)-9H-3,9’-bicarbazole
TSPO1 – diphenylphosphineoxide-4-(triphenylsilyl)phenyl
TSTC – 9-(4-triphenylsilanyl-(1,1’,4,1”)-terphenyl-4”-yl)-9H-carbazole
TXO-PhCz – 2-(9-phenyl-9H-carbazol-3-yl)-9H-thioxanthen-9-one 10,10-dioxide
ZITO - zinc-indium-tin-oxid

CONTENTS

1. INTRODUCTION

"And God said, let there be light: and there was light. And God saw the light, that it was good: and God separated the light from the darkness" – Genesis 1:3-4. As it was in the beginning, today, light is still the most significant phenomenon that helps the world to go round. The Sun was the main natural light source throughout all of Earth's history. Through the centuries, the desire of humankind to catch the light, to store it and to produce it has been increasingly growing. At the beginning, the main light source was the flame, then the industrial revolution brought light bulbs, later on, halogen lamps and fluorescent light bulbs appeared. The ability to produce light artificially made humanity more independent from the light of Sun.

The behavior of molecules under the exposure to radiation and the ability to convert the different kinds of energy to light are still one of the main challenges in science and technology. The breakthrough in synthetic chemistry and chemical engineering, the ability to design molecule structures of materials with the required properties and to synthesize them gave a rise to a variety of different electroactive compounds. Organic semiconductors are the most widely used organic electroactive materials. They are employed in optoelectronic devices such as organic and hybrid solar cells, organic light emitting diodes (OLEDs) and in organic electronics, mainly for the fabrication of organic field effect transistors (OTFTs). Among the huge amount of different organic electroactive materials reported, compounds having carbazole moiety occupy an important position [1-3]. Carbazole is a cheap heterocyclic aromatic compound, which is extracted mostly from coal tar [4]. This heterocyclic building block has attracted much attention due to the variety of possible substitutions, easy functionalization, good chemical stability and excellent charge transporting properties of the derivatives [5-7]. A search for organic electroactive materials with the desirable properties has to be performed, especially considering the possibilities of their large scale production

To prepare commercially available products, convenient synthetic routes are of great importance. Therefore, researchers engaged in the development of new organic semiconductors must focus on the number of steps and overall yields of the target products. Here are the following requirements for organic semiconducting materials, which are intended to be produced on an industrial scale, as well:

- High thermal, chemical and electrochemical stabilities, which are needed to ensure the long service time of optoelectronic devices.
- Ability to form stable molecular glasses by solution processing, which is of interest in the context of low-cost device fabrication.
- An effective light-to-electricity conversion in organic solar cells of organic semiconductors with a broad absorption spectra (low band gaps) are of great relevance.
- The fabrication of efficient OLEDs organic electroactive materials with a high luminescence quantum yield and good charge transporting properties are needed.

- Low costs of raw materials and of device fabrication.

An increasing interest in ambipolar organic semiconductors used in organic optoelectronics and electronics raises new requirements concerning the availability of starting compounds, simplicity of the synthesis and the properties of the target compounds. Perylene derivatives form a class of promising n-type organic semiconductors with effective luminescent characteristics [8,9]. Use of the combination of the modified perylene aromatic system and carbazole moiety is expected to result in effective ambipolar organic electroactive materials, which could enable the fabrication of effective fluorescent light emitting diodes. Due to its lactam rings, isoindigo moiety has a strong electron-withdrawing character, therefore, this unit is useful as an acceptor for donor-acceptor-donor or acceptor-donor-acceptor based systems [10]. In the researcher's opinion, using a carbazole-isoindigo-carbazole system it is possible to design and synthesize ambipolar compounds, with a broad UV-vis absorption spectra i.e. with a low band gap. The employment of such isoindigo-based materials in organic solar cells is still of great interest.

Helicenes represent an interesting type of heteroaromatic compounds with ortho-annulated rings. These helical systems are well known, due to their inherent chirality and their ability to behave as organic semiconductors [11]. Thus the synthesis of carbazole and quinolone based helical compounds and investigation of their behavior in the presence of UV-vis radiation is of great importance.

It is known that the introduction of electron-donating methoxy groups into carbazole moiety leads to the decrease of ionization potentials (IP) [12,13] of the derivatives, however there is still a lack of information on the impact of the number and positions of methoxy groups on properties of stand-alone carbazole and carbazole derivatives with extended π-conjugation.

The suitability of new promising organic semiconducting materials for large scale production is of great importance. Therefore, in the design of new organic electroactive materials, it is important that they could be prepared with high yields from relatively cheap and commercially available starting compounds by simple synthetic procedures.

The aim of this work was synthesis, studies and estimation of applicability in optoelectronic devices of new derivatives of carbazole in which different types of organic moieties are linked to the most reactive positions (C-3, C-6, C-2, C-7) of carbazole fragments. The following moieties were employed in the design and synthesis of new electroactive materials:

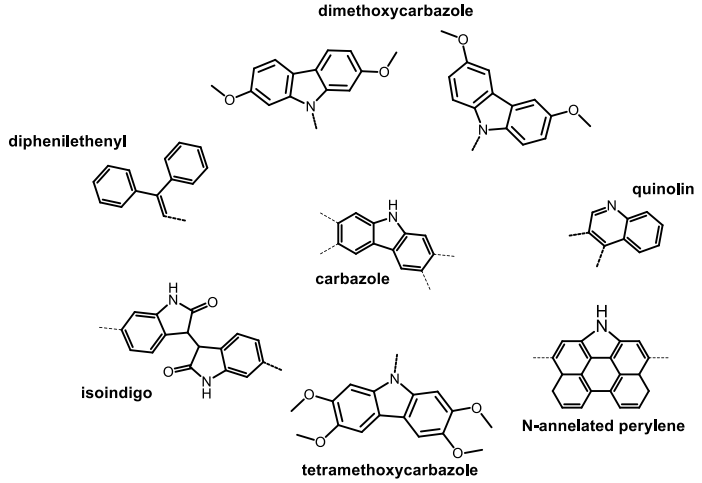

The following objectives were raised for the achievement of the thesis aim:

- Investigation of the synthesis and properties of isomeric diphenylethenyl-disubstituted dimethoxy carbazoles.
- Synthesis of new chiral carbazole-based helicenes, their separation, functionalization and investigation of the optical properties.
- Synthesis of the derivatives of N-annelated perylene and carbazole, investigation of their thermal, electrochemical, photophysical, photoelectrical and charge transporting properties, along with the estimation of applicability of the synthesized derivatives for the fabrication of effective OLEDs.
- Investigation of the influence of the amount of methoxy groups and their positions on the crystal structure of carbazole derivatives, and on their thermal and electrochemical properties; application of multimethoxysubstituted carbazole derivatives as strong electron-donors for the preparation of an effective hole transporting materials.
- Synthesis and investigation of the properties of electroactive carbazole derivatives containing isoindigo moiety and estimation of their applicability in organic photovoltaic devices.

The main statements of the doctoral thesis:

- Methoxycarbazole derivatives substituted with diphenylethenyl moieties possess high hole mobility, high thermal stability and show an aggregation induced emission phenomenon.
- N-annelated perylene derivatives as efficient green-emitting materials, with ambipolar charge-transporting properties, are suitable for the fabrication of effective OLEDs.

- Donor-acceptor-donor compounds based on carbazole and isoindigo moieties exhibit ambipolar charge transport and can be used as electron-donating materials in bulk heterojunction solar cells.

The novelty of the work:

- New glass forming isomeric 3,6-dimethoxy- and 2,7-dimethoxycarbazoles containing diphenylethenyl moieties, which possess high hole mobility, were synthesized and characterized. It was established that the derivatives of 2,7-dimethoxycarbazole exhibits an aggregation induced emission.
- New carbazolyl-substituted N-annelated perylenes with the different linking topologies of the chromophores were synthesized and the comparative analysis of their properties was performed. Using the newly synthesized compounds as emissive materials, the efficient fluorescent OLEDs with the brightness value exceeding 62000 cd/m^{2}and external quantum efficiency reaching 4.2% were fabricated.
- The influence of the amount of methoxy groups and their positions on the crystal structure of carbazole derivatives, and on their thermal, optical, electrochemical properties was investigated for the first time. It was established that the introduction of methoxy groups leads to the decrease of ionization potentials and to the increase of glass transition temperatures and melting points.
- New ambipolar carbazole and isoindigo derivatives, which possess broad absorption spectra, were synthesized and characterized. Using the newly synthesized materials, organic bulk heterojunction solar cells were fabricated and characterized.

The contribution of the author

The author synthesized six different series of carbazolyl based compounds and investigated their thermal, electrochemical, photophysical, photoelectrical and charge transporting properties. The author participated in OLED preparation supervised by dr. Dmytro Volyniuk (KTU). The theoretical calculations were performed in contribution with dr. Gintautas Bagdziunas (Kaunas University of Technology, Kaunas) and prof. B. F. Minaev (Khmelnytsky National University, Ukraine). Bulk heterojunction solar cells were fabricated with the help of prof. L. Y. Chen (National Tsing-Hua University, Taiwan).

2. LITERATURE REVIEW

2.1. Evolution of organic electroluminescent devices

Electroluminescence (EL) is an electrical and optical phenomenon in which a material emits light in response to an electric current or to a strong electric field [14]. The first time it was observed was in a piece of carborundum crystal in 1907 [15]. The story of OLEDs started sixty years ago after Bernanose's experiment, who first observed EL in organic material by applying a high-voltage alternating current field to a crystalline film of acridine orange and quinacrine [16-19]. Fifteen years later, an EL cell using single crystals of anthracene was prepared and successfully tested on 400 V voltage, observing blue fluorescence [20]. Such a large operating voltage was the main circumstance that constrained commercialization and investments to this field. During the next twenty years, the first OLED was made using polyvinyl carbazole doped with acridine orange or perylene. The device was fabricated using an alkali cathode, which made a huge improvement in the OLED structure and empowered it to operate at lower voltages [21-23]. In 1987, Tang and co-workers reported on the first two-layer vacuum-deposited OLED based on small molecules, which was a turning point in EL device history [24-26]. To improve the light extraction, a transparent anode made from indium tin oxide (ITO) on a glass substrate was used. They used hole-transporting film of aromatic diamine, emitting a layer of tris-hydroxyquinoline aluminum (Alq_3) and magnesium as the electron-injecting cathode. The use of updated OLED versions allowed the operating voltage to be decreased to 10 V. A while later, a Cambrigde group published and patented the successful results of a single-layer prototype, by introducing conjugated polymer poly(p-phenylene vinylene) (PPV) into the OLED structure [27,28]. In 1991, the Heeger group prepared a modified PPV version named poly[2-methoxy-5-(2-ethylhexyloxy)-1,4-phenylenevinylene] or MEH-PPV[29], but due to its instability to photo-oxidation the work was abolished. In 1998, Forrest and co-workers[30] announced the first effective phosphorescent OLED (PHOLED) achieving 25% internal and 4% external quantum efficiency (EQE) by inducing energy transformation to light from both singlet and triplet (that constituted three-quarters of the bound electron-hole pairs) state excitons. During the next decade, much work was done to increase the PHOLEDs EQE from 15% to 19% or luminous power efficiency from 40 lm/W to 124 lm/W [31-33]. The usage of heavy metal complexes as an emitter has several disadvantages. Firstly, commonly used iridium is one of the rarest elements (abundance is 40 times less than that of gold) on the crust of the Earth [34], secondly, the recycling from the optoelectronic devices is inconceivable. The next reasonable breakthrough in OLED history was the year 2012. Adachi et al. [35] reported on the phenomenon of thermally activated delayed fluorescence (TADF) that drives a reverse (from T_1 to S_1) intersystem crossing using metal-free materials. The main dates throughout the history of OLED are presented on a time line at (Fig. 2.1). Additionally, below the time-line is the development of the flat OLED TV by the industry are shown.

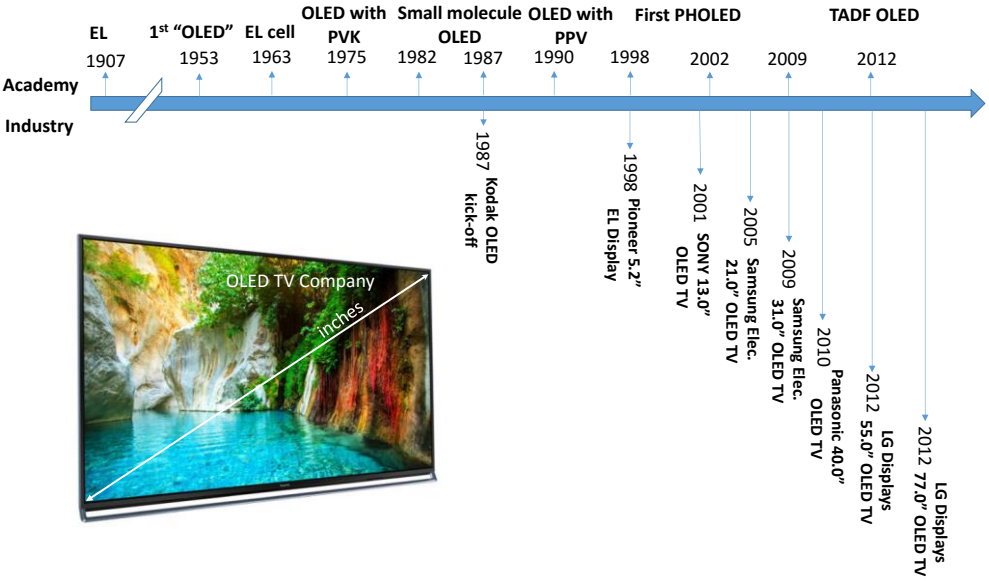

Fig. 2.1. OLED development stream though the history and OLED TV evolution

2.2. General information about OLEDs

2.2.1. Classification and structure

The average diameter of a human hair is 200 times thicker compared to todays novel multilayer EL device thickness [36]. OLED is an optoelectronic device made of thin organic semiconducting materials incorporated between two electrodes. Basic and enhanced OLED structures are shown in Fig. 2.2 and Fig. 2.3 [37], respectively.

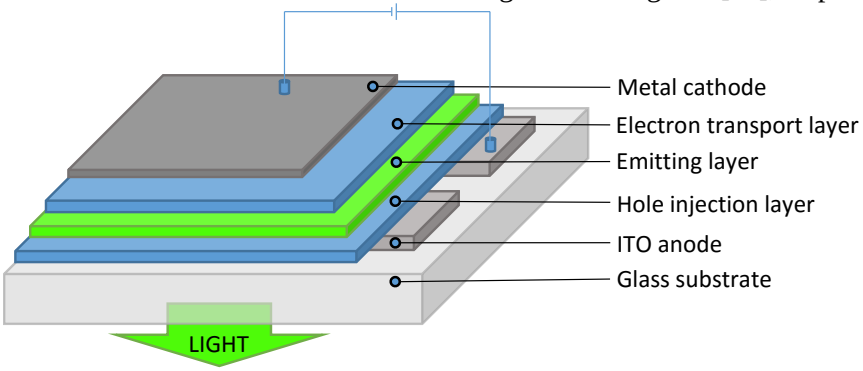

Fig. 2.2. Basic structure of sandwich-structured OLED

The OLED basic working principle is presented in Fig. 2.3. Inside the device, electrons and holes are injected from electrodes into the light emitting layer (LEL), where they subsequently recombine, resulting in light emission. Efficiency of the

device depends on the efficient injection of both electrons and holes. According to the number of layers between electrodes, OLEDs can be divided into three groups:

- Single layer OLEDs, which possess a simple single layer structure consisting of one emitting layer between an anode and cathode [38-40].
- Three-layered devices consisting of a hole transporting layer (HTL), LEL and an electron transporting layer (ETL) [41,42]. Generally such OLEDs possess three layers sealed between two electrodes, including the hole injection/transport layer, LEL and ETL.
- OLEDs with two additional layers: electron blocking layer (EBL) and hole blocking layer (HBL) [43].

The following paragraphs will focus on each layer, by introducing the role in the working device, requirements which have an influence on the effectiveness of the device and present the most popular compounds used. Information about layers is summarized in Table 2.1.

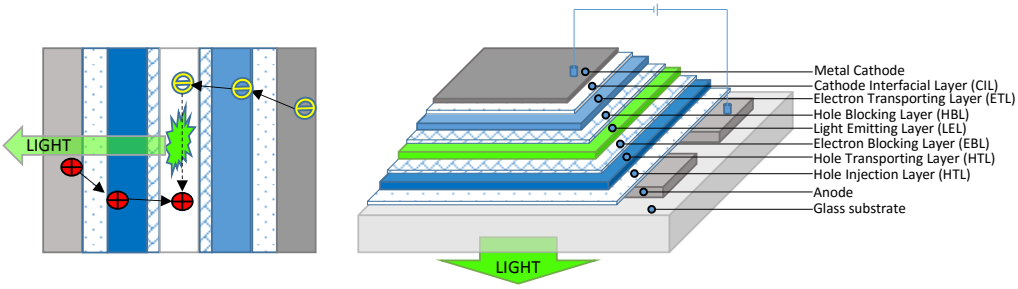

Fig. 2.3. Structure of sandwich-structured OLED and principle working mechanism

Table 2.1. The role of each OLED layer

Layer	**The role**	**Examples**
Substrate	Device foundation	Glass, plastic
Anode	The source of holes	ITO, GITO, ZITO
Hole Injection Layer (HIL)	To ease hole injection	PEDOT–PSS, SiO_2
Hole Transporting Layer	Positive charge transition	TCTA, TPD, NPB
Light Emitting Layer	Light source	Firpic, FCNIr
Electron Transporting Layer	Negative charge transition	Alq_3, BCP, TPBI
Cathode Interfacial Layer (CIL)	Cathode protection from oxidation	LiF, CaF_2, NaCl
Metal Cathode	The source of electrons	Au, Cu, Zn, Ag

According to the principles of exciton formation, OLEDs are classified into three categories (Fig. 2.4):

- Fluorescent OLEDs based on fluorescent emitting materials.

- Phosphorescent OLEDs based on organic host materials and triplet guest emitters i.e. organometallic complexes with heavy metals such as Ir, Pt and Os (dopants).
- OLEDs based on TADF.

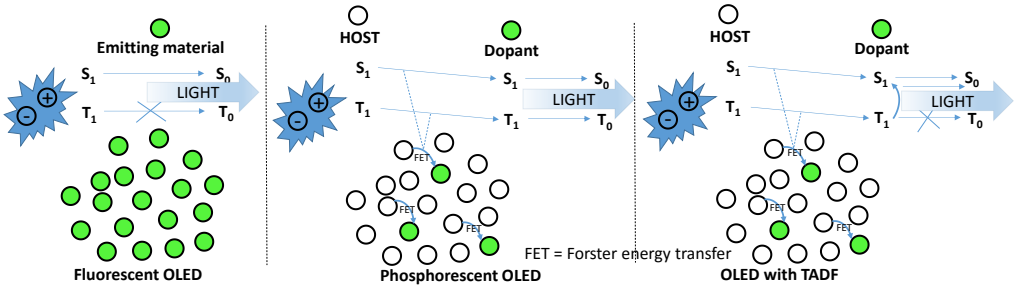

Fig. 2.4. Classification of OLEDs by working principle

2.2.2. The materials for cathode, anode, HIL and CIL

The main requirements for anode materials [37]:

1. Good optical transparency in the visible range.
2. High conductivity.
3. High work function (*WF*)
4. Good thermal and chemical stability.
5. Good film-forming properties.
6. Low fabrication cost.

Recently, ITO, known as the n-type semiconductor, is the academic/industry-dominant transparent conductive anode material for OLEDs [33,32,44-49]. When preparing optoelectronic devices, the most complicated point of using ITO is a low *WF* (~4.7 eV). The energy levels of commonly used materials for a host is ~5.8-6.0 eV. As a result, multiple charge transporting layers are needed to match such a low ITO energy.

The cathode is the opposite electrode to anode, which performs electron injection to the optoelectronic device. As in the case of an anode, the material used for a cathode plays a huge role to the device performance, i.e. the lower the energetic barrier between the cathode metal contact and ETL, the higher the density of electron reaches the LEL. The main cathode material requirements are: [37]

1. High conductivity.
2. Low working function.
3. Good film-forming properties.
4. Good thermal and chemical stability.
5. Highly reflective or transparent.

The usage of various metallic cathodes and their WF values are presented in Table 2.2 [50-52]:

Table 2.2. Different cathode characteristics

Metal	1st Ionization energy, eV[53]	Work function, eV
Eu	5.67	2.54
Yb	6.25	2.63
Ba	5.21	2.70
Sm	5.64	2.73
Li	5.39	2.95
Ca	6.11	3.00
Tm	6.18	3.12
Mg	7.65	3.70
Al	5.99	4.30
Ag	7.57	4.32
Zn	9.39	4.47
Cu	7.72	4.70
Au	9.22	5.10

The low *WF* correlates with low ionization energy, which implies a high chemical reactivity, i.e. the problem occurs in the contact between the cathode metal and organic layer. Moreover, low *WF* metals are susceptible to atmospheric oxidation. This issue was solved by researchers of the Kodak company [54], by preparing a two-layer cathode, which consisted of metal and a thin (~1.5 mm) insulating material layer deposited on top of the electrode (e.g., LiF, with band gap energy of 12 eV). This layer is named as the cathode interfacial layer. Due to the tunnel injection effect [55], the charge carries are injected to the organic material. Typical CIL materials are:

- LiF[56],CsF [57], CaF_2[58], NaCl [59];
- organic polymer surfactants [60];
- Li-doped Alq3 layer [61].

To improve the hole injection from an anode, HIL is used. This layer serves as an interface connection layer between the anode and HTL, which improves the film forming properties of HTL and facilitates the hole injection into HTL [37]. Additionally, HIL protects the LEL from the reactive ITO if HTL is absent. HIL materials should fit these requirements:

- highest occupied molecular orbital (HOMO) level should be between HOMO levels of the anode and HTL;
- minimal absorption of red, green, blues light which comes from LEL;
- high thermal and chemical stability.

Currently used HIL materials:

- porphyrinic metal complexes (CuPc) [62] (advantage: high thermal stability; disadvantage: HTM crystallization on the CuPc surface) [63];
- inorganic insulators (SiO_2, SiO_xN_y) [64,65];
- fluorocarbon polymers [66];
- conducting polymers such as (PEDOT–PSS) [67].

2.2.3. Hole transport layer

Due to high impact to OLED performance, HTL materials are commonly analyzed molecules. This layer serves as a pathway for holes to migrate from anode to LEL. The basic requirements for this type of materials are [68]:

- good hole mobility;
- high glass transition temperature to form thermally and morphologically stable film;
- low energy barrier for hole injection from anode to LEL, i.e. suitable HOMO;
- low impurity level, to exclude hole trapping;
- shallow lowest unoccupied molecular orbital (LUMO) energy, as it must act as EBL;
- high triplet energy, to isolate triplet excitons in the LEL.

According to these requirements, the commonly used hole-transporting compounds have triphenylamine and carbazole moieties. The examples of compounds used for HTL are shown in Fig. 2.5 [69-72].

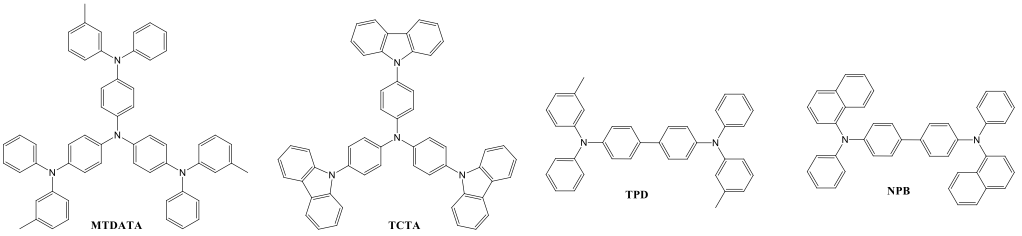

Fig. 2.5. Typical hole-transporting materials

2.2.4. Electron transport layer

ETL serves as a pathway for charge transport between a cathode and an emission layer. The structures of electron-transporting compounds usually contain electron withdrawing groups (cyano, oxadiazole etc.). The common requirements that must follow ETL materials are [37]:

- considerable electron mobility;

- suitable HOMO/LUMO to block holes and to ease electron injection;
- electrochemically stability, high thermal stability and not highly crystalline;
- high electron affinity;

The most popular among reported electron-transporting compounds are presented in Fig. 2.6 [73-76].

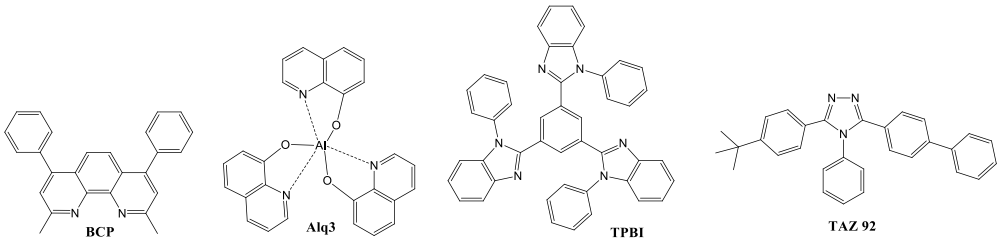

Fig. 2.6. Typical electron-transporting materials

2.2.5. Light-emitting layer

Due to the light output, the materials of LEL get most of the attention in fabrication of OLEDs. There are three types of materials used for LEL: hosts [68], which serve as a matrix for organometallic complexes [77]; highly emissive fluorescent materials, which serve as a light emitting source by themselves [78] and materials, used as dopants or matrix in OLEDs with a TADF effect [79]. The main four requirements that satisfy effective host materials are [80]:

- high thermal, chemical, electrochemical stability;
- high triplet energy for efficient energy transfer and higher than that of triplet emitters;
- balanced electron and holes transport properties to have more efficient recombination of positive and negative charges;
- HOMO should be deeper and LUMO should be shallower than that of the triplet emitter;
- bipolar charge transporting properties.

The basic requirements for effective non-doped and TADF emitters [37,79]:

- balanced HOMO and LUMO energy levels with HTL and ETL;
- high fluorescence quantum yield in the solid state;
- high thermal stability and ability to form molecular glasses;
- match the standard of International Commission on Illumination (CIE) 1931 coordinates: (0.30, 0.60) for green color, (≥0.62, ≤0.37) for red color, (0.14–0.16, 0.11–0.15) for blue color, (0.313, 0.329) for white color;
- small ΔE_{ST} (for TADF emitters only).

2.2.6. Estimation of characteristics of OLEDs

The source of EL are excitons resulting from the recombination of the positive and negative charges [37]. According to quantum mechanics, the ratio of singlet (one combination of antiparallel spins) and triplet excitons (three combinations of parallel spins) is 1:3 [81]. Thus, the fluorescent materials used for the emitting layer can reach the internal quantum efficiency (IQE) of 25%, while the emitters based on electrophosphorescence can reach 100% IQE [82]. The principle scheme of singlet and triplet radiation is shown in Fig. 2.7[83].

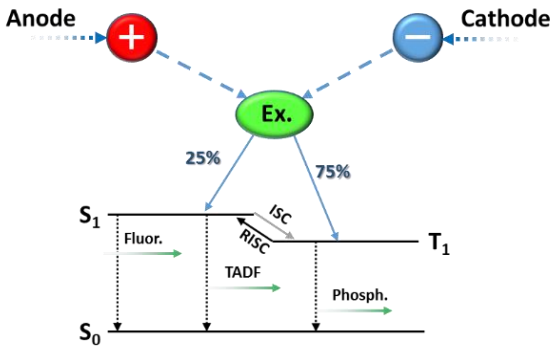

Fig. 2.7. Singlet and triplet exciton formation and radiation in OLEDs.

To make a quantitative assessment of OLED, five parameters are used [37]:

1. Turn on voltage (V_{on}, in V).
2. Brightness (L, in cd m^{-2}) or luminance; the level of light per unit area emitted by OLED.
3. The power efficiency (η_p, in lm/W); expressed by the ratio of total light output in lumens to electrical power in Watts.
4. The current efficiency (*LE*, in cd/A); defined by the ratio of the luminous intensity in a forward direction, and the current flowing through an OLED.
5. The external quantum efficiency (*EQE*, in %); expressed by the ratio between the number of emitted photons and the number of injected photons.

2.3. Carbazole-based molecular glasses as the components of OLEDs

To our knowledge, no comprehensive review on carbazole-based compounds used in OLEDs or PHOLEDs has been reported. Carbazolyl-containing derivatives can be used as emitters and as host materials of emitting layers. In this chapter a review of reported carbazole-based compounds which were employed in EL devices during the recent decade is discussed. In order to analyze the suitability of the reviewed compounds to the large scale production, the review will focus on the overall yield and the number of steps needed to obtain the final compound throughout all the

synthetic route. Additionally, the review will place emphasize on the glass-forming ability and the thermal stability, which are important properties of the compounds used in OLEDs. HOMO/LUMO energy levels and triplet energy values will also be discussed, since these characteristics predetermine the energetic compatibility of the layers. According to the role of the carbazole derivatives in OLEDs, they will be classified into three main groups, i.e. compounds for electrofluorescent OLEDs, compounds for electrophosphorescent devices (PHOLEDs) and compounds for OLEDs based on thermally activated delayed fluorescence (TADF).

2.3.1. Low-molar-mass hosts for PHOLEDs

Carbazole is still one of the most popular moieties used for the design and synthesis of host materials, since it fits most of the above mentioned requirements, i.e. high thermal, chemical stability, high triplet energy, solubility etc. In the past 10 years, nearly 200 PHOLED devices containing carbazole derivatives were reported. Doping them with different triplet emitters (Fig. 2.8) many scientific groups obtained different color PHOLEDs with external quantum efficiencies up to 33% [84]. The most convenient heavy metal based phosphorescent emitters of different color are presented inFig. 2.8:

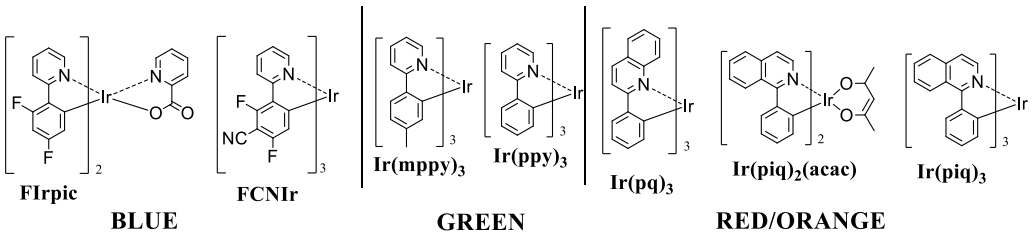

Fig. 2.8. Heavy metal based phosphorescent emitters

2.3.1.1. Carbazole-based hosts for blue PHOLEDs

Characteristics of carbazole-based hosts used in blue PHOLEDs are given in Table 2.3.

Table 2.3. Hosts for blue PHOLEDs doped with different Iridium complexes

Host	Yield, %	Synth. steps	HOMO, eV	LUMO, eV	E_T, eV	T_g, C^O	T_d, C^O	Dopant conc., %	V_{on}, V	L, cd m^{-2}	LE_{max}, cd A^{-1}	η_p, lm W^{-1}	EQE, %	EL λ_{max}	CIE1931, (x, y)	Ref. No.
Firpic																
CBZ1-F2	92	1	5.52	2.14	2.88	171	429	21%	-	39100	19.2	-	10.2		-	85
CPF	52	2	5.45	1.91	2.88	165	508	15%	5.1	25800	9.5	-	-	470	-	86
CPTBF	18	3	5.57	2.03	2.84	163	511	15%	4.3	25900	13.0	-	-	470	-	86
TBCPF	35	3	5.53	2.05	2.88	212	540	20%	4.2	23300	13.0	-	-	470	-	86
SiTCz_3c	36	2	6.01	2.44	3.00	152	-	10%	5.6	4000	-	-	7.2	472	0.15; 0.29	87
SiTCz_2c	22	2	6.01	2.49	3.00	149	-	10%	5.5	1500	-	-	8.0	468	0.15; 0.29	87
SiDCz_2b	27	2	6.05	2.50	3.00	99	-	10%	5.5	2500	-	-	8.2	468	0.15; 0.28	87
SiDCz_3b	39	2	6.01	2.44	3.00	120	-	10%	5.5	3000	-	-	8.3	472	0.15; 0.28	87
SiDCz_2b	27	2	6.05	2.50	3.00	99	-	2b/10%	4.5	8000	-	13.6	12.1	468	0.15; 0.28	87
SitCz	52	5	5.54	2.30	3.00	168	402	10%	3.6	10514	46.3	36.5	27.2	472	0.17; 0.34	88
CzPO1	37	2	5.78	2.20	2.81	111	391	10%	7.0	8000	3.8	-	2.0	475	0.15; 0.32	89
CzPO2	32	2	5.85	2.34	2.82	96	386	10%	7.4	11000	23.6	-	10.5	475	0.16; 0.32	89
BCzTPA	67	2	5.15	1.11	2.91	157	526	11%	2.8	5000	38.2	39.3	16.6	475	-	90
BCzPO	86	2	5.44	1.48	2.91	136	516	11%	2.9	5000	39.3	34.4	17.2	475	-	90
BCzTPM	66	2	5.26	1.14	2.87	-	529	11%	2.9	3000	44.5	45.5	19.6	475	-	90
BCzPh	52	1	5.31	1.16	2.87	105	399	11%	2.8	20000	43.9	45.2	19.8	475	-	90
TrzCz_4	37	4	5.61	2.09	2.76	218	426	15%	3.2	5827	21.1	18.7	-	485	-	91
TrzCz_3	39	4	5.62	2.15	2.70	116	452	15%	3.2	6916	17.7	13.6	-	485	-	91

Table 2.3. (continued)

Host	Yield, %	Synth. steps	HOMO, eV	LUMO, eV	E_T, eV	T_g, C^O	T_d, C^O	Dopant conc., %	V_{on}, V	L, cd m^{-2}	LE_{max}, cd A^{-1}	η_p, lm W^{-1}	EQE, %	EL λ_{max}	CIE1931, (x, y)	Ref. No.
TrzCz_1	40	4	5.61	2.32	2.58	-	453	15%	4.4	517	2.2	1.2	-	485	-	91
TrzCz_2	42	4	6.62	2.19	2.56	156	454	15%	5.0	532	1.5	1.3	-	485	-	91
mCPCzCN	32	3	5.66	2.23	2.78	167	437	8%	4.0	9184	19.3	10.5	9.2	475	0.16; 0.40	92
m-CzOCN	29	3	5.63	2.19	2.89	98	334	8%	3.6	12080	36.8	21.9	15.3	475	0.16; 0.38	92
m-CzCzCN	33	3	5.62	2.20	2.82	-	186	8%	3.9	12530	33.4	21.0	16.4	475	0.14; 0.35	92
o-CzCzCN	31	3	5.62	2.37	2.82	104	320	8%	4.8	24300	43.9	23.0	21.0	475	0.15; 0.35	92
m-CzSCN	29	3	5.63	2.20	2.78	111	330	8%	4.0	14730	46.1	23.4	23.3	475	0.17; 0.43	92
CzBPCb	34	3	6.09	2.58	2.75	-	-	10%	5.5	4600	47.0	35.0	27.5	480	-	93
BPTRZ	13	4	5.60	2.36	2.70	134	445	5%	6.0	24400	14.4	4.6	6.2	473	-	94
MBPTRZ	12	4	5.58	2.28	2.81	154	475	5%	5.0	30600	15.6	6.3	7.0	473	-	94
mCP	-	-	6.10	2.50	3.00	55	-	14%	4.3	5000	15.9	-	8.0	480	-	95
SimCP	-	-	6.10	2.50	3.00	101	-	14%	5.8	4000	22.1	-	13.0	480	-	95
SimCP2	-	-	6.10	2.50	3.00	144	-	14%	4.7	4000	38.9	-	21.0	480	-	95
CzDBF	53	2	5.90	2.42	2.82	-	-	5%	4.0	2000	-	-	23.9	480	0.15; 0.30	96
PCz-BFP	29	3	6.10	2.52	2.89	78	-	5%	3.5	8000	-	-	23.0	480	0.15; 0.33	97
35DCzPPy	65	3	6.18	-	2.71	107	461	11%	3.0	16000	-	45.8	20.7	480	-	98
26DCzPPy	65	3	6.05	-	2.71	102	455	11%	3.0	21000	-	50.6	24.5	480	-	98
pOXDDSiCz	33	3	5.49	2.31	2.67	190	435	15%	6.8	2021	8.2	3.2	3.7	490	0.16; 0.36	99
mOXDDSiCz	35	3	5.46	2.28	2.73	158	460	15%	7.2	3341	11.5	4.5	5.3	490	0.16; 0.34	99
DTCPFB	45	3	5.63	2.16	2.85	242	442	30%	6.0	5000	24.0	8.8	-	470	0.14; 0.23	100
PPO27	30	3	5.64	1.36	2.81	-	-	15%	3.0	10000	-	37.5	23.9	480	-	101
TRCz_6	56	3	-	-	2.90	-	-	6%	5.0	10000	14.2	-	9.8	-	0.14; 0.31	102
DCzGe	25	2	5.77	2.21	3.02	110	377	10%	10.1	10000	15.2	3.8	6.9	480	-	103

Table 2.3. (continued)

Host	Yield, %	Synth. steps	HOMO, eV	LUMO, eV	E_T, eV	T_g, C^O	T_d, C^O	Dopant conc., %	V_{on}, V	L, cd m^{-2}	LE_{max}, cd A^{-1}	η_p, lm W^{-1}	EQE, %	EL λ_{max}	CIE1931, (x, y)	Ref. No.
EBCz-ThX	63	2	5.95	2.63	2.94	227	400	15%	3.0	6000	23.8	12.4	11.5	480	-	104
BCz-Si	36	2	5.62	2.30	2.77	130	487	5%	3.2	18000	46.5	45.8	21.0	480	0.16; 0.39	105
CBP	92	1	5.54	2.23	2.66	62	-	8%	3.9	10935	10.7	8.5	5.2	475	0.15; 0.32	106
m-CBP	53	3	5.60	2.13	2.84	97	411	8%	4.3	21172	18.6	11.3	8.7	475	0.16; 0.32	106
o-CBP	33	3	5.55	2.19	3.00	82	317	8%	3.7	10252	29.9	25.3	14.2	475	0.16; 0.31	106
CzDPOTA	20	2	5.53	2.12	2.86	122	476	6%	3.1	7287	27.4	24.1	14.1	480	0.14; 0.32	107
TCTA	90	1	5.09	1.63	2.85	152	489	6%	3.2	5560	29.4	24.4	14.5	480	0.15; 0.31	107
DCzPOTA	21	2	5.44	2.05	2.84	148	471	6%	2.7	19910	33.0	36.9	16.9	480	0.14; 0.32	107
DBFDPOCz2	30	2	6.10	2.84	2.88	116	508	10%	2.4	5000	11.1	12.7	5.1	480	-	108
DBFSPOCz2	15	2	6.09	2.67	2.91	116	456	10%	2.4	6000	13.1	14.5	7.4	480	-	108
DBFDPOCz	22	2	6.10	2.73	2.88	116	463	10%	2.4	9000	19.1	19.9	9.6	480	-	108
DBFSPOCz	36	2	6.06	2.54	2.90	116	455	10%	2.5	8000	19.9	23.1	11.5	480	-	108
TCTP	24	2	5.25	1.67	3.03	163	497	8%	3.2	35100	35.0	-	15.9	-	0.15; 0.34	109
TPCz	24	3	6.27	2.69	3.07	143	506	8%	-	-	36.4	-	16.7	-	-	109
CzPAPm	28	4	5.88	2.34	2.56	175	473	5%	5.1	3247	6.7	3.1	-	475	0.15; 0.34	110
CzPPO	37	2	5.84	2.35	2.71	169	536	5%	4.5	6498	9.3	5.0	-	475	0.15; 0.35	110
CzPAMe	38	4	5.96	2.42	2.73	159	471	5%	5.6	2839	10.6	4.9	-	475	0.16; 0.39	110
SimCP2	-	-	6.10	2.44	2.70	144	466	5%	5.0	3775	9.2	2.8	-	475	0.15; 0.34	110
CPF	43	2	5.45	1.91	2.88	165	508	8%	4.0	21100	11.4	-	-	470	-	86
FCNIr																
PPO1	47	4	6.16	2.60	3.02	74	-	15%	6.0	-	20.5	14.3	17.1	-	0.14; 0.16	111
PPO2	28	4	6.31	2.77	3.02	123	-	15%	5.0	-	21.1	16.6	18.4	-	0.14; 0.15	111
PPO36	30	3	5.73	1.07	3.01	-	-	15%	4.0	2000	-	19.9	19.8	450	-	112

Table 2.3. (continued)

Host	Yield, %	Synth. steps	HOMO, eV	LUMO, eV	E_T, eV	T_g, C^O	T_d, C^O	Dopant conc., %	V_{on}, V	L, cd m^{-2}	LE_{max}, cd A^{-1}	η_p, lm W^{-1}	EQE, %	EL λ_{max}	CIE1931, (x, y)	Ref. No.
BCPCB	36	3	6.25	2.73	3.00	146	-	10%	5.5	3200	-	23.4	19.7	460	-	113
CPDBC	46	3	6.13	2.59	3.01	-	-	10%	5.0	4000	-	31.0	24.5	460	-	113
PPS21	29	3	6.14	2.58	3.00	120	-	15%	3.5	1100	-	-	12.0	482	0.14; 0.17	114
PPO21	29	3	6.25	2.68	3.01	111	-	15%	3.5	5000	22.5	19.0	19.2	482	0.14; 0.16	114
FCNIrpic																
mCPPO1	45	3	6.13	2.64	3.00	-	-	3%	4.2	4000	31.0	29.8	25.0	-	0.14; 0.17	115
bic-CMPC	28	2	6.16	2.76	2.95	140	377	10%	6.2	1000	-	-	13.1	470	0.14; 0.21	116
DBFSi. Ir(dbfmi)																
meta_CBP_2	24	2	5.56	2.17	2.97	107	349	20%. 5%	3.1	5000	0.9	0.6	0.5	450	-	117
meta_CBP_4	17	2	5.53	2.17	2.93	120	319	20%. 5%	4.0	9300	4.5	3.3	2.6	450	-	117
meta_CBP_1	20	2	5.65	2.15	2.98	-	315	20%. 5%	3.0	5300	11.5	10.2	8.2	450	-	117
meta_CBP_3	15	2	5.65	2.16	2.95	108	319	20%. 5%	3.6	10800	12.2	10.2	8.7	450	-	117
Ir(dbi)$_3$																
mCPPI	33	2	6.04	2.63	2.89	143	430	10%	3.5	9000	-	-	24.3	-	0.18; 0.38	118
mCP2PI	44	2	6.06	2.63	2.89	196	490	10%	4.0	8000	-	-	25.4	-	0.19; 0.39	118
fac-Ir(mpim)$_3$																
26DCzPPy	65	3	6.05	-	2.71	102	455	10%	2.8	12000	73.6	71.9	33.2	-	-	84

Tremendous effort was made investigating various host materials for blue PHOLEDs. Examples are presented in Table 2.3. Firpic is a dominant triplet emitter among the blue ones. The concentration of the dopant ranges from 5 to 21%, but it is not the main factor that predetermines performance of the devices. For example, some authors [85,99,104] reported on EL devices (15-21% of Firpic) with EQE reaching 12%, while other groups [96,97,105] presented PHOLEDs (concentration of Firpic less than 5% of) with EQE reaching 24%. Taking into account EQE, the best results were obtained by Lee et al. [93] in 2013 with the value of this parameter reaching 27,5%. They prepared the multilayer device consisting of HIL (PEDOT:PSS), HTL (TAPC), LEL and ETL (TSPO1), CIL(LiF) layers squeezed between electrodes. LEL consists of host CzBPCb (Fig. 2.9), based on carbazole and pyrido[2,3-b]indole moieties linked through a diphenyl-bridge, and 10% of dopant (Firpic). CzBPCb was prepared in three steps, with an overall yield of 34%. Brightness of the device was less than 5000 cd/m^2. Deng et al. [92], Xie et al. [105], Su et al. [98],Bin et al. [88] reported on the low turn-on voltage (<5.0V) EL devices with the EQE higher than 20%, a current efficiency reaching 40 cd/A and the brightness higher than 10000 cd/m^2. Deng et. al. [92] used simple carbazole based bipolar hosts o-CzCzCN and m-CzSCN (Fig. 2.9) containing ciano groups, which have a strong electron accepting ability.

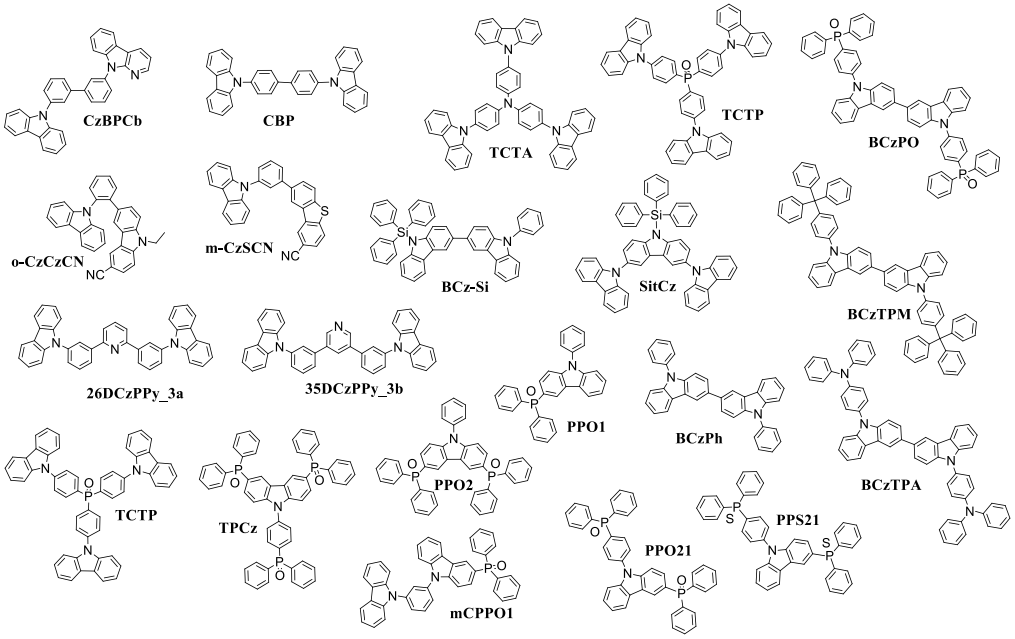

Fig. 2.9. Chemical structures of carbazole based host materials for blue PHOLEDs

The maximum brightness and current efficiency values of the prepared multilayer devices reached 24000 cd/m^2 and 46 cd/A, respectively. The device containing m-CzSCN showed the best results between carbazole and Firpic based PHOLEDs [92]. By introducing triphenyl silicon into the carbazole based derivatives, BCz-Si [105]

and SitCz[88] (Fig. 2.9) were synthesized. They were employed as host materials in blue PHOLEDs with EQE of 27.2 % and 21.0 %, respectively. For both these devices, EQE was quite high with half smaller value of current density of 40 mA/cm^2. BCz-Si was prepared in 2 steps with an overall yield of 36%, while its counterpart (SitCz) was prepared in a five step synthesis with an overall yield of 52%. Due to the shorter synthetic route, BCz-Si is more convenient for preparation on an industrial scale. In most of the studies, the scientific groups focus only on the PHOLED effectiveness, but not on the synthetic routes of host materials. Sasabe et al. [90] paid attention to both the yield of the host and to the efficiency of the device. They reported a one-step preparation with 52% overall yield of the bicarbazole compound BCzPh (Fig. 2.9), which was used to fabricate the low turn-on voltage (2.8 V) EL device with a reduced efficiency roll-off (EQE of 19.8 % at 100 cd/m^2 and 16.4 % at 1000 cd/m^2) and with a maximum brightness reaching 20000 cd/m^2. By attaching triphenylamine, tetraphenylmethane and triphenylphosphine oxide to bicarbazole moiety the same group prepared three compounds BCzTPA, BCzTPM and BCzPO (Fig. 2.9) with an overall yield of a two-step synthesis of 66, 67 and 86%, respectively. By employing these hosts (BCzTPA, BCzTPM, BCzPO) into the same multilayered device structure as BCzPh PHOLED, Sasabe et al. [90] reported about a 75% decrease of the device brightness. By doping 8% of FIrpic into 4,4',4"tri(N-carbazolyl)triphenylphosphine oxide (TCTP, Fig. 8) Ding et al. [109] prepared an effective PHOLED with the maximum brightness reaching 35000 cd/m^2 and an efficiency of 15.9%. TCTP is characterized by high glass transition and decomposition temperatures, with the values of 163 ºC and 497 ºC, respectively. In general, high morphological stability, easy preparation and the possibility to design effective PHOLED makes TCTP a promising candidate for production on an industrial scale.

The most effective PHOLED containing an other than Firpic emitter was reported by Udagawa et al. [84] with the maximum EQE, brightness, current and power efficiency of 33.2%, ~12000 cd/m^2, 73.6 cd/A and 71.9 lm/W, respectively. The emissive layer for the EL device was prepared by mixing 10% of blue-green emitter fac-Ir(mpim)$_3$ with a host material 26DCzPPy (Fig. 2.9) that consists of two carbazole moieties linked with a phenyl-pyridine-phenyl conjugated bridge. The efficiency roll-off of the reported device was found to be very small, with an EQE of 27% at 10000 cd/m^2. There are two limiting factors that hinder production of such a PHOLED on an industrial scale. Firstly, the device shows blue-green emission, i.e. there are two maxima (474, 510 nm) in the EL spectrum. Secondly, a three step synthesis of 26DCzPPy with 65% an overall synthesis yield is rather costly. The EL spectra of all PHOLED examples presented in Table 2.3 show one (FIrpic) or two (fac-Ir(mpim)$_3$) emission maxima in the range of 475-510 nm. Therefore, the EL devices exhibit blue-green, sky-blue, greenish-blue, bluish-green emissions, rather than deep blue. Replacing FIrpic or FCNIrpic with FCNIrpic and doping it into the carbazole and phosphine oxide based host material (PPO1, PPO2, Fig. 2.9) Jeon et al. [111] fabricated deep-blue PHOLEDs (CIE_{XY} 0.14, 0.15-0.16) with a maximum EQE efficiency reaching 18.4% and maximum current efficiency of 21.1 cd/A. Later,

the same group reported one more deep-blue PHOLED (CIE_{XY} 0.14, 0.16), prepared using bipolar host material (PPO21, Fig. 2.9) doped with 15% of FCNIr [114]. The EL device showed a low turn-on voltage of 3.5 V, maximum EQE of 19.2%, current efficiency of 22.5 cd/A and power efficiency of 19.0 lm/W. Jeon et al. [115] also reported on the host material mCPPO1 (Fig. 2.9), which was employed in the EL device (CIE_{XY} 0.14, 0.17), with the maximum EQE, current and power efficacy of 25%, 31.0 cd/A and 29.8 lm/W, respectively. In general, due to the low concentration of expensive iridium dopant (FCNIr) (3%) and an effective three-step synthesis (45% yield) of host material (mCPPO1), it seems to be promising for commercialization.

2.3.1.2. Carbazole based hosts for green PHOLEDs

Characteristics of carbazole-based hosts used in green PHOLEDs are given in Table 2.4.

Table 2.4. Hosts for green PHOLEDs doped with different Iridium complexes

Host	Yield, %	Synt. steps	HOMO, eV	LUMO, eV	E_T, eV	T_g, C^O	T_d, C^O	Dopant conc., %	V_{on}, V	L, cd m^{-2}	LE_{max}, cd A^{-1}	η_p, lm W^{-1}	EQE, %	EL λ_{max}, nm	CIE1931, (x, y)	Ref. No.
Ir(ppy)$_3$																
TSTC	8.3	4	6.00	2.50	2.40	-	-	6%	3.5	-	64.3	59.4	19.8	515	-	119
BCBP	14	3	5.45	2.13	2.60	173	412	9%	2.9	48420	52.7	41.1	13.7	-	0.26; 0.65	120
DCzP	47	2	5.59	2.59	2.28	-	-	5%	8.0	23000	11.0	-	-	-	0.33; 0.60	121
BIMCzNPh_3b	40	3	5.93	2.77	2.50	-	-	10%	4.1	4900	3.2	8.0	-	-	0.28; 0.52	122
BIMCzPh_3a	44	3	6.10	2.86	2.60	-	-	10%	3.6	4500	46.7	12.0	-	-	0.29; 0.61	122
CBP-CN	47	2	6.06	2.63	2.69	162	440	6%	3.6	98650	80.6	48.9	23.1	510	0.31; 0.62	123
TrzCz_4	37	4	5.61	2.09	2.76	218	426	8%	2.9	22500	32.7	22.1	-	510	-	91
TrzCz_3	39	4	5.62	2.15	2.70	116	452	8%	2.9	23771	28.9	21.8	-	510	-	91
TrzCz_1	40	4	5.61	2.32	2.58	-	453	8%	2.7	16796	11.7	11.1	-	510	-	91
TrzCz_2	42	4	6.62	2.19	2.56	156	454	8%	2.7	24544	13.0	11.2	-	510	-	91
CzDPhI_8	7	3	5.80	-	-	64	-	3%	3.2	860	8.7	5.5	-	-	0.31; 0.62	124
CzT_7	25	2	5.80	-	-	71	-	3%	3.2	2548	16.8	14.5	-	-	0.31; 0.62	124
Cz-PhI_6	45	2	6.00	-	-	31	-	3%	6.0	13660	23.0	6.8	-	-	-	124
PHI_M3	26	3	5.35	2.03	-	132	430	16%	4.4	11590	14.2	9.3	5.2	-	0.42; 0.46	125
PHI_M1	37	2	5.50	2.33	-	132	405	0.15nm	3.0	12920	20.0	12.3	6.9	-	0.25; 0.46	125
PHI_M2	6	4	5.35	2.22	-	207	515	15%	3.2	61500	33.3	23.0	9.5	-	0.32; 0.62	125
TP-mCP	10	3	5.68	2.11	2.63	159	436	8%	3.0	25000	64.0	49.0	20.3	-	0.28; 0.64	126
DTP-mCP	16	3	5.98	2.39	2.63	179	488	8%	3.0	20000	52.0	51.0	25.6	-	0.29; 0.63	126

Table 2.4. (continued)

Host	Yield, %	Synt. steps	HOMO, eV	LUMO, eV	E_T, eV	T_g, C^O	T_d, C^O	Dopant conc., %	V_{on}, V	L, cd m^{-2}	LE_{max}, cd A^{-1}	η_p, lm W^{-1}	EQE, %	EL λ_{max}, nm	CIE1931, (x, y)	Ref. No.
CZPT	27	3	5.76	-	3.20	-	500	6%	10.5	7000	3.0	-	-	530	-	127
Cz_G1	35	2	5.61	2.33	2.62	175	478	6%	5.9	10930	18.3	6.4	5.4	-	0.28; 0.62	128
Cz_G3	10	5	5.42	2.30	2.61	376	517	6%	4.8	11300	20.8	8.7	6.1	-	0.27; 0.62	128
Cz_G2	27	5	5.45	2.29	2.60	300	502	6%	5.1	11991	23.8	8.2	7.0	-	0.28; 0.63	128
Cz_G1	35	2	5.61	2.33	2.62	175	478	6%. OXD-7 30%	5.0	19220	34.5	13.2	10.2	-	0.27; 0.62	128
Cz_G3	10	5	5.42	2.30	2.61	376	517	6%. OXD-7 30%	3.8	19820	36.4	18.6	10.7	-	0.27; 0.62	128
Cz_G2	27	5	5.45	2.29	2.60	300	502	6%. OXD-7 30%	4.5	22020	38.7	15.7	11.4	-	0.28; 0.63	128
Spiro-2CBP	-	-	5.00	1.60	-	-	-	20%	4.0	28800	77.0	44.0	-	-	0.32; 0.62	129
ACBP	57	2	5.76	1.75	2.66	-	-	6%	3.3	2793	56.0	44.5	16.9	-	0.29; 0.63	130
Ir(mppy)$_3$																
PhosCz_3	65	2	5.70	2.10	3.00	108	454	15%	2.6	11530	35.3	33.5	9.6	511	-	131
PhosCz_5	62	2	5.20	1.70	2.99	-	433	15%	2.8	510	34.1	37.8	11.6	-	-	131
BCzPPm	40	4	5.69	1.89	2.77	56	448	11%	3.9	900	-	30.0	10.0	510	-	132
BCzPPh	35	3	5.68	-	2.79	51	436	11%	5.0	300	-	30.7	13.2	510	-	132
mCz_2	15	4	5.24	1.88	2.73	0	442	10%	3.6	3720	9.1	8.2	2.8	510	-	133
mCz_5	15	4	5.19	1.85	2.66	54	464	10%	3.1	1020	18.2	12.1	4.8	510	-	133
mCz_4	27	4	5.21	1.89	2.68	40	494	10%	3.0	1180	22.1	18.2	6.9	510	-	133
mCz_3	22	4	5.21	1.90	2.66	30	490	10%	2.8	2310	35.5	33.6	10.6	510	-	133
Cz(MP)2	60	1	5.20	1.80	2.80	59	-	10%	8.0	5000	20.0	-	5.9	520	-	134
TRZ-3Cz(MP)2	9	5	6.70	2.60	3.00	144	403	10%	7.0	18000	32.0	-	9.2	520	-	134

Table 2.4. (continued)

Host	Yield, %	Synt. steps	HOMO, eV	LUMO, eV	E_T, eV	T_g, C^O	T_d, C^O	Dopant conc., %	V_{on}, V	L, cd m^{-2}	LE_{max}, cd A^{-1}	η_p, lm W^{-1}	EQE, %	EL λ_{max}, nm	CIE1931, (x, y)	Ref. No.
TRZ-1Cz(MP)2	5	7	5.20	2.60	2.80	98	399	10%	6.0	11000	19.0	-	-	520	-	134
Cz-6PBI	21	3	5.64	2.30	2.66	223	519	10%	2.9	28000	47.8	29.6	-	-	0.30; 0.60	135
Cz-2PBI	26	3	5.61	2.05	2.67	143	386	10%	6.1	10000	41.3	13.9	-	-	0.31; 0.60	135
Cz-4PBI	27	3	5.61	2.15	2.67	196	492	10%	3.2	28000	44.5	28.3	-	-	0.31; 0.60	135
6Cz-PBI	35	2	5.26	2.01	2.66	285	510	10%	4.8	10000	27.5	14.3	-	-	0.32; 0.60	135
4Cz-PBI	37	2	5.29	2.01	2.67	233	458	10%	5.7	25000	29.6	10.5	-	-	0.31; 0.60	135
2Cz-PBI	38	2	5.46	1.98	2.68	186	408	10%	7.2	20000	38.9	12.2	-	-	0.31; 0.60	135
Ir(piq)$_3$																
CFL	41	5	6.00	2.60	-	151	-	10%	5.9	70000	39.0	25	11.0	-	0.30; 0.63	136
(TPm)$_2$Ir(acac)																
CzT	55	2	5.49	2.77	2.67	134	425	8%	2.8	110000	75.3	71.3	20.0	-	0.38; 0.59	137
Ir(pbi)$_2$(acac)																
CPhBzIm	62	3	5.49	2.37	2.48	170	480	10%	2.0	96000	62.0	62.0	19.2	-	0.42; 0.56	138

The conventional metal-based complexes used for green EL devices are $Ir(mppy)_3$ and Ir(ppy). Combining carbazole and triphenylene moieties, Lee et al. [126] synthesized two host materials (DTP-mCP and TP-mCP, Fig. 2.10), which possess high glass transition temperatures (179 °C and 159 °C) and high thermal stability.

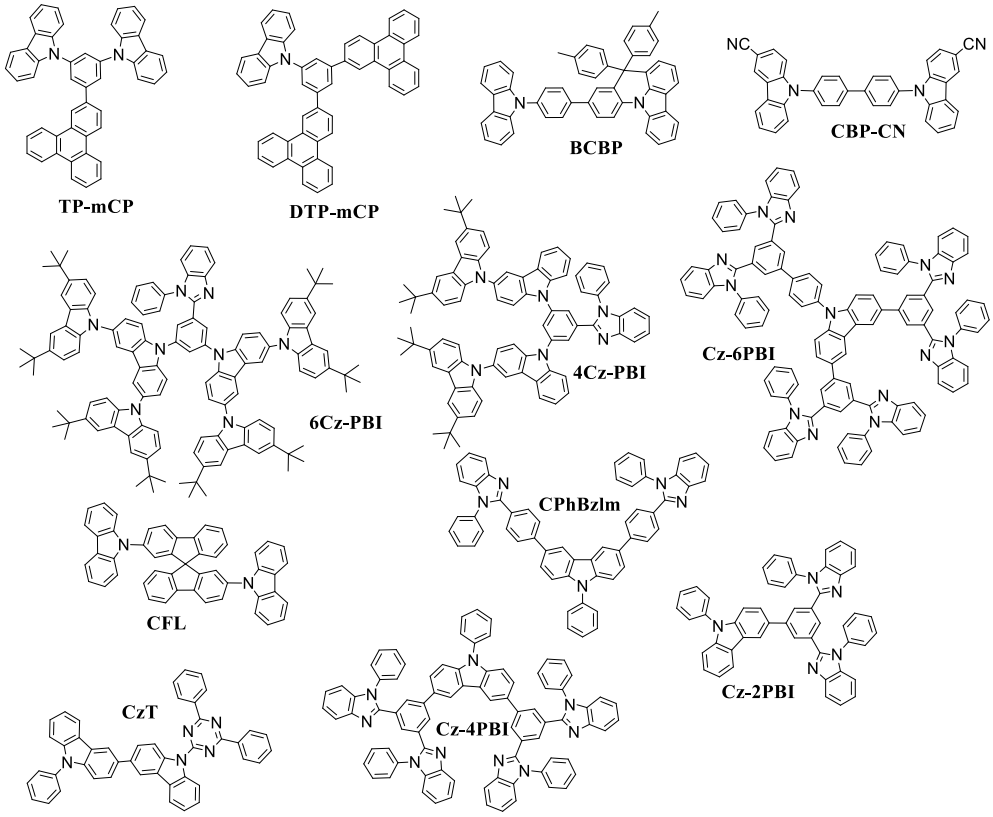

Fig. 2.10. Chemical structures of carbazole based hosts for green PHOLEDs

The temperatures of the onset of thermal degradation were found to be 488°C and 436°C, respectively. Both compounds were tested as the hosts for green PHOLED doping with 8% of $Ir(ppy)_3$. The maximum EQE, current and power efficiency of the DTP-mCP, TP-mCP containing EL devices, were found to be 25.6 and 20.3%, 52.0 and 64.0 cd/A, 51.0 and 49.0 lm/W, respectively. Both devices reached brightness higher than that of 20000 cd/m^2. The limiting factor that could hinder commercialization of these materials is a non-effective synthesis (3 steps, the overall yield <16%). Jiang et al. [120] reported on a PHOLED based on an asymmetric CBP derivative (BCBP, Fig. 2.10) as a host of an emitting layer with the maximum brightness close to 50000 cd/m^2. Unfortunately, the synthesis of BCPB was non-effective with the low yield of the target product (<15%). Zhang and co-workers [123] prepared another CBP derivative (CBP-CN) in a two-step synthesis by

incorporating a ciano group onto each carbazole moiety with an overall yield reaching 47%. By doping CBP-CN with 6% of $Ir(ppy)_3$, green PHOLED was fabricated, which exhibited a maximum brightness close to 10000 cd/m^2, power efficiency of 80.6 lm/W and an external quantum yield of 23.1%. Currently, this is one of the most effective reported green PHOLEDs fabricated using $Ir(ppy)_3$ as a triplet emitter. Ban et al. [135] prepared a series of two or three step synthesis of bipolar hosts with a different number of linked carbazole and benzimidazole moieties (2Cz-PBI, 4Cz-PBI, 6Cz-PBI, Cz-2PBI, Cz-4PBI, Cz-6PBI, Fig. 2.10) with an overall yield ranging from 21 to 38% [135]. With the exception of Cz-2PBI, all the compounds were employed as hosts of the light emitting layers of PHOLED by mixing 10% of green dopant ($Ir(mppy)_3$). The maximum brightness of the devices ranged from 10000 to 28000 cd/m^2, current and power efficiency ranged from 29.6 to 47.8 cd/A and from 10.5 to 29.6 lm/W, respectively. The lowest turn-on voltages (2.9-3.2 V) were observed for the PHOLEDs prepared using Cz-4PBI and Cz-6PBI. Spirobifluorene linked with two carbazole moieties (CFL, Fig. 2.10) exhibiting a high glass transition temperature (151 ^{o}C) was also used as a host for green PHOLED [136]. The devices emitting layer, which was prepared by mixing CFL with 10% of $Ir(piq)_3$, gave the maximum brightness of 70000 cd/m^2, EQE of 11%, current and power efficiencies of 39.0 cd/A and 25.0 lm/w, respectively. However, the five-step synthesis is the limiting factor for commercialization of CFL. The promising hosts for green PHOLEDs with respect of commercialization (high-yield synthesis and high PHOLED efficiency) were reported by Chang et al. [137] and Hung et al. [138]. Chang et al.[137] prepared a bipolar host (CzT) containing dicarbazole and triazine moieties with an overall yield of 55%. By incorporating the mixture of CzT with 8% of $(Tmp)_2Ir(acac)$, the EL device was fabricated with a maximum brightness reaching 110000 cd/m^2 and EQE of 20.0%. Hung and co-workers [138] achieved the benzimidazole-carbazole based product (CPhBzIm, Fig. 2.10) in three steps with an overall yield of 62%. The PHOLED with low turn-on voltage (2.0 V) PHOLED, maximum brightness of 96000 cd/m^2 and EQE reaching 19.2% was prepared using the CPhBzIm as host and $Ir(pbi)_2(acac)$ as the triplet emitter with the mass ratio of 90 to 10.

2.3.1.3. Carbazole based hosts for orange and red PHOLEDs

Characteristics of carbazole-based hosts used in orange PHOLEDs are given in Table 2.5.

Table 2.5. Hosts for orange PHOLEDs doped with different Iridium complexes

Host	Yield, %	Synth. steps	HOMO, eV	LUMO, eV	E_T, eV	T_g, C^O	T_d, C^O	Dopant conc., %	V_{on}, V	L, cd m^{-2}	LE_{max}, cd A^{-1}	η_p, lm W^{-1}	EQE, %	EL λ_{max}, nm	CIE1931, (x, y)	Ref. No.
Ir(pq)$_3$																
CzPPQCz	70	2	5.83	2.71	2.51	138	421	4%	2.7	120274	51.2	50.1	17.2	582	0.55; 0.45	139
CzPPCzQ	70	2	5.79	2.50	2.95	145	419	4%	3.0	144746	59.4	53.4	21.6	586	0.56; 0.44	139
CzPPQ	85	1	5.77	2.45	2.61	90	345	4%	3.0	129885	75.8	68.1	25.6	580	0.55; 0.45	139
Ir(pq)$_2$pic																
CPBDC	46	3	6.13	2.59	3.01	-	-	5%	4.0	1000	-	-	15.1	583	-	140
Ir(2-phq)$_3$																
NFBC	47	2	5.90	2.90	2.32	183	484	2%	3.7	18000	32.0	26.5	15.3	600	0.57; 0.42	141
DFBC	45	2	5.80	2.50	2.33	192	480	2%	3.0	18000	20.1	21.0	-	584	0.55; 0.42	142
TCzMe	68	2	5.48	1.71	2.94	130	404	20%	2.5	10000	-	16	7.5	600	-	143
Ir(2-PhPyCz)$_2$(acac) yellow																
CzOXD	67	1	5.50	2.50	2.45	65	460	7%	5.5	15232	20.0	5.0	-	-	0.48; 0.53	144
(t-bt)$_2$Ir(acac)																
CzPhONI	11	4	5.60	3.10	2.51	142	474	24%	3.1	41710	44.2	33.3	16.5	-	0.52; 0.47	145
(CF3-bt)$_2$Ir(acac)																
CMP	31	4	5.32	2.19	2.90	296	469	10%	5.0	2157	26.6	14.6	9.6	-	0.49; 0.47	146
CPMP	15	5	5.30	2.18	2.90	233	424	10%	4.7	4186	31.6	16.6	11.2	-	0.50; 0.47	146
(CF3-bt)$_2$Ir(acac). OXD-7																
CMP	31	4	5.32	2.19	2.90	296	469	10%.30%	4.1	6989	35.5	22.5	13.0	-	0.50; 0.47	146

Table 2.5. (continued)

Host	Yield, %	Synth. steps	HOMO, eV	LUMO, eV	E_T, eV	T_g, C^O	T_d, C^O	Dopant conc., %	V_{on}, V	L, cd m^{-2}	LE_{max}, cd A^{-1}	η_p, lm W^{-1}	EQE, %	EL λ_{max}, nm	CIE1931, (x, y)	Ref. No.
CPMP	15	5	5.30	2.18	2.90	233	424	10%. 30%	4.5	6993	39.5	25.5	14.4	-	0.51; 0.47	146
Cz_G1	35	2	5.61	2.33	2.62	175	478	8%. 30%	4.1	9745	22.2	13.9	7.9	-	0.51; 0.47	128
Cz_G2	27	5	5.45	2.29	2.60	300	502	8%. 30%	3.9	12050	32.2	20.2	11.4	-	0.51; 0.48	128
Cz_G3	10	5	5,42	2,30	2,61	376	517	8%, 30%	3,8	10810	30,5	19,2	10,8	-	0,51; 0,48	128
Os complex																
CzPhO	34	1	5,78	2,33	2,71	105	365	4%	2,5	52624	34,8	45,2	14,3	-	0,54; 0,46	147
PO-01																
26PyzCz	92	1	5,83	2,80	2,51	127	410	6%	4,0	20000	65,5	51,9	-	-	0,48; 0,50	148

Table 2.6. Hosts for red PHOLEDs doped with different Iridium complexes

Host	Yield, %	Synth.	HOMO, eV	LUMO, eV	E_T, eV	T_g, C^O	T_d, C^O	Dopant conc., %	V_{on}, V	L, cd m^{-2}	LE_{max}, cd A^{-1}	η_p, lm W^{-1}	EQE, %	EL λ_{max},nm	CIE1931, (x, y)	Ref. No.
Ir(piq)$_3$																
CzPPQ	85	1	5.77	2.45	2.61	90	345	4%	2.9	61485	24.8	24.4	19.3	620	0.67; 0.33	139
CzPPCzQ	70	2	5.79	2.50	2.95	145	419	4%	3.1	65867	24.4	20.5	19.4	620	0.67; 0.33	139
CzPPQCz	70	2	5.83	2.71	2.51	138	421	4%	3.0	68384	27.5	24.1	21.4	620	0.67; 0.33	139
Ir(piq)$_2$(acac)																
MTXSFCz	40	4	5.75	2.93	2.9	127	456	10%	4.4	27031	13.8	8.2	15.6	640	0.68; 0.32	149
BBTC	28	3	5.68	2.33	2.51	148	482	8%	2.9	82625	16.4	13.0	19.3	-	0.68; 0.32	150

Table 2.6. (continued)

Host	Yield, %	Synth. steps	HOMO, eV	LUMO, eV	E_T, eV	T_g, C^O	T_d, C^O	Dopant conc., %	V_{on}, V	L, cd m^{-2}	LE_{max}, cd A^{-1}	η_p, lm W^{-1}	EQE, %	EL λ_{max}, nm	CIE1931, (x, y)	Ref. No.
Ir(phq)$_2$(acac)																
BT-mCP	20	5	5.66	2.18	2.26	150	430	8%	2.5	12000	19.5	20.4	10.3	-	0.62; 0.37	151
BT-PC	32	4	5.96	2.57	2.26	110	393	5%	2.5	12000	23.6	24.7	12.8	-	0.63; 0.38	151
Ir(DBQ)2(acac)																
t-CmOxa	40	3	6.14	2.62	-	76	387	4%	4.0	13790	-	9.89	9.5	610	0.66; 0.34	152
Ir(2-PhDeCz)$_2$(acac)																
CzOXD	67	1	5.50	2.50	2.45	65	460	5%	11.3	4894	4.8	0.67	-	-	0.64; 0.36	144
(tmq)$_2$Ir(acac)																
BIQMCz	58	2	5.56	2.94	2.94	197	497	4%	3.1	62720	32.4	30.9	24.9	618	-	153

As described above, many carbazole based host materials have been developed and employed in blue and green PHOLEDs. However, carbazolyl-containing hosts are not very common in red or orange devices. Wang et al. [145] synthesized CzPhONI (Fig. 2.11) by incorporating carbazole and naphthalimide moieties. A PHOLED fabricated using CzPhONI as a host of emitting layer exhibited current efficiency of 44.2 cd/A with CIE_{XY} of (0.52, 0.47), maximum brightness of 41710 cd/m^2 and EQE of 16.5%. However, due to low overall yield (11%) of the five-step synthesis, CzPhONI does not seem to be promising for industrial production.

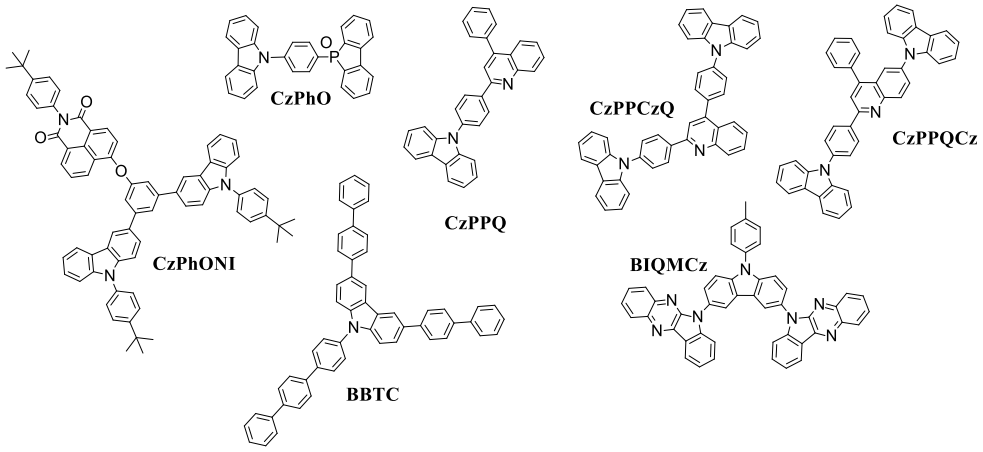

Fig. 2.11. Chemical structures of carbazole based host materials for red and orange PHOLEDs

Carbazole and phosphine oxide based host material (CzPhO, Fig. 2.11) was prepared in a one-step synthesis with an overall yield of 34% [147]. By doping CzPhO with Osmium-based orange emitter, a PHOLED with EQE of 14.3% and maximum external efficiency of nearly 53000 cd/m^2 was prepared. Utilizing the donor-acceptor approach, Chen et al. [139] synthesized three quinoline and carbazole based compounds (CzPPCzQ, CzPPQCz, CzPPQ, Fig. 2.11). CzPPCzQ and CzPPQCz) were obtained in a two-step synthesis with an overall yield reaching 70%, while CzPPQ was obtained in a one-pot synthesis with a high yield of 85%. All three compounds were employed as the host materials in orange PHOLEDs doped with 4% of iridium based complex ($Ir(pq)_3$). The devices exhibited a high maximum brightness ranging from 120000 to 145000 cd/m^2 (51.0-76.0 lm/W) and an EQE ranging from 17.2 to 25.6%. Due to the simplicity of the synthesis, CzPPQ might be the promising candidate for industrial production.

Characteristics of carbazole-based hosts used in red PHOLEDs are given in Table 2.6. Compared to the number of already published blue, green and orange PHOLEDs, there are few reports on carbazole-based hosts used for red PHOLEDs. However, recently reported red PHOLEDs demonstrated high efficiency. Kwak et al. [150] reported on carbazole derivative BBTC (Fig. 2.11) containing diphenyl and terphenyl moieties, which was obtained in a three-step synthesis route with an overall

yield of 28%. Red PHOLED doped with $(piq)_2Ir(acac)$ showed a low turn on voltage of 2.9 V, maximum brightness of 82625 cd/m^2 (16.4 cd/A, 13.0 lm/W) and EQE reaching 19.3%. Su et al. [153] fabricated a PHOLED using carbazole and indoloquinoxaline based bipolar host material (BIQMCz, Fig. 2.11) with 4% of deep-red emitter $(tmq)_2Ir(acac)$. The PHOLED showed a maximum EQE of 25.0 % with EL emission wavelength of 618 nm. A PHOLED based on BIQMCz showed double the value of maximum current and power efficiency (32.4 cd/A and 30.9 lm/W, respectively) than the device containing BBTC. Moreover, BIQMCz was prepared in two steps with an overall yield of 58%. Efficient red PHOLED was reported by Chen et al.[139]. The host materials (CzPPCzQ, CzPPQCz & CzPPQ, Fig. 2.11) were used to fabricate the devices with $Ir(piq)_3$ as an emitter. The devices containing CzPPCzQ, CzPPQCz and CzPPQ showed a maximum EQE of 19.4%, 21.4% and 19.3%, respectively. All the devices showed small roll-off with only 1-3% fall at 1000 cd/m^2. Although PHOLEDs based on CzPPCzQ and CzPPQCz showed higher efficiency, CzPPQ as a host material has apparently more perspectives for synthesis on an industrial scale, as it was prepared in a one-pot synthesis with the overall yield of 85%.

2.3.2. Derivatives of carbazole as emitters for fluorescent OLEDs

To eliminate phase separation and concentration quenching in the emissive layer and to exclude heavy-metal complex usage as dopant in the emissive layer, non-doped devices could be the option for large scale applications (Table 2.7). Gong et al. [154] reported tetraphenylethene substituted carbazole derivatives Cz-1TPE, Cz-2TPE(3,6) ,Cz-2TPE(2,7), Cz-3TPE and Cz-4TPE (Fig. 2.12) prepared in three steps with an overall yield ranging from 36 to 71%.

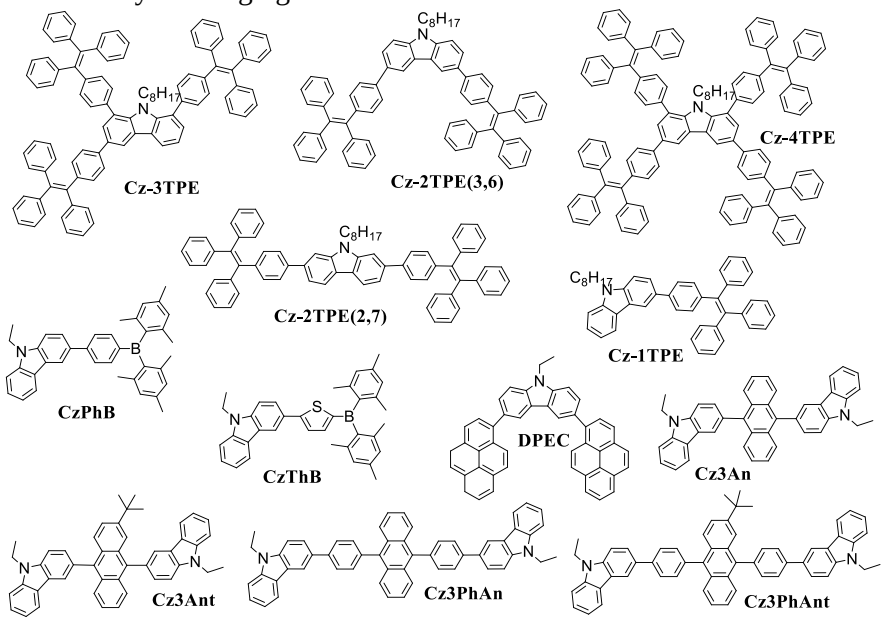

Fig. 2.12. Chemical structures of carbazole based compounds as emitters for blue OLEDs

Table 2.7. Carbazole based materials for blue OLEDs

Host	Yield, %	Synth. steps	HOMO, eV	LUMO, eV	Φ_{SOL}, %	Φ_{FILM}, %	T_g, C^O	T_d, C^O	V_{on}, V	L, cd m^{-2}	LE_{max}, cd A^{-1}	η_p, lm W^{-1}	EQE, %	EL λ_{max}, nm	CIE1931, (x, y)	Ref. No.
DDPFTBC	-	-	5.70	2.90	-	-	-	-	2.8	14000	8.7	9.1	-	492	0.18; 0.36	155
BF4	15	5	5.00	2.86	80 [c]	-	39	-	5.0	534	0.04	-	0.02	450	0.19; 0.21	156
Cz-NPh	51	3	5.12	2.15	-	-	90	320	3.0	8207	2.0	1.5	2.3	460	0.14; 0.09	157
Cz-SiPh	51	3	5.32	2.19	-	-	80	311	10.1	450	0.5	0.1	3.3	450	0.15; 0.11	157
CzThB	59	2	5.80	3.07	99 [h]	51	91	354	5.5	28300	10.1	4.9	6.9	473	0.13; 0.21	158
CzPhB	54	2	5.92	2.91	97 [h]	54	102	360	6.5	5350	3.3	1.3	4.3	449	0.15; 0.09	158
CzTrDPh_1	19	3	-	-	80 [d]	65	-	-	10.3	66	0.08	-	-	430	0.28; 0.20	159
TCPC-6	24	3	5.47	-	99 [b]	-	108	385	5.0	398	1.4	-	3.7	425	0.16; 0.05	160
TCTP-4	12	3	5.49	-	99 [b]	-	143	420	5.0	403	0.9	-	2.5	-	0.16; 0.05	160
3.7-DBTOC	21	3	-	2.10	98 [c]	-	-	223	3.6	11422	3.3	-	2.0	475	0.16; 0.22	43
2.8-DBTOC	15	3	-	1.85	48 [c]	-	-	240	3.8	1716	0.6	-	0.6	450	0.16; 0.13	43
BSB-Cz	48	3	5.80	3.10	100 [e]	-	113	341	-	-	-	-	2.0	444	-	161
CzPhOMe_2	57	3	5.67	2.50	19 [g]	-	-	-	8.5	-	0.06	-	-	420	0.22; 0.21	162
CzPyr_5	60	3	5.74	2.80	56 [g]	-	-	-	9.0	-	0.1	-	-	460	0.18; 0.21	162
CzPhCOMe_4	48	3	5.90	3.00	21[g]	-	-	-	3.0	1088	0.8	-	-	460	0.19; 0.23	162
CzPhCN_3	58	3	5.97	2.93	96 [g]	-	-	-	3.0	628	1.1	-	-	430	0.17; 0.08	162
Den11	44	4	5.60	2.60	95 [b]	-	-	-	3.2	1000	0.4	-	-	-	0.15; 0.10	163
Den12	8	6	5.70	2.70	94 [b]	-	-	-	3.7	2000	0.7	-	-	-	0.15; 0.09	163
CFP	50	2	5.49	2.35	84 [e]	-	95	390	4.0	6033	1.1	-	0.12	434	0.16; 0.14	164
CFTP	42	4	5.43	2.61	36 [e]	-	98	408	4.1	7277	2.5	-	0.16	480	0.16; 0.36	164
CzF4	21	4	5.55	2.55	91[a]	69	-	394	6.9	5135	1.8	0.85	-	416	0.16; 0.09	165
CzF1	52	2	5.63	2.47	97 [a]	59	45	352	4.7	714	0.9	0.50	-	437	0.17; 0.12	165
CzF2	28	3	5.58	2.52	98 [a]	67	64	383	5.1	1410	1.4	0.76	-	443	0.18; 0.19	165

Table 2.7. (continued)

Host	Yield, %	Synth. steps	HOMO, eV	LUMO, eV	Φ_{SOL}, %	Φ_{FILM}, %	T_g, C^O	T_d, C^O	V_{on}, V	L, cd m^{-2}	LE_{max}, cd A^{-1}	η_p, lm W^{-1}	EQE, %	EL λ_{max}, nm	CIE1931, (x, y)	Ref. No.
CzF3	21	4	5.56	2.53	88 [a]	67	70	389	4.7	1507	1.3	0.74	-	446	0.18; 0.19	165
OxCz_2	21	4	5.29	2.04	99 [f]	36	-	-	3.9	-	-	-	0.2	453	0.16; 0.12	166
OxCz_1	22	4	5.26	1.80	88 [f]	38	-	-	4.2	-	-	-	5.0	431	0.16; 0.08	166
OxCz_3	24	4	5.25	1.97	86 [f]	17	-	-	3.0	-	-	-	0.5	484	0.18; 0.27	166
OxCz_6	34	6	5.20	1.80	99 [f]	21	-	-	3.2	-	-	-	0.6	452	0.16; 0.11	166
OxCz_7	39	3	5.40	1.70	95 [f]	29	-	-	3.7	-	-	-	0.5	428	0.16; 0.05	166
OxCz_5	41	4	5.15	1.77	96 [f]	20	-	-	3.0	-	-	-	2.0	453	0.15; 0.10	166
OxCz_4	48	4	4.88	1.76	80 [f]	17	-	-	2.8	-	-	-	1.5	455	0.15; 0.18	166
DPEC	80	2	5.50	2.60	73 /	-	-	-	3.1	10000	4.8	-	-	460	0.15; 0.18	167
CzPhTr_4	31	3	5.48	2.32	97 [d]	-	-	418	9.0	74	0.01	-	-	-	0.25; 0.23	168
Cz3An	42	2	5.48	2.68	71 [c]	24	-	448	3.3	12270	5.1	-	-	468	0.15; 0.22	169
Cz3Ant	42	2	5.50	2.71	83 [c]	27	-	401	3.1	12841	3.4	-	-	494	0.22; 0.38	169
Cz3PhAn	20	4	5.52	2.73	72 [c]	25	-	495	3.1	37423	4.0	-	-	504	0.23; 0.40	169
Cz3PhAnt	19	4	5.56	2.78	85 [c]	28	169	486	3.0	23049	4.7	-	-	470	0.16; 0.23	169
CzIm_M1	37	2	5.50	2.33	70 [b]	65	132	405	4.5	3342	0.7	0.48	1.9	420	0.17; 0.05	125
CzIm_M4	8	2	5.35	2.06	55 [b]	32	220	530	3.2	5446	1.3	0.76	2.1	424	0.17; 0.08	125
CzIm_M5	30	3	5.53	2.10	99 [b]	81	153	475	6.2	4822	0.9	0.30	1.5	424	0.17; 0.08	125
CzIm_M3	26	3	5.35	2.03	50 [b]	24	132	430	4.0	3602	0.6	0.32	1.5	420	0.17; 0.05	125
CzIm_M2	6	4	5.35	2.22	68 [b]	59	207	515	3.4	4543	1.5	0.86	3.0	428	0.17; 0.06	125
Cz-1TPE	66	3	5.44	2.18	0.37 [b]	45	21	331	3.5	2585	3.5	2.1	-	492	0.18; 0.34	154
Cz-2TPE(3.6)	71	3	5.53	2.34	0.16 [b]	51	65	449	3.5	1353	4.9	3.9	-	500	0.20; 0.40	154
Cz-2TPE(2.7)	65	3	5.39	2.28	0.23 [b]	61	138	443	4.2	1129	5.5	3.1	-	492	0.20; 0.38	154
Cz-4TPE	36	3	5.39	2.26	0.22 [b]	48	94	463	3.6	2088	3.1	1.8	-	492	0.20; 0.38	154

Table 2.7. (continued)

Host	Yield, %	Synth. steps	HOMO, eV	LUMO, eV	Φ_{SOL}, %	Φ_{FILM}, %	T_g, C^O	T_d, C^O	V_{on}, V	L, cd m^{-2}	LE_{max}, cd A^{-1}	η_p, lm W^{-1}	EQE, %	EL λ_{max}, nm	CIE1931, (x, y)	Ref. No.
Cz-3TPE	60	3	5.37	2.21	0.18 [b]	58	70	493	3.3	986	3.1	2.2	-	492	0.20; 0.39	154
DTPCZ	4	4	4.98	1.75	0.38 [b]	-	123	241	6.0	4624	4.3	-	-	464	0.18; 0.21	170
CzSiSF	37	3	5.62	2.39	-	-	156	487	4.8	615	0.32	-	0.48	410	-	171
CzPySiSF	11	4	5.63	2.43	-	-	179	502	5.8	627	0.35	-	0.59	408	-	171
CBZDPA	21	3	5.94	3.07	94 [e]	60	188	416	3.5	3377	5.7	3.9	4.5	454	0.17; 0.17	172
MTPC-Et	-	-	5.20	2.00	-	-	-	-	4.5	1600	-	-	3.3	408	-	173
MTPC-Me	-	-	5.20	2.00	47 [e]	-	220	351	4.0	900	-	-	2.3	408	-	173
StiCz1	59	3	5.05	2.05	44 [a]	-	-	268	3.0	8703	3.3	1.9	2.3	454	0.17; 0.19	174
StiCz2	38	5	5.17	2.17	49 [a]	-	-	403	4.0	5533	2.9	2.0	2.4	454	0.16; 0.15	174
StiCz3	40	5	5.00	2.05	10 [a]	-	-	349	3.0	1081	2.8	2.3	1.3	484	0.20; 0.31	174
DEC	68	2	5.60	2.50	-	-	-	-	-	-	-	-	1.5	420	0.19; 0.21	175

[a] in toluene; [b] in THF; [c] in $CHCl_3$; [d] in DCM; [e] in CH_2Cl_2; [f] in cyclohexane; [g] in CH_3CN; [h] in EtOAc

Due to the aggregation induced emission (AIE) phenomenon, all the compounds exhibit a high PL quantum yield in the solid state reaching 61%. The materials were employed as emitters in a multilayer device with EQE ranging from 1.8 to 3.9% and a brightness reaching 2585 cd/m^2. Taking into account the synthesis route, glass transition temperature (138 ºC) and the effectiveness of the OLED, Cz-2TPE(2,7) could be a promising candidate for industrial production. A series of effective blue or blue-green fluorescent devices with brightness reaching 38000 cd/m^2 were prepared by Chang and co-workers [169] using carbazole and anthracene derivatives Cz3An, Cz3Ant, Cz3PhAn and Cz3PhAnt (Fig. 2.12) as the emitters. Although Cz3PhAn and Cz3PhAnt showed the highest brightness and thermal stability, Cz3An and Cz3Ant seem to be more suitable for industrial production, because of the higher overall yields and the shorter synthetic routes compared to Cz3PhAn and Cz3PhAnt. Promising results in the synthesis of blue emitters, with overall yields ranging from 54 to 80% were reported by Lin et al.[158]and Tong et al. [167] Tong and co-workers [167] designed a deep blue OLED (CIE_{XY} 0.15, 0.18) using a derivative of carbazole and pyrene DPEC (Fig. 2.12) for the preparation of the emissive layer. The low turn-on voltage (~ 3.1 V) fluorescent device exhibited a maximum brightness of nearly 10000 cd/m^2. Due to the high yield of the synthesis (two steps, ~80 %) DPEC can be of interest for production on an industrial scale. Lin et al.[158] synthesized bipolar compounds CzPhB, CzThB (Fig. 2.12) possessing carbazole and dimesitylborane moieties in two steps with an overall yield ranging from 54 to 59%. Employing CzPhB and CzThB in the multilayered blue fluorescent devices, the maximum brightness of 5350 and 28300 cd/m^2, maximum current efficiencies of 3.3 and 10.1 cd/A and EQE of 4.3 and 6.9 %, respectively, were achieved.

Compared to blue emitting devices, the number of reports on effective non-blue fluorescent OLEDs based on carbazole derivatives as emitters is rather scarce (Table 2.8). Usluer et al. [176,177], reported on green (EL wavelength 512-516 nm) OLEDs based on thermally stable (T_d> 500 ºC, T_g> 160 ºC) derivatives of carbazole with fluorene (OFC-G2,SFC-G2, SFCT-G2, SFC-G1 in Fig. 2.13) and spirobifluorene (SBFC-G2,SBFCT-G2,OFCT-G2 in Fig. 2.13). The brightness of the fluorescent OLEDs ranged from 10000 to 25000 cd/m^2. Although the highest brightness was shown by SBFC-G2, SFCT-G2, SFC-G2, SBFCT-G2 based OLEDs, the device based on OFC-G2 could be the best choice for industrial application, because of the high yielded (~ 65%) of the three-step synthesis. Albrecht [178] and co-workers fabricated an OLED with a maximum EQE and power efficiency of 3.4% and 8.5 lm/W, respectively using G3TAZ material as an emitter. Due to the six step synthesis, G3TAZ does not look to be promising for commercialization. A series of thiophene-containing derivatives of carbazole and pyrene (CFT2P, CFT3P, CFT4P in Fig. 2.13) were synthesized and employed in green and orange OLEDs with the maximum brightness reaching 49000 cd/m^2[164]. Due to low yields (<27%) and the complicated synthesis (>6 steps), the derivatives (CFT2P, CFT3P, CFT4P) are not promising for production on the industrial scale.

Table 2.8. Carbazole based materials for green, yellow and orange OLEDs

Host	Yield, %	Synth.	HOMO, eV	LUMO, eV	Φ_{SOL}/ Φ_{FILM}, %	T_g, C^O	T_d, C^O	V_{on}, V	L, cd m^{-2}	LE_{max}, cd A^{-1}	η_p, lm W^{-1}	EQE, %	Color	EL λ_{max}, nm	CIE193, (x, y)	Ref. No.
G2-PTP-G2	14	6	5.10	2.73	31 [c]/ -	172	544	4.0	1000	0.4	-	-	yellow	570	0.50; 0.49	179
Cz-Ph3	60	2	5.13	2.26	-	70	293	3.3	5393	1.7	0.7	0.7	green	520	0.23; 0.55	157
CFT2P	27	6	5.36	2.69	34 [e]/ -	102	416	2.2	48800	11.2	-	0.5	green	509	0.27; 0.61	164
CFT3P	17	8	5.28	2.74	10 [e]/ -	116	420	2.8	28722	3.1	-	0.1	green	531	0.37; 0.59	164
CFT4P	14	10	5.21	2.77	8 [e]/ -	118	445	2.5	24096	3.1	-	0.1	orange	552	0.45; 0.51	164
OFC-G2	61	3	5.38	2.14	35 [c]/ -	253	505	4.0	19800	3.6	-	-	green	516	0.28; 0.52	177
SBFCT-G2	52	5	5.36	2.18	11 [c]/ -	227	617	2.5	25400	7.7	-	-	green	516	0.28; 0.53	177
OFCT-G2	65	3	5.39	2.21	5 [c]/ -	186	500	5.0	11300	2.8	-	-	green	520	0.29; 0.55	177
SBFC-G2	49	5	5.45	2.21	11 [c]/ -	-	650	3.0	23100	3.1	-	-	green	516	0.28; 0.53	177
SFCT-G2	32	6	5.37	2.19	4 [c]/ -	205	586	3.0	23000	3.7	-	-	green	516	0.28; 0.54	177
SFC-G1	41	4	5.59	2.16	37 [c]/ -	166	552	6.0	10800	2.2	-	-	green	512	0.27; 0.49	177
SFC-G2	30	6	5.46	2.22	9 [c]/ -	-	629	2.5	22400	1.9	-	-	green	512	0.28; 0.52	177
G2TAZ	41	4	5.76	3.01	94 [a] / 52	-	592	3.3	1000	-	6.0	2.4	green	510	0.25; 0.49	178
G3TAZ	21	6	5.72	2.97	100 [a] / 31	-	620	3.5	1100	-	8.5	3.4	green	510	0.27; 0.49	178
G4TAZ	7	7	5.68	2.80	94 [a] / 9	-	633	3.5	300	-	3.0	1.5	green	510	0.23; 0.37	178

[a] in Toluene; [b] in THF; [c] in $CHCl_3$; [d] in DCM; [e] CH_2Cl_2; [f] in cyclohexane; [g] in CH_3CN; [h] in EtOAc.

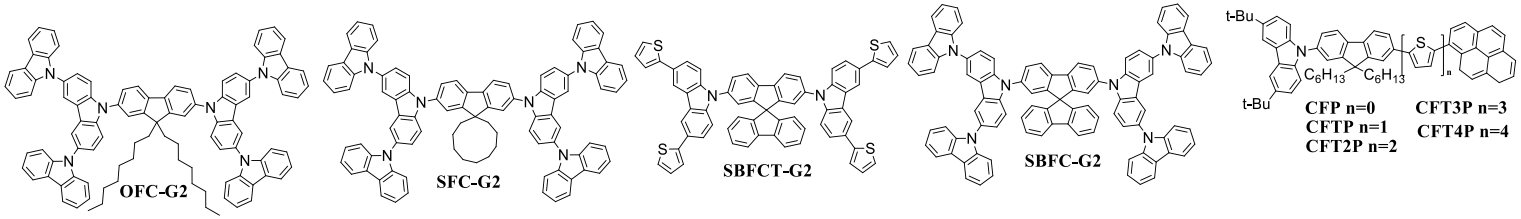

Fig. 2.13. Chemical structures of carbazole based materials for effective non-blue OLEDs

2.3.3. Carbazolyl-containing compounds for OLEDs based on thermally activated delayed fluorescence

In 2009, Adachi and co-workers [180] reported on the mechanism of thermally activated delayed fluorescence (TADF), which gave the opportunity to fabricate OLEDs with a metal-free emissive layer and to harvest both singlet and triplet excitons altogether as shown in Fig. 2.7. In addition, it was found that triplet-triplet annihilation, which could reduce the device efficiency in PHOLEDs with a narrow charge recombination zone [68], was eliminated in the TADF based devices. Three years later, Adachi et al. [181,182] made a real breakthrough in OLEDs, by presenting the TADF-based device with a maximum EQE of 19.5%. They prepared new derivatives 4CzIPN, 2CzPN and 4CzTPN-Ph (Fig. 2.14) based on carbazole (electron-donor) and dicyanobenzene (electron acceptor) moieties in a one-step synthesis with overall yields of 90%, 8,5% and 79%, respectively. By embedding these compounds as dopants in 4,4'-9-bis(carbazol-9-yl)biphenyl (CBP) (5% of 4CzIPN, 4CzTPN-Ph) or in 1,3-bis(9-carbazolyl)benzene (mCP) (6% of 2CzPN), Adachi and co-workers[181,182] fabricated green, blue and orange OLEDs with a maximum EQE of 19.5%, 13.6% and 11.2%, respectively. Hirata et. al.[183] reported on triazine and carbazole based TADF dopants (TRZ-Cz_1a, TRZ-Cz_2c, TRZ-Cz_2b, TRZ-Cz_2a in Fig. 2.14).

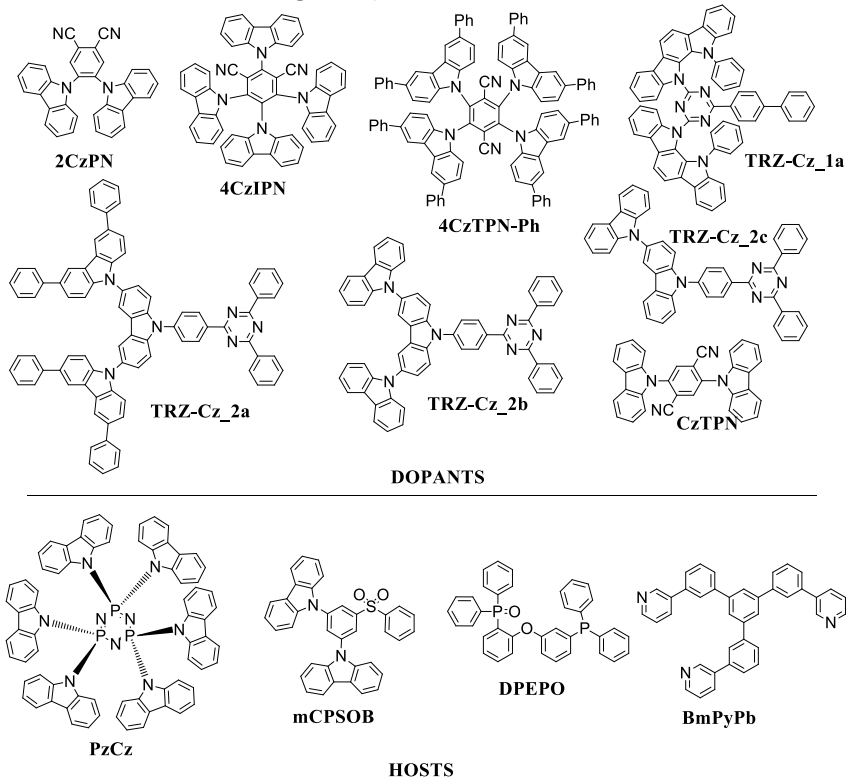

Fig. 2.14. Chemical structures of carbazole derivatives used in OLEDs based on TADF

Table 2.9. Characteristics of the compounds and the devices based on thermally activated delayed fluorescence

Dopant	Yield, %	Syn. St.	HOMO, eV	LUMO, eV	$E_T/\Delta E_{ST}$, eV	Host	V_{on}, V	L, cd m^{-2}	LE_{max}, cd A^{-1}	η_p, lm W^{-1}	EQE, %	Color	EL λ_{max}, nm	CIE1931, (x, y)	Ref. No.
SPhCz_3	73	1	5.81	2.52	- / 0.32	10% in DPEPO	3.7	400	-	-	9.9	blue	-	0.15; 0.07	184
CzT1	55	2	5.49	2.77	- / 0.085	3% in DPEPO	4.0	400	-	9.7	6.0	green	530	0.23; 0.40	185
DMOC	79	2	5.55	-	- / 0.24	10% in DPEPO	4.0	2544	24.0	-	14.5	blue	460	0.16; 0.16	186
4CzTPN-Ph	79	1	-	-	-	5% in CBP	-	-	-	-	11.2	orange	-	-	181
4CzIPN	90	1	5.80	3.41	2.40 / -	5% in CBP	-	-	-	-	19.5	green	-	-	181
2CzPN	8.5	1	5.80	3.00	-	5% in PPT	-	-	-	-	8.0	blue	-	-	181
4CzIPN	90	1	5.80	3.41	2.40 /-	2% in PPO27	4.0	2000	-	52.0	24.2	green	-	0.20; 0.48	187
Cz2BP_1	90	1	5.74	2.64	3.10 / 0.21	6% in DPEPO	4.3	510	9.3	-	8.1	blue	-	0.16; 0.14	188
CC2BP_2	89	1	5.65	2.63	3.02 / 0.14	6% in DPEPO	4.4	3900	25.5	-	14.3	sky-blue	-	0.17; 0.27	188
CzTPN	17	3	6.20	3.50	2.73 / 0.08	4% in PzCz	4.2	18800	37.2	24.4	15.0	blue-green	494	0.18; 0.45	189
4CzIPN	90	1	5.80	3.41	2.40 /-	4% in PzCz	4.5	49200	60.2	38.6	18.2	green	506	0.20; 0.54	189
m-ATP-CDP	37	3	5.70	3.10	3.02 / 0.26	6% in mCP	4.8	3290	13.4	6.4	7.5	sky-blue	500	-	190
CzPAPCz	14	3	6.10	3.60	- / 0.16	10% in CBP	3.7	20000	-	-	9.0	orange	574	-	191
TXO-PhCz	41	3	5.78	3.58	- / 0.09	5% in mCP	4.7	21000	76.0	70.0	21.5	green	520	0.31; 0.56	192
TRZ-Cz_1a	7	4	-	-	- / 0.09	6% in DPEPO	4.2	4000	-	-	7.7	sky-blue	506	0.26; 0.43	183
TRZ-Cz_2c	23	3	-	-	- / 0.32	6% in DPEPO	4.2	10000	-	-	14.6	sky-blue	477	0.18; 0.28	183
TRZ-Cz_2b	7	4	-	-	- / 0.28	6% in DPEPO	4.2	12000	-	-	16.8	sky-blue	478	0.17; 0.27	183
TRZ-Cz_2a	1	4	-	-	- / 0.09	6% in DPEPO	4.2	20000	-	-	20.6	sky-blue	487	0.19; 0.35	183
2CzPN	8.5	1	5.80	3.00	-	6% in mCP	-	-	-	-	13.6	sky blue	483	0.17; 0.30	182
4CzIPN	90	1	5.80	3.41	2.40 / -	3% in mCP:BmPyPb	3.5	4000	-	56.6	28.6	green	-	0.21; 0.53	193

At 6% dopant concentration in the bis[2-(diphenylphosphino)phenyl]ether oxide (DPEP), the maximum EQE of the sky-blue OLED ranged from 7.7% (for TRZ-Cz_1a) to 20.6% (for TRZ-Cz_2a). Although the significant efficiency was achieved using TRZ-Cz_2a, very low overall yield (1%) of its synthesis makes it not very promising with respect to production on a larger scale. Adachi et al. [189] reported on the synthesis of hosts for OLEDs based on TADF. A compound consisting of six carbazoles moieties linked to a cyclophosphazene core (PzCz in Fig. 2.14) was employed in a multilayered OLED by doping it with 4% of carbazole based derivatives (CzTPN and 4CzIPN). Devices based on CzTPN and 4CzIPN emitted green light with a maximum brightness of 20000 and 49200 cd/m^2, efficiency of 37.2 and 60.2 cd/A, and a maximum EQE of 15.0 and 18.2%, respectively. Due to the high overall yield (>50%) of the one-step synthesis, 4CzIPN and CzPz make a promising combination for an effective green OLED. 4CzIPN is one of the most popular carbazole based dopants for green TADF based devices. A series of green TADF-based OLEDs were prepared using PPO27 [187], mCP:BmPyPb[193] and mCPSOB[194] as host materials. The device with an EQE of 28.6% was achieved by employing the mixture of host materials with the different triplet energy (mCPwith the triplet energy of 2.90eV and BmPyPb with the triplet energy of 2.78eV). With respect to brightness, current and power efficiency and low roll-off, the best results were achieved for an OLED using mCPSOB as the host material (20000 cd/m^2, 81.2 cd/A, 79.0 lm/W).

2.4. Conclusions from the literature review

The analysis of more than 275 OLEDs was conducted (~190 PHOLEDs, ~85 OLEDs), which were prepared using carbazole based materials and found that there is a limited number of promising compounds with respect to the possibilities of large scale production. Many scientific groups focus their attention on the device efficiency but not on the efficiency of the synthesis of new electroactive compounds used in OLEDs. The most promising compounds for large scale production from those reviewed in this chapter are summarize in Table 2.10. In the case of the blue PHOLEDs, the highest value of EQE (~21%) was achieved using a bicarbazole derivative possessing triphenylsilyl moiety (BCz-Si) [105], while the most promising compound with respect to industrial production that could be easily achievable (one step, 52% yield) is bicarbazolyl derivative (BCzPh) [90]. The device fabricated using this compound showed an EQE of 19.8% and maximum brightness of 20000 cd/m^2. The analysis of the literature revealed two promissing host materials for green PHOLEDs that can be produced on a large scale. The first one is based on a bipolar host material based on bicarbazole and triazine moieties (CzT) [137], which was achieved in a 3 step synthesis with an overall yield of 55%. By employing it as a host material in a green PHOLED, the maximum EQE of 20.0 % and brightness of 110000 cd/m^2 were reported [137]. The second promising host for green PHOLED (EQE = 19.2 %, L=96000 cd/m^2) is CPhBzIm [138]. It is achieved in by a three step synthetic route with an overall yield of 62 %. In the case of an orange PHOLED, an efficient device (EQE = 25.6 %, L= 129885 cd/m^2) can be fabricated using

carbazole–quinoline hybrid (CzPPQ) [139] which is prepared in a one-pot synthesis with an overall yield of 85%. The red PHOLED was prepared using the same host material (CzPPQ) but a different Iridium complex [139] with an EQE of 19.3 % and maximum brightness of 61485 cd/m^2. Another promising red PHOLED (L = 62720 cd/m^2, EQE = 24.9 %) was obtained employing an indoloquinoxalinyl and carbazole based derivative (BIQMCz) [153], as host material, which was synthesized in two steps with an overall yield of 58 %. Based on the TADF effect, one green and one blue OLED can be chosen as promising candidates for large scale application. The green device (EQE = 18.2 %, L= 49200 cd/m^2) was based on 4CzIPN (1 step, 90 % overall yield) doped in PzCz (1 step, 54 % overall yield) host material [189] and the blue one (EQE = 14.6 %, L= 10000 cd/m^2) was prepared using a carbazole-triazole based material (TRZ-Cz_2c, 3 steps, 37 % overall yield) doped in commercially available host material (DPEPO) [183].

Among the reported materials for fluorescent OLEDs, only several compounds can be considered for large scale application. For the blue OLED, based on the bipolar fluorophore (CzThB, 2 steps, 59% overall yield) [158] possessing carbazole and dimesitylborane moieties might be the field of interest. For a green light emitting device; fluorene-carbazole dendrimer (OFC-G2, 3 steps, 61 % overall yield) [176] can be regarded as a promising candidate for large-scale production. The blue OLED reached a maximum brightness of ca. 50000 cd/m^2, while the green device showed a maximum brightness less than 20000 cd/m^2.

Table 2.10. Promising materials for large scale applications

Color	Type of device	Material for LEL	Synthesis	Device parameters
Blue	PHOLED	BCz-Si [105](host) TCTP [109] (host) BCzPh[90] (host)	2 steps, 36 % yield 2 steps, 24 % yield 1 step, 52 % yield	18000 cd/m^2, 21.0 % 35100 cd/m^2, 15.9 % 20000 cd/m^2, 19.8 %
Green	PHOLED	CzT [137] (host) CPhBzIm [138] (host)	3 steps, 55 % yield 3 steps, 62 % yield	110000 cd/m^2, 20.0 % 96000 cd/m^2, 19.2 %
Red	PHOLED	CzPPQ [139](host) BIQMCz [153](host)	1 step, 85 % yield 2 steps, 58 % yield	61485 cd/m^2, 19.3 % 62720 cd/m^2, 24.9 %
Orange	PHOLED	CzPPQ [139](host)	1 step, 85 % yield	129885 cd/m^2, 25.6 %
Blue	TADF OLED	TRZ-Cz_2c[183](dopant) DPEPO (Host)	3 steps, 23 % yield	10000 cd/m^2, 14.6 %
Green	TADF OLED	4CzIPN [189] (dopant) PzCz (Host)	1 step, 90 % yield 1 step, 54 % yield	49200 cd/m^2, 18.2 %
Blue	OLED	CzThB [158]	2 steps, 59 % yield	28300 cd/m^2, 6.9 %
Green	OLED	CFT2P [164] OFC-G2 [176]	6 steps, 27 % yield 3 steps, 61 % yield	48800 cd/m^2, 0.5 % 19800 cd/m^2, -

The greatest progress was done in the field of synthesis and application of host materials for PHOLEDs. However the usage of an environmentally unfriendly and

expensive heavy metal complexes, emissive layer phase separation, triplet-triplet annihilation makes them expensive, non-friendly for the environment and inefficient for long lasting devices. Recently, the OLEDs with TADF effect started to displace the PHOLEDs from the top of the efficient device position. Although TADF OLEDs are friendly for the environment and as efficient as PHOLEDs, the preparation of the TADF compounds and the devices are rather complicated. Therefore, the appliance of TADF fluorescent devices for high scale industry is still problematic and non-cost-effective. OLEDs exploiting singlet excitons do not lose their importance and have a number of advantages against the devices exploiting both singlet and triplet excitons. The fabrication of fluorescent devices using layer by layer evaporation method is simple and there is no need of a concentration control, as LEL consists of one material only. Furthermore, the simplicity of the synthesis of the singlet emitters and of fabrication of OLEDs could decrease their cost. However, the choice of organic materials, which could be employed as emitters or hole transporting materials in effective blue or green fluorescent devices, is limited. For continued research, carbazole moiety was selected due to its high thermal stability, good charge transporting properties and easy functionalization.

3. EXPERIMENTAL

3.1 Instrumentation

^{1}H and ^{13}C nuclear magnetic resonance (NMR) spectra were recorded using a Varrian Unity Inova (300 MHz (^{1}H), 75.4 MHz (^{13}C)) and Bruker Avance III 400 spectrometer (400 MHz (^{1}H), 100 MHz (^{13}C)) apparatus. Chemical shifts (δ) are reported in parts per million (ppm) referenced to a tetramethylsilane or internal (NMR) solvent signal.

Infrared (IR) spectra were recorded on a Perkin Elmer Spectrum GX spectrometer. The spectra of the solid compounds were recorded using KBr pellets.

Mass spectrometry (MS) was performed with the Bruker maxis 4G.

High resolution mass spectrometry (HRMS) was performed using EI (70 eV ionization energy). Exact mass measurements were performed in the EI mode at a resolution of 10000 and also on a quadrupole orthogonal acceleration time-of-flight mass spectrometer.

Elemental analysis was performed with an Exeter Analytical CE-440 Elemental.

Melting points (m.p.) of the synthesized compounds were estimated using Electrothermal Mel-Temp apparatus.

For the X-ray crystallography analysis diffraction data was collected on a Bruker-Nonius Kappa CCD single diffractometer using graphite monochromated Mo-Kα radiation (λ = 0.71073 Å). The crystal structure was analyzed solved by direct methods [SIR-97] and refined by full-matrix least squares [SHELXL-97]. Mercury 3.3 software [195] was used for molecular graphics.

UV spectra were recorded with an Aventes AvaSpec-2048XL spectrometer.

Fluorescence (FL) spectra and fluorescence decay curves of the dilute THF solutions and of the solid films of the compounds were recorded by an Edinburgh Instruments FLS980 spectrometer. Fluorescence quantum yields were measured using an integrated sphere calibrated with two standards: quinine sulfate in 0.1 M H_2SO_4 and rhodamine 6G in ethanol.

CD measurements were performed on a Jasco J600 spectropolarimeter. The measurements were performed in quartz cuvettes. Photochemical reactions were performed in the photochemical reactor equipped with interchangeable light sources (300 nm, 350 nm lamps) using a quartz flask.

Differential scanning calorimetry (DSC) measurements were carried out in a nitrogen atmosphere with a Perkin Elmer at DSC 8500 equipment at a heating and cooling rate of 10 °C/min. An empty pan was used as a reference.

Thermogravimetric analysis (TGA) was performed on a Perkin Elmer TGA 4000 apparatus in a nitrogen atmosphere at a heating rate of 10 °C/min. The samples were filled with 2-3 mg of the investigated material.

Cyclic voltammetry (CV) measurements were carried out by a three-electrode assembly cell from a Bio-Logic SAS and a micro-AUTOLAB Type III potentiostat-galvanostat. The measurements were carried out with a glassy carbon electrode in dichloromethane solutions containing 0.1 M tetrabutylammonium hexafluorophosphate as electrolyte, $Ag/AgNO_3$ as the reference electrode, and a Pt wire counter electrode. The samples were filled with diluted solution of the investigated materials in dichloromethane (10^{-3} M). Prior to each measurement, the solutions were bubbled with inert gases (Ar or N_2).

The ionization energies of the films of the synthesized compounds were measured by an electron photoemission in air method as described before [196]. The samples for the measurements were prepared by dissolving the materials in THF and by coating on Al plates pre-coated with a ca. 0.5 μm thick methylmethacrylate and methacrylic acid copolymer adhesive layer [197]. The measurement method was, in principle, similar to that described in the literature [198].

The charge transport properties of the drop-casted thin amorphous layer of the materials were investigated by xerographic time-of-flight (XTOF) method, using the experimental setup described in the literature [199,200]. The samples were prepared by casting the solutions of the materials with or without bisphenol-Z polycarbonate on to an ITO covered substrate. The charge carriers were generated at the sample surface by illumination with pulses of nitrogen laser (pulse duration was 2 ns, wavelength 337 nm). A high electric field was created using negative or positive corona charging.

The charge carrier mobility (μ) measurements of the vacuum deposited layers of target materials were also carried out by the time-of-flight (TOF) method [201]. The sandwich-like samples (ITO/compounds/Al) were used for measurements. The layers of materials were prepared on precleaned ITO-coated glass substrates from Sigma-Aldrich, with a sheet resistance of 70-100 Ω/sq. Then, Al electrodes were evaporated at a pressure below 5×10^{-5} mbar. ITO-coated glass substrates were cleaned by successive washing with deionized water, THF, and trichloroethene in an ultrasonic bath. Each operation lasted over 5 minutes. The deposition rates of materials and Al were 0.2–0.3 Å/s and ~15 Å/s, respectively. The thicknesses of the films of the target compounds vary from 0.65 to 2.5 μm, respectively, and the active

area of the obtained samples was 6 mm^2. The layers were undertaken by exciting materials through the ITO layer. The charge carriers were generated at the layer surface by illumination with a Nd:YAG laser EKSPLA NL300 (pulse duration was 3-6 ns, wavelength 355 nm). The total photogenerated charge was kept small enough to avoid space charge effects. The electronic time response of the measurement circuit ($\tau = RC$) was always selected to be smaller than the transit time ($\tau << t_{tr}$). The transit time was determined from the kink point in the transient photocurrent curves. The transit time t_{tr} with the applied bias (V) indicates the passage of holes through the entire thickness of the cell (d) and enabled the determination of the hole mobility as $\mu = d^2/U \times t_{tr}$. The experimental setup consisted of a delay generator Tektronix AFG 3102C and a digital storage oscilloscope Tektronix TDS 3032C.

OLEDs with the structures: Device A: ITO/CuI(8nm)/DMAC36(20nm)/NP-3-Cz(30nm)/ Bphen(20nm)/ Ca(50nm)/ Al(200nm); Device B: ITO/CuI(8nm)/DMAC36(20nm)/NP-9-Cz(30nm)/ Bphen(20nm)/ Ca(50nm)/ Al(200nm); Device C: ITO/CuI(8nm)/DMAC36(20nm)/NP-2-Cz(30nm)/ Bphen(20nm)/ Ca(50nm)/ Al(200nm), were fabricated by a step-by-step deposition of different organic layers and metal electrodes onto precleaned indium–tin-oxide (ITO)-coated glass substrate under a vacuum of 10^{-5} Torr. CuI and 3,6-di[di(4-methylphenyl)amino]-9-ethylcarbazole (DMAC36) were used for the preparation of HTL [202], Bphen was applied as the ETL [203]. Since Ca is highly reactive and corrodes quickly in the ambient atmosphere, a Ca layer topped with 200 nm aluminum (Al) layer was used as the cathode. The active area of the obtained devices was 3x6 mm^2. The density current-voltage and luminance-voltage characteristics were measured using a semiconductor parameter analyzer (HP 4145A) in air without passivation immediately after the formation of the device. The brightness measurements were done using a calibrated photodiode [202]. The EL spectra were recorded with an Ocean Optics USB2000 spectrometer.

The solution processed BHJ organic solar cells with ITO/PEDOT:PSS/active layer/LiF/Al were prepared by a step-by-step of ITO coated glass substrate, organic layers and metal electrodes. Water solution of PEDOT:PSS was spin casted onto the cleaned ITO substrate to obtain a film with a thickness of about 60 nm. The layer was dried at a temperature of 120 ^oC. A mixture of the compound and PCBM with weight ratios of 1:1.5, 1:2, 1:3 and 1:4 in chlorobenzene solution was spin casted onto the top of the PEDOT:PSS. The active layer thickness is about 130 nm. The aluminum electrode was thermally deposited on the top of active layer under a vacuum of 10^{-5} Torr. The current-voltage (J-V) characteristics of the BHJ organic solar cells were measured using a computer controlled Keithley 238 source meter in dark as well as under simulated AM1.5G illumination of 100 mW/cm^2.

3.2 Computational details

Time dependent density function theory (TD-DFT) calculations of UV-vis spectra of **3a-b** were performed with the Gaussian 09 software package [204]. The geometries of the molecules of **3a** and **3b** were optimized from X-ray data as the starting point using B3LYP functional and 6-31G(d,p) basis set, followed by calculations of their harmonic vibrational frequencies to verify their stability. All the calculated vibrational frequencies are real, which indicates the true minimum of the total energy on the potential energy hypersurface. The alkyl chains were approximated by methyl groups to reduce the computational time. The simulations were performed for the THF solutions using a polarizable continuum model (IEFPCM) to assess the influence of the solvent polarity onto the molecular vertical excitation energies. The half-width at *1/e* of the peak maximum σ value of 0.25 eV was used in this work. Up to 10 lowest energies of the excited states were calculated.

Electron transfer rate constant (k_i) for pathway *I* was calculated using the current equation:

$$k_i = \frac{2\pi}{\hbar} |H_i|^2 \frac{1}{\sqrt{4\pi\lambda \boldsymbol{k_b T}}} \exp\left(-\frac{(\lambda + \Delta G^0)^2}{4\lambda k_b T}\right) \quad (1)$$

where H_i is the electronic coupling between the initial and final states, λ is the reorganization energy ($\lambda = \lambda_{in} + \lambda_{out}$, i.e. the sum of both inner and outer-sphere), ΔG^0 is the total Gibbs free energy change for the electron transfer reaction, k_b is the Boltzmann constant and *T* is the absolute temperature (298 K).

The internal reorganization energy (λ_{in}) value was calculated at the B3LYP/6-311+G(d,p) level in vacuum according to the following equation:

$$\lambda_{in} = [E^{\pm}(g^0) - E^{\pm}(g^{\pm})] + [E^0(g^{\pm}) - E^0(g^0)] \quad (2)$$

where *E* corresponds to the energy of the neutral molecule (g^o) in the geometry of the cationic/anionic species ($g^{\pm}$).

The electronic coupling (transfer) integrals H_i were estimated using the energy splitting in dimmer method [205] at the long-range corrected hybrid density functional wB97X-D [206] and 6-31G(d) basis set using the Spartan'14 package [207] in vacuum:

$$H_i = \frac{E_{L+1(H)} - E_{L(H-1)}}{2} \quad (3)$$

where $E_{L[H]}$ and $E_{L+1[H-1]}$ are the energies of the LUMO and LUMO+1 (HOMO and HOMO−1) levels taken from the neutral state from the crystal structures of the molecules.

The diffusion coefficient (*D*) for migration of electrons or holes in the dimmers was calculated using the current equation (4) [208]:

$$D = \frac{1}{2N} \frac{\sum d_i^2 k_i^2}{\sum k_i} \quad (4)$$

where N is the dimensionality of the crystal ($N=3$) and d_i is the distance between the dimmers mass centers.

The drift mobility (μ_0) in the absence of an electric field was calculated using the single-step approximation:

$$\mu_0 = \frac{e \cdot D}{k_b T} \quad (5)$$

where e is the electron charge, $T=298$ K.

The equilibrium structural parameters of the **NP-9-Cz**, **NP-3-Cz**, **NP-2-Cz** molecules were optimized at the B3LYP/6-31G(d) [209-211] level of the density functional theory (DFT) using the Gaussian 09 software package [204]. The experiment has also calculated the vibrational frequencies for the studied compound in order to verify determination of the true minimum on potential energy surface (PES). All vibrational frequencies are found to be real, which indicates the location of the sought-for energy minimum. The electronic absorption spectra of the studied molecules have been calculated by the time dependent (TD) DFT method [212] in the THF medium considering the polarized continuum model PCM) [213] using the same B3LYP/6-31G(d) approach.

Reorganization energy values for the electron (λ_-) and hole (λ_+) carriers have been calculated using the following equation, as this is being widely used for estimation of the charge transport properties of organic materials [214]:

$$\lambda_{-/+} = (E^*_{-/+} - E_{-/+}) + (E^{**}_{-/+} - E_0) \quad (6)$$

where E_0 is the optimized ground state energy of the neutral molecule, $E_{-/+}$ is the energy of the optimized anionic/cationic species, $E^{**}_{-/+}$ is the energy of the neutral molecule at the anionic/cationic geometry and $E^*_{-/+}$ is the energy of the anionic/cationic molecule at the optimized geometry of the neutral species. All calculations are performed on the PDC supercomputers of the Royal Institute of Technology, Stockholm.

The electronic circular dichroism (CD) spectra were calculated using TD-DFT with the B3LYP hybrid function combined with the 6-31G(d,p) basis set and PCM for chloroform. The excited states were calculated up to the 15 lowest energies. The rotational strength velocity (R_{vel}) and length formalism (R_{len}) were calculated. Both formalisms were almost identical. Rotatory strengths were estimated in cgs units of 10^{-40} esu cm erg G^{-1}, where 1 esu cm erg G^{-1} corresponds to $3.336 \cdot 10^{-15}$ C m J T^{-1} in

SI units. The CD spectra of the individual conformers were visualized using SpecDis version 1.61. The half-width at *1/e* of the peak maximum σ value of 0.30 eV and R_{vel} were used in this work. The calculated CD spectra were not wavelength corrected.

3.3 Materials

Carbazole (>96.0%, TCI Europe), N-bromosuccinimide (NBS, 99%, Aldrich), potassium hydroxide (≥90.0%, Reachem), copper(I) iodide (98%, Aldrich), sodium (99%, Aldrich), 2-ethylhexylbromide (95%, Aldrich), potassium carbonate (≥99.5%, Reachem), diphenylacetaldehyde (95%, Aldrich), (rac)-camphor-10-sulfonic acid (CSA, 98%, Aldrich), 1-Br-3-methylbutane, copper (spheroidal >10 microns, 99%, Aldrich), tetrabutylammonium hydrogensulfate (97%, Aldrich),n-butyllithium (2.5 M in hexanes, Aldrich),2-iso-propoxy-4,4,5,5-tetramethyl-1,3,2-dioxaborolane (97%, Aldrich), bis(triphenylphosphine) palladium(II) dichloride (98%, Aldrich), perylene (≥99.0%, Aldrich), triphenylphosphine (≥95.0%, Aldrich), 18-Crown-6 (99%, Aldrich), Acetic acid (glacial, 99.8%, Lach-Ner).

Chemicals received from commercial sources were used without further purification. Solvents used in reactions were freshly distilled, or were otherwise used as received.

Table 3.1. Reference to the synthesis of the compounds

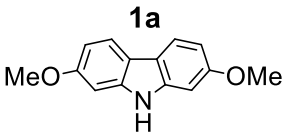

Chemical Formula: $C_{14}H_{13}NO_2$

2,7-Dimethoxycarbazole (**1a**, FW=227 g/mol, m.p.: 270-272 ºC, lit.: 272–274 ºC) was achieved by an Ullmann-coupling and a Cadogan cyclization as reported in the literature [215,216]. ^{1}H NMR (400 MHz, DMSO) δ 10.98 (s, 1H), 7.83 (d, *J* = 8.5 Hz, 2H), 6.93 (d, *J* = 2.2 Hz, 2H), 6.72 (dd, *J* = 8.5, 2.3 Hz, 2H), 3.82 (s, 6H). ^{13}C NMR (101 MHz, DMSO) δ 157.6, 141.0, 120.0, 116.5, 107.3, 94.7, 55.2.

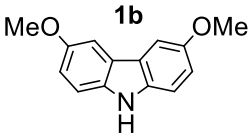

Chemical Formula: $C_{14}H_{13}NO_2$

3,6-Dimethoxycarbazole(**1b**, FW=227 g/mol, m.p.: 130-131 ºC, lit.: 131-133 ºC) was prepared by bromination and methoxylation reactions by the procedures described in literature [217,218]. ^{1}H NMR (300 MHz, $CDCl_3$) δ 7.74 (s, 1H), 7.49 (d, *J* = 2.5 Hz, 2H), 7.22 (dd, *J* = 8.8, 0.5 Hz, 2H), 7.03 (dd, *J* = 8.8, 2.5 Hz, 2H), 3.91 (s, 6H). ^{13}C NMR (75 MHz, $CDCl_3$) δ 153.7, 135.4, 123.8, 115.3, 111.7, 102.94, 56.2.

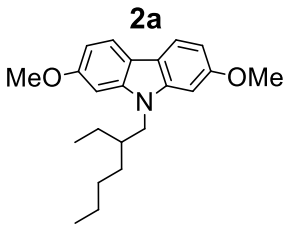

Chemical Formula: $C_{22}H_{29}NO_2$

9-(2-Ethylhexyl)-2,7-dimethoxycarbazole (**2a**) was prepared by the reaction of 2,7-dimethoxycarbazole with an excess of 2-ethylhexylbromide under the basic conditions in the presence of a phase transfer catalyst. 2,7-Dimethoxycarbazole (**1a**, 0.40 g, 1.8 mmol), 2-ethylhexylbromide (0.38 g, 2.1 mmol), potassium carbonate (0.10 g, 0.70 mmol), potassium hydroxide (0.30 g, 5.3 mmol) and catalytic amount of tetrabutylammonium hydrogensulfate were refluxed (2 h) in acetone (14 ml). After, a thin layer chromatography (TLC) (acetone/hexane, 1:10) control, when the starting compound **1a** disappeared, the reaction was terminated, cooled down to room temperature, treated with ethyl acetate and washed with distilled water. The organic layer was dried over anhydrous Na_2SO_4, filtered and the solvents were removed. The residue was purified by silica-gel column chromatography using the mixture of hexane and acetone (20:1) as the eluent. The yield of yellowish crystals was 75 %(0.45 g, FW = 339 g/mol, m.p.: 86-88 ºC). ^{1}H NMR (400 MHz, $CDCl_3$) δ 7.77 (dd, *J* = 7.9, 1.0 Hz, 2H), 6.75 – 6.72 (m, 4H), 3.99 – 3.92 (m, 2H), 3.84 (s, 6H), 2.00 – 1.93 (m, 1H), 1.33 – 1.18 (m, 8H), 0.84 (t, *J* = 7.4 Hz, 3H), 0.80 (t, *J* = 7.2 Hz, 3H).^{13}C NMR (75 MHz, $CDCl_3$, δ, ppm): 158.0, 142.4, 120.0, 116.9, 106.5, 93.8, 55.6, 47.3, 39.1, 30.9, 28.8, 24.4, 23.0, 14.0, 10.9.

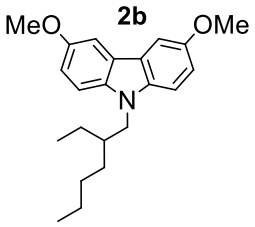

Chemical Formula: $C_{22}H_{29}NO_2$

9-(2-Ethylhexyl)-3,6-dimethoxycarbazole (**2b**) was synthesized by a similar procedure as compound **2a** using 3,6-dimethoxycarbazole (**1b**, 0.5 g, 2.2 mmol), 2-ethylhexylbromide (0.51 g, 2.6 mmol), potassium carbonate (0.12 g, 0.88 mmol), potassium hydroxide (0.37 g, 6.6 mmol), catalytic amount of tetrabutylammonium hydrogensulfate and 15 ml of acetone. The yield was 77 % (0.58 g) of yellowish oil. ^{1}H NMR (300 MHz, $CDCl_3$, δ, ppm): 7.50 (s, 2H, Ar), 7.23 (d, *J*=8.9 Hz, 2H, Ar), 7.05 (dd, J_1=8.9 Hz, J_2=2.5 Hz, 2H), 4.05 (d, *J*=7.4 Hz, 2H, NCH_2), 3.90 (s, 6H, OCH_3), 2.02-1.93 (m, 1H, CH), 1.33–1.19 (m, 8H, CH_2), 0.86 (t, *J*=7.4 Hz, 3H, CH_3), 0.83 (t, *J*=7.3 Hz, 3H, CH_3). ^{13}C NMR (75 MHz, $CDCl_3$, δ, ppm): 153.0, 136.5, 122.6, 114.9, 109.7, 102.8, 56.0, 47.5, 39.5, 30.9, 28.8, 24.3, 23.0, 14.0, 10.9.

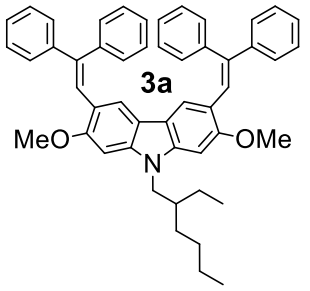

Chemical Formula: $C_{50}H_{49}NO_2$

3,6-Bis(2,2-diphenylethenyl)-9-(2-ethylhexyl)-2,7-dimethoxy-carbazole(**3a**). 9-(2-ethylhexyl)-2,7-dimethoxy-carbazole (**2a**, 0.37 g, 1.08 mmol), diphenylacetaldehyde (0.46 g, 2.37 mmol) were dissolved in toluene (5 ml) at a reflux temperature and catalyzed by CSA (0.30 g, 1.29 mmol). Water generated during the course of the reaction (8 h) was removed by a Dean–Stark trap. After TLC control (ethyl acetate/hexane, 1:10), when the starting compound **2a** disappeared, the reaction was terminated, cooled down to room temperature, treated with ethyl acetate and washed with distilled water. The organic layer was dried over anhydrous Na_2SO_4, filtered and concentrated under a vacuum. The residue was purified by silica-gel column chromatography using the mixture of hexane and ethyl acetate (20:1) as the eluent and recrystallized from the mixture of hexane and ethylacetate. The yield of yellow crystals was 35 %(0.26 g, FW = 695 g/mol, m.p.: 166-167 °C).^{1}H NMR (300 MHz, $CDCl_3$) δ 7.38 – 7.17 (m, 22H), 6.89 (s, 2H), 6.65 (s, 2H), 3.97 – 3.94 (m, 2H), 3.86 (s, 6H), 2.01 – 1.94 (m, 1H), 1.39 – 1.25 (m, 8H), 0.98 – 0.86 (m, 6H).^{13}C NMR (75 MHz, $CDCl_3$, δ, ppm): 156.7, 144.3, 141.3, 141.2, 140.5, 130.6, 128.5, 128.2, 127.9, 127.0 (two peaks are overlapping), 124.0, 120.9, 119.2, 116.2, 91.2, 55.9, 47.3, 39.4, 31.1, 29.0, 27.1, 24.6, 23.2, 14.2, 11.1.IR ($\bar{\upsilon}$, cm^{-1}):3080, 3051, 3024 (arene C−H, 3100-3000 cm^{-1}); 2959, 2924, 2872, 2855 (aliphatic C−H, 3000-2850 cm^{-1}); 1605, 1492, 1463, 1443 (C−C in Ar, 1600-1585, 1500-1400 cm^{-1}); 1300, 1264, 1239 (C−N in Ar, 1335-1250 cm^{-1}); 1195, 1166, 1127 (C−O−C, 1250-1050 cm^{-1}); 807, 762, 697 (C−H in Ar, 900-675 cm^{-1}) cm^{-1}.EI-MS m/z 695.3751 (M+) (calcd 695.3763). Anal. Calcd for $C_{50}H_{49}NO_2$ (%): C 86.29, H 7.10, N 2.01, O 4.60. Found (%): C 86.21, H 7.16, N 2.06.

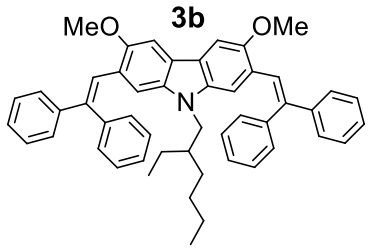

Chemical Formula: $C_{50}H_{49}NO_2$

2,7-Bis(2,2-diphenylethenyl)-9-(2-ethylhexyl)-3,6-dimethoxy-carbazole(**3b**). It was synthesized by a similar procedure as compound **3a** using 9-(2-ethylhexyl)-3,6-dimethoxycarbazole (**2b**, 0.50 g, 1.47 mmol), diphenylacetaldehyde (0.69 g, 3.53 mmol), (rac)-camphor-10-sulfonic acid (0.41 g, 1.767 mmol) and 5 ml of toluene. The residue was purified by silica-gel column chromatography using the mixture of hexane and ethyl acetate (20:1) as the eluent and recrystallized from hexane. The yield of yellow crystals was 31 %(0.32 g, FW = 695 g/mol, m.p.: 144-145 ^{o}C).^{1}H NMR (400 MHz, $CDCl_3$) δ 7.32 – 7.16 (m, 24H), 6.59 (s, 2H), 3.89 (s, 6H), 3.19 – 3.07 (m, 2H), 1.53 – 1.47 (m, 1H), 1.14 – 1.05 (m, 3H), 0.97 – 0.87 (m, 3H), 0.79 (t, *J* = 7.3 Hz, 3H), 0.71 – 0.64 (m, 2H), 0.52 (t, *J* = 7.3 Hz, 3H).^{13}C NMR (100 MHz, $CDCl_3$, δ, ppm):152.1, 144.0, 141.8, 141.2, 136.2, 130.8, 128.8, 128.2, 128.0, 127.4, 127.2, 125.5, 124.3, 121.6, 110.8, 101.0, 56.5, 47.4, 38.5, 30.6, 28.4, 27.1, 24.0, 23.4, 14.3, 10.9. IR ($\bar{\upsilon}$, cm^{-1}): 3077, 3054, 3021 (arene C−H, 3100-3000 cm^{-1}); 2954, 2930, 2870, 2858 (aliphatic C−H, 3000-2850 cm^{-1}); 1597, 1490, 1470, 1429 (C−C in Ar, 1600-1585, 1500-1400 cm^{-1}); 1310, 1269 (C−N in Ar, 1335-1250 cm^{-1}); 1201, 1160, 1063 (C−O−C, 1250-1050 cm^{-1}); 823, 774, 764, 696 (C−H in Ar, 900-675 cm^{-1}) cm^{-1}. EI-MS m/z 695.3740 (M+) (calcd 695.3763). Anal. Calcd for $C_{50}H_{49}NO_2$ (%): C 86.29, H 7.10, N 2.01, O 4.60. Found (%): C 86.19, H 7.17, N 2.08.

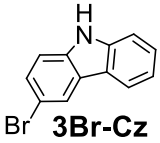

Chemical Formula: $C_{12}H_8BrN$

3-Bromo-9H-carbazole (**3Br-Cz**) was prepared by bromination reaction following the procedure described in literature [217].

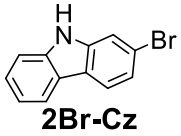

Chemical Formula: $C_{12}H_8BrN$

2-Bromo-9H-carbazole (**2Br-Cz**) was achieved by the nitration and a Cadogan cyclization procedure as reported in the literature [216].

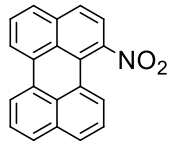

NP

Chemical Formula: $C_{20}H_{11}NO_2$

1-Nitroperylene (**NP**) was prepared from perylene according to the reported procedure [219]. Its identity was confirmed by ^{1}H NMR. ^{1}H NMR (300 MHz, $CDCl_3$) δ 8.17 (t, *J* = 7.0 Hz, 2H), 7.76 (dd, *J* = 15.5, 7.7 Hz, 3H), 7.66 (d, *J* = 8.6 Hz, 2H), 7.59 – 7.46 (m, 3H), 7.41 (t, *J* = 7.9 Hz, 1H).

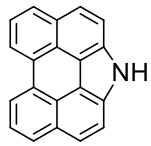

H-NP

Chemical Formula: $C_{20}H_{11}N$

1H-Phenanthro[1,10,9,8-cdefg]carbazole (**H-NP**) was prepared from 1-nitroperylene according to the literature procedure [220]. The chemical structure was confirmed by ^{1}H NMR. ^{1}H NMR (400 MHz, DMSO) δ 12.20 (s, 1H), 8.73 (d, *J* = 7.5 Hz, 2H), 8.17 (d, *J* = 8.0 Hz, 2H), 7.95 (q, *J* = 8.8 Hz, 4H), 7.81 (t, *J* = 7.8 Hz, 2H).

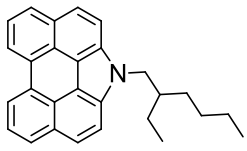

A-NP

Chemical Formula: $C_{28}H_{27}N$

1-(2-Ethylhexyl)-1H-phenanthro[1,10,9,8-cdefg]carbazole (**A-NP**). The following were added to the solution of 1H-phenanthro[1,10,9,8-cdefg]carbazole (**H-NP**) (1.1 g, 4.2 mmol) in acetone (100 mL): potassium carbonate (0.23 g, 1.7 mmol), potassium hydroxide (0.70 g, 12.5 mmol), catalytic amount of tetrabutylammonium hydrogen sulfate and an excess of 2-ethylhexylbromide (0.96 g, 5.0 mmol). The reaction mixture was allowed to reflux for 2 hours. After TLC control, the reaction was terminated, cooled down to room temperature, treated with ethyl acetate and washed with distilled water. The organic layer was dried over anhydrous Na_2SO_4, filtered and the solvents were removed. After, the column chromatography, which was performed using acetone/hexane (1:40) as an eluent compound, **A-NP** (1.25 g, 90 %), was obtained as yellow crystals. ^{1}H NMR (700 MHz, $CDCl_3$) δ 8.64 (d, *J* = 7.4 Hz, 2H), 8.12 (d, *J* = 7.9 Hz, 2H), 7.89 (d, *J* = 8.7 Hz, 2H), 7.80 (t, *J* = 7.7 Hz, 2H), 7.75 (d, *J* = 8.7 Hz, 2H), 4.55 – 4.47 (m, 2H), 2.24 – 2.17 (m, 1H), 1.47 – 1.23 (m, 8H), 0.94 (t, *J* = 7.5 Hz, 3H), 0.87 (t, *J* = 7.3 Hz, 3H). ^{13}C NMR (176 MHz, $CDCl_3$) δ 132.3, 130.5, 128.9, 125.1, 125.0, 124.6, 123.7, 120.8, 117.5, 113.6, 49.9, 41.5, 31.1, 28.9, 24.4, 23.1, 14.2, 10.9.

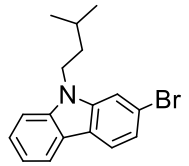

2Br-ACz

Chemical Formula: $C_{17}H_{18}BrN$

2-Bromo-9-isopentyl-carbazole (**2Br-ACz**) was synthesized by a similar procedure to compound **A-NP** using 2-bromo-9H-carbazole (**2Br-Cz**, 2.0 g, 8.1 mmol), 1-Br-3-methylbutane (1.6 g, 10.6 mmol), potassium carbonate (0.4 g, 3.3 mmol), potassium hydroxide (1.4 g, 24 mmol), catalytic amount of tetrabutylammonium hydrogensulfate and 150 ml of acetone. Purified by column chromatography using hexane to obtain **2Br-ACz** as slightly yellowish crystals (Yield 82 %). ^{1}H NMR (700 MHz, $CDCl_3$) δ 8.06 (d, *J* = 7.7 Hz, 1H), 7.93 (d, *J* = 8.2 Hz, 1H), 7.53 (d, *J* = 1.4 Hz, 1H), 7.49 (t, *J* = 7.6 Hz, 1H), 7.39 (d, *J* = 8.1 Hz, 1H), 7.33 (dd, *J* = 8.2, 1.5 Hz, 1H), 7.25 (t, *J* = 7.4 Hz, 1H), 4.28 – 4.24 (m, 2H), 1.75 – 1.70 (m, 3H), 1.04 (d, *J* = 6.2 Hz, 6H); ^{13}C NMR (176 MHz, $CDCl_3$) δ 141.2, 140.6, 126.2, 122.5, 122.0, 122.0, 121.6, 120.5, 119.4, 119.4, 111.8, 108.9, 41.7, 37.5, 26.3, 22.7.

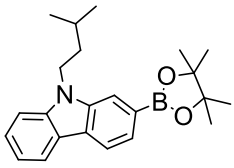

2BCz

Chemical Formula: $C_{23}H_{30}BNO_2$

9-Isopentyl-2-(4,4,5,5-tetramethyl-1,3,2-dioxaborolan-2-yl)-carbazole (**2-BCz**) was synthesized by a procedure reported in literature [221] using 2-bromo-9-isopentyl-9H-carbazole (**2Br-ACz**) (1.0 g, 3.2 mmol), 2.78 mL of n-butyllithium (7.0 mmol, 2.5 M in hexane), 2-isopropoxy-4,4,5,5-tetramethyl-1,3,2-dioxaborolane (0.71 g, 3.8 mmol) and dry THF (20 mL). After completion of the reaction, the mixture was extracted with EtOAc, dried over Na_2SO_4, and concentrated. The crude product was purified by column chromatography using acetone/hexane (1:40) as an eluent to obtain the compound (**2-BCz**) (0.74 g, 64%) as yellowish crystals. ^{1}H NMR (700 MHz, $CDCl_3$) δ 8.13 (t, *J* = 7.7 Hz, 2H), 7.89 (s, 1H), 7.71 (d, *J* = 7.7 Hz, 1H), 7.50 (t, *J* = 7.6 Hz, 1H), 7.42 (d, *J* = 8.2 Hz, 1H), 7.24 (t, *J* = 7.4 Hz, 1H), 4.39 – 4.36 (m, 2H), 1.79 – 1.72 (m, 3H), 1.42 (s, 12H), 1.05 (d, *J* = 6.3 Hz, 6H); ^{13}C NMR (176 MHz, $CDCl_3$) δ 140.9, 140.0, 126.3, 125.5, 125.1, 122.8, 121.0, 119.8, 118.8, 115.1, 115.0, 108.8, 83.9, 41.48, 37.8, 26.3, 25.1, 22.9.

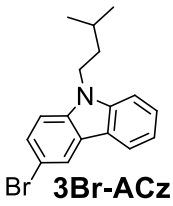

3Br-ACz

Chemical Formula: $C_{17}H_{18}BrN$

3-Bromo-9-isopentyl-carbazole (**3Br-ACz**) was synthesized by a similar procedure as compound **A-NP** using 3-bromo-9H-carbazole (**3Br-Cz**, 1.5 g, 6.1 mmol), 1-Br-3-methylbutane (1.2 g, 7.9 mmol), potassium carbonate (0.3 g, 2.4 mmol), potassium hydroxide (1.0 g, 18 mmol), catalytic amount of tetrabutylammonium hydrogensulfate and 120 ml of acetone. Purified by column chromatography using acetone/hexane (1:40) to obtain **3Br-ACz** as slightly yellowish crystals (Yield 83 %). ^{1}H NMR (700

MHz, $CDCl_3$) δ 8.22 (d, *J* = 2.0 Hz, 1H), 8.06 (d, *J* = 7.8 Hz, 1H), 7.56 (dd, *J* = 8.6, 1.9 Hz, 1H), 7.52 (t, *J* = 7.1 Hz, 1H), 7.41 (d, *J* = 8.2 Hz, 1H), 7.29 – 7.25 (m, 2H), 4.25 (d, *J* = 15.2 Hz, 2H), 1.75 – 1.67 (m, 3H), 1.04 (d, *J* = 6.6 Hz, 6H).^{13}C NMR (176 MHz, $CDCl_3$) δ 140.6, 139.0, 128.3, 126.4, 124.7, 123.2, 121.9, 120.7, 119.3, 111.6, 110.1, 108.9, 41.5, 37.5, 26.2, 22.7.

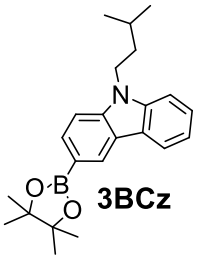

Chemical Formula: $C_{23}H_{30}BNO_2$

9-Isopentyl-3-(4,4,5,5-tetramethyl-1,3,2-dioxaboro-lan-3-yl)-carbazole (**3-BCz**) was synthesized by a similar procedure as compound **2-BCz** using 3-bromo-9-isopentyl-9H-carbazole (**3Br-ACz**, 0.8 g, 2.5 mmol), 2.23 mL n-butyllithium (5.6 mmol, 2.5 M in hexane), 2-isopropoxy-4,4,5,5-tetramethyl-1,3,2-dioxaborolane (0.57 g, 3.0 mmol) and dry THF (15 mL). The mixture was extracted with EtOAc, dried over Na_2SO_4, and concentrated. The crude product was purified by column chromatography using acetone/hexane (1:40) as an eluent to obtain compound **3-BCz** (0.63 g, 68%) as yellowish oil. ^{1}H NMR (700 MHz, CDCl3) δ 8.52 (s, 1H), 8.05 (d, *J* = 7.7 Hz, 1H), 7.84 (d, *J* = 9.1 Hz, 1H), 7.37 (t, *J* = 7.6 Hz, 1H), 7.32 – 7.28 (m, 2H), 7.16 – 7.13 (m, 1H), 4.23 – 4.19 (m, 2H), 1.66 – 1.56 (m, 3H), 1.31 (s, 12H), 0.92 (d, *J* = 6.5 Hz, 6H).

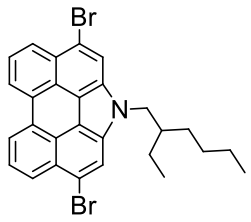

A-NP-Br

Chemical Formula: $C_{28}H_{25}Br_2N$

3,10-Dibromo-1-(2-ethylhexyl)-1H-phenanthro[1,10,9,8-cdefg]carbazole (**A-NP-Br**). To the solution of compound **3** (1.2 g, 3.2 mmol) in DMF (50 mL), NBS (1.1 g, 6.4 mmol) was added, and the mixture was stirred at room temperature for 1 h. The mixture was extracted with EtOAc, dried over Na_2SO_4, and concentrated. The crude product was purified by column chromatography using hexane as an eluent to give compound **A-NP-Br** (1.39 g, 82%) as a orange crystals.^{1}H NMR (400 MHz, $CDCl_3$) δ 8.47 (d, *J* = 7.6 Hz, 2H), 8.21 (d, *J* = 8.2 Hz, 2H), 7.83 – 7.76 (m, 4H), 4.19 – 4.07 (m, 2H), 2.02 – 1.94 (m, 1H), 1.34 – 1.22 (m, 8H), 0.92 – 0.83 (m, 6H); ^{13}C NMR (176 MHz, CDCl3) δ 131.7, 129.7, 127.8, 125.5, 125.1, 123.9, 121.8, 118.1, 117.1, 116.1, 50.0, 41.3, 30.9, 28.7, 24.4, 23.1, 14.2, 10.9.

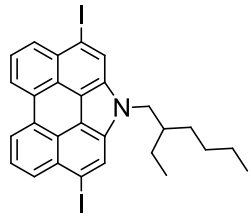

A-NP-I

Chemical Formula: $C_{28}H_{25}I_2N$

3,10-Diiodo-1-(2-ethylhexyl)-1H-phenanthro[1,10,9,8-cdefg]carbazole (**A-NP-I**). It was synthesized according to the Tucker procedure [222] using 1-(2-ethylhexyl)-1H-phenanthro[1,10,9,8-cdefg]carbazole **3** (0.5 g, 1.3 mmol), glacial acetic acid (15 mL), potassium iodide (0.29 g, 1.7 mmol) and potassium iodate (0.43 g, 2.0 mmol). After TLC control the reaction was terminated, cooled down to room temperature, treated with ethyl acetate and washed with distilled water. After, the column chromatography, which was performed using hexane as an eluent compound **A-NP-I** (0.58 g, 70 %), was obtained as dark yellow crystals. ^{1}H NMR NMR (700 MHz, $CDCl_3$) δ 8.55 (d, *J* = 7.2 Hz, 2H), 8.19 – 8.14 (m, 4H), 7.83 (t, *J* = 7.8 Hz, 2H), 4.30 – 4.22 (m, 2H), 2.08 – 2.02 (m, 1H), 1.45 – 1.28 (m, 8H), 0.91 (t, *J* = 7.4 Hz, 3H), 0.87 (t, *J* = 7.3 Hz, 3H). ^{13}C NMR (176 MHz, $CDCl_3$) δ 132.5, 130.0, 129.7, 129.4, 125.8, 123.9, 123.4, 121.9, 116.9, 93.1, 50.0, 41.3, 30.8, 28.7, 24.4, 23.2, 14.2, 11.0.

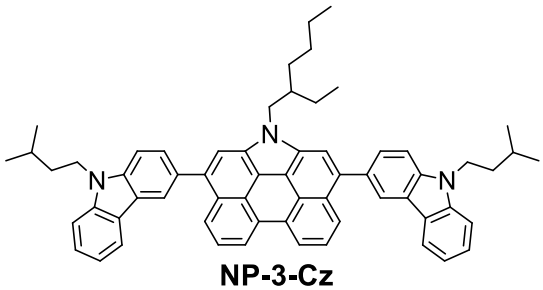

NP-3-Cz

Chemical Formula: $C_{62}H_{61}N_3$

1-(2-Ethylhexyl)-3,10-bis(9-isopentyl-9H-carbazol-3-yl)-1H-phenanthro[1,10,9,8-cdefg] carbazole (**NP-3-Cz**) was synthesized by the Suzuki-Miyaura coupling reaction following the procedure reported in literature [223] using 3,10-dibromo-1-(2-ethylhexyl)-1H-phenanthro [1,10,9,8-cdefg]carbazole (**A-NP-Br**, 0.35 g, 0.65 mmol), 9-isopentyl-3-(4,4,5,5-tetramethyl-1,3,2-dioxaborolan-2-yl)-9H-carbazole (**3-BCz**, 0.55, 1.5 mmol), potassium carbonate (0.34 g, 2.5 mmol), bis(triphenylphosphine) palladium(II) dichloride (0.05 molar equiv.), THF (15 mL) and water (2 mL). After completion of the reaction the mixture was extracted with EtOAc, dried over Na_2SO_4, and concentrated. The crude product was purified by column chromatography using acetone/hexane (1:40) as an eluent to obtain compound **NP-3-Cz** (0.32 g, 58 %) as yellow crystals. m.p.: 221-222 °C. ^{1}H NMR (400 MHz, $CDCl_3$) δ 8.72 (d, *J* = 7.5 Hz, 2H), 8.46 (s, 2H), 8.23 (d, *J* = 8.3 Hz, 2H), 8.17 (d, *J* = 7.7 Hz, 2H), 7.90 – 7.83 (m, 4H), 7.78 (t, *J* = 7.9 Hz, 2H), 7.59 (d, *J* = 8.4 Hz, 2H), 7.55 – 7.45 (m, 4H), 7.29 – 7.22 (m, 2H), 4.61 (d, *J* = 7.5 Hz, 2H), 4.41 (t, *J* = 7.9 Hz, 4H), 2.37 – 2.27 (m, 1H), 1.90 – 1.74 (m, 6H), 1.47 – 1.22 (m, 8H), 1.09 (d, *J* = 6.3 Hz, 12H), 0.94 (t, *J* = 7.4 Hz, 3H), 0.83 (t, *J* = 7.1 Hz, 3H). ^{13}C NMR (101 MHz, $CDCl_3$) δ 140.9, 139.7, 138.3, 132.9, 132.5, 130.9, 128.6, 128.4, 125.9, 125.1, 124.7, 124.6, 123.2, 123.1, 122.2, 120.9, 120.7, 119.0, 116.8, 114.7, 108.9,

108.5, 50.0, 41.7, 41.3, 37.8, 30.9, 28.7, 26.4, 24.3, 23.2, 22.8, 14.2, 11.0. IR ($\bar{\upsilon}$, cm^{-1}): 3053 (arene C−H, 3100-3000 cm^{-1}); 2953, 2929, 2869 (aliphatic C−H, 3000-2850 cm^{-1});1598, 1487, 1468 (C-C in Ar, 1600-1585, 1500-1400 cm^{-1}); 1353, 1304, 1273 (C−N in Ar, 1350-1250 cm^{-1});892, 862, 794, 762, 746, 731 (C−H in Ar, 900-675 cm^{-1}); m/z: 848 ($[M + H]^+$).

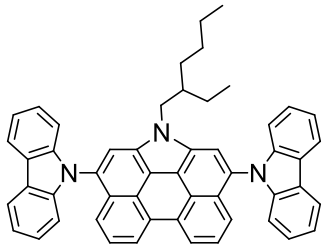

NP-9-Cz

Chemical Formula: $C_{52}H_{41}N_3$

3,10-Di(9H-carbazol-9-yl)-1-(2-ethylhexyl)-1H-phenanthro[1,10,9,8-cdefg]carbazole (**NP-9-Cz**) was achieved by an Ullmann-coupling procedure as reported in literature [224] using diiodo derivative **A-NP-I** (0.25 g, 0.40 mmol), carbazole (0.17 g, 1.0 mmol), potassium carbonate (0.44 g, 3.2 mmol), copper (0.10 g, 1.6 mmol) and 18-crown-4 ether (0.05 molar equiv.). After completion of the reaction, the mixture was filtered through a glass filter. The crude product was purified by column chromatography using hexane as an eluent to give compound **NP-9-Cz** (0.12 g, 43 %) as yellow crystals. ^{1}H NMR (700 MHz, $CDCl_3$) δ 8.77 (d, *J* = 7.1 Hz, 2H), 8.30 (d, *J* = 7.8 Hz, 4H), 8.07 (s, 2H), 7.73 – 7.70 (m, 2H), 7.51 (d, *J* = 7.6 Hz, 2H), 7.42 – 7.38 (m, 4H), 7.36 (t, *J* = 7.4 Hz, 4H), 7.20 (d, *J* = 8.0 Hz, 4H), 4.64 – 4.56 (m, 2H), 2.26 – 2.20 (m, 1H), 1.47 – 1.18 (m, 8H), 0.91 (t, *J* = 7.4 Hz, 3H), 0.75 (t, *J* = 7.2 Hz, 3H); ^{13}C NMR (176 MHz, $CDCl_3$) δ 142.8, 132.6, 132.6, 131.6, 130.7, 127.1, 126.9, 126.3, 126.2, 126.2, 125.6, 125.2, 123.4, 122.7, 122.2, 120.6, 120.0, 117.5, 115.3, 110.5, 110.5, 50.5, 41.5, 31.1, 28.7, 24.3, 23.1, 14.1, 10.9.IR ($\bar{\upsilon}$, cm^{-1}): 3049 (arene C−H, 3100-3000 cm^{-1}); 2956, 2926, 2870 (aliphatic C−H, 3000-2850 cm^{-1}); 1596, 1567, 1477, 1450 (C-C in Ar, 1600-1585, 1500-1400 cm^{-1}); 1334, 1315, 1299 (C−N in Ar, 1350-1250 cm^{-1}); 860, 799, 744, 719(C−H in Ar, 900-675 cm^{-1}); m/z: 709 ($[M + H]^+$).

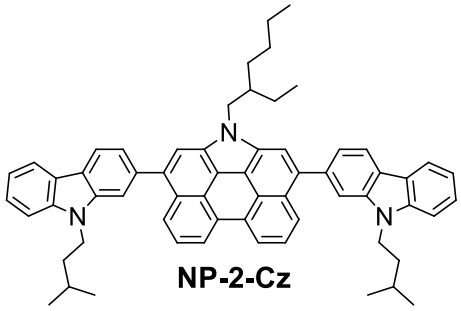

NP-2-Cz

Chemical Formula: $C_{62}H_{61}N_3$

1-(2-Ethylhexyl)-3,10-bis(9-isopentyl-9H-carbazol-2-yl)-1H-phenanthro [1,10,9,8-cdefg]carbazole (NP-2-Cz) was synthesized by a similar procedure as compound **NP-3-Cz** using 3,10-dibromo-1-(2-ethylhexyl)-1H-phenanthro[1,10,9,8-cdefg]carbazole (**A-NP-Br**, 0.35 g, 0.65 mmol), 9-isopentyl-2-(4,4,5,5-tetramethyl-1,3,2-dioxaborolan-2-yl)-9H-carbazole (**2-BCz**, 0.57, 1.6 mmol), potassium carbonate (0.34 g, 2.5 mmol),

bis(triphenylphosphine) palladium(II) dichloride (0.05 molar equiv.), THF (15 mL) and water (2 mL). After completion of the reaction the mixture was extracted with EtOAc, dried over Na_2SO_4, and concentrated. The crude product was purified by column chromatography using acetone/hexane (1:40) as an eluent to obtain compound **NP-2-Cz** (0.28 g, 51 %) as yellow crystals. ^{1}H NMR (700 MHz, $CDCl_3$) δ 8.77 – 8.71 (m, 2H), 8.31 – 8.24 (m, 4H), 8.22 (d, *J* = 7.6 Hz, 2H), 7.94 (s, 2H), 7.83 – 7.80 (m, 2H), 7.79 (s, 2H), 7.64 (d, *J* = 7.7 Hz, 2H), 7.53 (t, *J* = 7.2 Hz, 2H), 7.48 (d, *J* = 8.1 Hz, 2H), 7.31 (t, *J* = 7.0 Hz, 2H), 4.70 – 4.62 (m, 2H), 4.43 – 4.39 (m, 4H), 2.35 (d, *J* = 37.6 Hz, 1H), 1.85 (dd, *J* = 15.1, 6.9 Hz, 4H), 1.79 – 1.73 (m, 2H), 1.51 – 1.26 (m, 8H), 1.04 (d, *J* = 6.6 Hz, 12H), 0.98 (t, *J* = 7.4 Hz, 3H), 0.84 (t, *J* = 7.3 Hz, 3H); ^{13}C NMR (176 MHz, $CDCl_3$) δ 141.0, 140.7, 139.8, 138.6, 132.5, 130.9, 128.4, 128.3, 125.8, 125.1, 124.7, 123.0, 122.2, 121.8, 121.1, 120.6, 120.4, 119.1, 117.0, 114.7, 110.5, 108.8, 77.3, 77.2, 77.0, 68.1, 50.0, 41.6, 41.4, 37.8, 31.0, 28.9, 26.3, 24.3, 23.2, 22.8, 14.2, 10.9.IR ($\bar{\upsilon}$, cm^{-1}): 3050 (arene C−H, 3100-3000 cm^{-1}); 2954, 2927, 2868 (aliphatic C−H, 3000-2850 cm^{-1}); 1596, 1556, 1474, 1456 (C-C in Ar, 1600-1585, 1500-1400 cm^{-1}); 1323, 1304, 1243 (C−N in Ar, 1350-1250 cm^{-1}); 858, 824, 762, 746, 728 (C−H in Ar, 900-675 cm^{-1}); m/z: 848 ($[M + H]^+$).

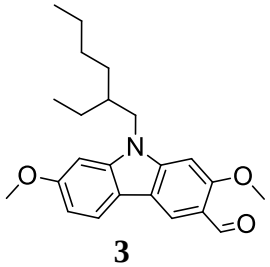

3

Chemical Formula: $C_{23}H_{29}NO_3$

9-(2-Ethylhexyl)-2,7-dimethoxycarbazole-3-carbaldehyde (3). To a solution of DMF (5.3 mL, 69 mmol) at 0°C, $POCl_3$(3.4 ml, 37 mmol) was added dropwise and the reaction mixture was stirred for 10 min to form the Vilsmeier salt. To this was added a solution of 9-(2-ethylhexyl)-2,7-dimethoxycarbazole**2** (1.55 g, 4.60 mmol) in DCE (10 mL) and the reaction mixture was stirred at room temperature for 2 h. The reaction mixture was then quenched with 1 M KOAc solution. Ethyl acetate was added and the two layers separated, the organic layer was washed with water, brine and dried over $MgSO_4$ and evaporated to dryness. Purification by column chromatography using acetone/heptane (1:5) as eluent gave aldehyde **3** (1.25 g, 74 %) as a yellow solid. mp 134-136 °C; MS (ESI+) *m/z* 368 [MH^+]; HRMS(ESI-TOF) m/z: calcd for $C_{23}H_{29}NO_3$: 368.2147; found: 368.2220 [M+H].^{1}HNMR (300 MHz, $CDCl_3$, 25°C, TMS) *δ* 10.47 (s, 1H), 8.44 (s, 1H), 7.89 (d, *J* = 8.4 Hz, 1H), 6.86 (dd, *J* = 8.5, 2.2 Hz, 1H), 6.80 (d, *J* = 2.1 Hz, 1H), 6.69 (s, 1H), 4.02 (d, *J* = 1.6 Hz, 1H), 4.00 (s, 1H), 3.91 (s, 3H), 2.05-1.97 (m, 1H), 1.41-1.27 (m, 8H), 0.94 (t, *J* = 7.4 Hz, 3H), 0.88 (t, *J* = 7.1 Hz, 3H).^{13}C NMR (75 MHz, $CDCl_3$, 25°C, TMS) δ: 189.5, 161.0, 159.0, 146.6, 143.1, 120.9, 120.6, 118.4, 117.3, 117.2, 107.9, 94.8, 90.9, 55.9, 55.8, 47.5, 39.2, 31.1, 28.9, 24.5, 23.1, 14.2, 11.1.

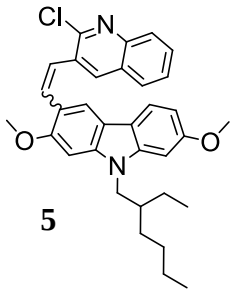

5

Chemical Formula: $C_{33}H_{35}ClN_2O_2$

3-(2-(2-Chloroquinolin-3-yl)vinyl)-9-(2-ethylhexyl)-2,7-dimethoxycarbazole (5). A solution of aldehyde **3** (0.380 g, 1.03 mmol) dropwise was added to a stirred solution of phosphonium salt **4** (0.617 g, 1.12 mmol) and sodium hydride (0.062 g, 2.60 mmol) in dichloromethane at 0 °C, after which the reaction mixture was stirred for 3 h. The crude product was purified by silica gel column chromatography using acetone/heptane (1:10) as eluent to obtain compound **5** (0.535 g, 98%, *Z/E*~2:1 from ^{1}HNMR) as a yellow solid. m.p. 166-168°C; MS (ESI+) *m/z* 527 [MH^+]; HRMS (ESI-TOF) m/z: calcd for $C_{33}H_{35}ClN_2O_2$: 527.2387; found: 527.2387 [M+H]; ^{1}HNMR (300 MHz, $CDCl_3$, 25°C, TMS) δ: 8.40 (d, *J* = 21.0 Hz), 8.25 (s, 1H), 8.04 – 7.92 (m), 7.85 (d, *J* = 8.0 Hz), 7.80 – 7.73 (m), 7.69 (t, *J* = 4.8 Hz), 7.66 – 7.53 (m), 7.52 (s), 7.49 (s), 7.41 – 7.30 (m), 7.13 – 7.11 (m), 7.09 – 7.05 (m), 6.88 – 6.83 (m), 6.80 (d, *J* = 4.1 Hz), 6.78 – 6.70 (m), 6.69 (d, *J* = 2.2 Hz), 6.66 (d, *J* = 2.2 Hz), 4.06 (dd, *J* = 7.4, 2.0 Hz), 4.02 (s, 3H), 4.00 (d, *J* = 2.1 Hz), 3.93 (s, 3H, OCH_3,minor isomer), 3.86 (s, 3H, OCH_3, major isomer), 3.83 (s, 3H, OCH_3, major isomer), 2.08 – 1.96 (m), 1.71 – 1.63 (m), 1.43 – 1.23 (m), 0.98 – 0.83 (m).^{13}C NMR (75 MHz, $CDCl_3$, 25°C, TMS)*δ* 158.5, 158.3, 156.4, 156.0, 151.1, 150.6, 146.7, 146.6, 142.8, 142.7, 142.4, 142.3, 137.7, 137.1, 133.1, 131.7, 131.0, 130.0, 129.8, 129.4, 128.4, 128.2, 127.9, 127.7, 127.6, 127.3, 127.2, 127.0, 126.9, 123.9, 121.1, 120.5, 120.2, 118.5, 118.0, 117.1, 117.0, 117.0, 116.9, 116.4, 107.1, 106.8, 94.4, 94.2, 91.7, 91.6, 56.0, 55.9, 55.8, 55.7, 47.5, 47.4, 39.3, 35.6, 31.2, 31.1, 29.0, 28.9, 26.6, 26.5, 24.5, 23.2, 23.1, 22.8, 14.2, 11.1.

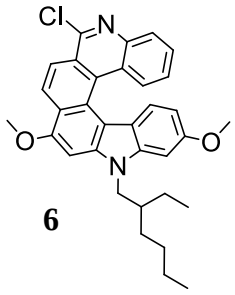

6

Chemical Formula: $C_{33}H_{33}ClN_2O_2$

2-chloro-7-(2-ethylhexyl)-5,9-dimethoxy-7H-carbazolo[3,4-k]phenanthridine (6). Argon was bubbled through a solution of compound **5** (0.150 g, 0.28 mmol, mixture of two isomers) in toluene (440 mL) later, iodine (0.094 g, 0.37 mmol) was added to it and then excess propylene oxide was added to the solution. A Rayonet photochemical reactor (wavelength used is 350 nm) was used for irradiation purpose and the reaction mixture was irradiated for 48-50 h, after which it was washed with aqueous $Na_2S_2O_3$, water and brine, dried over anhydrous $MgSO_4$ and evaporated to afford a dark yellow residue. Purification by column chromatography using Et_2O/acetone/heptane (1:1:40) as eluent gave the racemic diaza[6]helicene **6** (0.079 g, 53 %) as a light yellow solid. m.p.: 242-244 °C; MS (ESI+) *m/z* = 525

[MH]$^+$;HRMS (ESI-TOF) m/z: calcd for $C_{33}H_{33}ClN_2O_2$: 525.2231; found: 525.2277 [M+H];^{1}H NMR (300 MHz, $CDCl_3$, 25°C, TMS) δ 8.61 (d, J = 8.9 Hz, 1H), 8.28 – 8.18 (m, 3H), 7.69 – 7.62 (m, 1H), 7.27 – 7.20 (m, 2H), 6.92 (d, J = 1.9 Hz, 1H), 6.50 – 6.41 (m, 2H), 4.25 (d, J = 7.5 Hz, 2H), 4.20 (s, 3H), 3.88 (s, 3H), 2.24 – 2.13 (m, 1H), 1.55 – 1.34 (m, 8H), 1.03 (t, J = 7.3 Hz, 3H), 0.90 (td, J = 7.0, 1.9 Hz, 3H).^{13}C NMR (75 MHz, $CDCl_3$, 25°C, TMS) δ:157.3, 154.3, 151.2, 143.4, 141.7, 141.1, 131.7, 128.6, 128.2, 126.1, 125.5, 125.2, 124.4, 124.0, 123.4, 123.3, 119.6, 117.5, 117.4, 112.3, 106.3, 93.6, 92.9, 56.3, 55.7, 47.7, 39.7, 31.3, 29.2, 24.8, 23.2, 14.2, 11.1.

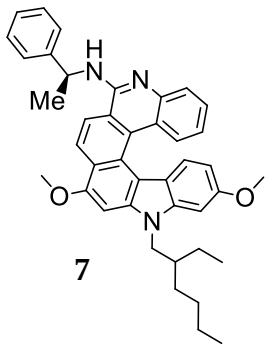

7

Chemical Formula: $C_{41}H_{43}N_3O_2$

7-(2-ethylhexyl)-5,9-dimethoxy-N-((S)-1-phenylethyl)-7H-carbazolo[3,4-k]phenanthridin-2-amine (7). (*S*)-α-methyl benzylamine (37μL, 0.29 mmol), Cs_2CO_3 (0.931 g, 2.86 mmol), *rac*-BINAP (0.007 g, 5 mol %), and $Pd(OAc)_2$ (0.005 g, 10 mol %) were added to a solution of **6** (0.120 g, 0.23 mmol) in dry toluene (25 mL) and the reaction mixture was stirred at 80 °C for 12 h. Subsequently, the mixture was diluted with ethyl acetate (40 mL) and washed with water (3×20 mL). The organic fraction was dried over $MgSO_4$ and filtered, and the solvent was removed under vacuum. After column chromatographic purification using Et_2O: acetone: heptane (1:1:20) as eluent, a 1:1 mixture of diastereomers (0.074 g, 53%) was obtained as a yellow solid. These diastereomers were readily separated by silica gel column chromatography. m.p. 77-78°C; MS (ESI+) *m/z* = 610 [MH]$^+$;HRMS (ESI-TOF) m/z: calcd for $C_{41}H_{43}N_3O_2$: 610.3355; found: 610.3431 [M+H];^{1}HNMR (300 MHz, $CDCl_3$, 25°C, TMS, single diastereomer) δ 8.45 (d, J = 8.7 Hz, 1H), 8.00 (d, J = 7.1 Hz, 1H), 7.88 (d, J = 7.6 Hz, 1H), 7.73 (d, J = 8.8 Hz, 1H), 7.60 (d, J = 7.2 Hz, 2H), 7.45 (t, J = 6.9 Hz, 1H), 7.38 (t, J = 7.4 Hz, 2H), 7.31 – 7.26 (m, 1H), 7.13 (s, 1H), 6.92 – 6.85 (m, 2H), 6.69 (d, J = 8.9 Hz, 1H), 6.43 (dd, J = 8.9, 2.3 Hz, 1H), 5.85-5.76 (m, 1H), 5.59 (d, J = 6.6 Hz, 1H), 4.22 (d, J = 7.3 Hz, 2H), 4.16 (s, 3H), 3.86 (s, 3H), 2.21 – 2.11 (m, 1H), 1.82 (d, J = 6.7 Hz, 3H), 1.51 – 1.28 (m, 8H), 1.00 (t, J = 7.3 Hz, 3H), 0.89 (t, J = 6.6 Hz, 3H). ^{13}C NMR (100 MHz, $CDCl_3$, 25°C, TMS) δ: 157.0, 154.2, 152.7, 141.4, 141.0, 131.1, 128.6, 128.1, 127.9, 127.1, 126.8, 126.3, 126.1, 124.3, 122.8, 122.7, 121.9, 121.6, 119.6, 117.8, 115.0, 112.2, 106.2, 93.4, 91.9, 56.2, 55.7, 47.6, 39.7, 31.3, 31.3, 29.9, 29.2, 29.1, 24.8, 23.2, 22.7, 14.2, 11.3, 11.1.

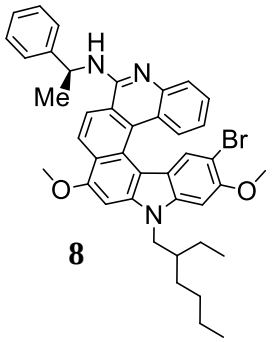

8

Chemical Formula: $C_{41}H_{43}N_3O_2$

10-bromo-7-(2-ethylhexyl)-5,9-dimethoxy-N-((S)-1-phenylethyl)-7H-carbazolo[3,4-k]phenanthridin-2-amine (8).To a solution of compound **7** (25 mg, 0.041 mmol) in chloroform (5 mL) at -40 °C, NBS (6.9 mg, 0.038 mmol) was added and reaction mixture was stirred at this temperature for 3 h. After 3 h the reaction mixture was diluted with ethyl acetate. The organic layer was washed with water, brine and dried over $MgSO_4$ and the solvent was removed under vacuum. The crude product was purified by silica-gel column chromatography using heptane/CH_2Cl_2/acetone (20:1:1) as the eluent. Compound **8** (23 mg, 82 %) was obtained as a yellow solid. M.p. 70-73°C; MS (ESI+) *m/z* 689 $[MH]^+$;HRMS (ESI-TOF) m/z: calcd for $C_{41}H_{42}BrN_3O_2$: 688.2534; found: 688.2536, 690.2526, 691.2549 [M+H]; ^{1}HNMR (600 MHz, $CDCl_3$, 25°C, TMS) δ: 8.46 (d, *J* = 8.7 Hz, 1H), 7.94 (d, *J* = 8.1 Hz, 1H), 7.86 (d, *J* = 8.2 Hz, 1H), 7.76 (d, *J* = 8.7 Hz, 1H), 7.62 (d, *J* = 7.7 Hz, 2H), 7.54 (t, *J* = 7.5 Hz, 1H), 7.40 (t, *J* = 7.7 Hz, 2H), 7.32 – 7.27 (m, 1H), 7.13 (s, 1H), 6.92 (t, *J* = 7.3 Hz, 1H), 6.89 (s, 1H), 6.82 (s, 1H), 5.84 – 5.78 (m, 1H), 5.66 – 5.59 (m, 1H), 4.25 (d, *J* = 7.3 Hz, 2H), 4.18 (s, 3H), 3.97 (s, 3H), 2.18 – 2.11 (m, 1H), 1.83 (d, *J* = 6.7 Hz, 3H), 1.51 – 1.39 (m, 8H), 1.04 – 0.99 (m, 3H), 0.91 – 0.87 (m, 3H).^{13}C NMR (100 MHz, $CDCl_3$, 25°C, TMS) δ: 154.7, 152.8, 152.6, 145.1, 144.8, 141.2, 139.7, 131.0, 129.7, 128.9, 128.4, 127.9, 127.4, 127.0, 126.5, 124.3, 123.0, 122.6, 121.5, 121.4, 121.1, 119.8, 118.3, 115.4, 111.1, 102.5, 92.1, 91.7, 56.5, 56.2, 50.9, 47.6, 39.8, 31.4, 29.2, 24.8, 23.1, 22.4, 14.2, 11.3.IR ($\bar{\upsilon}$, cm^{-1}): 3410 (N−H, 3500-3200 cm^{-1}); 3009 (arene C−H, 3100-3000 cm^{-1}); 2956, 2927, 2871 (aliphatic C−H, 3000-2850 cm^{-1}); 1594, 1572, 1503, 1450 (C-C in Ar, 1600-1585, 1500-1400 cm^{-1}); 1339, 1307(C−N in Ar, 1350-1250 cm^{-1}); 1233, 1216, 1199, 1080(C−O−C, 1250-1050 cm^{-1}); 885, 770 (C−H in Ar, 900-675 cm^{-1});

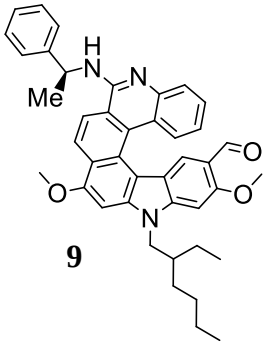

9

Chemical Formula: $C_{42}H_{43}N_3O_3$

7-(2-ethylhexyl)-5,9-dimethoxy-2-(((S)-1-phenyleth yl)amino)-7H-carbazolo[3,4-k]phenanthridine-10-carbaldehyde (9). To a solution of DMF (0.050 mL, 0.66 mmol) at 0°C, $POCl_3$(0.03 ml, 0.33 mmol) was added dropwise and the reaction mixture was stirred for 10 min to form the Vilsmeier salt. To this was added a solution of compound **7** (20 mg, 0.033 mmol) in DCE (3 mL) and the reaction mixture was stirred at room temperature for 3 h. The reaction mixture was poured into crushed ice. Ethyl acetate was added and the

two layers separated, the organic layer was washed with water, brine and dried over $MgSO_4$ and evaporated to dryness. Purification by column chromatography using acetone/heptane (1:5) as eluent gave aldehyde **9** (8.9 mg, 42 %) as a yellow solid. m.p. 92-94°C; MS (ESI+) *m/z* 638 $[MH]^+$;HRMS (ESI-TOF) m/z: calcd for $C_{42}H_{43}N_3O_3+NH_4$: 655.3304; found: 655.3367 $[M+NH_4]$;^{1}HNMR (300 MHz, $CDCl_3$, 25°C, TMS) δ: 9.91 (s, 1H), 8.46 (d, *J* = 8.8 Hz, 1H), 7.95 (d, *J* = 8.1 Hz, 1H), 7.88 (d, *J* = 7.2 Hz, 1H), 7.77 (d, *J* = 8.9 Hz, 1H), 7.62 (d, *J* = 7.4 Hz, 2H), 7.53 – 7.45 (m, 1H), 7.41 (t, *J* = 7.4 Hz, 2H), 7.33 – 7.27 (m, 1H), 7.16 (s, 1H), 7.13 (s, 1H), 6.86 – 6.78 (m, 2H), 5.89 – 5.77 (m, 1H), 5.60 (d, *J* = 5.0 Hz, 1H), 4.26 (d, *J* = 7.3 Hz, 2H), 4.18 (s, 3H), 4.00 (s, 3H), 2.21 – 2.12 (m, 1H), 1.82 (d, *J* = 6.7 Hz, 3H), 1.56 – 1.32 (m, 8H), 1.04 (td, *J* = 7.3, 2.1 Hz, 3H), 0.90 (t, *J* = 6.3 Hz, 3H).^{13}C NMR (100 MHz, $CDCl_3$, 25°C, TMS) δ: 189.6, 158.8, 155.1, 152.6, 145.1, 144.5, 142.0, 130.1, 128.9, 128.6, 127.9, 127.4, 127.0, 124.4, 123.3, 122.54, 122.49, 121.5, 121.45, 121.41, 121.3, 120.0, 119.9, 117.9, 117.5, 116.0, 112.4, 91.8, 90.8, 56.2, 55.9, 50.8, 47.7, 39.8, 32.1, 31.4, 29.2, 24.8, 23.1, 14.2, 11.3.IR ($\bar{\upsilon}$, cm^{-1}): 3430 (N−H, 3500-3200 cm^{-1}); 3012 (arene C−H, 3100-3000 cm^{-1}); 2955, 2927, 2857 (aliphatic C−H, 3000-2850 cm^{-1}); 1738 (C=O, 1750-1650 cm^{-1}); 1595, 1572, 1558, 1493 (C-C in Ar, 1600-1585, 1500-1400 cm^{-1}); 1366, 1337(C−N in Ar, 1350-1250 cm^{-1}); 1234, 1215, 1200, 1080 (C−O−C, 1250-1050 cm^{-1}); 815, 765 (C−H in Ar, 900-675 cm^{-1});

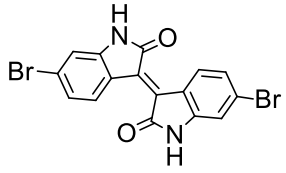

ISO

Chemical Formula: $C_{16}H_8Br_2N_2O_2$

6,6′-Dibromoisoindigo (**ISO**) was prepared according to the literature procedure [225] from 6-bromoisatin and 6-bromooxindole. ^{1}H NMR (300 MHz, DMSO) δ 11.09 (bs, 2H), 8.99 (d, *J* = 8.7 Hz, 2H), 7.18 (dd, *J* = 8.7, 2.0 Hz, 2H), 7.00 (d, *J* = 2.0 Hz, 2H).

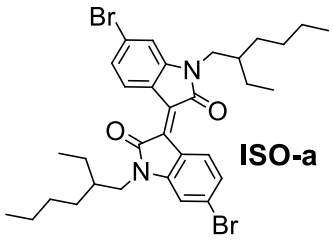

ISO-a

Chemical Formula: $C_{32}H_{40}Br_2N_2O_2$

1,1'-Bis(2-ethylhexyl)-6,6′-dibromo isoindigo (**ISO-a**) was synthesized by alkylation reaction described in literature [225]. ^{1}H NMR (300 MHz, $CDCl_3$) δ 9.03 (d, *J* = 8.6 Hz, 2H), 7.15 (dd, *J* = 8.6, 1.9 Hz, 2H), 6.88 (d, *J* = 1.8 Hz, 2H), 3.68 – 3.53 (m, 4H), 1.87 – 1.77 (m, 2H), 1.40 – 1.25 (m, 16H), 0.97 – 0.85 (m, 12H).

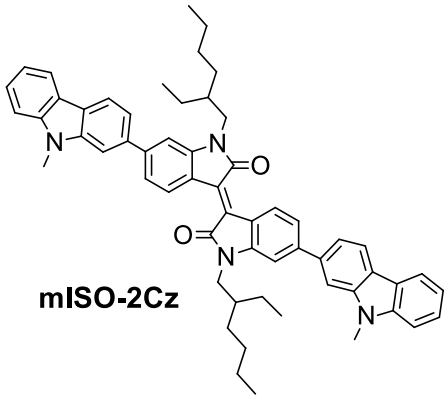

Chemical Formula: $C_{58}H_{60}N_4O_2$

1,1'-Bis(2-ethylhexyl)-6,6'-bis(9-methyl-9H-carbazol-2-yl)-isoindigo (**mISO-2Cz**) was synthesized by the Suzuki-Miyaura coupling reaction by a similar procedure as compound **12** using 1,1'-bis(2-ethylhexyl)-6,6′-dibromoisoindigo (0.40 g, 0.62 mmol), 9-methyl-2-(4,4,5,5-tetramethyl-1,3,2-dioxaborolan-2-yl)-9H-carbazole (0.44 g, 1.43 mmol), potassium carbonate (0.33 g, 2.4 mmol), bis(triphenylphosphine) palladium(II) dichloride (0.05 molar equiv.), 16 mL of THF and 2.5 mL of water. After completion, the mixture was extracted with DCM, dried over Na_2SO_4, and concentrated. The crude product was purified by column chromatography using DCM/hexane (1:1) to give compound **mISO-2Cz** (0.30 g, 58 %) as dark red crystals. m.p.: 235-236 ^oC. ^1H NMR (300 MHz, $CDCl_3$) δ 9.27 (d, *J* = 8.4 Hz, 2H), 8.20 – 8.10 (m, 4H), 7.62 (d, *J* = 1.0 Hz, 2H), 7.54 – 7.48 (m, 4H), 7.46 – 7.40 (m, 4H), 7.31 – 7.25 (m, 2H), 7.08 (s, 2H), 3.90 (s, 6H), 3.79 – 3.71 (m, 4H), 1.98 – 1.89 (m, 2H), 1.49 – 1.30 (m, 16H), 1.02 – 0.89 (m, 12H).^{13}C NMR (75 MHz, $CDCl_3$) δ 168.9, 146.0, 145.8, 141.9, 141.6, 138.4, 132.54, 130.2, 126.2, 123.0, 122.6, 121.2, 120.9, 120.8, 120.6, 119.3, 118.4, 108.7, 107.1, 106.9, 44.3, 37.9, 31.0, 29.3, 29.1, 24.4, 23.3, 14.3, 11.0.IR ($\bar{\upsilon}$, cm^{-1}): 3040 (arene C−H, 3100-3000 cm^{-1}); 2953, 2927, 2868 (aliphatic C−H, 3000-2850 cm^{-1}); 1739, 1687 (C=O, 1750-1650 cm^{-1}); 1608, 1555, 1454 (C-C in Ar, 1600-1585, 1500-1400 cm^{-1}); 1348, 1325, 1247(C−N in Ar, 1350-1250 cm^{-1}); 871, 847, 811, 746, 773 (C−H in Ar, 900-675 cm^{-1}); m/z: 846 ($[M + H]^+$). Anal. Calcd for $C_{58}H_{60}N_4O_2$ (%):C 82.43, H 7.16, N 6.63, O 3.79. Found (%): C 82.32, H 7.22, N 6.70.

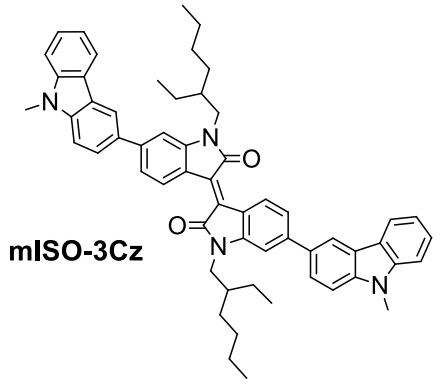

Chemical Formula: $C_{58}H_{60}N_4O_2$

1,1'-Bis(2-ethylhexyl)-6,6'-bis(9-methyl-9H-carbazol-3-yl)-isoindigo (**mISO-3Cz**) was synthesized by a similar procedure as compound **mISO-2Cz**, using 1,1'-bis(2-ethylhexyl)-6,6′-dibromoisoindigo (0.70 g, 1.1 mmol), 9-methyl-3-(4,4,5,5-tetramethyl-1,3,2-dioxaborolan-2-yl)-9H-carbazole (0.73 g, 2.4 mmol), potassium carbonate (0.57 g, 4.1 mmol), bis(triphenylphosphine) palladium(II) dichloride (0.05 molar equiv.), 24 mL of THF and 3.5 mL of water. After completion, the mixture was extracted with DCM, dried over Na_2SO_4, and concentrated. The crude product was purified by column chromatography using DCM/hexane (1:1) to give compound **mISO-3Cz**

(0.56 g, 60 %) as dark violet crystals. m.p.: 284-285 °C. ^{1}H NMR (400 MHz, $CDCl_3$) δ 9.23 (d, *J* = 8.3 Hz, 2H), 8.34 (d, *J* = 1.3 Hz, 2H), 8.16 (d, *J* = 7.7 Hz, 2H), 7.77 (dd, *J* = 8.5, 1.5 Hz, 2H), 7.52 (t, *J* = 7.4 Hz, 2H), 7.48 – 7.38 (m, 6H), 7.28 (t, *J* = 7.4 Hz, 2H), 7.06 (s, 2H), 3.86 (s, 6H), 3.82 – 3.65 (m, 4H), 2.01 – 1.87 (m, 2H), 1.52 – 1.29 (m, 16H), 1.00 – 0.95 (m, 6H), 0.91 (t, *J* = 6.9 Hz, 6H).^{13}C NMR (101 MHz, CDCl3) δ 169.0, 145.8, 145.8, 141.6, 141.1, 132.2, 131.7, 130.1, 126.2, 125.1, 123.5, 123.0, 120.7, 120.6, 120.4, 119.4, 118.8, 109.0, 108.8, 106.6, 44.2, 37.9, 31.0, 29.4, 29.0, 24.3, 23.3, 14.3, 11.0.IR ($\bar{\upsilon}$, cm^{-1}): 3041 (arene C−H, 3100-3000 cm^{-1}); 2955, 2924, 2855 (aliphatic C−H, 3000-2850 cm^{-1}); 1682 (C=O, 1750-1650 cm^{-1}); 1612, 1597, 1455, 1432 (C-C in Ar, 1600-1585, 1500-1400 cm^{-1}); 1357, 1275, 1249 (C−N in Ar, 1350-1250 cm^{-1}); 839, 830, 793, 742, 726 (C−H in Ar, 900-675 cm^{-1}); m/z: 846 ([M + H]$^+$). Anal. Calcd for $C_{58}H_{60}N_4O_2$ (%):C 82.43, H 7.16, N 6.63, O 3.79. Found (%): C 82.30, H 7.25, N 6.71.

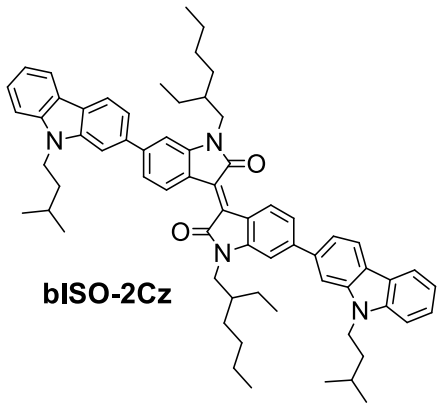

Chemical Formula: $C_{66}H_{76}N_4O_2$

1,1'-Bis(2-ethylhexyl)-6,6'-bis(9-isopentyl-9H-carbazol-2-yl)-isoindigo (**bISO-2Cz**) was synthesized by a similar procedure as compound **mISO-2Cz** using 1,1'-bis(2-ethylhexyl)-6,6′-dibromoiso indigo (0.45 g, 0.70 mmol), 9-isopentyl-2 (4,4,5,5-tetramethyl-1,3,2-dioxaborolan-2-yl)-9H-carbazole (**2-BCz**, 0.56 g, 1.5 mmol), potassium carbonate (0.37 g, 2.7 mmol), bis(triphenylphosphine) palladium(II) dichloride (0.05 molar equiv.), 16 mL of THF and 2.5 mL of degased water. After completion, the mixture was extracted with DCM, dried over Na_2SO_4, and concentrated. The crude product was purified by column chromatography using DCM/hexane (1:1) to give compound **bISO-2Cz** (0.39 g, 59 %) as dark red crystals.^{1}H NMR (400 MHz, $CDCl_3$) δ 9.30 (d, *J* = 8.3 Hz, 2H), 8.17 (d, *J* = 8.1 Hz, 2H), 8.14 (d, *J* = 7.7 Hz, 2H), 7.63 (s, 2H), 7.54 – 7.48 (m, 4H), 7.47 – 7.42 (m, 4H), 7.27 (t, *J* = 7.2 Hz, 2H), 7.12 (d, *J* = 1.1 Hz, 2H), 4.41 – 4.35 (m, 4H), 3.84 – 3.72 (m, 4H), 2.03 – 1.92 (m, 2H), 1.83 – 1.71 (m, 6H), 1.51 – 1.33 (m, 16H), 1.06 (d, *J* = 6.3 Hz, 12H), 0.99 (t, *J* = 7.3 Hz, 6H), 0.91 (t, *J* = 7.0 Hz, 6H); ^{13}C NMR (101 MHz, $CDCl_3$) δ 168.8, 146.1, 145.7, 141.0, 140.8, 138.3, 132.5, 130.1, 126.0, 123.0, 122.6, 121.2, 120.8, 120.8, 120.6, 119.1, 118.2, 108.7, 107.1, 107.0, 44.2, 41.4, 37.8, 37.6, 30.7, 28.9, 26.9, 26.2, 24.2, 23.2, 22.6, 14.2, 10.9.IR ($\bar{\upsilon}$, cm^{-1}): 3045 (arene C−H, 3100-3000 cm^{-1}); 2956, 2927, 2870 (aliphatic C−H, 3000-2850 cm^{-1}); 1684 (C=O, 1750-1650 cm^{-1}); 1606, 1456, 1443(C-C in Ar, 1600-1585, 1500-1400 cm^{-1}); 1348, 1327, 1249 (C−N in Ar, 1350-1250 cm^{-1}); 877, 850, 809, 745, 723 (C−H in Ar, 900-

675 cm^{-1});m/z: 958 ($[M + H]^+$). Anal. Calcd for $C_{66}H_{76}N_4O_2$ (%):C 82.80, H 8.00, N 5.85, O 3.34. Found (%): C 82.70, H 8.09, N 5.91.

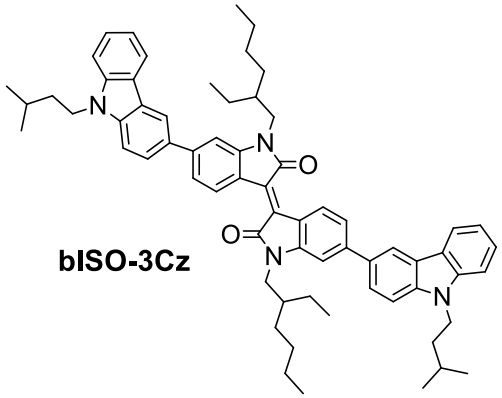

Chemical Formula: $C_{66}H_{76}N_4O_2$

1,1'-Bis(2-ethylhexyl)-6,6'-bis(9-isopentyl-9H-carbazol-3-yl)-isoindigo (**bISO-3Cz**) was synthesized by a similar procedure as compound **bISO-2Cz** using 1,1'-bis(2-ethylhexyl)-6,6′-dibromoisoindigo (**3-BCz**, 0.42 g, 0.65 mmol), 9-isopentyl-2-(4,4,5,5-tetramethyl-1,3,2-dioxaborolan-3-yl)-9H-carbazole (0.52 g, 1.4 mmol), potassium carbonate (0.34 g, 2.5 mmol), bis(triphenylphosphine) palladium(II) dichloride (0.05 molar equiv.), 15 mL of THF and 2.5 mL of degased water. After completion, the mixture was extracted with DCM, dried over Na_2SO_4, and concentrated. The crude product was purified by column chromatography using DCM/hexane (1:1) to give compound **bISO-3Cz** (0.38 g, 60 %) as dark violet crystals. m.p.: 237-238 ºC. ^{1}H NMR (400 MHz, $CDCl_3$) δ 9.26 (d, *J* = 8.3 Hz, 2H), 8.37 (d, *J* = 1.6 Hz, 2H), 8.18 (d, *J* = 7.7 Hz, 2H), 7.78 (dd, *J* = 8.5, 1.7 Hz, 2H), 7.55 – 7.46 (m, 4H), 7.46 – 7.40 (m, 4H), 7.28 (t, *J* = 7.5 Hz, 2H), 7.08 (s, 2H), 4.37 – 4.31 (m, 4H), 3.83 – 3.68 (m, 4H), 2.02 – 1.90 (m, 2H), 1.81 – 1.70 (m, 6H), 1.52 – 1.32 (m, 16H), 1.05 (d, *J* = 6.3 Hz, 12H), 0.98 (td, *J* = 7.3, 1.4 Hz, 6H), 0.92 (t, *J* = 7.0 Hz, 6H); ^{13}C NMR (101 MHz, $CDCl_3$) δ 169.0, 145.8, 145.8, 140.9, 140.4, 132.2, 131.7, 130.1, 126.2, 125.1, 123.6, 123.1, 120.8, 120.7, 120.4, 119.3, 118.9, 109.1, 109.0, 106.6, 77.2, 44.3, 41.6, 37.9, 37.7, 30.9, 29.0, 26.3, 24.3, 23.3, 22.8, 14.3, 11.0.IR ($\bar{\upsilon}$, cm^{-1}): 3042 (arene C−H, 3100-3000 cm^{-1}); 2953, 2930, 2868 (aliphatic C−H, 3000-2850 cm^{-1}); 1705 (C=O, 1750-1650 cm^{-1}); 1601, 1458, 1430(C-C in Ar, 1600-1585, 1500-1400 cm^{-1}); 1352, 1333, 1246(C−N in Ar, 1350-1250 cm^{-1}); 869, 854, 810, 735 (C−H in Ar, 900-675 cm^{-1}); m/z: 958 ($[M + H]^+$). Anal. Calcd for $C_{66}H_{76}N_4O_2$ (%):C 82.80, H 8.00, N 5.85, O 3.34. Found (%): C 82.68, H 8.07, N 5.90.

Chemical Formula: $C_{14}H_{11}Br_2NO_2$

3,6-Dibromo-2,7-dimethoxy-9H-carbazole was synthesized by a simple bromination procedure [217] using 2,7-Dimethoxycarbazole (**2DMCz**, 0.8 g, 3.5 mmol), NBS (2.5 g, 14 mmol) and 30 mL of DMF. The reaction mixture was stirred at room temperature for 1.5 hours. After TLC control the reaction mixture was poured into water and extracted with ethylacetate. The organic layer was dried with Na_2SO_4,

filtered and concentrated under vacuum. The residue was purified chromatographically using hexane and ethyl acetate (10 : 1) as the eluent. The yield of white crystals was 70 %(1.30 g, FW = 385 g/mol).

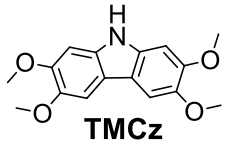

Chemical Formula: $C_{16}H_{17}NO_4$

2,3,6,7-Tetramethoxy-9H-carbazole was prepared by the methoxylation procedure [218] using metallic sodium (1.0 g, 3.1 mmol), absolute MeOH (16 ml), CuI (2.5 g, 4.2 mmol), dry DMF (33 ml) and 3,6-Dibromo-2,7-dimethoxy-9H-carbazole (1.0 g, 3.1 mmol) at a reflux temperature, which was stirred for 2 hours under an argon atmosphere. After TLC control the reaction mixture was cooled and EtOAc was added. Then the mixture was filtered through a glass filter and washed with water. The organic layer was dried with Na_2SO_4, filtered and concentrated under vacuum. The residue was purified chromatographically using hexane and acetone (10:1) as the eluent. The yield of white crystals was 51 %(0.45 g, FW = 287 g/mol).^{1}H NMR (400 MHz, DMSO) δ 10.61 (s, 1H), 7.56 (s, 2H), 6.97 (s, 2H), 3.83 – 3.82 (m, 12H). ^{13}C NMR (101 MHz, DMSO) δ 147.8, 143.4, 134.2, 115.0, 102.8, 94.9, 56.2, 55.7.IR ($\bar{\upsilon}$, cm^{-1}): 3405 (N−H, 3500-3200 cm^{-1}); 3003 (arene C−H, 3100-3000 cm^{-1}); 1491, 1473, 1446 (C-C in Ar, 1600-1585, 1500-1400 cm^{-1}); 1363, 1272(C−N in Ar, 1350-1250 cm^{-1}); 1223, 1196, 1159(C−O−C, 1250-1050 cm^{-1}); 837, 774 (C−H in Ar, 900-675 cm^{-1}); m/z: 288 ([M + H]$^+$).

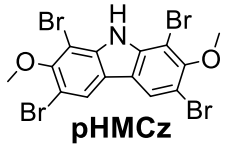

Chemical Formula: $C_{14}H_9Br_4NO_2$

1,3,6,8-Tetrabromo-2,7-dimethoxy-9H-carbazole was synthesized according to the procedure as compound **pTMCz** using 2,7-Dimethoxycarbazole (**2DMCz**, 1.1 g, 4.8 mmol), NBS (1.6 g, 9.2 mmol) and 25 mL of DMF. The reaction mixture was stirred at room temperature for 1.5 hours. The organic layer was dried with Na_2SO_4, filtered and concentrated under vacuum. The residue was purified chromatographically using hexane and ethyl acetate (10:1) as the eluent. The yield of white crystals was 72 %(1.38 g, FW = 543 g/mol).^{1}H NMR (400 MHz, DMSO) δ 11.37 (s, 1H), 8.53 (s, 2H), 3.87 (s, 6H).

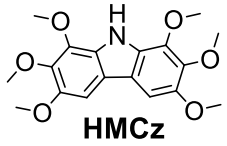

Chemical Formula: $C_{18}H_{21}NO_6$

1,2,3,6,7,8-Hexamethoxy-9H-carbazole was synthesized to the procedure as compound **TMCz** using 1,3,6,8-tetrabromo-2,7-dimethoxy-9H-carbazole (**pHMCz**, 0.40 g, 0.74 mmol), metallic sodium (0.34 g, 14.7 mmol), absolute MeOH (4 ml), CuI (0.84 g, 4.4 mmol), dry DMF (8 ml) and

at a reflux temperature, which was stirred for 2 hours under an argon atmosphere. After TLC control the reaction mixture was cooled and EtOAc was added. Then the mixture was filtered through a glass filter, washed with brine, dried with Na_2SO_4, filtered and concentrated under vacuum. The residue was purified chromatographically using hexane and acetone (10:1) as the eluent. The yield of white crystals was 7 % (0.018 g, FW = 347 g/mol). ^{1}H NMR (700 MHz, DMSO) δ 10.81 (s, 1H), 7.42 (s, 2H), 3.94 (s, 6H), 3.87 (s, 6H), 3.81 (s, 6H). The structure was proven by X-ray crystalography.IR ($\bar{\upsilon}$, cm^{-1}): 3431, 3408 (N−H, 3500-3200 cm^{-1}); 3023 (arene C−H, 3100-3000 cm^{-1}); 1574, 1494, 1468 (C-C in Ar, 1600-1585, 1500-1400 cm^{-1}); 1336, 1303, 1266(C−N in Ar, 1350-1250 cm^{-1}); 1219, 1206, 1159(C−O−C, 1250-1050 cm^{-1}); 827, 810 (C−H in Ar, 900-675 cm^{-1}); m/z: 348 ([M + H]$^+$).

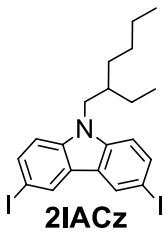

Chemical Formula: $C_{20}H_{23}I_2N$

9-(2-Ethylhexyl)-3,6-diiodo-9H-carbazole (**2IACz**) was prepared by the Tucker iodination [222] and alkylation reaction [226] procedure. ^{1}H NMR (400 MHz, $CDCl_3$) δ 8.32 (d, *J* = 1.4 Hz, 2H), 7.70 (dd, *J* = 8.6, 1.7 Hz, 2H), 7.14 (d, *J* = 8.6 Hz, 2H), 4.07 (dd, *J* = 7.5, 2.1 Hz, 2H), 2.01 – 1.94 (m, 1H), 1.38 – 1.21 (m, 8H), 0.92 – 0.83 (m, 6H).

General procedure for Ullmann reaction. To a solution of 9-(2-ethylhexyl)-3,6-diiodo-9H-carbazole (**2IACz**,1 equiv.) and methoxysubstituted carbazole (2.2 equiv.) in o-DCB was added potassium carbonate (8 equiv.) at 110 ºC, 18-crown-4 (5 mol %) and copper powder (4 equiv.) at 150 ºC and refluxed under argon at 180 ºC. After TLC control the reaction was stopped, cooled and filtered. The solvent was removed under reduced pressure and the residue was purified chromatographically using respective eluent.

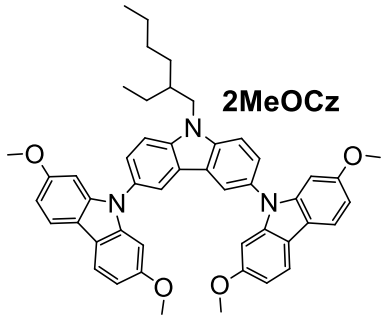

Chemical Formula: $C_{48}H_{47}N_3O_4$

3,6-Bis(2,7-dimethoxycarbazole-9-yl)-9-(2-ethylhexyl)carbazole (**2MeOCz**). Synthesis according to the general procedure using 9-(2-ethylhexyl)-3,6-diiodo-9H-carbazole(**2IACz**, 0.30 g, 0.56 mmol), 2,7-dimethoxycarbazole(**2DMCz**, 0.28 g, 1.3 mmol), potassium carbonate (0.62 g, 4.5 mmol), 18-crown-4 (0.007 g, 5 mol %) and copper powder (0.14 g, 2.3 mmol). The product was purified chromatographically using hexane:ethylacetate (20:1) as the eluent. Yield of white powder was 68 % (0.28 g, FW = 730 g/mol). m.p.: 290-291 ºC.^{1}H NMR (700 MHz, $CDCl_3$) δ 8.22 (d, *J* = 1.8 Hz, 2H), 7.92 (d, *J* = 8.5 Hz, 4H), 7.68 – 7.62

(m, 4H), 6.87 (dd, *J* = 8.5, 2.2 Hz, 4H), 6.78 (d, *J* = 2.1 Hz, 4H), 4.41 – 4.33 (m, 2H), 3.79 (s, 12H), 2.27 – 2.21 (m, 1H), 1.59 – 1.34 (m, 8H), 1.07 (t, *J* = 7.4 Hz, 3H), 0.94 (t, *J* = 7.3 Hz, 3H); ^{13}C NMR (101 MHz, $CDCl_3$) δ 158.5, 143.5, 140.9, 129.4, 126.1, 123.6, 120.2, 119.9, 117.4, 110.7, 108.1, 94.4, 77.2, 55.8, 48.2, 39.9, 31.2, 29.0, 24.7, 23.3, 14.2, 11.2. IR ($\bar{\upsilon}$, cm^{-1}): 3015 (arene C−H, 3100-3000 cm^{-1}); 2942, 2930, 2890 (aliphatic C−H, 3000-2850 cm^{-1}); 1503, 1477, 1433 (C-C in Ar, 1600-1585, 1500-1400 cm^{-1}); 1341, 1293(C−N in Ar, 1350-1250 cm^{-1}); 1205, 1165, 1135 (C−O−C, 1250-1050 cm^{-1}); 834, 817, 798, 764 (C−H in Ar, 900-675 cm^{-1}); m/z: 731 ($[M + H]^+$). Anal. Calcd for $C_{48}H_{47}N_3O_4$ (%):C, 78.98; H, 6.49; N, 5.76; O, 8.77. Found (%): C 78.82, H 6.56, N 5.84.

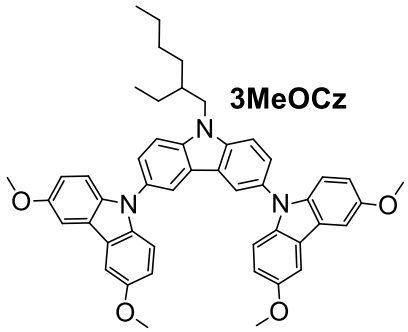

Chemical Formula: $C_{48}H_{47}N_3O_4$

3,6-Bis(3,6-dimethoxycarbazole-9-yl)-9-(2-ethylhexyl)carbazole (**3MeOCz**). Synthesis according to the general procedure using 9-(2-ethylhexyl)-3,6-diiodo-9H-carbazole(**2IACz**, 0.23 g, 0.43 mmol), 3,6-dimethoxycarbazole(**3DMCz**, 0.22 g, 0.95 mmol), potassium carbonate (0.48 g, 3.5 mmol), 18-crown-4 (0.006 g, 5 mol %) and copper powder (0.11 g, 1.7 mmol). The product was purified chromatographically using hexane:ethylacetate (20:1) as the eluent. Yield of white powder was 75 % (0.24 g, FW = 730 g/mol). m.p.: 203-204 ^{o}C. ^{1}H NMR (700 MHz, $CDCl_3$) δ 8.21 – 8.19 (m, 2H), 7.62 (d, *J* = 1.2 Hz, 4H), 7.59 (d, *J* = 2.5 Hz, 4H), 7.30 (d, *J* = 8.9 Hz, 4H), 7.04 (dd, *J* = 8.9, 2.5 Hz, 4H), 4.37 – 4.30 (m, 2H), 3.96 (s, 12H), 2.25 – 2.19 (m, 1H), 1.58 – 1.33 (m, 8H), 1.04 (t, *J* = 7.4 Hz, 3H), 0.94 (t, *J* = 7.3 Hz, 3H); ^{13}C NMR (176 MHz, $CDCl_3$) δ 154.0, 140.6, 137.6, 129.9, 125.8, 123.5, 123.4, 119.5, 115.3, 110.8, 110.4, 103.1, 77.2, 56.3, 48.1, 39.8, 31.2, 29.0, 24.7, 23.3, 14.2, 11.2. IR ($\bar{\upsilon}$, cm^{-1}): 3005 (arene C−H, 3100-3000 cm^{-1}); 2967, 2945 (aliphatic C−H, 3000-2850 cm^{-1}); 1531, 1442, 1412 (C-C in Ar, 1600-1585, 1500-1400 cm^{-1}); 1352, 1295(C−N in Ar, 1350-1250 cm^{-1}); 1208, 1172, 1120(C−O−C, 1250-1050 cm^{-1}); 842, 810, 771, 752 (C−H in Ar, 900-675 cm^{-1}); m/z: 731 ($[M + H]^+$). Anal. Calcd for $C_{48}H_{47}N_3O_4$ (%):C, 78.98; H, 6.49; N, 5.76; O, 8.77. Found (%): C 78.85, H 6.53, N 5.86.

3,6-Bis(2,3,6,7-tetramethoxycarbazole-9-yl)-9-(2-ethylhexyl)carbazole (**TMeOCz**). Synthesis according to the general procedure using 9-(2-ethylhexyl)-3,6-diiodo-9H-carbazole(**2IACz**, 90 mg, 0.17 mmol), 2,3,6,7-

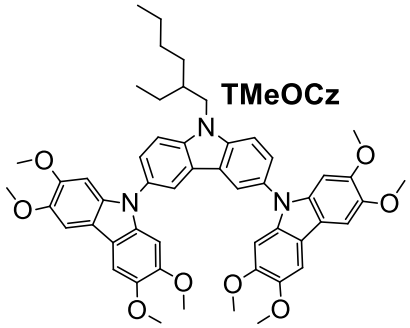

dimethoxycarbazole(**TMCz**, 107 mg, 0.37 mmol), potassium carbonate (187 mg, 1.3 mmol), 18-crown-4 (2 mg, 5 mol %) and copper powder (43 mg, 0.68 mmol). The product was purified chromatographically using hexane:ethylacetate (20:1) as the eluent. Yield of white powder was 42 % (60 mg, FW = 850 g/mol). ^{1}H NMR (700 MHz, $CDCl_3$) δ 8.25 (d, *J* = 1.8 Hz, 2H), 7.67 (d, *J* = 41.3 Hz, 4H), 7.50 (s, 4H), 6.82 (s, 4H), 4.42 – 4.34 (m, 2H), 4.04 (s, 12H), 3.82 (s, 12H), 2.28 – 2.23 (m, 1H), 1.60 – 1.35 (m, 8H), 1.08 (t, *J* = 7.4 Hz, 3H), 0.93 (t, *J* = 7.3 Hz, 3H); ^{13}C NMR (101 MHz, $CDCl_3$) δ 148.5, 144.7, 140.8, 136.5, 130.0, 126.1, 123.6, 119.7, 115.5, 110.7, 102.1, 93.8, 77.2, 56.8, 56.4, 48.2, 39.9, 31.2, 28.9, 24.7, 23.3, 14.2, 11.2. IR ($\bar{\upsilon}$, cm^{-1}): 3010 (arene C−H, 3100-3000 cm^{-1}); 2953, 2924, 2854 (aliphatic C−H, 3000-2850 cm^{-1}); 1613, 1487, 1474, 1438 (C-C in Ar, 1600-1585, 1500-1400 cm^{-1}); 1340, 1296(C−N in Ar, 1350-1250 cm^{-1}); 1197, 1163, 1105 (C−O−C, 1250-1050 cm^{-1}); 848, 836, 814, 753(C−H in Ar, 900-675 cm^{-1}); m/z: 851 ($[M + H]^+$).

4. RESULTS AND DISCUSSION

4.1 Isomeric diphenylethenyl-disubstituted dimethoxycarbazoles

Carbazole derivatives have attracted much attention because of their flexible synthesis and wide range of applications, such as organic light emitting diodes, organic thin film transistors and solid-state dye-sensitized solar cells [227-230]. The carbazole moiety can be easily modified via its C-3 and C-6 positions [231]. There is a substantial number of studies on 3,6-substituted carbazole derivatives and on their optoelectronic applications. In comparason, less research was done on 2,7-substituted carbazole derivatives. Until recently, the main obstacle was the lack of an efficient synthesis procedure for these compounds. The obstacle disappeared when convenient synthetic pathways towards 2,7-dihalocarbazoles were reported [232,233]. Since then, ongoing studies of 2,7-disubstituted carbazole compounds revealed substantially higher hole mobilities compared to those of 3,6-disubstituted counterparts [5]. In this work, the convenient synthetic method of 2,7-diphenylethenyl disubstituted carbazole derivative by the direct reaction of 3,6-dimethoxy substituted carbazole derivative with diphenylacetaldehyde is demonstrated. During research the isomeric compound from 2,7-dimethoxy substituted carbazole derivative was synthesized and a comparative study of the properties of the obtained materials using theoretical and experimental tools was performed. Diphenylethenyl-disubstituted derivatives of carbazole were earlier prepared by the multi-step synthetic route, the last step of which was Pd-catalyzed Suzuki coupling of diphenylethenyl borolane with the corresponding dibromocarbazole derivatives [234,235], which showed good performance as hole-transporting blue emitters in electroluminescent devices. In some fields of application, such as dye-sensitized solar cells, electrochemically stable hole-transporting materials with low ionization potentials are required. It is known that the introduction of methoxy groups into the structures of aromatic amines, as well as the attachment of methoxy-substituted diphenylamino groups to the carbazole moieties, lead to the decrease of the ionization potential [12,13]. The possibility to monitor ionization potentials is also important in the fabrication of OLEDs. The hole-injection barrier differences can strongly affect the efficiency of the devices. The role of the methoxy groups is found to be related to the mesomeric (p-donor) effect and the possibility to establish hydrogen bonds [236]. The stronger influence was observed for *para*-methoxy substituted derivatives, as compared to *ortho*- and *meta*-methoxy substituted derivatives [13,236]. The *para*-methoxy substituted derivatives also showed the highest hole mobilities [13,236]. The effect of the methoxy substitution in carbazole derivatives on their photophysical and photoelectrical properties, to the best of our knowledge, has not yet been studied. Electrochemical and thermal stability is another important property of organic semiconductors. This can lead to the corresponding device degradation [237-240]. It

is known that 2,7-substituted derivatives of carbazole show irreversible oxidation with the formation of new carbazolyl derivative [241]. By introducing methoxy or diphenylethenyl groups into C-3 and C-6 positions of carbazole moiety compounds have been obtained that demonstrate reversible oxidation and higher electrochemical and thermal stability, in contrast to the non-substituted counterparts [5,234].

4.1.1 Synthesis

Diphenylethenyl-substituted dimethoxycarbazoles (**3a**, **3b**) were synthesized by condensation of the appropriate derivative of dimethoxycarbazole with diphenylacetaldehyde (Scheme 4.1). This synthetic method of diphenylethenyl-disubstituted derivatives is superior with respect of that reported earlier for the synthesis of the similar derivatives containing no methoxy groups [234]. It does not require the preparation of diphenylethenyl borolane and bromination of carbazole.

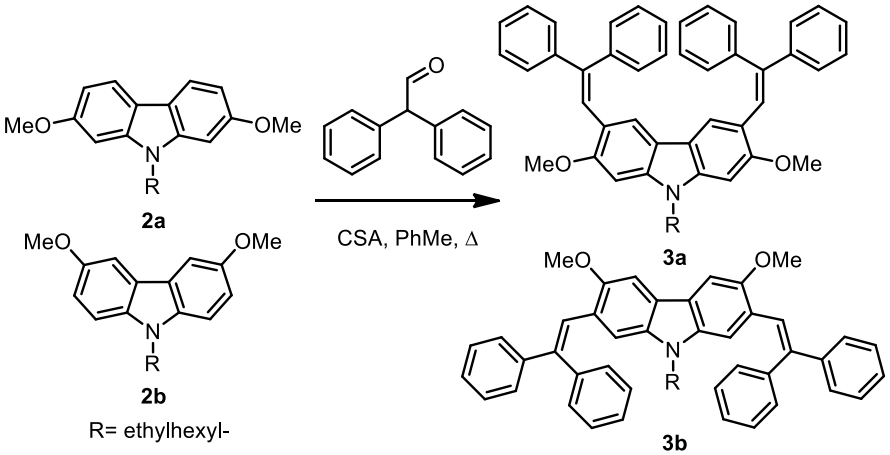

Scheme 4.1. Synthesis of **3a** and **3b**

The starting compound **2a** was prepared by three steps. 2,7-Dimethoxycarbazole (**1a**) was obtained by an Ullmann-coupling followed by a Cadogan cyclization reaction using triphenylphosphine as reported in literature [215,216]. Alkylation with 2-ethylhexylbromide was performed by the conventional procedure [242]. Compound **2b** was synthesized starting from 3,6-dimethoxycarbazole (**1b**), which was prepared by bromination of carbazole with N-bromosuccinimide (NBS) in dimethylformamide (DMF), followed by the direct methoxide displacement of bromine [217,218] and alkylation by the same procedure as mentioned above. The synthesized compounds were identified by elemental analysis, IR, ^{1}H and ^{13}C NMR, and MS. Compounds **3a**, **3b** were found to be soluble in common organic solvents such as tetrahydrofuran, toluene and chloroform.

4.1.2 Crystal structures

According to quantum chemical calculations molecular structures of 2,7-dimethoxycarbazole, derivatives (**2a**, **3a**) exhibit relatively high ground state dipole moments (4.53 and 5.98 D, accordingly). At the same time, the derivatives of 3,6-dimethoxycarbazole (**2b**, **3b**) are non-polar with low ground state dipole moments (0.30 and 0.69 D). Therefore, one could expect much stronger intermolecular dipole – dipole interaction in case of crystals of **3a** than for **3b**, which in the absence of molecular dipole is built by weaker London dispersion forces. The oak ridge thermal ellipsoid plot (ORTEP) projections of **3a-b** are shown in Fig. 4.1and the crystallographic data is listed inTable 4.1.

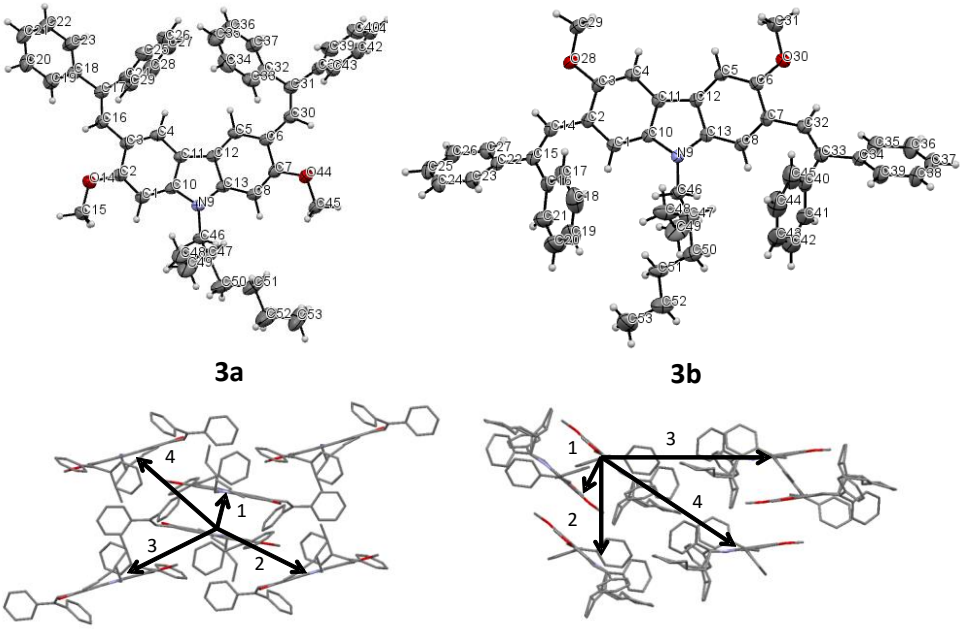

Fig. 4.1. ORTEP diagrams, packing in the crystals and the possible intermolecular charge-hopping channels of **3a-b**

The racemic compound **3a** crystallizes into the orthorhombic crystal system with space group P-b-c-a. The π-frameworks of **3a** have non-planar geometry and the alkyl chains are extended out of the molecular plane. The analysis of the packing pattern of the molecules of **3a** in the crystalline state revealed that the molecules form columns of alternating opposite interactions, such as C-H···O bonding, which occurs between the enantiomers held together with the different kinds of weak hydrogen atom at C-15 and the oxygen atom O-44 of methoxy groups with the distance of 2.664 Å, C-H···C bonding, which occurs between the hydrogen atom at C-15 and the carbon atom C-45 or between the hydrogen atom at C-53 and the carbon atom C-16 with the distances of 2.712 Å and 2.738 Å, respectively. The distances along the different planes of carbazole rings vary from 3.54 to 3.63 Å. The crystal of

3b is formed from (*S)*-enantiomer only and is held by C-H···C interactions between the hydrogen atoms at C-29, C-31 and C-49, and carbon atoms C-8, C-6, C-3 and C-10 with the distances of 2.861, 2.899, 2.874 and 2.785 Å, respectively. The C-H···O interactions between the molecules of **3b** was not observed. The angles between ethenyl double bond and the carbazole plane of the molecules **3a** (28.5˚, 22.4˚) and **3b** (26.1˚, 22.5˚) were measured. These values were found to be comparable to those of 2-methoxycarbazole 3,6-disubstituted with the diphenylethenyl moieties (30.11˚, 23.78˚) [243].

Table 4.1. Crystalographic data of **3a** and **3b**

	3a	**3b**
Chemical formula	$C_{50}H_{49}NO_2$	$C_{50}H_{49}NO_2$. ½ CH_3OH
Crystal system	orthorhombic	monoclinic
Formula weight	695.93	695.93
Shape	yellow plate	yellow plate
Space group	P b c a	P 21/n
***a* / Å**	16.3265(2)	20.8163(5)
***b* / Å**	18.2018(2)	7.6277(2)
***c* / Å**	26.5776(3)	26.4292(5)
***α* / º**	90.00	90.00
***β* / º**	90.00	91.0202(15)
***γ* / º**	90.00	90.00
***V* / Å^3**	7898.1(2)	4195.78(17)
Z	8	2
***D* / g cm^{-3}**	1.171	1.118
***Measurement temp.*/ K**	173	193

4.1.3 Thermal properties

The thermal properties of the synthesized compounds were estimated by DSC and TGA. The thermal characteristics are collected in Table 4.2. Compounds **3a** and **3b** possess high thermal

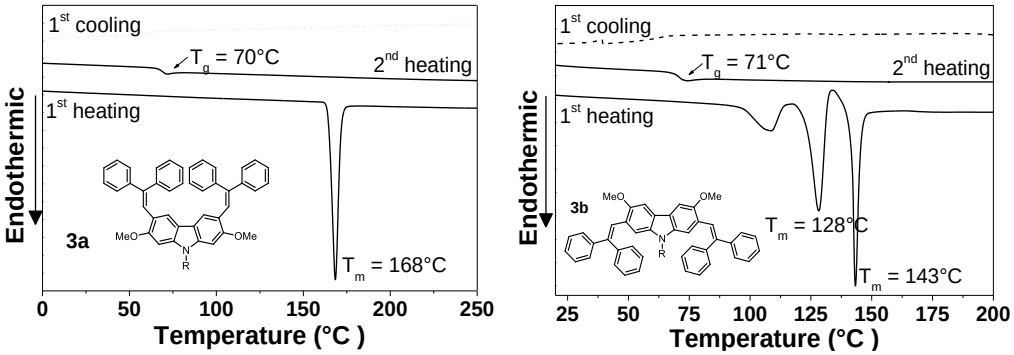

Fig. 4.2. DSC curves of **3a** and **3b** (scan rate 10 °C/min, N_2 atm.)

stability with 5% weight loss temperatures (T_d) of 405 °C and 376 °C, respectively. The DSC measurements showed that **3a** and **3b** are able to form molecular glasses. Compounds **3a** and **3b** were isolated after the synthesis as crystalline substances and their first DSC heating scans revealed endothermal melting signals (Fig. 4.2.). Due to the presence of stronger dipole – dipole interactions the crystals of **3a** showed by 25 °C higher melting point than those of **3b**. Compound **3b** exhibited polymorphism, which is rather often observed for organic glass forming molecular materials [244]. The ability to form more than one crystal structure could be the result of the weak dipole-dipole interaction between the molecules of **3b** [245]. No crystallization was observed during the cooling scans, which indicated the transition from the melt to the glassy state. In the second and the following DSC heating scans **3a** and **3b** exhibited glass transitions at 70 and 71 °C, respectively. This observation shows that the linking topology of **3a-b** has no effect on their glass transition temperatures.

4.1.4 Optical and photophysical properties

The normalized absorption and fluorescence spectra of the dilute solutions in THF and the solid films of **3a** and **3b** are shown in Fig. 4.3.

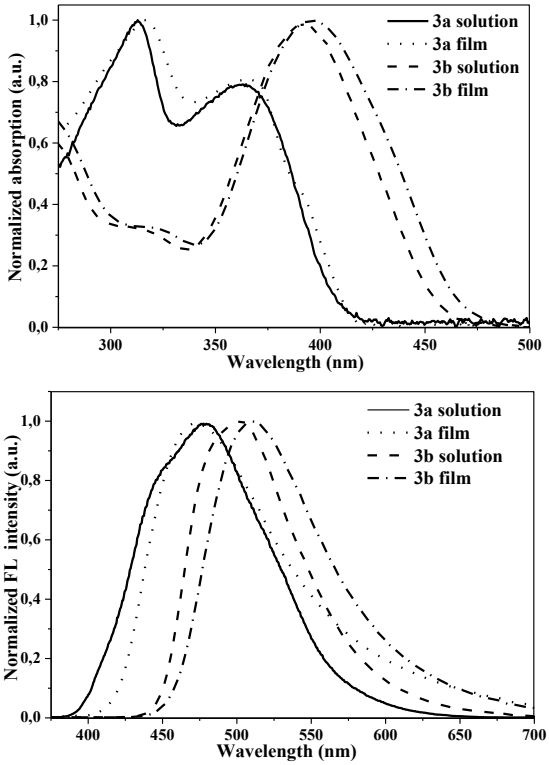

Fig. 4.3. UV-vis and fluorescence spectra of dilute THF solutions (10^{-5} M) and of the films of compounds **3a**, **3b**. λ_{ex}= 350 nm

The optical and photophysical characteristics are summarized in Table 4.2. The absorption maxima of the dilute solutions of **3a** and **3b** were detected at 362 nm and 392 nm, respectively. UV-vis spectrum of **3b** showed considerable bathochromic effect of 30 nm with respect to the spectrum of its counterpart **3a**. These results provide evidence for more effective and prolonged conjugation length in **3b** compared to **3a** [246].

Table 4.2. Thermal,optical and photophysical characteristics of compounds **3a** and **3b.**

	T_m / T_g [a] / T_d [b], °C	$\lambda^{abs}_{max\ sol}$ / $\lambda^{abs}_{max\ film}$, nm	$\lambda^{em}_{max\ sol}$ / $\lambda^{em}_{max\ film}$, nm	Stokes shift, nm	Φ_{sol}/ Φ_{film}, %	τ_{sol}/ τ_{film}, ns	χ^2_{sol}/ χ^2_{film} [c, d]	$k_{r\ sol}$ / $k_{r\ film}$, 10^8 s^{-1} [c]	$k_{nr\ sol}$ / $k_{nr\ film}$, 10^8 s^{-1} [c]
3a	168 / 70 / 405	362 / 365	473 / 476	111	1.20 / 2.20	0.10 (96%), 5.48 (4%) / 0.28 (86%), 3.7 (14%)	1.08/1.18	1.2 / 0.8	98.8 / 34.9
3b	128,143 / 71 / 376	392 / 396	501 / 510	109	34.9/ 11.8	3.96 / 0.69(77%), 3.03(23%)	1.07/1.21	0.9 / 1.7	1.6 / 12.8

[a] - determined by DSC, scan rate 10 °C/min, N_2 atmosphere; [b] - 5% weight loss determined by TGA, heating rate 10 °C/min, N_2 atmosphere; [c] counted for the most prevalent state; [d] the chi-square values show the quality of the fit.

Compounds **3a** and **3b** showed emission in the blue and green regions with the emission maxima at 473 and 501 nm, respectively. Fluorescence spectra of **3a** and **3b** exhibited considerable red shifts with respect to those of the starting compounds (**2a** and **2b**, Fig. 4.4).

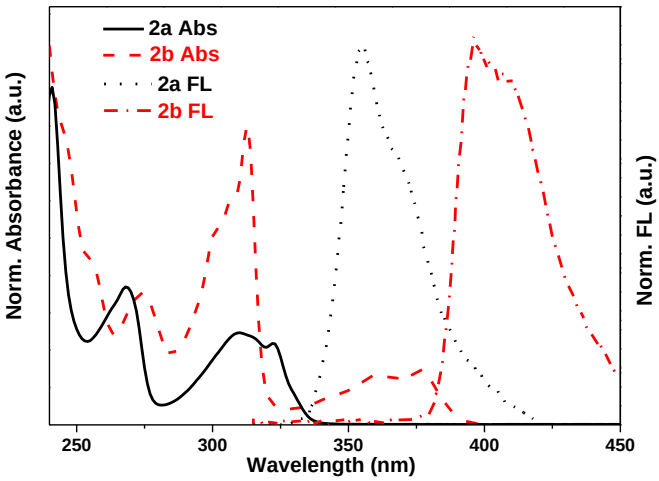

Fig. 4.4. UV-vis and fluorescence spectra of dilute THF solutions (10^{-5} M) of compounds **2a**, **2b**. λ_{ex}= 350 nm

The target compounds **3a** and **3b** are characterized by long Stokes shifts (~110 nm), which implies that the structures of the emitting state and ground state are rather different. This difference apparently originates from the zwitterionic state of the excited molecules **3a-b** [247,248]. The absorption and emission spectra of the solvent casted solid amorphous films of **3a** and **3b** were found to be similar to the corresponding spectra of the solutions, but exhibited small red-shifts. Both the solid films and the dilute solutions of **3b** showed higher fluorescence quantum yields as compared to those of **3a**. This observation can be explained by the different zwitterionic states of 3,6-dimethoxy- and 2,7-dimethoxycarbazoles containing diphenylethenyl moieties [234]. Compound **3a** exhibited the phenomenon of aggregation induced emission, which is illustrated by Fig. 4.5a.

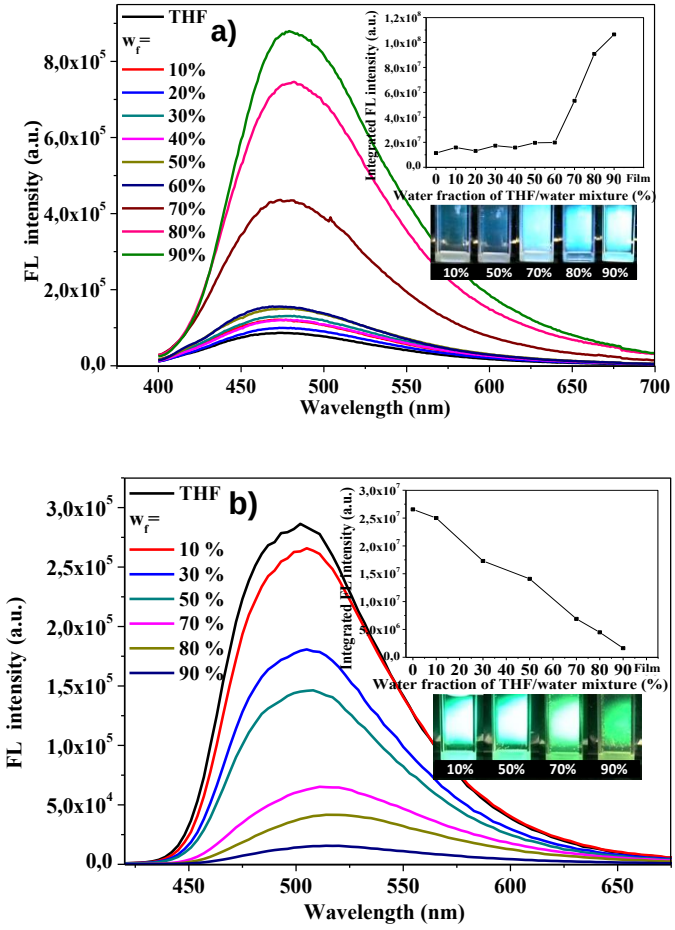

Fig. 4.5. Fluorescence spectra of the molecular dispersions of **3a** (a) and **3b** (b) in water–THF mixtures (10^{-4}–10^{-5} M). The inset depicts the changes of fluorescence peak intensity. (w_f -water fraction of THF/water mixture (%)).λ_{ex}= 350 nm

The FL intensity of the THF solution was very low and was almost unchanged when water was added up to 60% (*v/v*), but then started to increase sharply upon further addition of water. These results indicate that the molecules of compound **3a** started to aggregate when the volume fraction of water reached 70%. Clearly, the fluorescence behavior of **3a** is typical of an AIE luminogen [249]. The high ground state dipole moment and high dipole-dipole interaction between the molecules of compound **3a** results the restrictions of the molecular motions, which can be a key factor explaining the aggregation induced emission [250]. The X-ray analysis data of **3a** (Fig. 4.1) show that the neighboring dimers, which are arranged parallel but with the opposite induced dipole moments (IDM) of the excited state, can form configuration favorable for the formation of J-aggregates [251]. This presumption is confirmed by fluorescence spectroscopy. The intensity maxima of aggregation induced emission are batochromically shifted by ca. 15 nm compared to the emission maxima of dilute solutions in THF. The totally opposite effect of aggregation-caused quenching was observed for isomer **3b** (Fig. 4.5b). In the case of **3b**, the closest dimers are parallel and IDM (Fig. 4.1) are of the opposite direction. However, the ground state dipole moment of **3b** is very small (0.69 D). Therefore IDM is also small and they have no substantial effect on IDM of the surrounding molecules. For this reason, no shift in fluorescence spectra was observed and the aggregation induced quenching was monitored. Fig. 4.6 shows fluorescence decay curves of the dilute THF solutions and of the solid films of **3a** and **3b**.

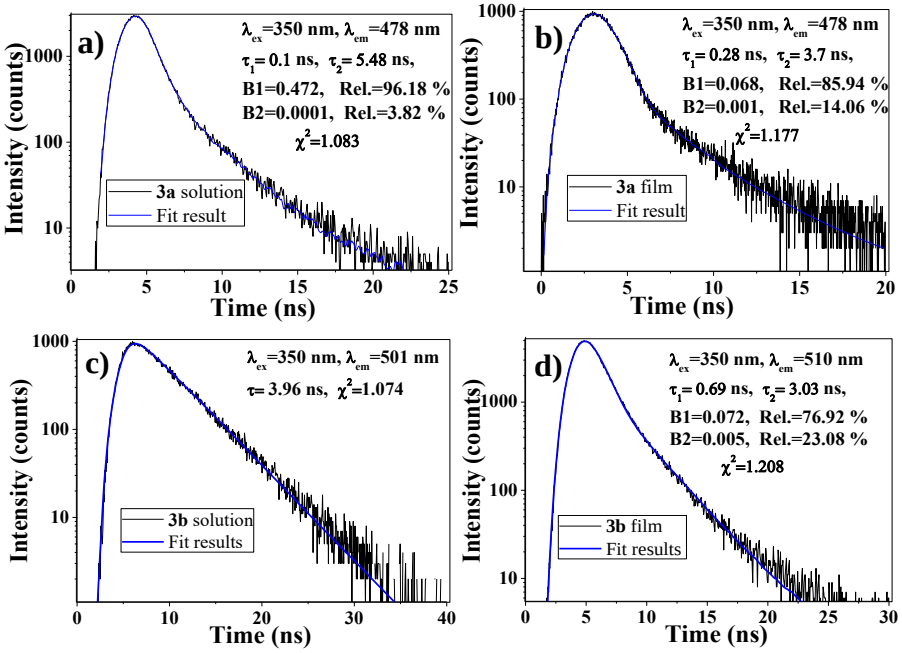

Fig. 4.6. Fluorescence decay curves of the dilute (10^{-5}M) solutions in THF and of the solid films of **3a** (a,b) and **3b** (c,d). Blue lines indicate single or double exponential fits to the experimental data. Fluorescence lifetimes (τ) are indicated

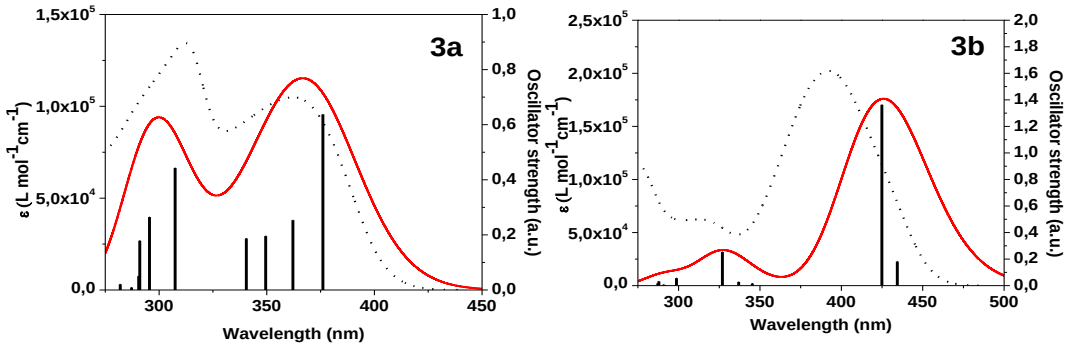

Fig. 4.7. Comparison of the experimental (black-dot) and calculated **3a** and **3b** (red) UV-vis spectra at the B3LYP/6-31G(d,p)/PCM(THF) level (σ = 0.25 eV); bars represent the oscillator strength

Table 4.3. Properties of the selected transitions and their contribution to the UV-vis spectra of **3a-b** calculated at the B3LYP/6-31G(d,p)/PCM(THF) level

	Exp UV λ, nm	Cal UV λ, nm	Tr.	Osc. Stren. a.u.	Contributions (more than 20%)
3a	362	376	1	0.637	H→L (95%)
		362	2	0.254	H-1→L (90%)
	312	307	5	0.443	H→L+2 (77%)
		296	6	0.265	H-1→L+2 (63%)
3b	392	434	1	0.181	H→L(63%),H-1→L(35%)
		425	2	1.363	H→L(35%),H-1→L(63%)
	317	327	5	0.253	H-2→L(67%)

The derivative **3a** exhibited double exponential fluorescence decays originating from two different molecular excited states with the fluorescence life times (τ) of 0.10 and 5.48 ns for the solution and 0.28 ns 3.7 ns for the film with χ^2 ranging from 1.08 to 1.18 respectively. The fluorescence decay of the film of compound **3b** can also be described by the double exponential fit with the fluorescence lifetimes of 0.69 ns and 3.03 ns with χ^2 value of 1.21, while fluorescence decay of the dilute solution of **3b** was adequately described by the single exponential curve with the lifetime of 3.96 ns (χ^2 = 1.07). It is presumed that the emission with the shorter life time (0.1-0.7 ns) originates from the excited dimethoxycarbazole moiety, while the emission with the longer life time (3.0-5.5 ns) originates from the excited zwitterionic states of **3a-b** derivatives. To unveil the contributions of the competing radiative and nonradiative relaxation processes, the radiative (k_r) and nonradiative (k_{nr}) decay rate constants were calculated from the singlet excited state using the obtained values of Φ and τ by the following relations: $k_r = \Phi / \tau$, $k_{nr} = (1-\Phi) / \tau$. The results are summarized in Table 4.2. Interestingly, the calculated k_r and k_{nr} values of **3a-b** were found to be highly dependent on the position of methoxy and

diphenylethenyl moieties. For both the isomers **3a-b** the k_r values obtained for the solutions and the solid films showed no large differences, while the values of k_{nr} observed for the solutions and films of **3a** were found to be significantly higher than those of **3b**. Thus the nonradiative processes are predominant in the relaxation processes of excited states of compound **3a**.

In order to get more insight on the nature of the absorption bands of **3a-b**, TD-DFT calculations were performed. The significant similarities between the theoretical and experimental UV-vis spectra of **3a-b** were observed (Fig. 4.7). The excitation energies and oscillator strengths for the molecules **3a-b** are presented in Table 4.3.

The lowest energy band for **3a** is influenced by two transitions $S_0 \rightarrow S_1$ and $S_0 \rightarrow S_2$ with the maxima of ε at 376 and 362 nm, respectively. The first excitation with the oscillator strength of 0.637 for **3a** corresponds to the HOMO→LUMO transition (Fig. 4.8). This transition is localized on the diphenylethenyl and dimethoxycarbazole moieties. Therefore, this excitation corresponds to π-π^* transition for both conjugated chromophores. The absorption band with the maximum at 312 nm of **3a** corresponds to the calculated $S_0 \rightarrow S_5$ and $S_0 \rightarrow S_6$ transitions.The $S_0 \rightarrow S_5$ transition, according to the nomenclature of Platt [252] is named as ^1L_a transition because the orbitals on the carbazole moiety are oriented along the symmetry axis [253]. The absorption band with the similar wavelength for *N*-substituted 2,7-dimethoxycarbazole was observed experimentally [254]. Therefore, these excitations are assigned to π-π^* transition in the dimethoxycarbazole moiety. The situation with **3b** was found to be different. The lowest energy absorption band of **3b** is influenced by two lower energy transitions compared to those of **3a**, i.e. $S_0 \rightarrow S_1$ and $S_0 \rightarrow S_2$ transitions which manifest themselves at 434 and 425 nm, respectively. The attachment of methoxy groups at the C-3 and C-6 positions of the carbazole ring generates the intramolecular charge transfer (ICT) from carbazole to diphenylethenyl moieties, which subsequently results in the zwitterionic state. A positive charge is delocalized at the C-3 or C-6 positions of the carbazole moiety and a negative charge is on the diphenylethenyl moiety. The first $S_0 \rightarrow S_1$ excitation with the oscillator strength of 0.181 a.u of **3b** corresponds to the HOMO→LUMO and HOMO-1→LUMO transitions with 63 and 35 % contributions, respectively (Fig. 4.8). This excitation is a mixture of the π-π^* transitions of both conjugated chromophores and ICT transition from carbazole to diphenylethenyl moieties. In other words, $S_0 \rightarrow S_1$ can be regarded as zwitterionic transition in nature [234]. The electron density in the carbazole ring is delocalized symmetrically because of the ICT transition. The second $S_0 \rightarrow S_2$ excitation at 425 nm corresponds to the same $S_0 \rightarrow S_1$ transition, but the orbital contributions are 35 and 63 %, respectively. Similarly, this excitation is a mixture of the π-π^* transition of both conjugated chromophores and ICT transition from the carbazole to the diphenylethenyl moiety. The obtained oscillator strength (0.181 a.u) of the first excitation of **3b** is lower than that of **3a**. The UV absorption band at 317 nm is

influenced by $S_0 \rightarrow S_5$ excitation, which corresponds to the HOMO-2→LUMO transition. This $S_0 \rightarrow S_5$ excitation is the mixture of π-π^* transitions in the diphenylethenyl and carbazole chromophores. The energies of HOMO and LUMO of **3a-b** were calculated using the same method as for UV-vis spectra. The energies of HOMO and LUMO for **3a** were found to be -4.97 eV and -1.16 eV, respectively, and those observed for **3b** were -4.93 eV and -1.60 eV, respectively. The calculated HOMO energy levels are in good agreement with the experimental values (Table 4.4).

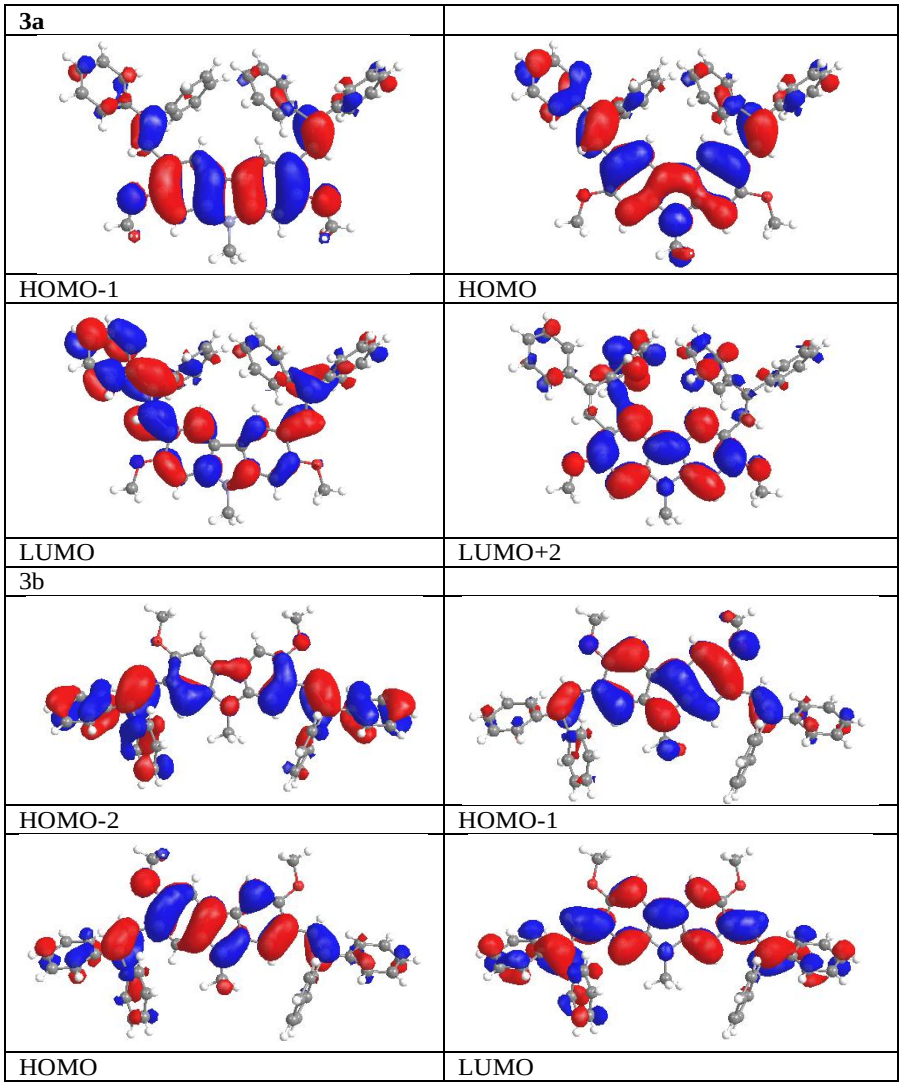

Fig. 4.8. The computed spatial distributions of HOMO and LUMO orbitals for **3a** and **3b**

4.1.5 Electrochemical properties and ionization potentials

Electrochemical properties of the solutions of the compounds in dichloromethane with 0.1 M tetrabutylammonium hexafluorophosphate as a supporting electrolyte were studied by the cyclic voltammetry using $Ag/AgNO_3$ as the reference electrode and a Pt wire counter electrode. The electrochemical characteristics are summarized in Table 4.4. The CV curves of **3a-b** are shown in Fig. 4.10.

Table 4.4. Electrochemical characteristics of **3a**, **3b** and **2a**, **2b**

	E_{onset}, V [a]	$E_{ox,pa}$, V [a]	$E_{ox,pc}$, V [a]	E_{HOMO}/ $E_{HOMO}{}^{DFT}$, eV [c]	E_g,eV[d]	IP, eV[e]
2a	0.41	0.53	- [f]	-5.17 / -	3.69	5.68
2b	0.35	0.51	0.33	-5.09 / -	3.16	5.50
3a	0.33	0.45	0.35	-5.06 / -4.97	3.05	5.38
3b	0.31	0.43	0.33	-5.03 /- 4.93	2.72	5.41

[a] Onset, oxidation and reduction potentials vs Fc.[c] $E_{HOMO(eV)} = -1.4E_{onset,ox(V)} - 4.6$, where $E_{onset,ox}$ was determined by solution-based CV [255].[d] The optical bandgap energies estimated from the absorption edges. [e] Ionization energy (*IP*) for the solid films was measured by the electron photoemission in air method. [f] Irreversible oxidation

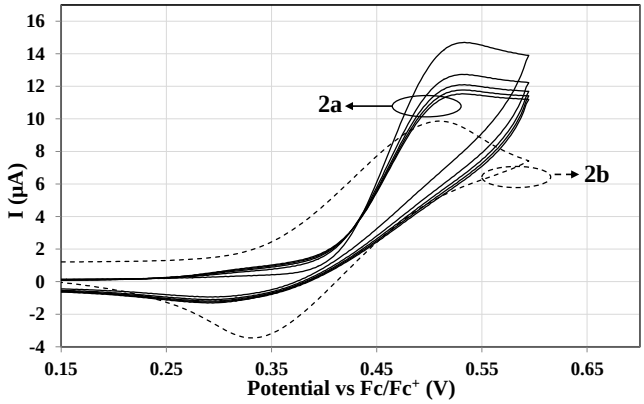

Fig. 4.9. Cyclic voltammograms of **2a-b** at 10^{-3} mol L^{-1} in a solution of in argon-purged TBAP (0.1 M) in CH_2Cl_2. v = 50 mV/s

No reduction waves were observed down to ca -1.5 V in CV curves of all the studied compounds. However, all the compounds showed the oxidation waves up to ca 0.31 V. The oxidation was only found to be irreversible for compound **2a** (Fig. 4.9), having unsubstituted C-3 and C-6 positions of carbazole ring. It was found to be quasi-reversible for **2b**. Irreversible oxidation of **2a** was followed by coupling of carbazole radical cations because of the higher electron spin density at the C-3 and C-6 positions [256] and formation of new carbazolyl-containing compounds [241].

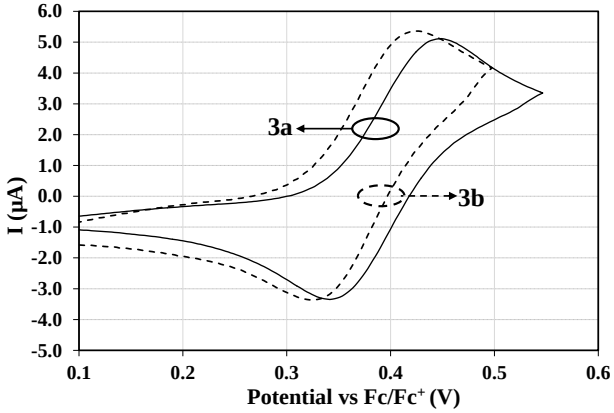

Fig. 4.10. Cyclic voltammograms of **3a-b** at 10^{-3}mol L^{-1} in a solution of argon-purged TBAP (0.1M) in CH_2Cl_2. *v*= 50 mV/s

The oxidation of **3a** and **3b** was found to be reversible up to ca 0.55 V. Precursor **2b** and compounds **3a-b** showed oxidation peaks at 0.51V, 0.45V and 0.43V, respectively, and after five repeated oxidation and reduction cycles their CV curves did not change. The oxidation of compound **2a** started at 0.41 V and, subsequently, the oxidation peak at 0.53 V was observed. The HOMO energy levels were determined using the relationship $E_{HOMO}(eV) = -1.4E_{onset,ox}(V) - 4.6$ [257]. The HOMO energy levels of the derivatives **3a** and **3b** were found to be comparable and slightly higher with respect to those of compounds **2a-b**.

The HOMO levels acquired from the DFT calculations and from CV measurements were found to be in good agreement for compounds **3a-b** and showed higher values compared to the diphenylethenyl-substituted derivatives of carbazole containing no methoxy groups [234]. The ionization potentials of the synthesized compounds were measured by the electron photoemission in air technique. The results are presented in Table 4.4. Usually, the photoemission experiments are carried out in vacuum, but in our case, the investigated organic compounds were stable with respect to oxygen and the measurements could be carried out in air. All the synthesized compounds showed lower *IP* values compared to compounds containing electronically isolated carbazole moieties having no substituents at the aromatic rings [258]. Methoxy-disubstituted carbazoles (**2a,b**) showed slightly higher *IP* than the target compounds (**3a**,**b**). Compounds **3a** and **3b** were found to exhibit comparable *IP* values. This observation proves our earlier finding that the alteration of the substitution patterns of carbazole moiety practically does not affect the ionization energy values [5].

4.1.6 Charge-transportingproperties

The hole-transporting properties of the layers of compounds **3a** and **3b** were studied by XTOF and TOF techniques. The sample of compound **3b** for the XTOF

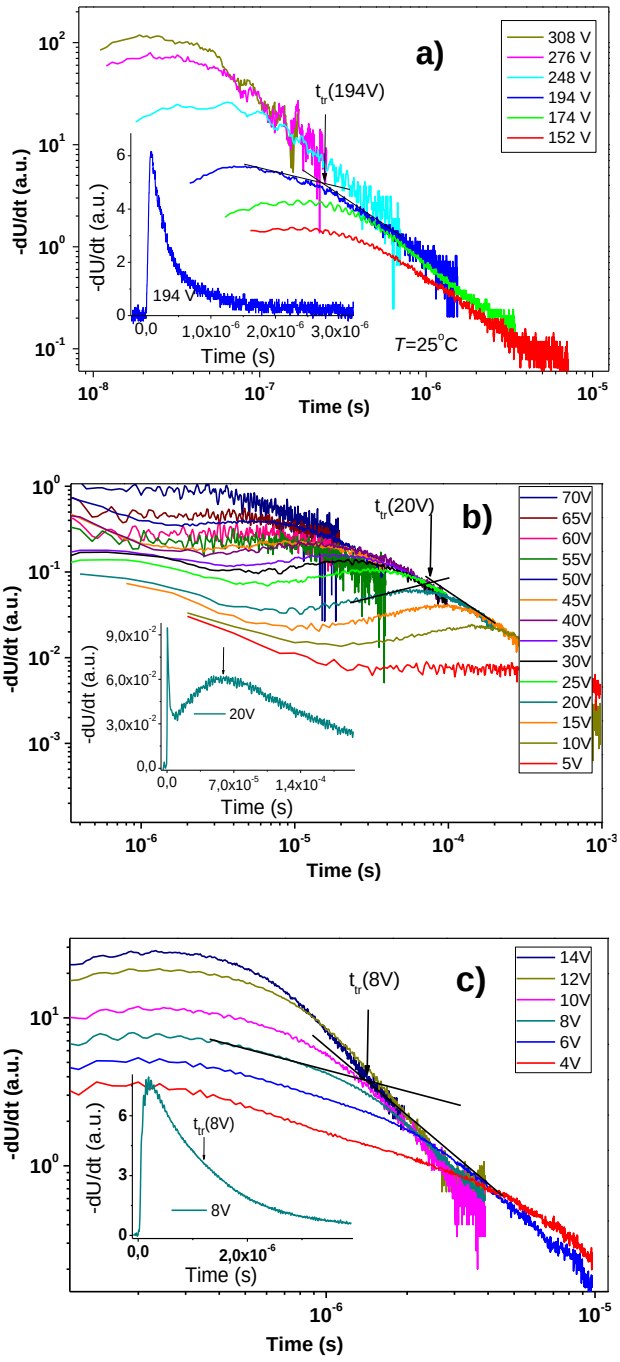

Fig. 4.11. XTOF transients for the drop-casted layer of **3b** (a) and TOF transients for the vacuum deposited layers of **3a** (b) and **3b** (c). The insets show transient curves in the linear plot

measurements was prepared by a drop casting technique with the layer thickness of ca. 2.5 μm.

Because of the high disposition to crystallization, it was not possible to obtain a good quality amorphous film of compound **3a** using the same film preparation method. The value of hole drift mobilities of layer **3b** was found to be 4.1×10^{-3} cm^2/Vs at an electric field of 1.23×10^6 V/cm.

Fig. 4.11a shows the hole photocurrent transients on log-log and linear (insets) scales that were observed for the layer of **3b**.

No transit times were detected in the linear plots, however, they were seen on log-log plots. This observation shows that dispersive hole transport is characteristic of the layer of **3b**. Hole-transporting properties of compounds **3a** and **3b** were also investigated by the TOF technique using the vacuum deposited amorphous layers. The layer thickness was in the range of 0.65-2.8 μm. Fig. 4.11b-c shows the hole photocurrent transients of **3a** and **3b** on log-log and linear (insets) scales. The different character of the transients is obvious. Compound **3a** showed low dispersion hole transport, while compound **3b** demonstrated high dispersion transport.

Fig. 4.12 shows the electric field dependencies of hole-drift mobility values (μ) for the layers of **3a** and **3b**. The logarithm of the hole-drift mobility values showed linear dependencies on the square root of the electric field. Similar characteristic dependences were observed for many amorphous (disordered) organic semiconductors and were explained in terms of the Bassler and Borsenberger model [259].

The zero field hole drift mobility (μ_0) and the field dependence parameter (α) were obtained by the extrapolation of the electric-field dependences of the hole drift mobilities to the zero electric field (Fig. 4.12, Table 4.5). Compound **3b** showed higher hole mobility and a little lower field dependence parameter than **3a**.

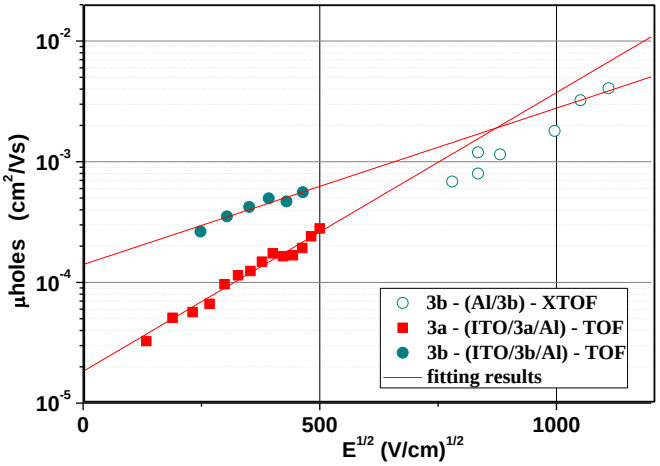

Fig. 4.12. Electric field dependencies of hole mobilities in the layers of **3a** and **3b**

Table 4.5. The hole mobility data for compounds **3a** and **3b**

	μ_0 / μ_0^{theor}, cm^2/Vs	μ, cm^2/Vs[a]	α, 10^{-3} cm/V
3a	1.8×10^{-5} / 7.7×10^{-6}	2.6×10^{-4}	5.3
3b	1.4×10^{-4} / 1.5×10^{-4}	6.2×10^{-4}	4.6

[a] mobility value at an electric field of 2.5×10^5 V/cm

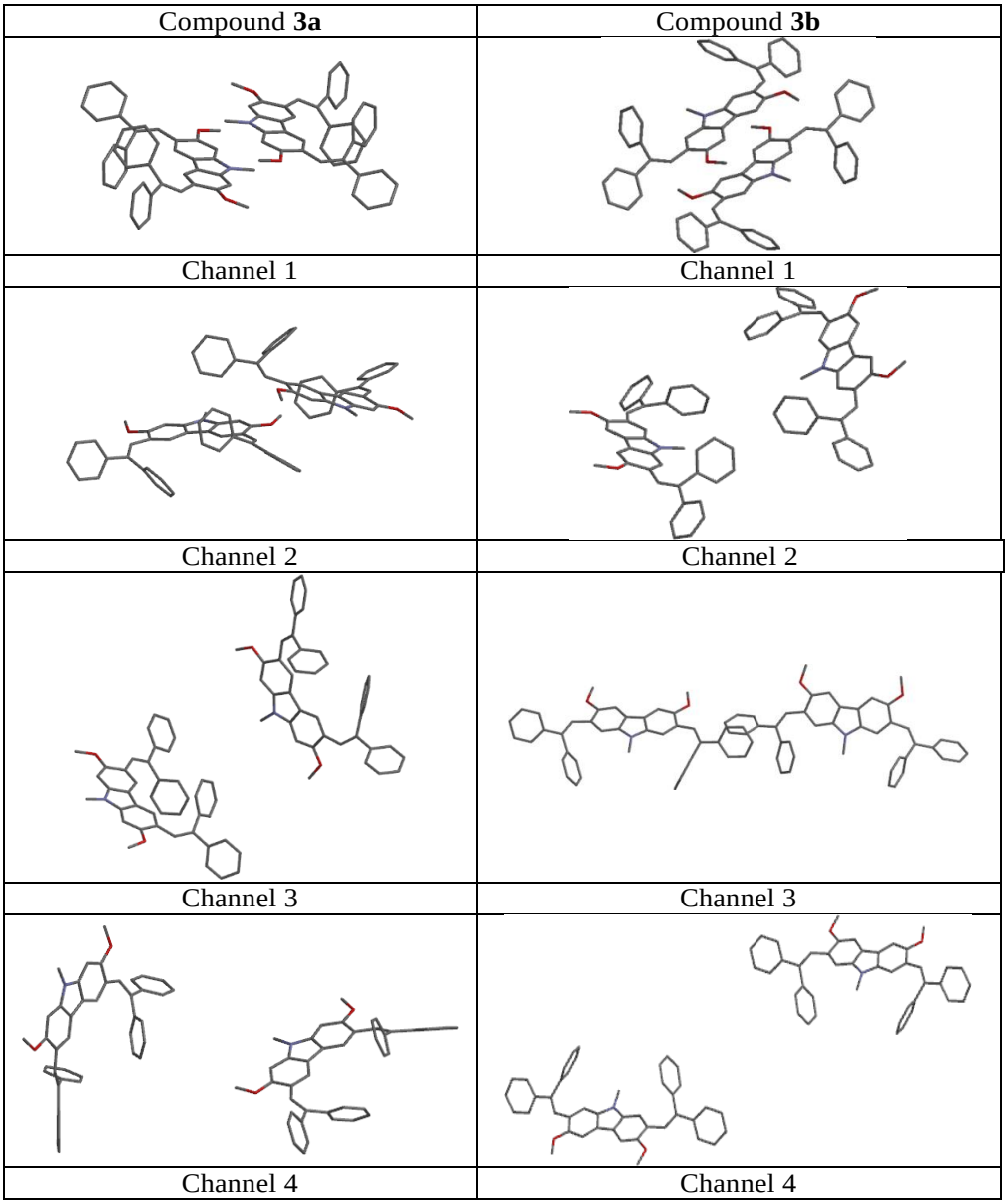

Fig. 4.13. The intermolecular charge-hopping channels for **3a-b** generated from X-ray data

To get a deeper insight into the hole-transporting properties of the isomers **3a-b**, theoretical calculations were performed. The crystal structure to a large extent determines the charge carrier transport pathways and charge mobilities in organic molecular crystals [260]. For some compounds the mesoscopically connected networks in the amorphous films are possible, even without a periodic order [261].

In this work, the crystal structures of **3a-b** were used to generate a wide variety of possible hopping pathways (dimmers) as showed in Fig. 4.1and Fig. 4.13.

According to the Holstein small polaron limit, the charge is localized on a single organic molecule. The standard Marcus-Hush model (equation 1) describes the rate of charge transfer between molecules [262]. Many theoretical and experimental studies concerning λ of single molecules were reported [263]. However, relevant for charge mobility is the charge reorganization energy of organic solids. The charge reorganization energy is the sum of inter- and intramolecular effects, where the intramolecular effects dominate the charge–phonon coupling. However, their energy is very small (10-100 meV) and the crucial point to access the impact to charge mobility in the solid state is not performed [264]. The other factor is a charge carrier polarization energy. The polarization energy is significant for the organic materials and ranges between -0.1 eV and -1.0 eV [265]. The polarization energy (P^+ and P^-) measures the contribution from intermolecular interactions in the crystal to hole and electron transport levels, and includes both an electrostatic and a polarization contribution[266]. P^+ energy is defined as the difference between the solid state and gas phase values of ionization potential [267]. It is assumed that the Gibbs free energy (ΔG^0) is approximately equal to the polarization energy for one dimension of the crystal for holes and can be described as $\Delta G^0 \approx -\frac{1}{3}P^+$. The P^+ energy can be estimated theoretically from the stand-alone molecule ionization potential (it can be obtained from vertical *IP* calculation in vacuum) and the *IP* of the solid state (it can be obtained from vertical *IP* calculation in one crystal lattice) using the formula $P^+ = IP_{solid} - IP_{vacuum}$. The calculated P^+ energy values were found to be -0.69 eV for **3a** and -0.57 eV for **3b**.

The internal reorganization energy (λ_{in}) values were calculated using the normal-mode analysis method (equation 2) [268]. The reorganization energies of **3a** and **3b** for holes (λ_+) were found to be 0.32 and 0.26 eV, and for electrons (λ_-) these energies were found to be 0.31 and 0.36 eV. These results show that the reorganization energies for holes and electrons of **3a-b** are somewhat similar.

The electronic coupling (transfer) integrals H_i for the pathways (see Fig. 4.1 and Fig. 4.13) were estimated using equation 3. This time, $E_{L[H]}$ and $E_{L+1[H-1]}$ are the energies of the LUMO and LUMO+1 (HOMO and HOMO−1) levels taken from the neutral state from the crystal structures of **3a-b**. The molecules in the crystal structures were not optimized. The 2-ethylhexyl chains were approximated by methyl groups to reduce computational time for the calculation of the reorganization energies and the electronic coupling integrals.

The diffusion coefficient (*D*) for migration of electrons or holes in the dimmers is given by equation 4. Then, according to the Einstein equation (5), the final drift mobility (μ_0) in the absence of an electric field was calculated.

The electronic coupling (transfer) integrals are very sensitive to the relative positions of molecules in the solid state [205]. The electronic couplings were evaluated using the dimmer model. Here, the single-crystal structures of **3a-b** were used to generate a wide variety of possible intermolecular charge-hopping channels (transport pathways shown in Fig. 4.1 and Fig. 4.13). The distances between molecular mass centers and charge transfer integrals for all hopping pathways are listed in Table 4.6:

The molecules of compound **3a** in channels 1 and 2 exhibit a close face-to-face stacking arrangement with a short interplanar distance of ca 3.6 Å. This stacked fashion provided high electronic coupling reaching 59 and 42 meV for holes. The channel 1 is not dominant in the charge carrier mobility between the molecules (Fig. 4.1, Table 4.6). The higher charge carrier mobilities were estimated for channels 2-4. This theoretical observation demonstrates that the orientation of dimmers is very important for charge carrier mobility.

Table 4.6. The data of the theoretical calculation of hole mobility at 298 K

Dimension (N=1) for **3a**	d, Å	Angle, deg.[a]	H_h, meV	k_h,10^8 s^{-1} for holes	$\mu_{0\,h}$, 10^{-5} cm^2/Vs
1	3.58	180	59	3.94	0.98
2	10.4	163	42	2.01	4.22
3	14.6	48	34	1.29	5.39
4	15.8	77	32	1.18	5.72
3a	D_h, 10^{-6} cm^2/s		$\mu_{0\,h}$, 10^{-6} cm^2/s/V		
N=3	0.25		7.65		
Dimension (N=1) for **3b**	d, Å	Angle, deg.[a]	H_h, meV	k_h,10^7 s^{-1} for hole	$\mu_{0\,h}$, 10^{-5} cm^2/Vs
1	6.00	180	110	672	47.1
2	11.5	122	11	5.79	1.49
3	17.2	58	31	47.7	27.4
4	22.7	180	0.2	0.002	0.0047
3b	D_h, 10^{-6} cm^2/s		$\mu_{0\,h}$, 10^{-4} cm^2/s/V		
N=3	3.89		1.51		

[a] the torsions angle between dipoles of the ^1L_a transition of carbazole moiety in dimmers.

The orientation of dimmers was estimated from the torsion angle between dipoles of ^1L_a transition in carbazole moiety. This transition dipole is parallel to the N-C(alkyl) bond and is located on the carbazole moiety. The transition dipoles of molecules **3a** in channel 1 are parallel but with the opposite direction (Fig. 4.1 and Fig. 4.13). Taking into account the distances between dimmers, the molecular orientation has a crucial role in charge carrier mobility. This effect is even clearer in the case of compound **3b**. The higher hole mobility was estimated for channel 1 as compared with 2-4 channels. The transition dipoles of molecules **3b** in channel 1 are parallel and with the same direction. These observations are well in line with the exciton coupling model in the molecular spectroscopy [269]. In other words, the excitonic coupling between the molecules plays a crucial role in charge carrier

mobility. The calculated charge carrier mobilities are in good agreement with the experimental data (Table 4.5). Considering the different polarity, the different charge carrier mobilities of the target compounds **3a-b** can be explained. According to some authors, [270,271] a higher induced dipole moment may cause lower charge mobility.

Concluding, 2,7-Dimethoxy and 3,6-dimethoxy carbazole derivatives possessing diphenylethenyl moieties (**3a-b**) were synthesized by condensation of the corresponding derivative of dimethoxycarbazole (**2a-b**) with diphenylacetaldehyde. The structures of the synthesized compounds were proven by X-ray crystallography. Both of the isomers exhibit high thermal stability and form molecular glasses. Since the majority of molecules in the crystal structure of **3a** form *J*-aggregates, this compound showed the effect of aggregation induced emission, while the other isomer, i.e. **3b**, showed the effect of aggregation-caused quenching. Both target compounds (**3a-b**) showed comparable ionization potentials of ca. 5.4 eV, which are lower compared to those of the parent dimethoxycarbazoles (**2a-b**). The derivative **3b** showed superior charge transporting properties relative to its counterpart **3a**. The TOF hole drift mobilities in its amorphous layers exceeded 10^{-3} cm^2/Vs at high electric fields. The pronounced differences in charge carrier mobility, thermal and optical properties were justified by the theoretical study using DFT and TD-DFT calculations. According to them, the target molecules of **3a** were found to be highly polar with the ground state dipole moment of 5.98 D, in contrast to the molecules of **3b** having the ground state dipole moment of ca. 0.69 D. The polarity has shown a crucial effect on the molecular arrangement in the crystals, consequently on the thermal transitions (polymorphism) and on the charge-transporting properties of the isomers.

4.2 Chiral carbazole based diaza[6]helicenes

Helicenes belong to an interesting class of polycyclic aromatic or heteroaromatic compounds with ortho-annulated rings. These unique and extended aromatic systems are well known for their inherent chirality [272-279]. The system cannot remain planar as the number of ortho-annulated rings increases, and releases the streric strain by adopting either the *P*- or *M*-configuration [280]. These unique three-dimensional aromatic systems are thermally stable and have attracted an ever-increasing amount of attention, and their chemistry has been considerably enriched owing to their interesting optical and electronic properties [281,282].

Helicenes, with heteroaromatic units incorporated in the π-systems, have been extensively studied due to their interesting self-assembly in the solid state [283], their ability to behave as organic semiconductors [11], and their use in optical resolutions [284,285]. Furthermore, the potential applications of the enantiomerically pure functionalized derivatives of (hetera) helicenes can be realized, as they are configurationally stable and form supramolecular architectures that exhibit second-order nonlinear optical and chiro-optical properties [281,282].

The last decade has highlighted carbohelicenes [278,286,287] as helical dominating frameworks, but heterahelicenes, [288] for example aza- and thiahelicene have also emerged as a very attractive class of molecules. The ambiguities associated with an all-benzene helix can be removed by the introduction of a hetereoaromatic unit. Azahelicenes belongs to a subgroup of heterahelicenes, with possible applications in fields such as light-emitting devices and chemosensors [289]. Azahelicene derivatives have also been reported to have applications in enantioselective transformations, as chiral inducers, in the field of asymmetric catalysis [290,291], self assembly [292], and metal coordination complexes [293].

Classical photochemical cyclization have been described by Caronna *et al*. [294,295], and is one of the most utilized methods for the synthesis of azahelicenes. A versatile synthetic method was described by Harrowven and coworkers [296,297,298] based on Bu_3SnH-mediated coupling. Furthermore, metal-catalyzed cyclizations [298], include the [2 + 2 + 2] cycloisomerization of triynes [297], and palladium catalyzed arylations. Recently, Lui *et al*. [299] described the synthesis of carbazole based diaza[7]helicenes and described their application as a deep-blue emitter in OLED. This new class of helicenes, with a carbazole framework, could open new possibilities for the utilization of helicene derivatives in OLEDs and also have potential applications in other fields of organic electronics [300,301]. We envisage that combining the carbazole unit to the readily available quinoline building block previously synthesized by us, would result in the formation of a donor-acceptor hybrid system with interesting electronic properties and potential applications in organic electronics. Furthermore, chiral resolution via diastereomeric separation and post-cyclization functionalization could be realized with this system leading to a chiral helical donor-acceptor hybrid system, which is an added advantage over the previously synthesized chiral diaza[5]helicenes by this methodology.

In the present work, this quinoline and 9-(2-ethylhexyl)-2,7-dimethoxycarbazole-3-carbaldehyde as building blocks is utilized to synthesize carbazole based helicenes. These bifunctional systems comprising of chloroquinoline and carbazole units are a useful combination. The chloro group can be substituted with a chiral amine, leading to diastereomeric separation, and the chiral forms can further be functionalized *via* electrophilic substitution on the carbazole unit. Post-cyclization functionalization via substituting the carbazole unit opens new opportunities for the synthesis of chiral functionalized materials.

4.2.1 Synthesis of carbazole based diaza[6]helicene

In the present approach 9-(2-ethylhexyl)-2,7-dimethoxycarbazole-3-carbaldehyde **3** was utilized as one of the building block. This building block **3** was prepared in two steps from 2,7-dimethoxycarbazole **1**, which was prepared according to earlier reported procedures [215]. Alkylation of compound **1** was done using 2-ethylhexylbromide according to the literature procedure [217] to obtain alkylated product **2** in 75% yield. Vilsmeier-Haack formylation of compound **2** gave the aldehyde **3** in 74% yield (Scheme 4.2). Wittig olefinationof phosphonium salt **4**, prepared according to the literature procedure [302] and aldehyde **3** using NaH as a

base in CH_2Cl_2, gave the asymmetric precursor **5** (*Z:E* ~2:1) in 98% yield. The alkene was obtained with a moderate degree of *Z* selectivity. Characterization of compound **5** was fully done by ^1H and ^{13}C NMR spectroscopy and HRMS.

The ratio of the isomers was determined by integration of the ^1H NMR spectrum to be *Z/E*=2:1. A high ratio of cis-isomer, which is beneficial during the irradiation process as compared to the trans-isomer which shows poor solubility was observed. The precursor **5** obtained was subjected to oxidative photocyclization using iodine and toluene as the solvent (1.0 mM) (Scheme 4.3).

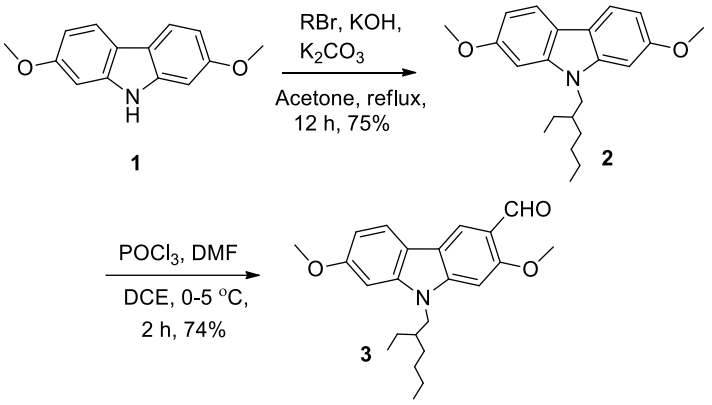

Scheme 4.2. Synthesis of 9-(2-ethylhexyl)-2,7-dimethoxycarbazole-3-carbaldehyde **3**

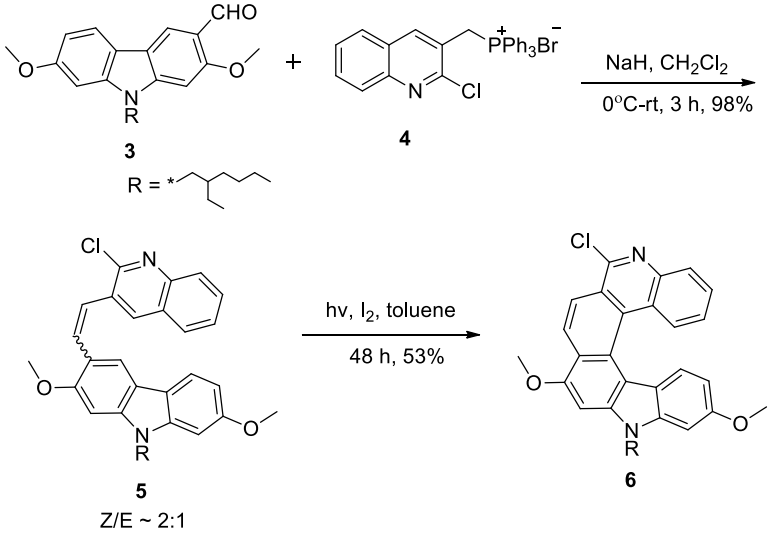

Scheme 4.3. Synthesis of carbazole based diaza[6]helicene via Wittig reaction and photochemical cyclization

A Rayonet photochemical reactor with interchangeable light sources (wavelength used is 350 nm) was used for the irradiation process, to obtain the diaza[6]helicene **6** in 53% yield. Compound 6 was characterized by HRMS and NMR spectroscopy.

4.2.2 Resolution via diastereomeric separation

Based on our previous knowledge of resolution *via* diastereomeric separation using a chiral amine, the chloro group was substituted utilizing the Buchwald-Hartwig amination reaction [302]. Amination reaction of **6** with *S*-(-)-α-methyl benzylamine using Cs_2CO_3, as the base, 10 mol% $Pd(OAc)_2$, 5 mol% *rac*-BINAP, and toluene as the solvent gave the desired product **7** in 53 % yield (1:1 mixture of diastereomers) (Scheme 4.4). The ratio was determined by integrating the ^{1}H NMR spectra.

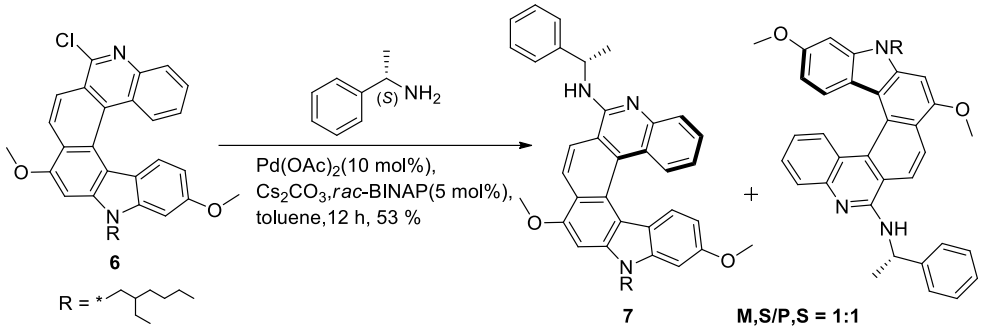

Scheme 4.4. Resolution via diastereomeric separation

The obtained diastereomers were readily separated via standard chromatography. The ease of separation of the chiral forms led to better characterization (NMR and CD spectroscopy) and utilization in further functionalization. These diastereomers were configurationally very stable at room temperature. (Qualitative analysis showed that these diastereomers were stable for 12 hours at 150 °C, there is no observable racemization after heating the diastereomers at 150˚C for 12 hours).

4.2.3 Functionalization of chiral forms via electrophilic substitution

Functionalization of the chiral forms of diaza[6]helicene was done utilizing the carbazole unit. The helicene core was functionalized *via* electrophilic substitution reactions.

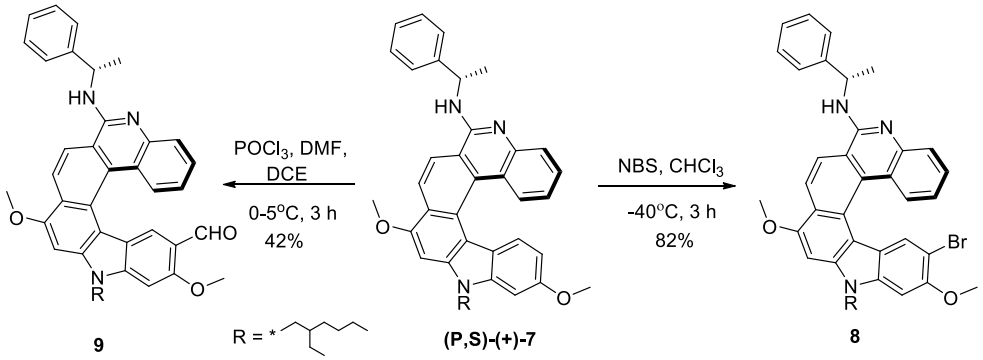

Scheme 4.5. Functionalization of chiral forms *via* electrophilic substitution

The substitution of diastereomer ***(P,S)-(+)-7*** with bromine was done using NBS and $CHCl_3$[303] as the solvent at -40 °C to furnish the brominated diaza[6]helicene **8** in 82 % yield. In addition to the references given, to prove the electrophilic substitution reaction position as depicted in Scheme 4.5, the electrostatic charges of the ***(P,S)-(+)-7*** diastereomer were calculated using the B3LYP/6-31G(d,p) method. The observed values at C-1, C-3 and C-8 positions of the carbazole fragment were found to be -0.429, -0.420 and -0.356, respectively. Although C-1 is slightly (0.009) electron richer than C-3, the higher reactivity of C-3 could be attributed to lower steric shielding by the methoxy group present at the C-2 position. Vilsmeier-Haack formylation of diastereomer ***(P,S)-(+)-7*** using DMF and $POCl_3$ gave the formyl substituted diaza[6]helicene **9** in 42% yield. The structural identity of the substituted azahelicenes was confirmed by NMR, HRMS and CD spectroscopy.

4.2.4 Optical properties

The absorption spectra for compounds **6**, **7**, **8** and **9** in dilute $CHCl_3$ solutions are shown in Fig. 4.14. Hypsochromic shift is observed for compound **7** compared to helicene **6,** which could be a result of the substitution of the helicene core with the amine. The spectra of compounds **8, 9** are comparable to **7.**

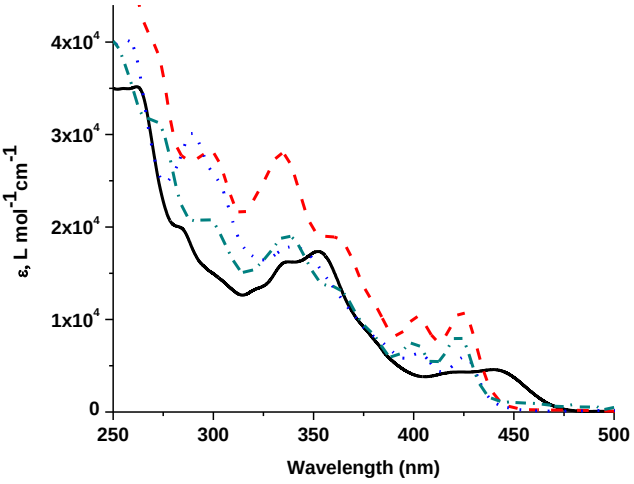

Fig. 4.14. UV-visible spectra of compounds **6-(**black), **7-(**dash), **8**-(dash dot), **9**-(dot) in dilute $CHCl_3$ solution (10 µM)

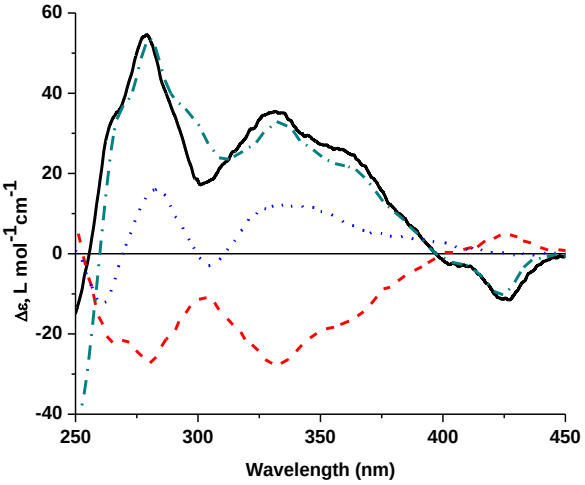

Fig. 4.15. CD spectrum of diastereomer ***(P,S)-(+)*-7(**black), (***M*,**S)-(-)-7 (**dash), (***P*,***S***)-(+)-**8 (**dash dot),***(P,S)-(+)*-**9** (dot) in dilute $CHCl_3$ solution (10 μM).

In the CD spectrum of the diastereomer **(+)-7** (Fig. 4.15) a small negative peak was observed, followed by several large positive bands.

As expected, the spectrum of the other diastereomer **(-)-7** is the mirror image of this. Based on earlier literature [304], it is commonly accepted that the sign of the CD-β-band is representative of the absolute configuration of the helicene, with a positive band corresponding to the P helicity and vice versa. Based on this, P helicity to diastereomer (+)-**7** and M helicity to diastereomer (-)-7 can be attributed.

4.2.5 Theoretical calculations

CD calculations of the obtained three most stable conformers were performed, using TD-DFT with the B3LYP functional 6-31G(d,p) basis set and PCM in chloroform [305,306]. The CD spectra of the most populated conformers were calculated and Boltzmann-averaged (see Table 4.7, Fig. 4.16, Fig. 4.17, Fig. 4.18, Fig. 4.19). In many cases, the conformational equilibrium has an influence on the CD spectra [307]. The results of the conformational analysis of **7** show changes on CD spectra ranging between 350-370 nm. The shoulders in this range in the experimental CD spectra at 366 and 360 nm for diastereomers ***(M,S)*-7** and ***(P,S)*-7** are the effect of different conformers (Fig. 3b, 3d). Excitation energies, oscillator and rotatory strengths for the diastereomers of helicene **7** (*conf1*) are presented in Table 4.7.

Table 4.7. Computational data of the selected transitions and their contribution to the CD spectra of helicene ***(P,S)-(+)-*7**(*conf1*) and ***(M,S)-(-)-*7** (*conf1*) calculated at the TD-B3LYP/6-31G(d,p)/PCM(chloroform) level

Comp.	Exp. CD, λ, nm ($\Delta\varepsilon$)	Calc. CD λ, nm	Trans.	Oscill. strength	Rotatory strength, cgs units	Contributions
***(M,S)*-7**	427 (4.7)	405	1	0.155	50.1	HOMO→LUMO (95%)
	366 (-31)	354	3	0.337	-56.9	HOMO→LUMO+1 (66%)
	333 (-28)	277	4	0.176	-58.8	HOMO-2→LUMO (87%)
	280 (-27)	286	8	0.114	-159	HOMO→LUMO+2 (74%)
***(P,S)*-7**	427 (-11)	399	1	0.152	-38.3	HOMO→LUMO (91%)
	360 (25)	348	3	0.175	35.6	HOMO→LUMO+1 (53%)
	332 (35)	275	4	0.248	81.3	HOMO-2→LUMO (62%)
	298 (54)	280	10	0.032	133	HOMO→LUMO+2 (32%)

The molecular orbitals (MO) of the diastereomer ***(M,S)*-7** were analyzed, since the (*S)*-α-methyl benzylamine moiety has no effect on the MO of helicene. For the helicene ***(M,S)*-7** the lowest energy and small intensity with positive Cotton effect (CE) band at 427 nm was influenced by one transition $S_0 \rightarrow S_1$ at 405 nm. The first excitation with the oscillator strength of 0.155 for ***(M,S)*-7** corresponds to the HOMO→LUMO transition. This transition is localized on the helicene moiety and is assigned to the forbidden ^1L_b transition, by the Platt's nomenclature [252]. This transition is known to be less useful for the analysis of the CD spectra of helicenes [308]. The bands with strong negative Cotton effects (CE) were observed at 277 and 286 nm for ***(M,S)*-7**, which are assigned as ^1B_a and ^1B_b transitions, respectively.

The signs of these CEs can be readily used as tools for the estimation of the absolute configuration of helicenes. Clearly visible levorotatory electron density migration was observed from the transition $S_0 \rightarrow S_4$ which corresponds to 87% of the transition HOMO-2→LUMO. The electron density in the orbital HOMO-2 is located on carbazole and quinoline parts of helicene. After excitation, the electrons migrate to the quinoline part (LUMO). Comparing and interpreting the theoretical and experimental data *P* (dextrorotatory) and *M* (levorotatory) helicities were obtained and significant agreement between the CD characteristics of the helicenes was observed (Fig. 4.16, Fig. 4.17, Fig. 4.18, Fig. 4.19). The main CD bands were predicted with the correct Cotton effect and the positions were found to be comparable with the experimental spectra for both compounds.

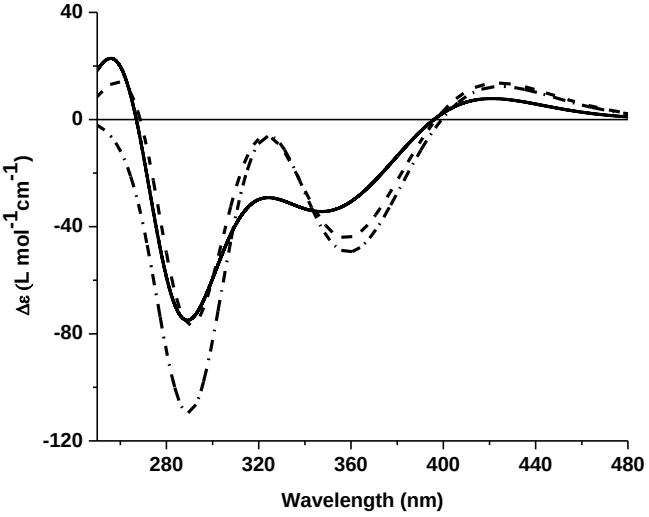

Fig. 4.16. Theoretical CD spectra for individual conformers of diastereomer ***(M,S)*-7** (*conf1* (dot), *conf2* (dash), *conf3* (dash dot)) and Boltzmann-averaged CD spectra (solid)

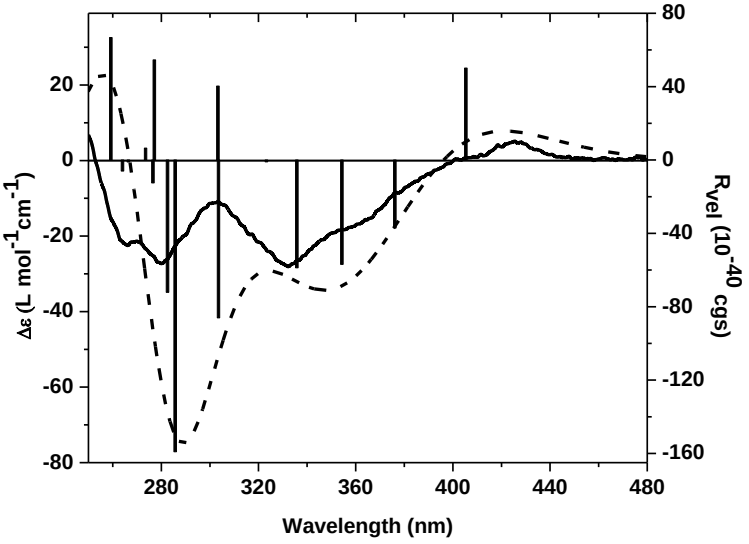

Fig. 4.17. Comparison of the experimental (solid) and theoretical (dash) CD spectra of most stable conformer of diastereomer ***(M,S)-(-)*-7** was calculated at the TD-B3LYP/6-31G(d,p) level (σ=0.30 eV) for Boltzmann-averaged of the three most stable conformers (black) CD spectra; bars represent the rotatory strength for the most abundant *conf1*

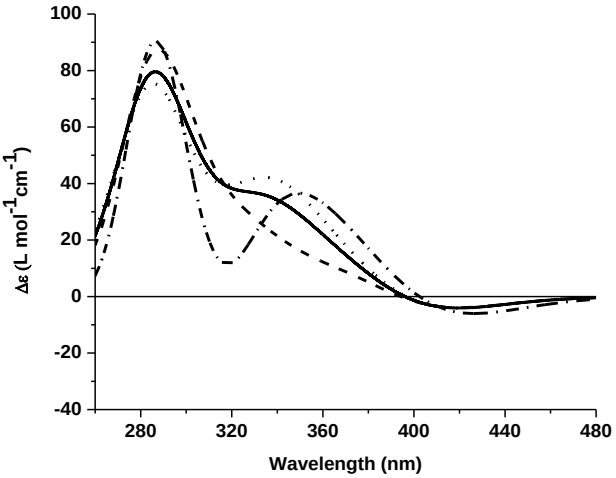

Fig. 4.18. Theoretical CD spectra for individual conformers of diastereomer ***(P,S)-(+)*-7** (*conf1* (dot), *conf2* (dash), *conf3* (dash dot)) and Boltzmann-averaged CD spectra (solid)

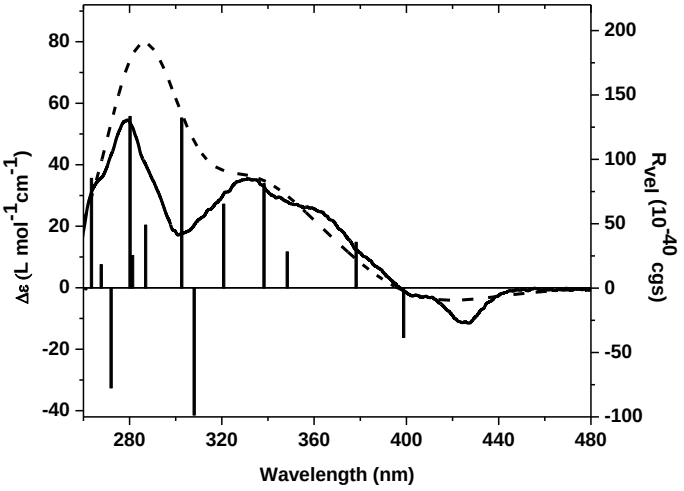

Fig. 4.19. Comparison of experimental (solid) and theoretical (dash) CD spectra of diastereomers ***(P,S)*-7**, calculated at the TD-B3LYP/6-31G(d,p) level (σ=0.30 eV) for Boltzmann-averaged of the three most stable conformers (black) CD spectra; bars represent the rotatory strength for the most abundant *conf1*

Additionally, DFT calculations were performed for helicene **7** to study the HOMO and LUMO electronic distribution. Due to the strong electron-donating property of carbazole moiety and electron-accepting property of quinoline species of the helicene, the HOMO of **7** was mainly dispersed over the carbazole moiety, while

their LUMO was localized on the quinoline part. (Fig. 4.20) The HOMO and LUMO energy levels were calculated for helicenes ***(M,S)*-7** and ***(P,S)*-7** to be −4.95/−1.38 eV and -5.10/-1.48 eV, respectively. Taking into account the semiconducting properties, these compounds act as electron donors and their HOMO is about -5 eV. Moreover, for electron transporting n-type organic semiconductors, quite low LUMO (~-3.0 eV) is needed [309]. In our case, the LUMO is below – 1.5 eV. This observation shows that these compounds can be potentially of interest as hole-transporting p-type semiconductors.

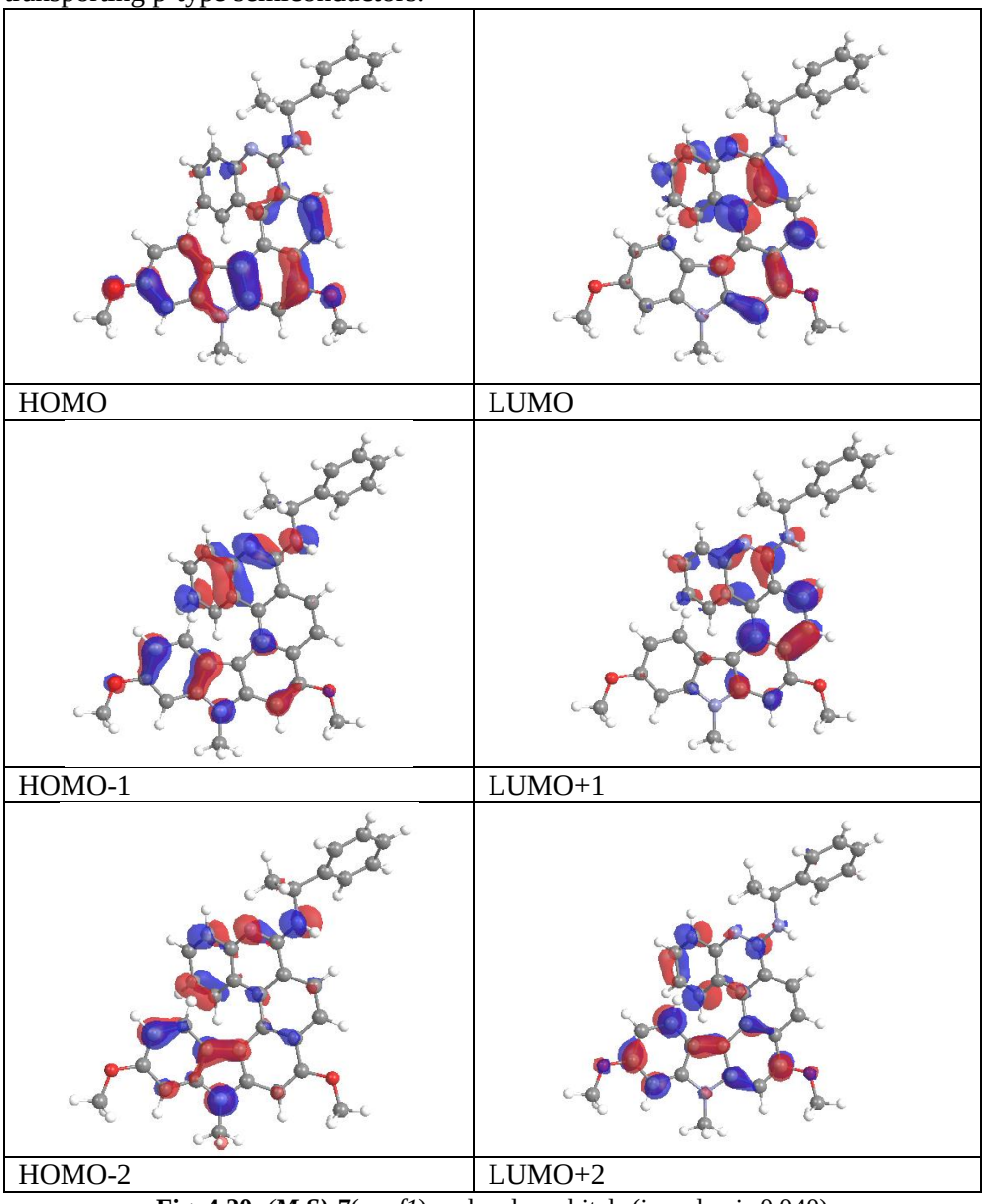

Fig. 4.20. ***(M,S)*-7**(*conf1*) molecular orbitals (isovalue is 0.040)

To summarize, an efficient method for the synthesis of carbazole based diaza[6]helicenes has been developed. The presence of bifunctional units in this strategy provides researchers with an opportunity for the substitution of the chloro group of quinoline unit leading to the resolution of the racemic helicene and further functionalization of the chiral forms utilizing the carbazole unit. Electrophilic substitution reactions were performed, resulting in the formation of functionalized chiral materials. The bromine and aldehyde groups are an ideal starting point for further elaboration. It is envisaged that the bromine or the aldehyde can further be converted to groups suitable in catalysis. An efficient synthetic methodology with ease of further functionalization provides the chirals forms of diaza[6]helicenes for various applications.

4.3 Derivatives of N-Annelated perylene and carbazole

Increasing interest in the application of ambipolar organic semiconductors for fabrication of efficient organic light emitting devices requires balanced charge carrier transport and high solid-state photoluminescence (PL) quantum yields of emitting materials [310-312]. Numerous emissive donor-acceptor combinations, including bipolar low-molar-mass compounds [313,314], conjugated-polymer blends [315], organic molecules mixtures [202,316,317] and organic-inorganic host-guest systems [318-320]were used for the OLEDs fabrication. Perylene derivatives form a class of interesting n-type organic semiconductors owing to an excellent charge carrier transport together with the outstanding chemical, thermal and photochemical stability [223,321]. Very high electron mobility of perylene derivatives has qualified them to be widely employed in electronic and optoelectronic devices [309,322]. Carbazole derivatives have also been extensively studied as the hole-transporting or emitting materials for OLEDs [323,324]. The combination of hole-transporting carbazole and with electron-transporting perylene at the molecular level may lead to new donor-acceptor molecular materials with interesting and useful optical and charge-transporting properties that are important for various device applications.

On the basis of experimental studies and quantum chemical calculations in this work, the impact of linking topology on the thermal, electrochemical optical and photophysical properties of the newly synthesized derivatives of N-annelated perylene and carbazole and demonstrate their applicability for the fabrication of highly efficient OLEDs have been disclosed.

4.3.1 Synthesis

The synthetic route to the target compounds **NP-9-Cz**, **NP-3-Cz**, **NP-2-Cz**, consisting of N-annulated perylene core and the differently linked carbazolyl substituents, are shown in

Scheme **4.6**. **NP-3-Cz**, **NP-2-Cz** were synthesized by the Suzuki-Miyaura coupling reaction [223] of **A-NP-Br** with 9-isopentyl-3-carbazolyl and 9-isopentyl-2-carbazolyl boronic acid pinacol ester, respectively. **NP-9-C** was obtained by

Ullmann-coupling [215] of iodinated precursor **A-NP-I** and carbazole. Halogenated N-annulated perylene was prepared in four steps, including nitration of commercially available perylene [219] followed by a Cadogan cyclization using triphenylphosphine [216], alkylation with 2-ethylhexylbromide [242] and bromination reaction with NBS in DMF [217] or Tucker iodination [222]. The boronic acid pinacol esters of carbazole (**3-BCz**, **2-BCz)** were prepared from 3-bromocarbazole (**3Br-Cz**) and 2-bromocarbazole (**2Br-Cz**) by N-alkylation and borylation using the procedure reported in literature [321]. The current synthetic route could be applied on industrial scales using the technological scheme shown in Appendix Fig. II.

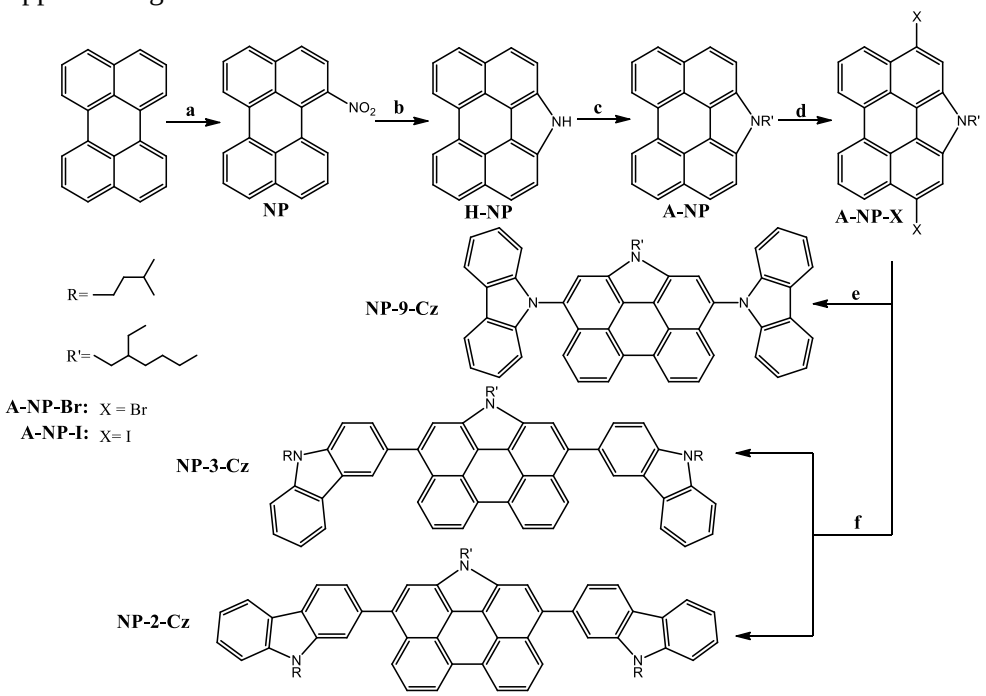

Scheme 4.6. Synthesis of **NP-9-Cz**, **NP-3-Cz**, **NP-2-Cz**. Reagents and conditions: (a) fuming HNO_3/H_2O = 1/1.6 (v/v), 1,4-dioxane, 60°C, 30 min; (b) PPh3, o-DCB, 180 °C, 12 h; (c) $C_8H_{17}Br$, K_2CO_3, KOH, TBAHS, Δ, 2 h; (d) NBS, DMF, 0 °C, 2 h (X = Br) / glacial acetic acid, KI, KJO_3, Δ, 2 h (X = I); (e) carbazole, Cu, K2CO3, 18-crown-6, o-DCB, 180 °C, 15 h; (f) **3-BCz** (**2-BCz**) $Pd(Ph_3)_2Cl_2$, KOH, THF–H_2O, 80 °C, 10–12 h

The chemical structures of the compounds were confirmed by ^1H and ^{13}C NMR and MS. In addition, the single crystal of **mISO-2Cz** was grown from a dilute THF/hexane solution and X-ray analysis was performed. The ORTEP projection of **mISO-2Cz** is presented in Fig. 4.21. The target compounds **NP-9-Cz**, **NP-3-Cz**, **NP-2-Cz** were found to be soluble in common organic solvents, such as chloroform, toluene, acetone and tetrahydrofuran.

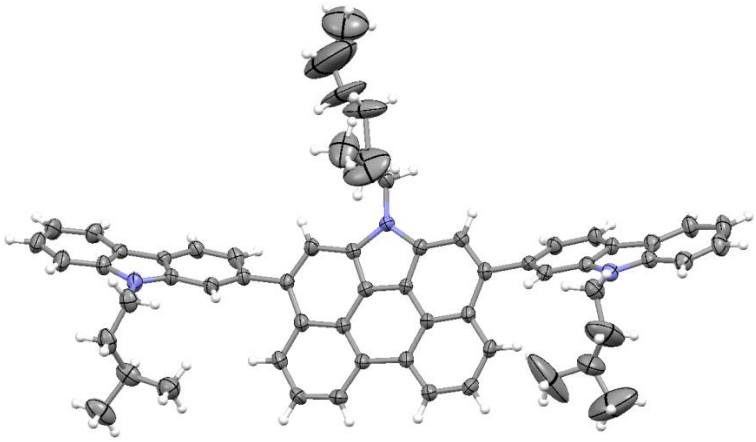

Fig. 4.21. ORTEP projection of the crystal structure of **mISO-2Cz**. Displacement ellipsoids are drawn at 30% probability level

4.3.2 Thermal properties

Thermal transitions of **NP-3-Cz, NP-9-Cz, NP-2-Cz** were investigated by TGA and DSC. The DSC curves of **NP-3-Cz** and **NP-2-Cz** are shown in Fig. 4.22. and the thermal characteristics of all three compounds are collected in Table 4.8. **NP-3-Cz, NP-9-Cz** and **NP-2-Cz** were found to exhibit very high thermal stability. Their 5% weight loss temperatures range from 400 °C to 457 °C. The slightly lower thermal stability of **NP-9-Cz** can apparently be explained by the fact that the C–N bonds between the carbazole and phenanthrocarbazole moieties are less stable than the corresponding C–C links.

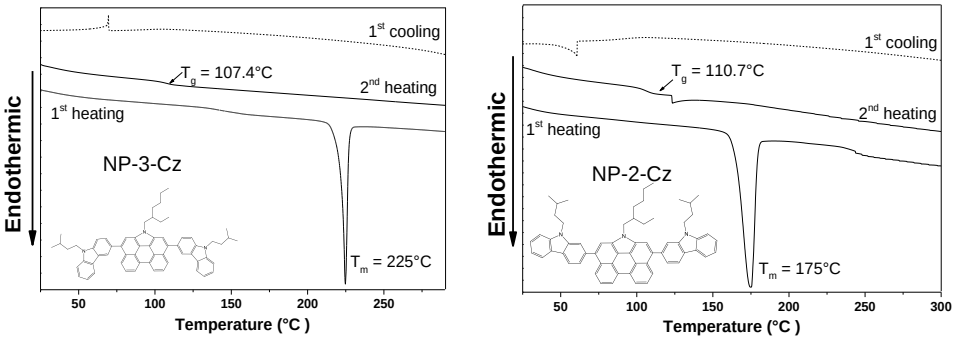

Fig. 4.22. DSC curves of **NP-3-Cz** and **NP-2-Cz** (scan rate 10 °C/min, N_2 atmosphere)

The melting points determined from the sharp endothermic peaks in the thermograms of DSC were found to be 225, 241 °C, 175 °C for **NP-3-Cz**, **NP-9-Cz** and **NP-2-Cz** respectively. No exothermic peaks associated with crystallization were observed for compounds **NP-3-Cz** and **NP-2-Cz** when their melted samples were cooled down to room temperature and an amorphous solid was formed. When the

melted sample of **NP-9-Cz** was cooled down, a broad exothermic peak due to crystallization was observed at ca 215 °C.

Table 4.8. Thermal characteristics of **NP-3-Cz, NP-9-Cz, NP-2-Cz**

	T_m, °C[a]	T_g, °C[a]	T_d, °C[a]
NP-3-Cz	225	107	457
NP-9-Cz	241	–	400
NP-2-Cz	175	111	457

[a]determined by DSC and TGA, scan rate 10 °C/min, N_2 atmosphere.

On repeated heating cycles, the samples of **NP-3-Cz** and **NP-2-Cz** showed glass transitions at 107 °C and 111 °C, respectively, and no other signals were observed. Meanwhile, on the second heating scan, compound **NP-9-Cz** demonstrated an endothermic melting peak at the same temperature (241 °C) as was observed on the first heating cycle. Thus, it was not possible to transform **NP-9-Cz** into the glassy state by slow cooling from melt. The stronger disposition to crystallization of **NP-9-Cz**, having no branched alkyl chains at carbazole moieties, may be due to a more favorable arrangement and stacking in the crystal as compared to **NP-3-Cz** and **NP-2-Cz**. Nevertheless, thin uniform films of **NP-9-Cz** could be prepared by solution processing and by vaccuum evaporation.

4.3.3 Optical and photophysical properties

UV and FL spectra of the dilute solutions of **NP-3-Cz**, **NP-9-Cz** and **NP-2-Cz** in THF and of the solid films are shown in Fig. 4.23 and Fig. 4.24. The optical and photophysical characteristics are summarized in Table 4.9

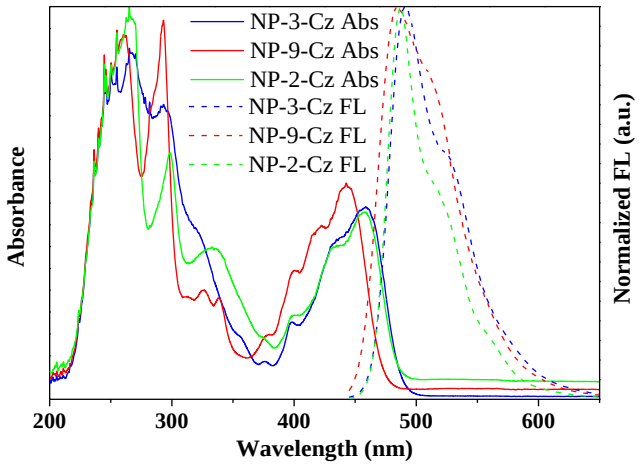

Fig. 4.23. UV-vis and normalized fluorescence spectra (λ_{ex}=350 nm) of dilute THF solutions (10^{-5} M) of **NP-3-Cz**, **NP-9-Cz** and **NP-2-Cz**

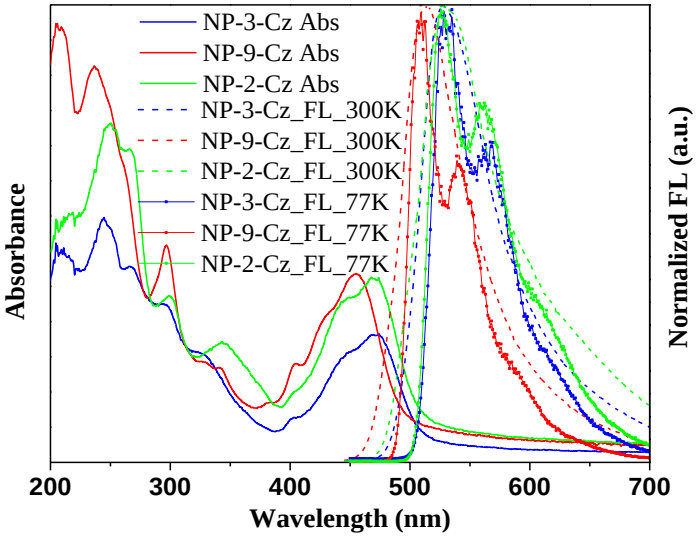

Fig. 4.24. Absorption and fluorescence spectra of the solid films of **NP-3-Cz**, **NP-9-Cz** and **NP-2-Cz**

Table 4.9. Optical and photophysical characteristics of compounds **NP-3-Cz**, **NP-9-Cz** and **NP-2-Cz**

	$\lambda^{ab}_{max,}$ / $\lambda^{ab}_{max\ film,}$(nm)	$\lambda^{em}_{max\ sol}$ / $\lambda^{em}_{max\ film}$, (nm)	Stokes shift, nm	Φ_{Sol} / Φ_{Film}, %	$S_1{}^a$ / $S_1{}^b$, eV	T_1, eV	f_{S0S1}	τ, (ns)	χ^2	k_{rad} (10^8 s^{-1}ns)	k_{nrad} (10^8 s^{-1}ns)
NP-3-Cz	458 / 472	491 / 528	33/56	76 / 33	2.56 / 2.69	1.76	0.90	3.15	1.15	2.4	0.8
NP-9-Cz	443 / 455	485 / 514	42/59	68 / 51	2.54 / 2.79	1.80	0.49	4.07	1.08	1.7	0.8
NP-2-Cz	457 / 471	487 / 528	30/57	61 / 42	2.53 / 2.72	1.76	1.06	2.62	1.18	2.3	1.5

[a] singlet levels of investigated molecules have been taken as the energies of maxima of FL spectra.
[b] triplet levels of investigated molecules have been calculated using the TD-DFT/B3LYP/6-31G(d) method with the PCM solvent approach (THF was used as the model solvent accordingly to the experimental measurements).

UV spectra of the dilute solutions and of the solid films of **NP-3-Cz** and **NP-2-Cz** have comparable absorption profiles. The absorption bands observed in spectra of the solutions of **NP-3-Cz**, **NP-9-Cz** and **NP-2-Cz** in the region of 285-310 nm can be assigned to nπ* transition of carbazole moiety [5,325]. The lowest-energy absorption bands observed at 460 nm in the UV spectra of the solutions of **NP-3-Cz** and **NP-2-Cz** are red shifted by ca. 20 nm relative to that of **NP-9-Cz.** These absorption bands can be attributed to the ππ* transition in the annelated perylene core [219], whiah are in good agreement with the quantum-chemical calculations. As can be seen from Fig. 4.25, both HOMO and LUMO orbitals are localized on the central 1H-phenanthro[1,10,9,8-cdefg]carbazole core with small contributions on the peripheral carbazole moieties. It should be noted that the minor charge transfer

from the carbazole fragment to the phenanthrocarbazole fragment occurs upon the HOMO-LUMO transition for all the compounds. The share of charge-transfer configuration increases in the series of **NP-2-Cz, NP-3-Cz and NP-9-Cz**, which corresponds to the decreasing of the oscillator strength ($f_{S_0S_1}$) of the first singlet-singlet transition. This result corresponds to the lower radiation rate constant for luminescence of **NP-9-Cz** because of the $f_{S_0S_1}$ being directly proportional to the k_{rad} values in accordance with the following equation: $k_{rad} = \nu^2 f_{S_0S_1}/1.5003$, where ν is the wave number for the corresponding transition $S_0 \rightarrow S_1$ (represented in cm^{-1}). These results provide evidence of a more effective conjugation of π-electrons in the molecules of **NP-3-Cz** and **NP-2-Cz** compared to that in **NP-9-Cz**. Dilute solutions of compounds **NP-3-Cz**, **NP-9-Cz** and **NP-2-Cz** show intense green emission with the wavelengths of intensity maxima ranging between 485 and 491 nm and fluorescence quantum yields ranging from 61 to 76 %. The emission intensity maxima of the solid samples are red-shifted up to 40 nm and the quantum yield values are lower by 20-40 %. It has to be stressed that the global PECs minima of the ground and first excited (S_1) singlet states almost coincide because of the small Stocks shift and mirror relationship for absorption and fluorescence spectral contours. Another indirect confirmation of this conclusion comes from this work UB3LYP and TD DFT calculation of the excited triplet state (T_1) and its comparison with the properties of S_0, S_1 states. The T_1 and S_1 states are both produced by HOMO-LUMO excitation, thus their geometrical characteristics are similar. On the other hand, geometry optimization of the T_1 structure provides quite similar parameters to the ground state one. Thus, it can be concluded that the calculated oscillator strength values for the first singlet-singlet electronic transition determines directly the intensity of the reverse emissive $S_1 \rightarrow S_0$ transition. This fact allows the high quantum yields values for **NP-3-Cz**, **NP-9-Cz** and **NP-2-Cz** by the high TD DFT calculated values of $f_{S_0S_1}$ to be explained.

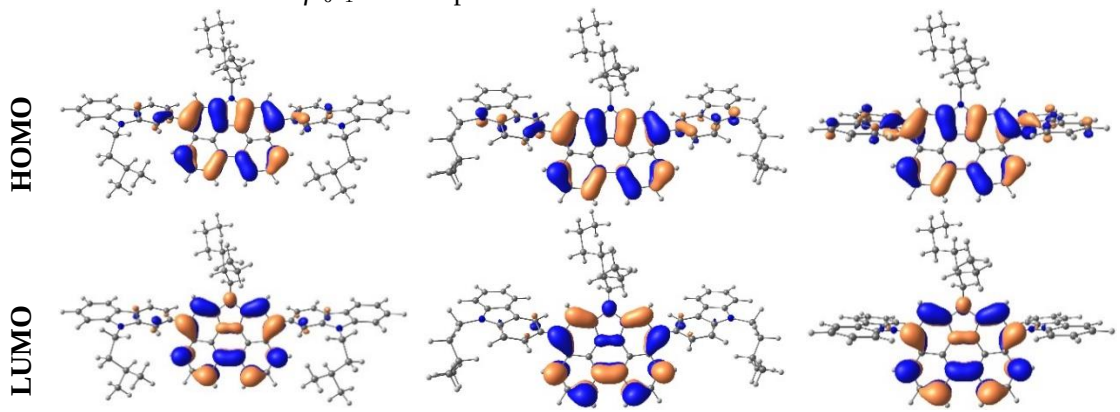

Fig. 4.25. Frontier molecular orbitals of **NP-2-CzNP-3-Cz** and **NP-9-Cz** stacked dimer calculated with the B3LYP/6-31G(d) method

To get a deeper insight into the photophysical properties of **NP-3-Cz**, **NP-9-Cz** and **NP-2-Cz**, the fluorescence decay curves of the solutions were recorded.

Fluorescence decay curves were well described by the single-exponential functions for all the target compounds (Fig. 4.26). Compounds **NP-3-Cz**, **NP-9-Cz** and **NP-2-Cz** showed close values of fluorescence life time (τ), which were found to be 3.15, 4.07 and 2.62 ns, respectively. The radiative (k_r) and nonradiative (k_{nr}) decay rate constants of the singlet excited state were calculated using the following equations: $k_r = \Phi / \tau$, $k_{nr} = (1-\Phi) / \tau$. The estimated values are summarized in Table 2. Compounds **NP-3-Cz** and **NP-2-Cz** exhibited almost the same k_r values while k_{nr} was found to be almost 2 times higher for **NP-2-Cz**. As a consequence, the more preferable nonradiative processes in the solution of the **NP-2-Cz** compound showed approximately a 15 % lower fluorescence quantum yield as compared to **NP-3-Cz**. Fig. 4.24 shows the absorption and emission spectra of the solid films of the target compounds. The lowest-energy absorption band of **NP-3-Cz**, **NP-9-Cz** and **NP-2-Cz** were observed at 528, 514, and 528 nm, respectively. The lowest energy absorption bands of the thin films of **NP-3-Cz**, **NP-9-Cz** and **NP-2-Cz** exhibited red-shifts of ca. 30 nm with respect to those of the dilute solutions. This difference is generally a result of the intermolecular interactions in the solid state.

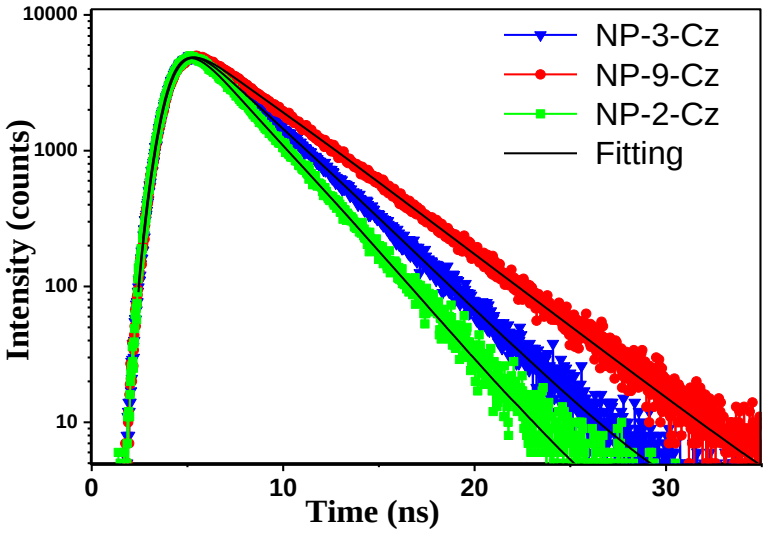

Fig. 4.26. Fluorescence decay curves of the dilute (10^{-5}M) solutions in THF of **NP-3-Cz**, **NP-9-Cz**, **NP-2-Cz**

4.3.4 Electrochemical and photoelectrical properties

The electrochemical properties of **NP-9-Cz**, **NP-3-Cz** and **NP-2-Cz** were investigated by CV to analyze energy transfer processes and the reversibility of oxidation-reduction processes. The CV curves of **NP-9-Cz**, **NP-3-Cz** and **NP-2-Cz** are shown in Fig. 4.27. The electrochemical characteristics are summarized in Table 4.10. The cyclic voltammograms of **NP-3-Cz**, **NP-9-Cz** and **NP-2-Cz** exhibited two reversible oxidation waves with peaks at 0.29, 0.63, 0.41 V (vs Fc/Fc^+) of the first wave and 0.64, 0.97, 0.91 V of the second wave, respectively.

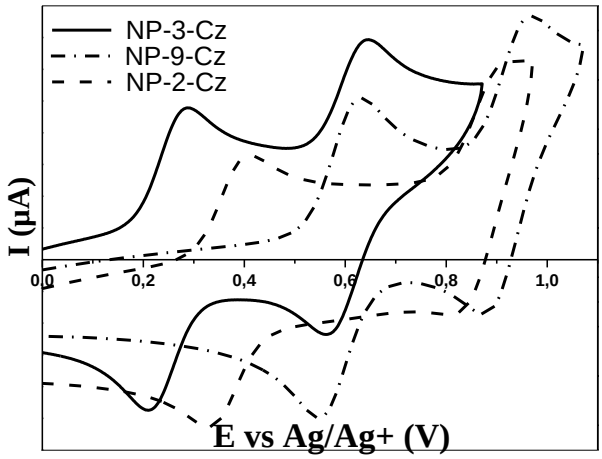

Fig. 4.27. Cyclic voltammograms of **NP-9-Cz**, **NP-3-Cz** and **NP-2-Cz** at 10^{-3} mol L^{-1} in a solution of in argon-purged TBAP (0.1 M) in CH_2Cl_2. v = 50 mV/s

Table 4.10. Electrochemical characteristics of **NP-3-Cz**, **NP-9-Cz** and **NP-2-Cz**

	E_{onset}, V [a]	$E_{ox,pa}$, V	$E_{ox,pc}$, V	$E_{1/2}$, V	E_{HOMO} [b] / E_{HOMO} ^{DFT}., eV [c]	E_{LUMO} ^{DFT}., eV [c]	E_g [d] / E_g ^{DFT}., eV [c]	IP, eV [e]
NP-3-Cz	0.19	0.29/0.64	0.21	0.25	-4.95/-4.73	-1.62	2.54 / 3.11	5.14
NP-9-Cz	0.52	0.63/0.97	0.55	0.59	-5.43/-5.16	-2.00	2.61 / 3.16	5.53
NP-2-Cz	0.31	0.41/0.91	0.33	0.37	-5.12/-4.82	-1.62	2.55 / 3.20	5.20

Each measurement was calibrated with ferrocene (Fc)

[a] E_{ox}^{pa} , E_{ox}^{pc} –peak potentials corresponding to successive molecular oxidations.

[b] $E_{HOMO}(eV) = -1.4E_{onset,ox}(V) - 4.6$

[c] theoretical values of E_{HOMO} and E_{LUMO} have been calculated at the B3LYP/6-31G(d) level of theory accounting the solvent effect.

[d] optical bandgap energies E_g estimated from the absorption edges.

[e] Ionization potentials of the solid samples were estimated by electron photoemission in air.

The redox processes of the solutions were found to be stable with no obvious changes during subsequently repeated scanning (over 5 cycles). The HOMO energy levels of **NP-3-Cz**, **NP-9-Cz** and **NP-2-Cz** were estimated to be -4.95, -5.43 and -5.12 eV respectively, according to the relationship $E_{HOMO}(eV) = -1.4E_{onset,ox}(V) - 4.6$ [257] where $E_{onset,ox}$ is the onset of the first oxidation wave[255]. The DFT-calculated HOMO energy levels are in good agreement with the experimentally estimated values (Table 4.10), while the theoretical bandgap energies deviate to a greater extent from the experimental values since the calculated E (LUMO) energies are evidently overestimated, which is a known problem of DFT.

Ionization potentials of the solid layers of the synthesized compounds were measured by the electron photoemission in air technique. The photoelectron emission spectra of **NP-3-Cz**, **NP-9-Cz** and **NP-2-Cz** are presented in Fig. 4.28.

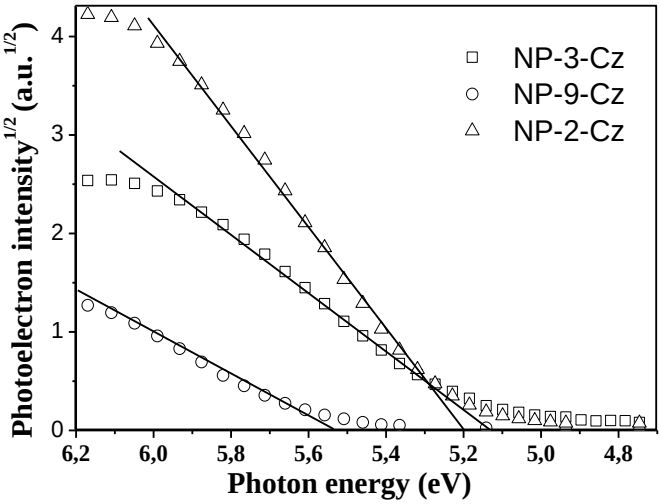

Fig. 4.28. Photoelectron emission spectra of the thin films of **NP-3-Cz**, **NP-9-Cz** and **NP-2-Cz**

The *IP* values were obtained from the intersection of the linear parts of the photoelectron spectra drawn with an abscissa axis. The ionization potential values vary in range from 5.14 to 5.53 eV. The *IP* value observed for **NP-9-Cz** was found to be 0.3 eV higher compared to those of **NP-3-Cz** and **NP-2-Cz**.

4.3.5 Charge-transporting properties

To characterize the charge transporting properties, the layers of the synthesized compounds **NP-3-Cz**, **NP-9-Cz** and **NP-2-Cz** were investigated using the TOF technique at room temperature in air. The layers of the samples were prepared by vacuum deposition. The layer thickness varied from 1.0 to 4.2 nm. Fig. 4.29 shows the hole and electron photocurrent transients on log-log and linear (insets) scales that were observed for the layers of **NP-3-Cz**, **NP-9-Cz** and **NP-2-Cz.**

The layers of all the synthesized compounds were found to be capable of transporting both holes and electrons in air with good agreement to the close values of the DFT calculated electron (λ_e) and hole (λ_h) reorganization energies (the higher λ values corresponds to the lower parameters of conductivity), i.e. the **NP-3-Cz**, **NP-9-Cz** and **NP-2-Cz** films possess the ambipolar semiconductive nature. Fig. 4.30 shows the electric field dependencies of charge carrier mobilities (μ) for the layers of **NP-3-Cz**, **NP-9-Cz** and **NP-2-Cz.** The linear dependencies of charge mobilities on the square root of the electric field ($E^{1/2}$) were observed for all the synthesized compounds. Such dependency was previously observed and explained by Borsenberger [259].

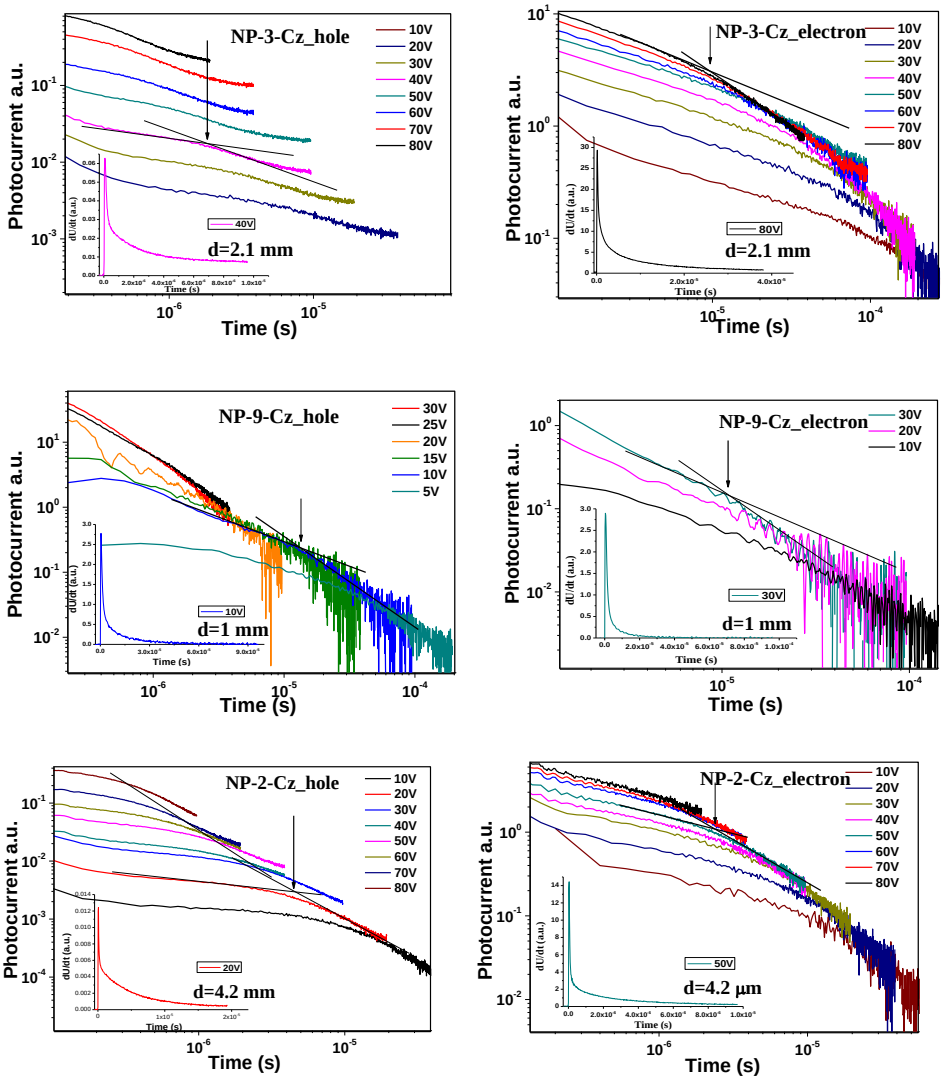

Fig. 4.29. TOF transients for the vacuum deposited layers of **NP-3-Cz**, **NP-9-Cz** and **NP-2-Cz** in the log-log scales. The insets show transient curves of electrons and holes at the corresponding surface voltages in the linear plot

The zero electric field charge mobility (μ_0) and field dependence parameter (α) were calculated using Poole–Frenkel relationship: $\mu=\mu_0 \exp(\alpha\sqrt{E})$. The TOF hole and electron mobility data for all the compounds (**NP-3-Cz**, **NP-9-Cz**, **NP-2-Cz**) are summarized in Table 4.11.

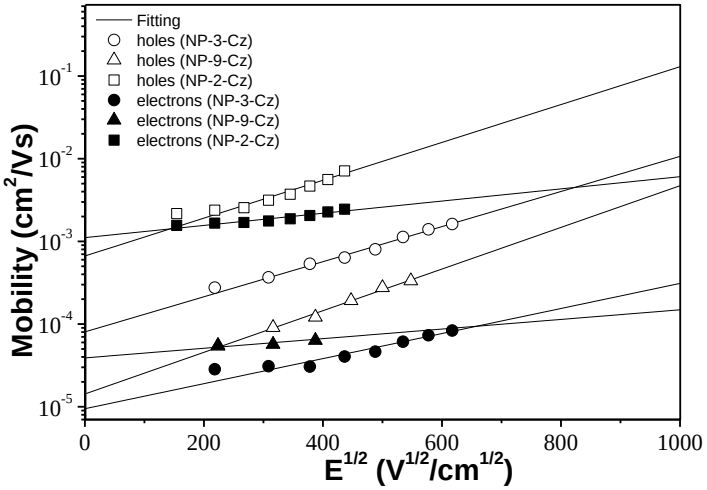

Fig. 4.30. Electric field dependencies of hole and electron mobilities in the layers of **NP-3-Cz**, **NP-9-Cz** and **NP-2-Cz**.

Table 4.11. The hole-electron mobility data for compounds **NP-3-Cz**, **NP-9-Cz** and **NP-2-Cz**.

Comp.	*d*, [μm]	μ_{0h} / μ_{0e},[cm²/Vs][b]	μ_h / μ_e, [cm²/Vs][a]	α *10⁻³, [cm/V]	λ_e, eV[c]	λ_h, eV[c]
NP-3-Cz	2.1	8.2×10^{-5} / 9.4×10^{-6}	9.1×10^{-4} / 5.4×10^{-5}	4.9 / 3.5	0.25	0.25
NP-9-Cz	1.0	1.4×10^{-5} / 2.2×10^{-5}	2.5×10^{-4} / 3.9×10^{-4}	5.8 / 1.4	0.22	0.37
NP-2-Cz	4.2	6.6×10^{-4} / 1.1×10^{-3}	9.3×10^{-3} / 2.6×10^{-3}	5.3 / 1.7	0.29	0.21

[a] mobility value at an electric field of 2.5×10^5 V/cm

[b] the zero-field hole and electron drift mobility

[c] the electron (λ_e) and hole (λ_h) reorganization energies obtained from the B3LYP/6-31G(d) calculations

The TOF measurements revealed, by nearly one, the order of magnitude higher hole and electron mobilities in the layer of **NP-2-Cz** against those of the layers of **NP-3-Cz** and **NP-9-Cz**. The zero field electron mobility of the vacuum deposited layer of **NP-2-Cz** was found to be higher than 10^{-3}cm^{2}V^{-1}s^{-1} at room temperature. At the electric field of 2.5×10^5 V/cm, hole-mobility values of the layers of **NP-3-Cz**, **NP-9-Cz** and **NP-2-Cz** were found to be 9.1×10^{-4},2.5×10^{-4}, 9.3×10^{-3}cm^{2}V^{-1}s^{-1}, while the electron-mobility values were 5.4×10^{-5}, 1.3×10^{-4}, 2.6×10^{-3}, 2.6×10^{-3}cm^{2}V^{-1}s^{-1}, respectively. The highest charge mobilities in the layers of **NP-2-Cz** can apparently be explained by a more effective conjugation of electrons between perlyne and carbazole moieties. This conclusion is in good agreement with the lowest value of λ_h for the **NP-2-Cz** molecule, while the λ_h value contradicts the experiment, this can be explained by the crucial role of charge transfer integrals, which depend on the crystal structure of the **NP-2-Cz** (this aspect has not been taken into account in the realized DFT calculations).

4.3.6 Performance in OLEDs

EL spectra of the fabricated OLEDs (Fig. 4.31) were found to be similar to the PL spectrum of the films of **NP-3-Cz**, **NP-9-Cz** and **NP-2-Cz**. (Fig. 4.32). Thus, the layers of the newly synthesized compounds were responsible for the OLED emission. The EL spectrum of device B was found to be wider with a lower-energy maximum at 490 nm.

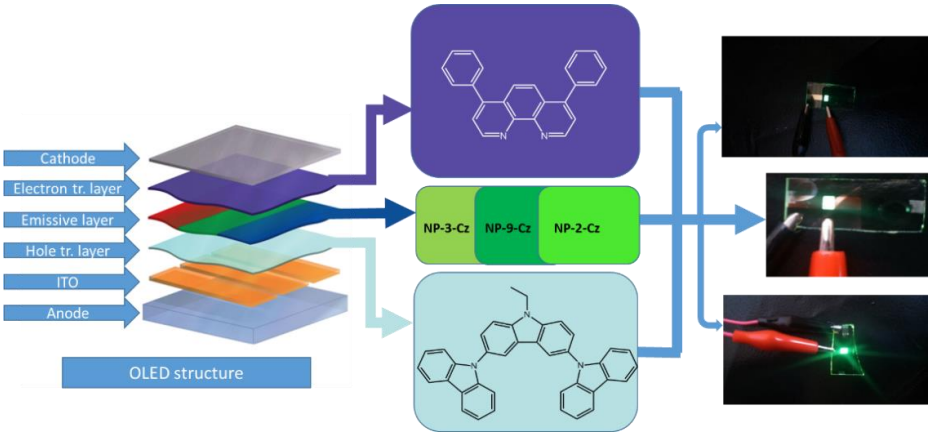

Fig. 4.31. OLED structure and photos of the devices A, B and C

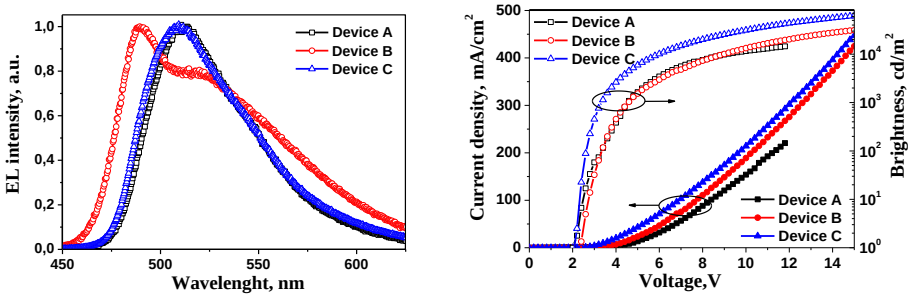

Fig. 4.32. EL spectra (left), current density-voltage and brightness-voltage characteristics (right) of the devices A, B and C

Table 4.12. Characteristics of the devices A, B and C

	Max. EQE and current efficiency	Max. power efficiency	Turn-on voltage	Max. brightness
Device A	3.7%, 12.9 cd/A	8.8 lm/W	2.0 V	14500 cd/m^2 (11.8 V, 220 mA/cm^2)
Device B	1.9%, 6.5 cd/A	5 lm/W	2.2 V	31300 cd/m^2 (15 V, 425 mA/cm^2)
Device C	4.2%, 14.6 cd/A	11.4 lm/W	2.0 V	62000 cd/m^2 (15 V, 450 mA/cm^2)

The basic characteristics of the fabricated devices A, B and C are presented in Table 4.12. The high brightness of the fabricated devices (Fig. 4.32) can be explain

by the high emission quantum yields of the films of **NP-3-Cz**, **NP-9-Cz** and **NP-2-Cz** and ambipolar charge-transporting properties of these compounds**.**

The best characteristics observed for Device C can apparently be explained by favourable charge-transporting properties of **NP-2-Cz**. Moreover, LUMO energy levels of **NP-3-Cz** and **NP-2-Cz** matched with the energy levels of the anodes, which provide low turn-on voltage of the devices (2.0 V) (Fig. 4.32).

In conclusion, N-annelated perylenes containing two differently linked carbazolyl substituents were synthesized and their thermal, optical, photophysical and electrochemical properties were studied. The synthesized compounds were found to be efficient green-emitting fluorophores. They were used for the fabrication of the emissive layers of the effective and highly luminous OLEDs. The brightness value exceeding 62000 cd/m^2 and EQE of 4.2% were recorded. We suggest that such high efficiencies of the fabricated devices are due to the high fluorescence quantum yields of compounds in the solid state, as well as due to the high and balanced electron and hole mobilities. The TDDFT calculated values of the S_0–S_1 oscillator strengths were found to be very high and consequently causes the high fluorescence ability. The oscillator strengths (0.9, 0.49, 1.06) are in correlation with the brightness (14500, 31300 and 62000 cd/m^2) and EQE (3.7, 1.9, 4.2 %) values that were observed for the fabricated OLEDs.

4.4 Di-, tetra-, hexamethoxycarbazole derivatives

There is a substantial number of studies on 3,6-disubstituted and 2,7-disubstituted carbazole derivatives and their applications [227-229]. Incomparison, less research has been carried out on multisubstituted carbazole derivatives. Working on the synthesis of multisubstituted derivatives of carbazole it was observed that for the 3,6-substituted derivatives of carbazole the most reactive positions are C-3 and C-6 followed by the C-1 and C-8 positions [6]. In the current work, a series of carbazole derivatives substituted with two, four and six methoxy groups at C-1, C-2, C-3, C-6, C-7 and C-8 positions will be presented. The impact of methoxy groups on aromatic system of carbazole and subsequently on the optical, thermal, electrochemical and photophysical properties of its derivatives will also be analyzed. In addition, the comparative study with the 3,6-disubtituted carbazole derivatives and discussion of the key differences of the thermal, optical, photophysical and charge-transporting properties will be presented. Finally, the theoretical calculations of all methoxy-substituted derivatives will be presented, along with a comparison of the data obtained from the experimental results.

4.4.1 Synthesis

The disubstituted compounds (**2DMCz**, **3DMCz**) were prepared in two steps, starting from anisole and carbazole derivatives, respectively, using the previously reported methods (Scheme 4.7) [215-218]. 2,3,6,7-Tetramethoxycabazole (TMCz) and 1,2,3,6,7,8-hexamethoxycarbazole (HMCz) were obtained from the

disubstituted derivative 2DMCz, via bromination [217] and methoxylation [218] reactions. The compounds were identified by ^{1}H and ^{13}C NMR spectrometries.

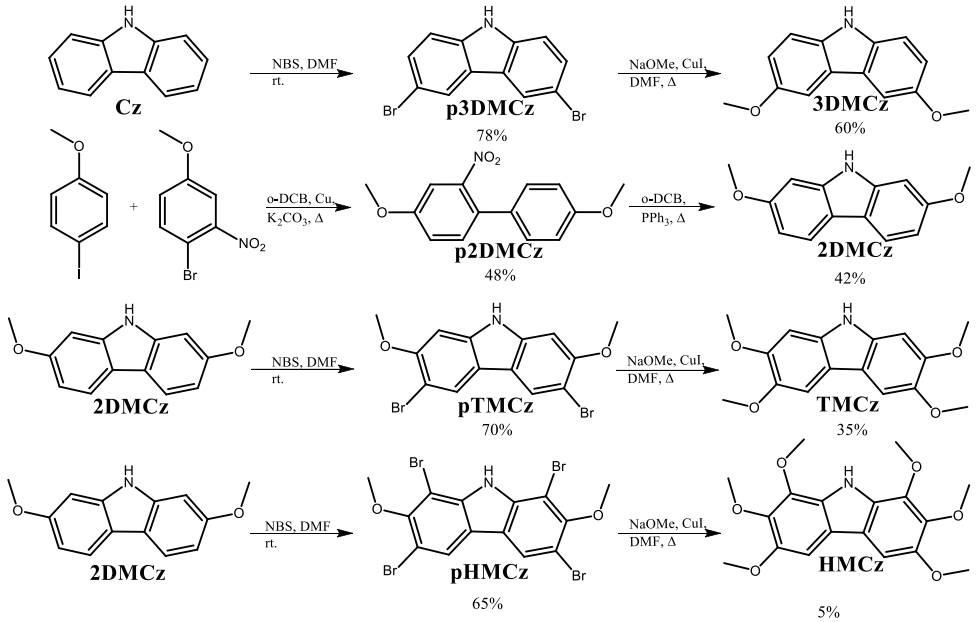

Scheme 4.7. Synthesis of di, tetra and hexamethoxycarbazole derivatives **3DMCz, 2DMCz, TMCz, HMCz**

4.4.2 Crystal structures

Single crystals of **3DMCz, 2DMCz, TMCz, HMCz** and **Cz** suitable for X-ray analysis were grown from the diluted solutions. The ORTEP drawings and packing in the crystals are shown in Fig. 4.33 and the crystalographic data is summarized in Table 4.13. The tetra- and hexamethoxy derivatives (**TMCz** and **HMCz)** crystalize into the monoclinic crystal systems with space group $P2_1$ (#4), while dimethoxycarbazole derivatives (**3DMCz** and **2DMCz**) form crystals with triclinic (space group P-1 (#2) and orthorhombic (space group P212121 (#19)) crystal systems, respectively. The methoxy groups of **3DMCz**, **2DMCz**, **TMCz** lay in the same plane as the carbazole aromatic rings. In the case of **HMCz**, due to steric overcrowding in the space around carbazole aromatic system, the methoxy groups bent below or above the carbazole plane. In the crystals, the molecules are held together with different types of interactions: N-H···O, C-H···O, N-H···CAr, C-H···CAr, ArC-H···CAr.

The strongest interactions, i.e. hydrogen bonds (N-H···O, C-H···O, Fig. 4.33), were observed for **3DMCz** and **HMCz** with the distances varying from 2.22 to 2.64 Å. The weaker interactions (N-H···CAr, C-H···CAr, ArC-H···CAr), with the distance higher than 2.72 Å, are common to all the other crystal structures described in this chapter.

Table 4.13. Crystalographic data of **Cz**, **3DMCz, 2DMCz, TMCz, HMCz**

	Cz	**3DMCz**	**2DMCz**	**TMCz**	**HMCz**
Chemical formula	$C_{12}H_9N$	$C_{14}H_{13}NO_2$	$C_{14}H_{13}NO_2$	$C_{16}H_{17}NO_4$ CH_2Cl_2	$C_{18}H_{21}NO_6$
Crystal system	orthorhombic	triclinic	orthorhombic	monoclinic	monoclinic
Formula weight	167.21	227.26	227.26	287.31	347.36
Shape	yellow, prism	colorless, chip	colorless, block	colorless, block	colorless, prism
Space group	Pnma (#62)	P-1 (#2)	P212121 (#19)	P21 (#4)	P21 (#4)
***a* / Å**	7.794(10)	6.338(7)	5.691(4)	11.240(9)	7.349(7)
***b* / Å**	19.19(2)	15.81(2)	7.584(7)	5.886(4)	8.146(8)
***c* / Å**	5.739(8)	18.75(2)	25.83(3)	26.47(2)	14.12(2)
***α* / º**	90.00	106.65(3)	90.00	90.00	90.00
***β* / º**	90.00	95.92(2)	90.00	90.052(7)	98.51(2)
***γ* / º**	90.00	91.708(4)	90.00	90.00	90.00
***V* / Å^3**	858(2)	1787(4)	1115(2)	1751(3)	836(2)
Z	4	6	4	4	2
***D* / g cm^{-3}**	1.294	1.267	1.354	1.366	1.380
***Temperature* / K**	298	298	298	298	298

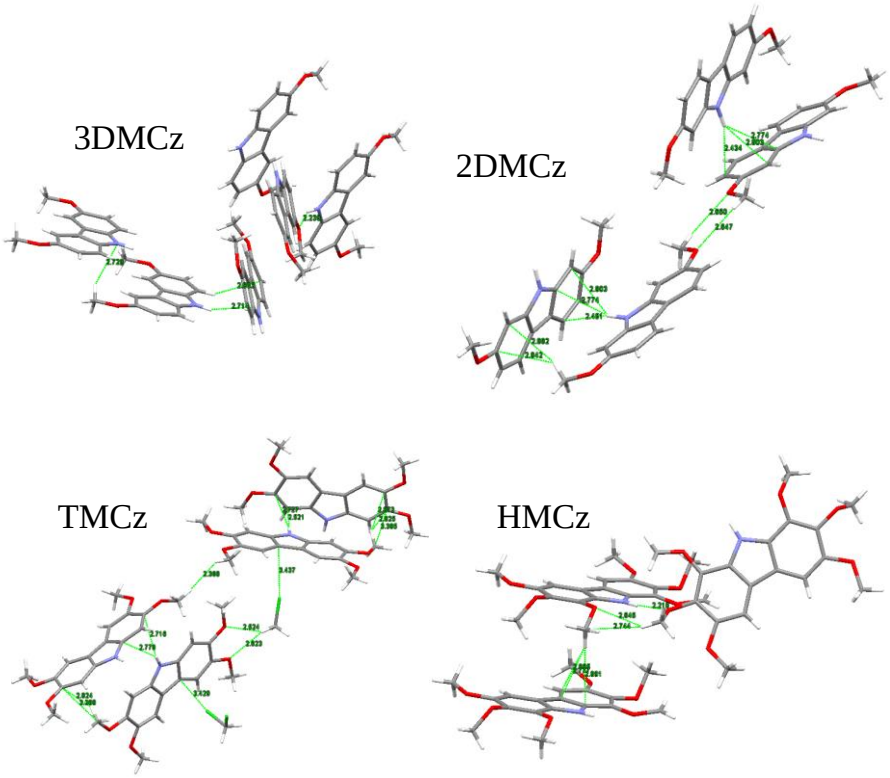

Fig. 4.33. Crystal packing and interactions of **3DMCz, 2DMCz, TMCz, HMCz**

4.4.3 Thermal properties

The glass-forming capabilities and thermal stability of the materials were estimated by DSC and TGA, respectively. The thermograms of the compounds (**3DMCz, 2DMCz, TMCz, HMCz**) are shown in Fig. 4.34 and the thermal characteristics are collected in Table 4.14. Due to the low molecular weight, the synthesized methoxycarbazoles are not capable of forming molecular glasses. These compounds showed moderate thermal stability with 5% loss temperatures between 227°C and 254°C. Compared to non-substituted stand-alone carbazole (**Cz**), methoxy groups have a positive influence on the degradation (sublimation) temperature of the compounds. The T_d values of **3DMCz**, **2DMCz**, **TMCz** and **HMCz** were found to be more than 30 °C higher than that of **Cz**. The increase of thermal stability could be interpreted in terms of hydrogen bonding between oxygen of the methoxy group and other hydrogen atoms (Fig. 4.33). In the first DSC heating scan, carbazole (**Cz**) showed an endothermal peak at 246 °C, while methoxysubstituted derivatives (**3DMCz**, **2DMCz**, **TMCz**, **HMCz**) showed their melting signals between 180 and 120 °C. Compared to **Cz**, the lower T_m values of **3DMCz**, **2DMCz**, **TMCz** and **HMCz** can be explained by the plasticizing effect of the methoxy groups.

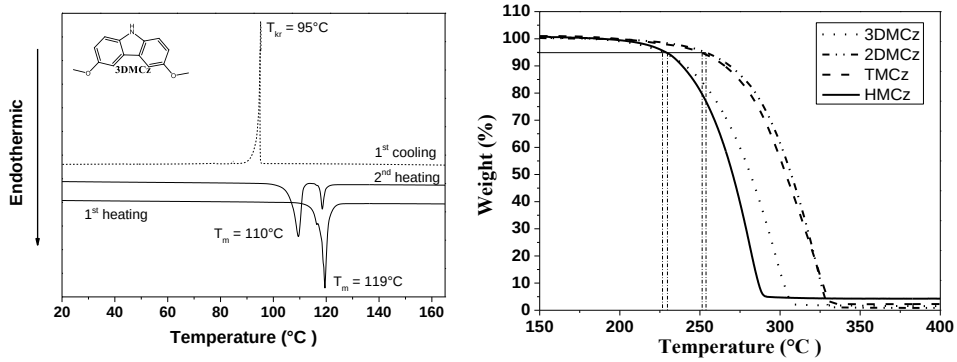

Fig. 4.34. DSC and TGA thermograms of methoxycarbazole derivatives

4.4.4 Optical and photophysical properties

UV-vis and FL spectra of the dilute solutions in THF of **3DMCz**, **2DMCz**, **TMCz**, **HMCz** are shown in Fig. 4.35. The optical characteristics are collected in Table 4.14. The methoxysubstituted carbazole derivatives (**3DMCz, 2DMCz, TMCz, HMCz**) showed the lowest absorption maxima wavelength values in the range of 321-366 nm. The number and position of methoxy groups at the carbazole moiety have a significant effect on the character of UV-vis spectra. The lowest energy absorption band of 3,6-dimethoxycarbazole (**3DMCz**) was observed at 366 nm, while the dimethoxy (**2DMCz**) and tetramethoxy (**TMCz**) counterparts showed blue shifts and the lowest energy absorption bands for these compounds were recorded at 320 nm. The multimethoxy-substituted carbazoles (**3DMCz, 2DMCz, TMCz, HMCz**) showed emission in the ultraviolet and violet regions with the wavelengths of emission maxima ranging from 343 to 390 nm. Fluorescence spectra

of the methoxycarbazole derivatives exhibited considerable redshifts of 17-47 nm with respect to non-substituted carbazole (**Cz**).

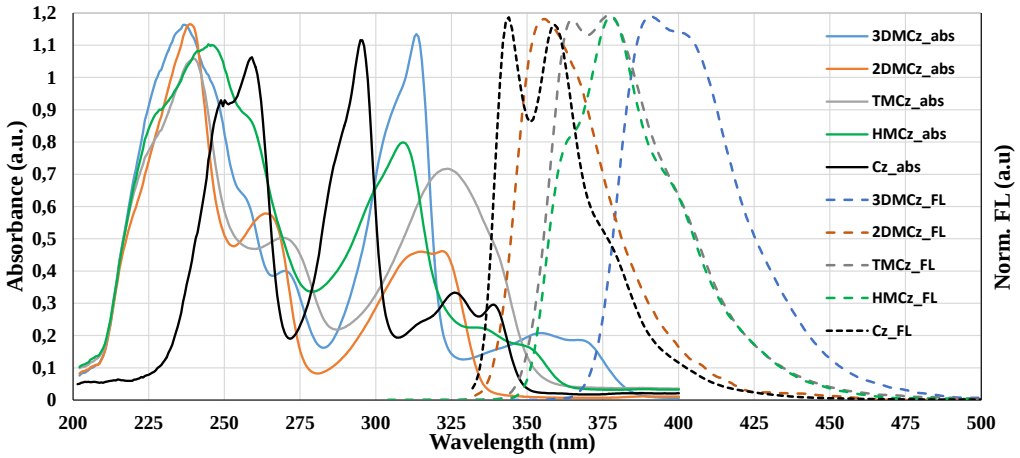

Fig. 4.35. UV-vis and normalized fluorescence spectra (λ_{ex}=350 nm) of dilute THF solutions (10^{-5} M) of **3DMCz**, **2DMCz**, **TMCz, HMCz** and **Cz**

In contrast to small Stokes shift estimated for carbazole solution, the methoxysubstituted derivatives (**3DMCz**, **2DMCz**, **TMCz**, **HMCz**) showed enlarged Stokes shift values of 18-36 nm. This observation implies noticeable differences between the emitting and ground state structures of methoxy derivatives (**3DMCz**, **2DMCz**, **TMCz**, **HMCz)**.

Table 4.14. Thermal and optical characteristics of **3DMCz**, **2DMCz**, **TMCz**, **HMCz** and **Cz**

	λ^{ab}_{max}, nm	λ^{em}_{max}, nm	Stokes shift, nm	T_{subl}, ◦C[b]	T_m, ◦C
3DMCz	366	390	24	227	120
2DMCz	320	357	37	254	140
TMCz	321	363	42	251	178
HMCz	346	378	32	230	-[a]
Cz	337	343	6	204	246

[a] not observed; [b] sublimation temperature

4.4.5 Electrochemical and photoelectrical properties

Electrochemical properties of the compounds (**3DMCz**, **2DMCz**, **TMCz**, **HMCz**) were studied by CV. The electrochemical data is collected in Table 4.15**.** The CV curves of the solutions of the studied compounds are shown in Fig. 4.36. No reduction waves were observed down to ca -1.5 V. Shigehare et al. [241] reported that C-1,8 positions of the carbazole moiety are the next reactive positions if C-3 and C-6 positions are occupied. It was noticed that 2,7-disubstituted (**2DMCz**) and

2,3,6,7-tetrasubstituted (**TMCz**) carbazole derivatives exhibited an irreversible oxidation peak and the formation of new carbazolyl-containing compounds, while 3,6-disubstituted (**3DMCz**) and 1,2,3,6,7,8-hexasubstituted (**HMCz**) compounds showed reversible oxidation processes. Compound **3DMCz** exhibited one oxidation peak at 0.62 V. **HMCz** showed two oxidation peaks at 0.48 and 0.83 V.

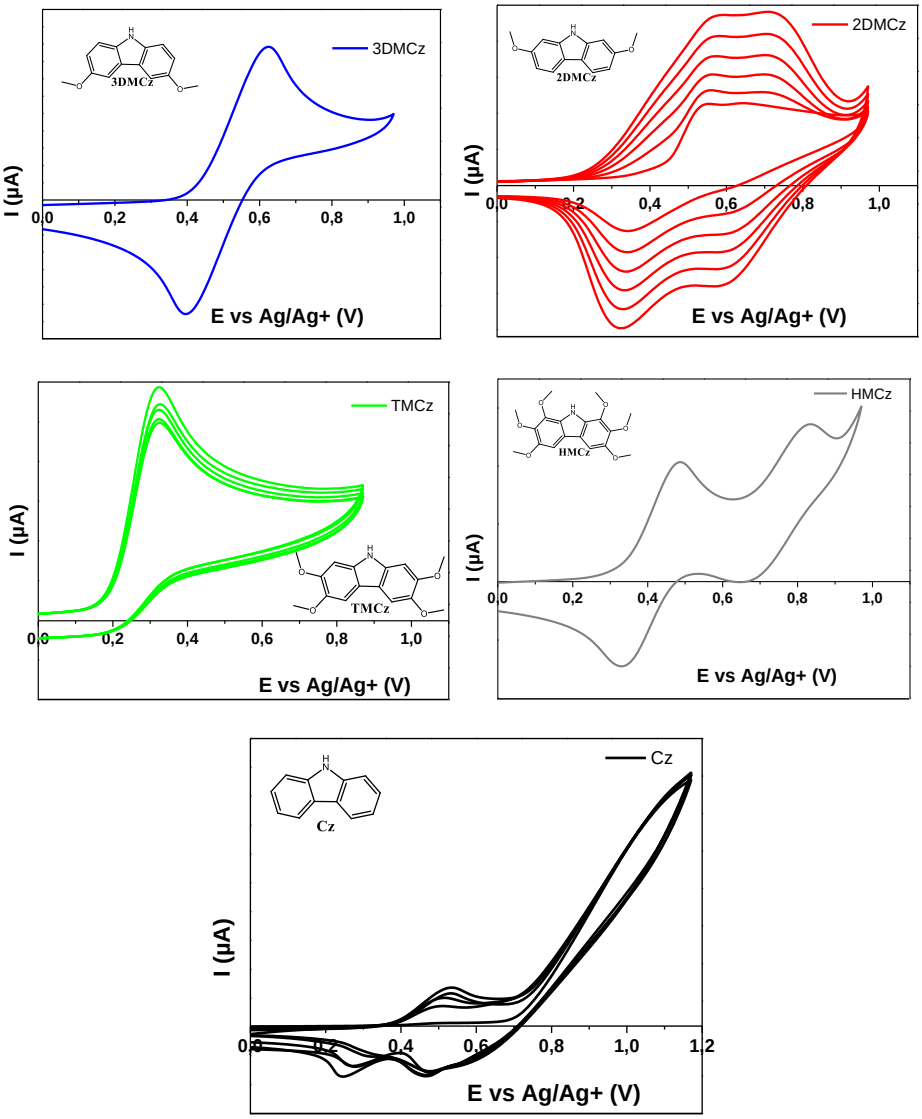

Fig. 4.36. Cyclic voltammograms of **3DMCz**, **2DMCz**, **TMCz, HMCz** and **Cz** at 10^{-3}mol L^{-1} in a solution of argon-purged TBAP (0.1M) in CH_2Cl_2. *v*= 50 mV/s

The irreversible oxidation of **2DMCz**, **TMCz** and **Cz** started at 0.44 V, 0.18 V and 0.70 V, respectively. Compared to **Cz** oxidation, methoxy substituted derivatives

3DMCz, **2DMCz**, **TMCz**, **HMCz** showed 50-75 % lower oxidation values in solutions.

Table 4.15. Electrochemical characteristics of **3DMCz**, **2DMCz**, **TMCz**, **HMCz** and **Cz**.

	E_{onset},V [a]	$E_{ox,pa}$, V [a]	$E_{ox,pc}$, V [a]	E_{HOMO}, (eV)[c]	E_g, (eV)[b]	IP, (eV)[b]
3DMCz	0.42	0.62	0.39	-5.31	3.25	5.45
2DMCz	0.44	-	-	-5.22	3.72	5.43
TMCz	0.18	-	-	-4.85	3.54	5.37
HMCz	0.34	0.48	0.33	-5.17	3.41	5.34
Cz	0.70	-	-	-5.58	3.58	5.68

[a] E_{oxpa} , E_{oxpc} –peak potentials corresponding to successive molecular oxidations.
[b] The optical bandgap energies E_g estimated from the absorption edges.
[c] $E_{HOMO}(eV) = -1.4E_{onset,ox}(V) - 4.6$ [257],where $E_{onset,ox}$ was determined by solution-based CV [255].
[d] IP for the solid films was measured by the electron photoemission in air method.

The HOMO energy values were calculated from CV results using the equation: $E_{HOMO}(eV) = -1.4E_{onset,ox}(V) - 4.6$. Compared to carbazole, compounds methoxysubstituted carbazole derivative showed the HOMO energy value increase by 0.30-0.50 eV. In addition, the experimental HOMO values are comparable to the theoretical results achieved using DFT calculations (Fig. 4.37, Table 4.15).

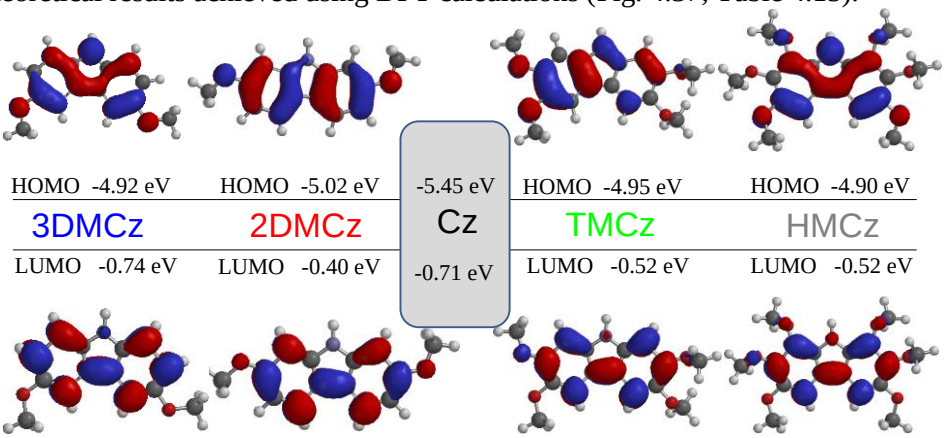

Fig. 4.37. Molecular orbitals of **3DMCz**, **2DMCz**, **TMCz, HMCz** calculated with the B3LYP/6-31** method

The IPs of the solid state were obtained using electron photoemission in air technique. The results are collected in Table 4.15. The *IP* values vary in the range from 5.34 eV to 5.45 eV. The lowest *IP* values were observed for tetra- and hexa-subtituted carbazole derivatives (**TMCz**, **HMCz**) with values of 5.37 eV and 5.34 eV, respectively, which are much lower compared to that of **Cz** (5.68 eV).

To summarize, four carbazole derivatives substituted with methoxy groups via C1, C2, C3, C6, C7 and C8 positions have been synthesized. All the structures were proven by X-ray crystallography. Moreover, from X-ray data it was observed that

methoxy groups of disubstituted (**3DMCz**, **2DMCz**) and tetrasubstituted (**TMCz**) carbazole derivatives lay in the same plane as carbazole aromatic rings, while, in the case of hexasubstituted carbazole (**HMCz**), they are bent above or below the carbazole plane. Additionally, due to hydrogen bonding between molecules, compounds containing methoxy groups showed a higher degradation (sublimation) temperature compared to that of carbazole temperature. Additionaly, compared to stand alone carbazole, the target methoxysubstituted compounds (**3DMCz**, **2DMCz**, **TMCz, HMCz**) showed a significant red-shifted FL spectra that consequently resulted in higher Stokes shift values. Carbazole derivatives substituted with two methoxy groups via C2 and C7 (**2DMCz**) or with four methoxy groups via C2, C3, C6 and C7-positions (**TMCz**) exhibited irreversible oxidation peaks, while 1,2,3,6,7,8-hexamethoxycarbazole (**HMCz**) and 3,6-dimethoxycarbazole (**3DMCz**) showed reversible oxidation processes. Moreover, DFT calculations revealed comparable experimental and theoretical HOMO values for all compounds. The estimated ionization energies of methoxysubstituted derivatives (**3DMCz**, **2DMCz**, **TMCz, HMCz**) vary in range from 5.35 eV to 5.45 eV and these values are lower compared to that of the carbazole IP values.

4.5 Synthesis and properties of glass-forming carbazole trimers containing methoxy-substituted carbazole moieties

4.5.1 Synthesis

The synthesis of the compounds **2MeOCz**, **3MeOCz**, **TMeOCz** consisting of N-alkylated carbazole core substituted at C-3 and C-6 with the different methoxy-carbazolyl substituents (**3DMCz**, **2DMCz**, **TMCz**) is shown in Scheme 4.8.

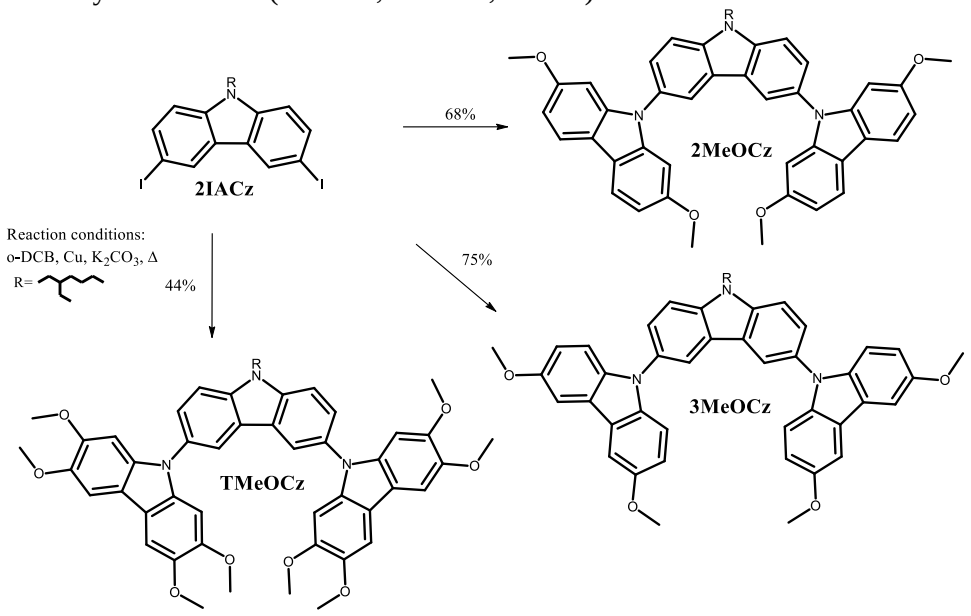

Scheme 4.8. Synthesis of di, tetra and hexamethoxycarbazole derivatives **2MeOCz**, **3MeOCz**, **TMeOCz**

Compounds **2MeOCz**, **3MeOCz**, **TMeOCz** were prepared in high yields using the modified Ullmann coupling reaction [326] of iodinated precursor (**2IACz**) with methoxylated derivatives **3DMCz**, **2DMCz**, **TMCz**. All the new compounds were identified by ^{1}H and ^{13}C NMR. At room temperature, **2MeOCz**, **3MeOCz**, **TMeOCz** were found to be soluble in acetone, DCM and THF.

4.5.2 Thermal properties

To investigate morphological and thermal stability under heating, compounds **2MeOCz**, **3MeOCz**, **TMeOCz** were analyzed by DSC and TGA. Thermal characteristics are collected in Table 4.16. The thermograms of the compounds are shown in Fig. 4.38.

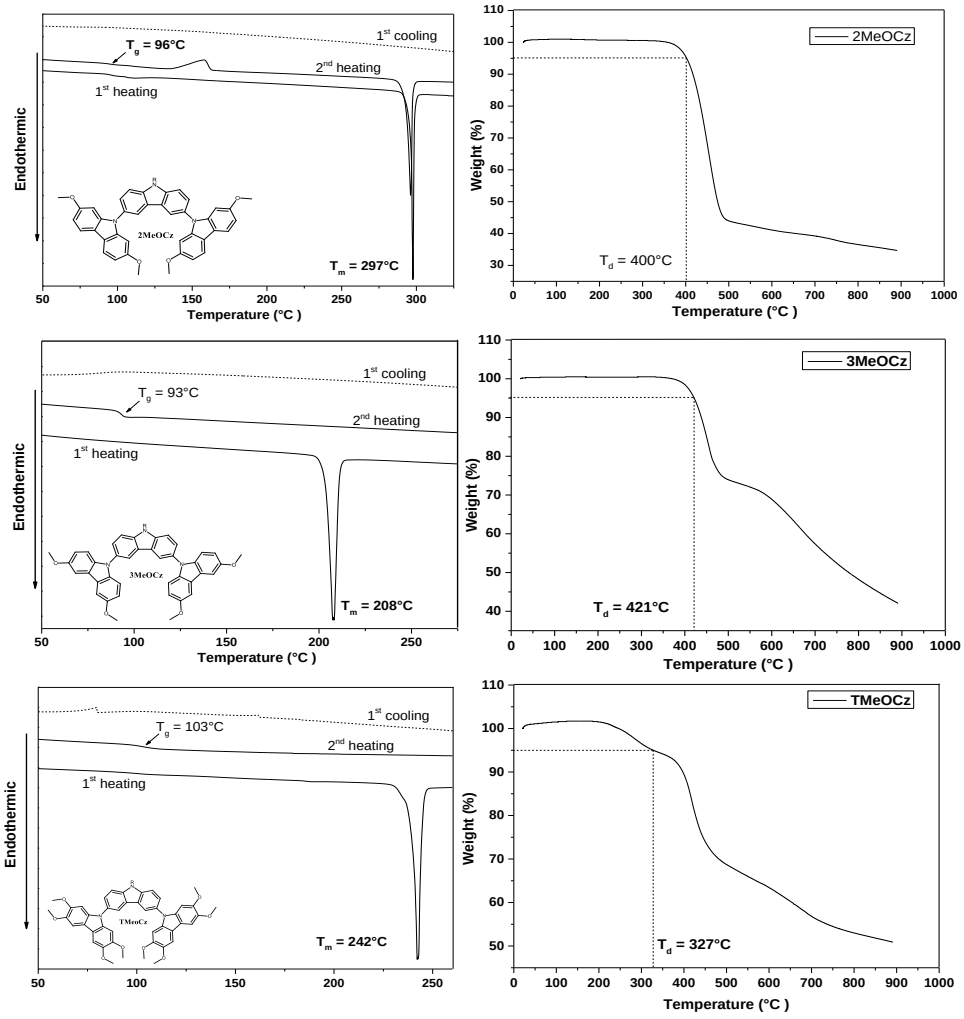

Fig. 4.38. DSC and TGA thermograms of**2MeOCz**, **3MeOCz**, **TMeOCz**

Compared with the thermal stability of the derivative having no methoxy groups (**1A**, 384 °C) [5], carbazole derivatives dimethoxycarbazole moieties (**2MeOCz**, **3MeOCz**) showed higher thermal stability with 5 % loss temperatures at 400 °C and 421 °C, respectively, while carbazole derivativepossessing tetramethoxycarbazole species (**TMeOCz)** showed relatively low degradation temperature with 5% temperature loss at 327 °C. DSC curves showed that all new compounds (**2MeOCz**, **3MeOCz**, **TMeOCz**) form molecular glasses with glass-transition temperatures ranging from 96 °C to 103 °C. Compounds **2MeOCz**, **3MeOCz**, **TMeOCz** were isolated as white crystals. In the first DSC scans, these compounds showed endothermal peaks of melting at 297 °C, 208 °C and 242 °C, respectively. In the case of **3MeOCz**, the exothermal peak of crystallization was observed during the second heating scan, which consequently caused one more endothermal peak of melting (at 297 °C) during the same scan. Compared to derivative with no methoxy groups **1A** [5], all the methoxylated derivatives (**2MeOCz**, **3MeOCz**, **TMeOCz**) showed higher thermal stability.

4.5.3 Optical properties

The UV-vis absorption and fluorescence spectra of the dilute THF solutions of compounds **2MeOCz**, **3MeOCz**, **TMeOCz** and **TCz** are presented in Fig. 4.39 and the data is collected in Table 4.16.

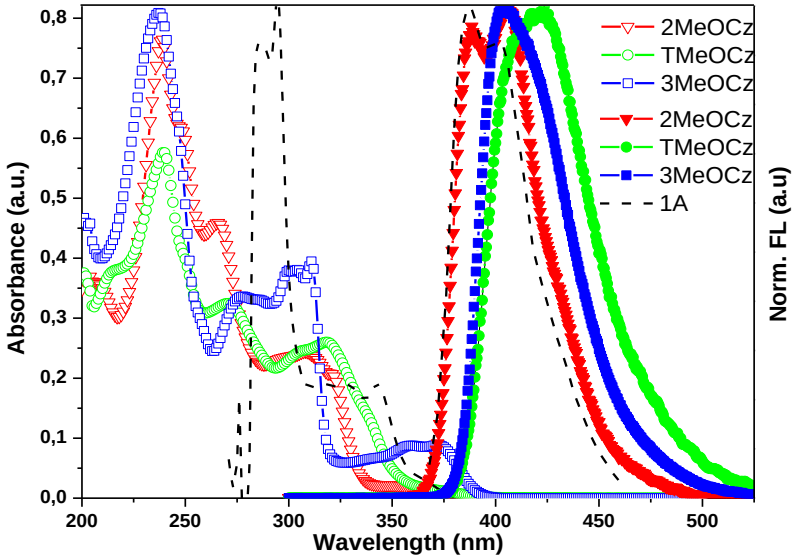

Fig. 4.39. UV-vis and normalized fluorescence spectra (λ_{ex}=350 nm) of dilute THF solutions (10^{-5} M) of **2MeOCz**, **3MeOCz**, **TMeOCz** and **1A**

Due to π-π* transitions, **2MeOCz**, **3MeOCz**, **TMeOCz** showed low energy absorption maxima at wavelengths ranging from 360 nm to 376 nm. Compared to carbazole trimer with no methoxy groups **1A** [5], the derivative containing 2,7-

dimethoxycarbazolemoiety (**2MeOCz**) showed a small blue-shift, while the derivatives containing 3,6-dimethoxycarbazole (**3MeOCz**) and 2,3,6,7-tetramethoxycarbazole (**TMeOCz**) moieties exhibited small red-shifts (5-9 nm). Dilute solutions of **2MeOCz**, **3MeOCz**, **1A** [5] exhibited close vibrational peaks in the FL spectra with the maximum intensity wavelengths of 389 nm, 404 nm, 391, respectively, while **TMeOCz** showed a 16-30 nm red-shifted emission spectrum with respect to other derivatives studied. The introduction of methoxy groups gave a rise of Stokes shift values in the following order: **1A**<**2MeOCz**<**3MeOCz**<**TMeOCz**.

Table 4.16. Thermal, optical and photophysical characteristics of compounds **2MeOCz**, **3MeOCz**, **TMeOCz** and **1A**

Material	T_m / T_g [a] / T_d [b], °C	λ^{ab}_{max}, nm	λ^{em}_{max}, nm	Stokes shift, nm	E_{onset}, V	$E_{ox,pa}$, V [c]	$E_{ox,pc}$, V [c]	E_{HOMO}, eV [e]	IP, (eV) [d]
2MeOCz	297 / 96 / 400	360	389	29	0.64	-	-	-5.50	5.40
3MeOCz	208 / 93 / 421	372	404	32	0.54	0.74	0.57	-5.36	5.19
TMeOCz	242 / 103 / 327	376	420	44	0.46	0.58	0.49	-5.24	5.44
1A [5]	182 / 82 / 384	367	391	24	0.57	-	-	-5.40	5.80

[a] - determined by DSC, scan rate 10 °C/min, N_2 atmosphere;
[b] - 5% weight loss determined by TGA, heating rate 10 °C/min, N_2 atmosphere;
[c] E_{oxpa}, E_{oxpc} –peak potentials corresponding to successive molecular oxidations.
[d] *IP* for the solid films was measured by the electron photoemission in air method.
[e] $E_{HOMO}(eV) = -1.4E_{onset,ox}(V) - 4.6$ [257],where $E_{onset,ox}$ was determined by solution-based CV [255].

4.5.4 Electrochemical and photoelectrical properties

The electrochemical behaviour of **2MeOCz**, **3MeOCz**, **TMeOCz** in solutions of dichloromethane were investigated by CV. The CV curves of the compounds are shown in Fig. 4.40.

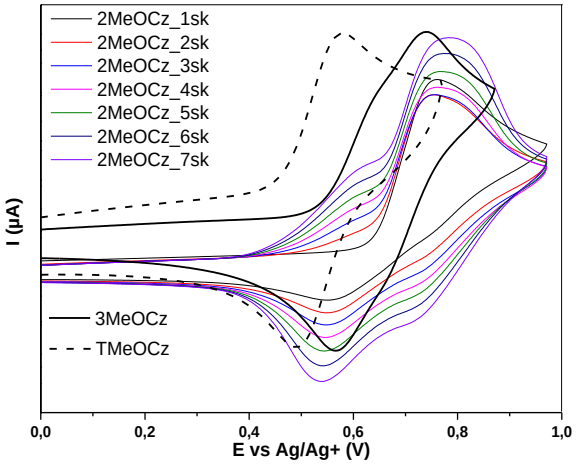

Fig. 4.40. Cyclic voltammograms of **2MeOCz**, **3MeOCz**, **TMeOCz** at 10^{-3}mol L^{-1} in a solution of argon-purged TBAP (0.1M) in CH_2Cl_2. *v*= 50 mV/s

After seven oxidation and reduction cycles, compounds **3MeOCz**, **TMeOCz** exhibited a reversible oxidation, while **2MeOCz** showed irreversible oxidation processes leading to the formation of new carbazole-based compounds [241]. The oxidation of the target compounds started in the range 0.46-0.64 V. The oxidation peaks of **2MeOCz**, **3MeOCz**, **TMeOCz** were observed at 0.75 V, 0.74 V and 0.58 V, respectively. The HOMO energy values were calculated from CV results using the equation $E_{HOMO}(eV) = -1.4E_{onset,ox}(V) - 4.6$. Compared to the compound with no methoxy groups (**1A**) [5],**3MeOCz**, **TMeOCz** derivatives showed higher HOMO energies with the values of -5.24 eV and -5.36 eV, respectively, while **2MeOCz** showed a lower HOMO energy with the value of -5.50 eV.

Ionization potential values of **2MeOCz**, **3MeOCz**, **TMeOCz** were measured by electron photoemission in air technique. The *IP* values (Fig. 4.41) ranging from 5.19 to 5.44 eV were obtained, which are much lower compared to the value of the derivative with no methoxy groups (**1A**, 5.80 eV) [5]. It seems that the position of methoxy groups in **2MeOCz** and**3MeOCz** derivatives has a substantial effect on the *IP* value. **2MeOCz** possessing 2,7-dimethoxycarbazole moieties showed a 0.2 eV higher *IP* value (5.40 eV), compared with the *IP* of **3MeOCz** with 3,6-dimethoxycarbazolule moieties (5.19 eV).

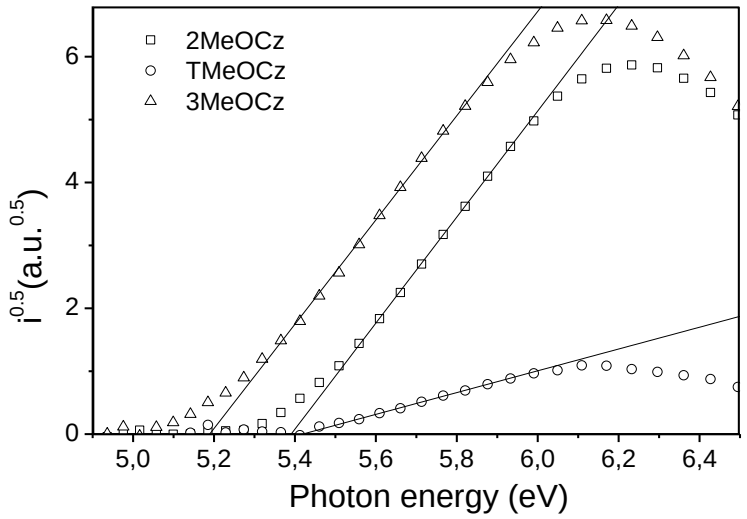

Fig. 4.41. Photoelectron emission spectra of the thin films of **2MeOCz**, **3MeOCz**, **TMeOCz**

4.5.5 Charge-transportingproperties

The charge-transporting properties of the layers of **2MeOCz**, **3MeOCz** and **TMeOCz** were studied by the TOF technique. The samples of compounds were prepared using the vacuum deposition technique with the layer thickness ranging from 1.4 to 4.8 μm . The linear dependencies of charge mobilities on the square root of the electric field ($E^{1/2}$) were observed for all the synthesized compounds (Fig.

4.42). Such dependency was previously observed and explained by Borsenberger [259]. The TOF measurements revealed by nearly one magnitude the higher hole mobilities in the layer of **3MeOCz** with respect to those of the layer of **TMeOCz**. The value of hole drift mobilities of the layer of **3MeOCz** was found to be 1.0×10^{-3} cm^2/Vs at the electric field of 5.0×10^5 V/cm. Zero field electron mobility of the layer of **2MeOCz** was found to be the highest among the compounds with the value of 1.0×10^{-5} $cm^2/V/s$. It is obvious that the position and amount of methoxy groups has an effect on the hole-transporting properties of the synthesized compounds (**2MeOCz**, **3MeOCz** and **TMeOCz**). All the methoxylated derivatives showed between 1-2 higher hole mobilities with respect to those recorded previously for derivative with no methoxy groups (**1A**) [5].

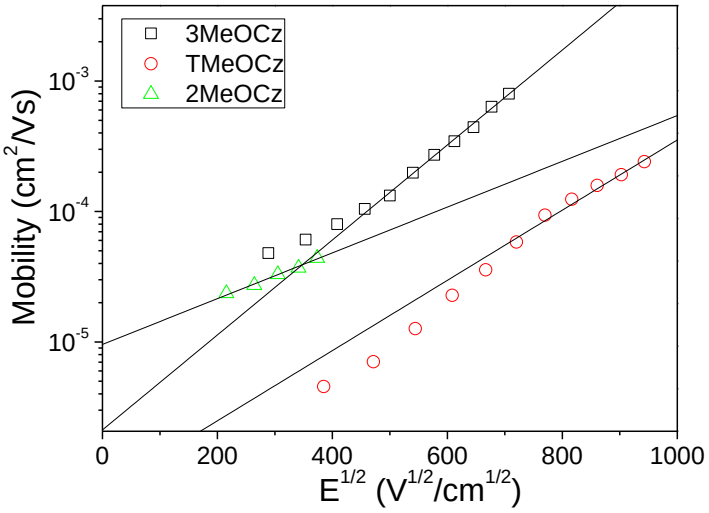

Fig. 4.42. Electric field dependencies of hole-drift mobilities for the vacuum deposited films of compounds**2MeOCz**, **TMeOCz** and **3MeOCz**measured by TOF method at room temperature

In conclusion, three new carbazole derivatives (**3MeOCz**, **2MeOCz** and **TMeOCz**) substituted via C-3 and C-6 positions with 3,6-dimethoxycarbazolyl, 2,7-dimethoxycarbazolyl and 2,3,6,7-tetramethoxycarbazolyl moieties were synthesized using the modified Ullmann coupling reaction. The derivatives show high melting points (>208 °C) and possess a glass transition temperature with the value ranging between 93 °C and 103 °C. Additionally, solutions of carbazole derivatives connected with 3,6-dimethoxycarbazole (**3MeOCz**) or 2,3,6,7-tetramethoxycarbazole (**TMeOCz**) fragments showed electrochemical stability in the range between 0.0-1.0 V, while the compound based on 2,7-dimethoxycarbazole (**2MeOCz**) exhibited irreversible oxidation. The ionization potentials vary in the range between 5.20 eV and 5.44 eV. An amporphous layers of **3MeOCz**, **2MeOCz**

and **TMeOCz** showed good hole transporting properties. In the case of **3MeOCz**, the TOF hole drift mobility value reached 10^{-3} cm^2/Vs at high electric fields.

4.6 Electroactive carbazole derivatives containing isoindigo moiety

For the preparation of optoelectronic devices such as OLEDs and bulk heterojunction organic solar cells, ambipolar electroactive compounds are more useful than hole-transporting compounds [327]. Isoindigo is one of the famous structures used as an electron acceptor unit for donor-acceptor-donor or acceptor-donor-acceptor based molecules [10]. In this work, the focus is on the synthesis and characterization of new ambipolar carbazole-isoindigo-carbazole (D-A-D) derivatives with different alkyl chains on carbazole moieties. The main aspects of the synthesis and characterization of the new derivatives, as well as of their physical, optical, thermal and electrochemical properties, will be reported. A comparative theoretical analysis of the new compounds was performed using DFT calculations. The effect of alkyl chain length on the thermal transitions and charge-transporting properties will also be analyzed. In addition, the results of tests of the selected compounds in the structures of bulk heterojunction organic solar cells will be reported.

4.6.1 Synthesis

The synthetic route to the isoindigo based compounds (**mISO-2Cz**, **mISO-3Cz**, **bISO-2Cz**, **bISO-3Cz**) with the differently linked carbazolyl substituents is shown in Scheme 4.9.

All the new derivatives with methyl (**mISO-2Cz**, **mISO-3Cz**) or isopentyl (**bISO-2Cz**, **bISO-3Cz**) alkyl chains on carbazole moiety were synthesized by the Suzuki-Miyaura coupling reaction [223] of **a-ISO** with 9-isopentyl-3-carbazolyl and 9-isopentyl-2-carbazolyl boronic acid pinacol ester (**3-mBCz**, **2-mBCz**) or 9-methyl-3-carbazolyl and 9-methyl-2-carbazolyl boronic acid pinacol ester (**3-BCz**, **2-BCz**), respectively. Halogenated isoindigo precursor (**ISO**) was prepared in two steps of commercially available 6-bromooxindole and 6-bromoisatin following the previous reported procedure [225]. To obtain the alkylated precursor (a-**ISO**) the reaction with 2-ethylhexylbromide was performed by the conventional procedure [242]. The boronic acid pinacol esters of carbazole (**3-mBCz**, **2-mBCz**, **3-BCz**, **2-BCz)** were prepared from 3-bromocarbazole (**3Br-Cz**) and 2-bromocarbazole (**2Br-Cz**) by N-alkylation reaction with iodomethane or 1-Br-3-methylbutane and borylation reaction using the procedure reported in the literature [321]. The chemical structures of the compounds were confirmed by ^{1}H and ^{13}C NMR and MS. The single crystal of **mISO-2Cz** was grown in the solvent mixture hexane/dicloromethane and the structure of **mISO-2Cz** was confirmed by X-ray crystallography results (Fig. 4.43). The target compounds **mISO-2Cz**, **mISO-3Cz**, **bISO-2Cz** and **bISO-3Cz** were found to be soluble in common chlorinated organic solvents such as chloroform, dichloromethane.

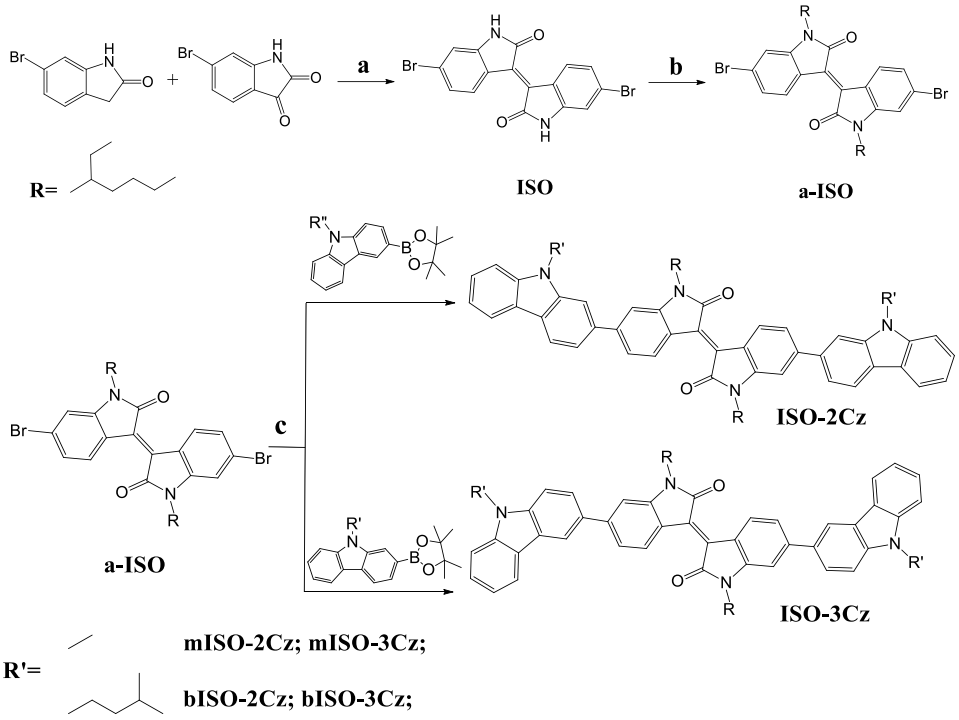

Scheme 4.9. Synthesis of isoindigo based derivatives **mISO-2Cz**, **mISO-3Cz**, **bISO-2Cz**, **bISO-3Cz**. Reagents and conditions:a) conc. HCl (cat.), acetic acid, 60°C, reflux 2 h (b) $C_8H_{17}Br$, K_2CO_3, KOH, TBAHS, Δ, 2 h; (c) $Pd(Ph_3)_2Cl_2$, KOH, THF–H_2O, 80 °C, 10–12 h

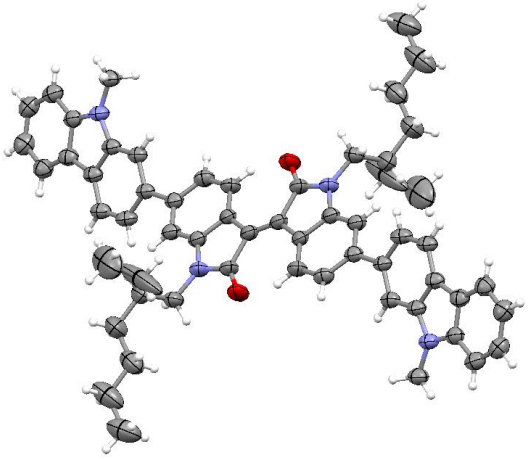

Fig. 4.43. ORTEP projection of the crystal structure of **mISO-2Cz**. Displacement ellipsoids are drawn at 30% probability level

4.6.2 Thermal properties

The thermograms of isoindigo based derivatives obtained by DSC and TGA are shown in Fig. 4.44 and Fig. 4.45. Thermal characteristics are collected Table 4.17.

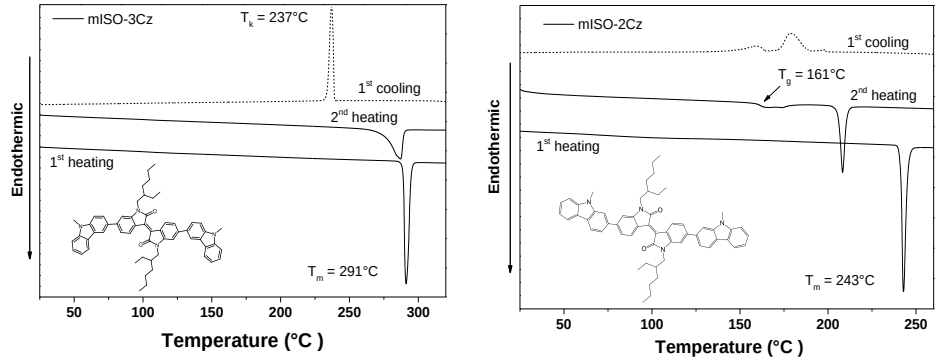

Fig. 4.44. DSC thermograms of **mISO-3Cz** and **mISO-2Cz**.

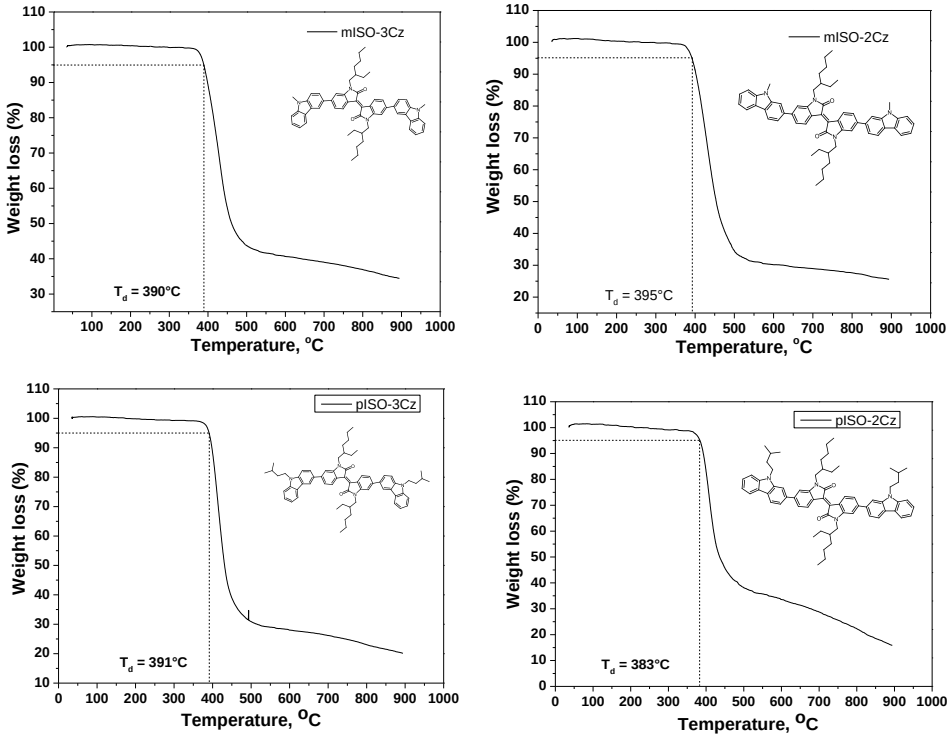

Fig. 4.45. TGA thermograms of **mISO-2Cz**, **mISO-3Cz**, **bISO-2Cz** and **bISO-3Cz**

From the TGA curves it is seen that the length of alkyl chain has no effect on thermal stability. The destruction temperatures of all isoindigo derivatives are comparable with the values ranging from 383 °C to 395 °C. Thermal behavior in DCS scans showed different behavior, depending not only on carbazole substitution position, but also the alkyl chain length as well. All the analyzed materials were

obtained as crystalline materials, therefore, from the first heating scan the melting point with the value ranging from 191 °C to 291 °C was observed. It is obvious that shorter alkyl chains causes higher molecule density in the crystal and stronger interactions, as well. Therefore, compared with **bISO-2Cz** derivative, **mISO-2Cz** and **mISO-3Cz** showed 50-100 °C higher melting points, exceeding 240 °C. Additionally, compounds with shorter alkyl chains (**mISO-2Cz**, **mISO-3Cz**) are very crystalline, therefore, the first cooling curve showed exothermic peaks of crystallization temperature. On the second heating scan of **bISO-2Cz** and **mISO-2Cz,** glass transition temperatures with the values of 60 °C and 161 °C, respectively were observed. In the case of **mISO-2Cz**, molecular glasses tend not to be very stable, therefore, during the second heating scan one more endothermic peak was observed.

4.6.3 Optical properties

UV-vis spectra of dilute solutions of isoindigo derivatives (**mISO-2Cz**, **mISO-3Cz**, **bISO-2Cz**, **bISO-3Cz**) are shown in Fig. 4.46. For comparison, the spectrum of precursor **a-ISO** is given. In UV-vis spectra of **mISO-2Cz**, **mISO-3Cz**, **bISO-2Cz**, **bISO-3Cz** a broad absorption covering almost all visible spectrum (380-750 nm) was observed.

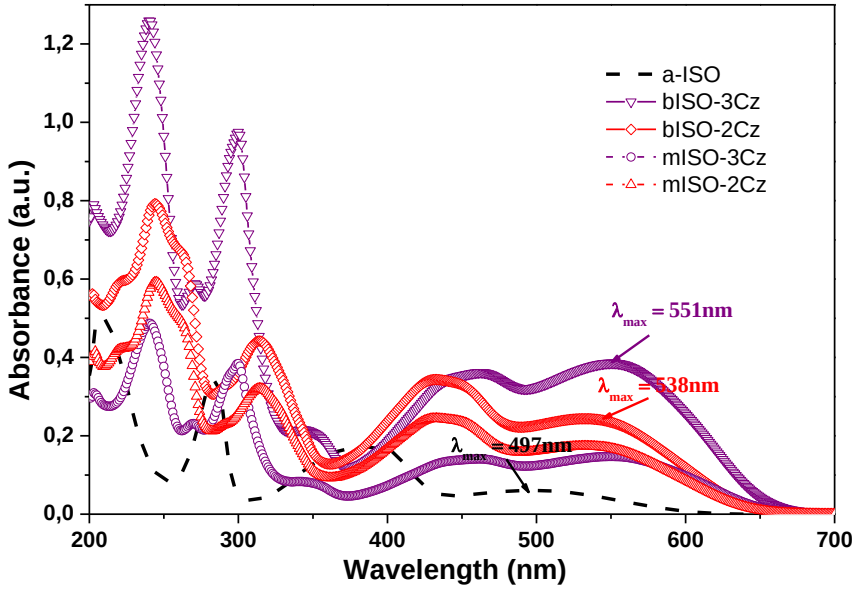

Fig. 4.46. UV-vis of dilute THF solutions (10^{-5} M) of **mISO-2Cz**, **mISO-3Cz**, **bISO-2Cz**, **bISO-3Cz** and the precursor **a-ISO**

Table 4.17. Thermal and optical characteristics of **mISO-2Cz, mISO-3Cz, bISO-2Cz, bISO-3Cz**

	T_m, °C[a]	T_g, °C[a]	T_d, °C[a]	$\lambda^{ab}_{max,/}$ (nm)	*IP*, (eV) [b]
a-iso	-	-	102	499	-
mISO-3Cz	291	-	390	551	5.32
mISO-2Cz	243	161	395	538	5.48
bISO-3Cz	-	-	391	551	5.28
bISO-2Cz	191	60	383	538	5.42

[a] determined by DSC and TGA, scan rate 10 °C/min, N_2 atmosphere.[b] ionization potential

Therefore, the isoindigo derivatives could be of interest for solar cells application. Compounds with different alkyl chains on carbazole moieties (**mISO-2Cz**, **bISO-2Cz** or **mISO-3Cz**, **bISO-3Cz**) possess similar profiles of UV spectra. Compared to **bISO-3Cz,** whose isoindigo moiety is linked to the carbazolyl group via C-3 position, the other isoindigo derivative, substituted with 2-carbazolyl fragment (**bISO-2Cz**), showed comparable absorption spectrum with the lowest energy absorption band observed at 538 nm. In addition, the UV-vis spectra of **mISO-2Cz, mISO-3Cz, bISO-2Cz, bISO-3Cz** showed considerable bathochromic effect of 30-50 nm with respect to the spectrum of their precursor **a-ISO**. These results provide evidence for more effective and prolonged conjugation length in the target compounds [246]. By exciting the solutions of the derivatives with radiation of different energy, the samples did not exhibited any emission up to 750 nm. This observation shows that non-radiative processes take place after excitation of the molecules.

4.6.4 Electrochemical and photoelectrical properties

The redox behavior was investigated and experimental HOMO/LUMO values were estimated using the CV technique. The CV curves and electrochemical characteristics of **bISO-2Cz** and **bISO-3Cz** are presented in Fig. 4.47 and Table 4.18, respectively.

Table 4.18. Electrochemical characteristics of **bISO-2Cz** and **bISO-3Cz**

	$E_{oxonset}$, V	$E_{ox,pa}$, V[a]	$E_{ox,pc}$, V[a]	$E_{redonset}$, V	$E_{ox,pa}$, V	$E_{ox,pc}$, V[a]	$E_{HOMO/LUMO}$, (eV)[b]
bISO-3Cz	0.55	0.65	0.55	-1.27	-1.38	-1.29	-5.37/-3.18
bISO-2Cz	0.68	-	-	-1.26	-1.36	-1.28	-5.55/-3.21

[a] E_{ox}^{pa} , E_{ox}^{pc}, E_{red}^{pa} , E_{red}^{pc}–peak potentials corresponding to successive molecular oxidations

[b] $E_{HOMO}(eV) = -1.4E_{onset,ox}(V) - 4.6$ [257], $E_{LUMO}(eV) = -1.19E_{onset,red}(V) - 4.78(V)$ [328] where $E_{onset,ox/red}$ was determined by solution based CV [255].

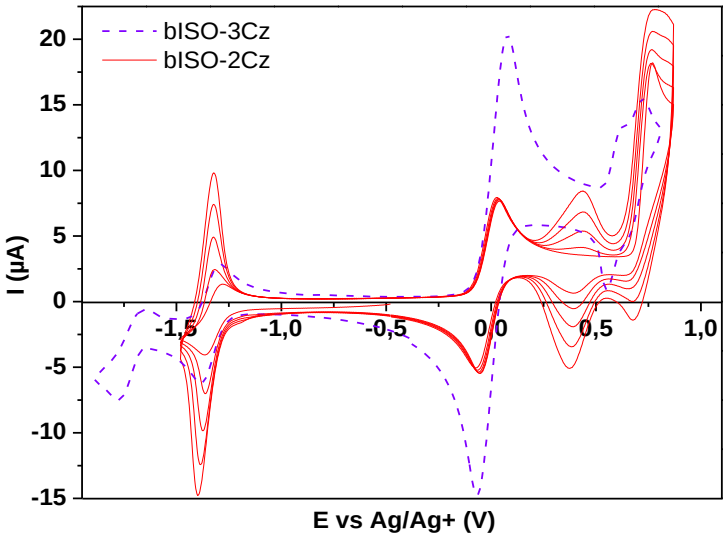

Fig. 4.47. Cyclic voltammograms of **bISO-2Cz** and **bISO-3Cz** at 10^{-3} mol L^{-1} in the solutions of argon-purged TBAP (0.1 M) in CH_2Cl_2. v = 50 mV/s

bISO-2Cz	
HOMO (-5.33 eV)	LUMO (-2.73 eV)
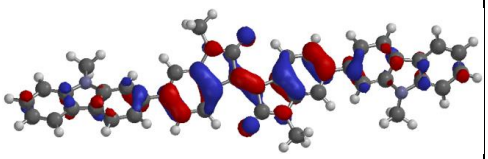	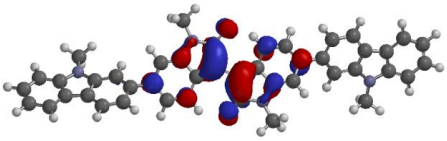
bISO-3Cz	
HOMO (-5.07 eV)	LUMO (-2.67 eV)
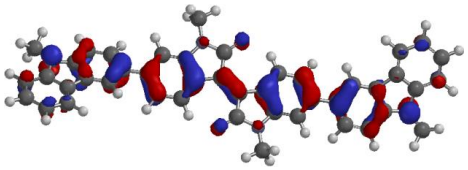	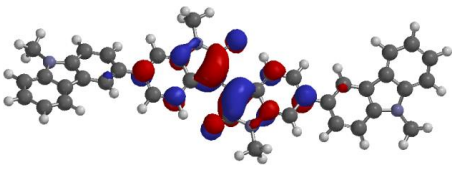

Fig. 4.48. The computed spatial distributions and the values of HOMO and LUMO orbitals for **bISO-2Cz** and **bISO-3Cz**

The isoindigo derivative containing the carbazolyl group linked vis C-3 position (**bISO-3Cz**) after five repeated CV scan cycles showed reversible oxidation and reduction peaks with the values of 0.55 V and -1.38 V, respectively. In the case of **bISO-2Cz**, in which the carbazolyl group is linked via its C-2, the irreversible oxidation and formation of new carbazole derivatives on the electrode were observed. HOMO and LUMO values were calculated using the formulas: $E_{HOMO}(eV) = -1.4E_{onset,ox}(V) - 4.6$ [257], $E_{LUMO}(eV) = -1.19E_{onset,red}(V) - 4.78(V)$ [328] formulas and ferrocene as the standard of the redox system [329]. The linking topology of isoindigo and carbazole moieties has a stronger effect on HOMO energy than on LUMO energy. In the case of **bISO-2Cz**, HOMO and LUMO values were found to be -5.55 eV and -3.21 eV, respectively, while in the case of **bISO-3Cz**, the values were slightly higher (-5.37 eV, -3.18 eV).

The theoretical energies of HOMO and LUMO of **bISO-2Cz** and **bISO-3Cz** were calculated using the B3LYP method with the 6-31G** basis set. LUMO orbitals are localized on the central isoindigo core, while HOMO orbitals are distributed on the peripheral carbazole moieties. The energies of HOMO and LUMO for **bISO-3Cz** (-5.07 eV and -2.67 eV) and for **bISO-2Cz** (-4.93 eV and -1.60 eV) are in good agreement with the experimental values (Fig. 4.48, Table 4.18).

The ionization potentials of **mISO-2Cz**, **mISO-3Cz**, **bISO-2Cz** and **bISO-3Cz** were established from electron photoemission in air spectra (Fig. 4.49).

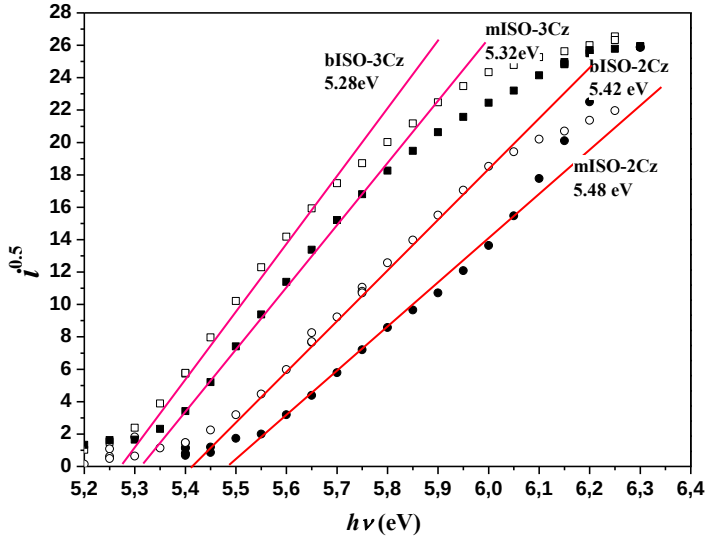

Fig. 4.49. Photoelectron emission spectra of the thin films of **mISO-2Cz**, **mISO-3Cz**, **bISO-2Cz** and **bISO-3Cz**

The ionization potentials of **mISO-2Cz**, **mISO-3Cz**, **bISO-2Cz** and **bISO-3Cz** were established from the electron photoemission spectra (Fig. 4.49). The position of the carbzolyl unit was found to have an effect on the IP values. **mISO-2Cz**, **bISO-2Cz** showed 0.2 eV lower *IP* compared to that of **mISO-3Cz**, **bISO-3Cz**. The length of the alkyl chain on the carbazolyl moiety did not have any effect on the *IP* value.

4.6.5 Charge-transporting properties

XTOF measurements were used to analyze charge-transporting properties of the isoindigo derivatives (**mISO-2Cz**, **mISO-3Cz**, **bISO-2Cz** and **bISO-3Cz**). The layers of the samples were prepared by the drop-casting technique. Due to high crystallinity of the isoindigo compounds, the layers were prepared from a mixture of the compound with inert polymer bisphenol-Z-polycarbonate (ratio of 1:3). The layer thickness varied from 1.7 to 8.0 nm.

Fig. 4.50 shows the electric field dependencies of hole and electron drift mobility values (μ) for the layers containing isoindigo derivatives. The layer of **bISO-2Cz** doped in PC-Z showed the ambipolar behaviour with hole and electron mobility values of 4.8×10^{-7} and 3.7×10^{-8}cm^2/V/s, respectively at an electric field of 2.5×10^5 V/cm. (Table 4.19).

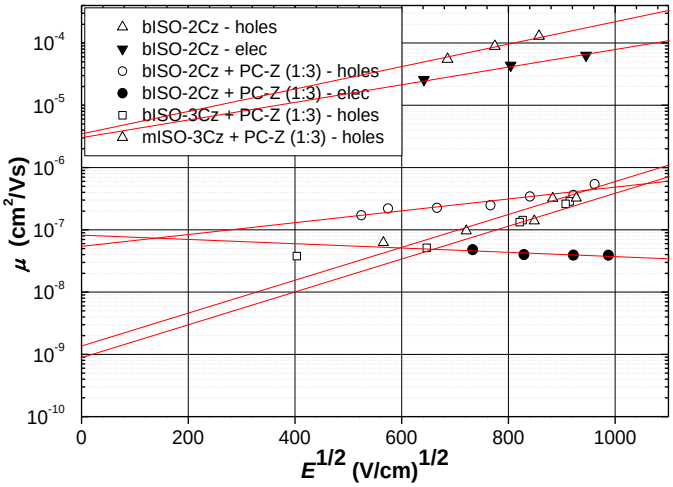

Fig. 4.50. Electric field dependencies of charge mobilities in the layers of isoindigo derivatives with (**mISO-3Cz, bISO-3Cz** and **bISO-2Cz**)or without (**bISO-2Cz**) bisphenol-Z polycarbonate

Table 4.19. Charge mobility data for**mISO-2Cz, mISO-3Cz, bISO-2Cz** and **bISO-3Cz**

Compound	*d*, [μm]	μ_{0h} / μ_{0e}, [cm^2/V/s]	μ_h / μ_e, [cm^2/V/s][a]	α *10^{-3}, [cm/V]
mISO-3Cz + PC-Z, 1:3	5.0	1.7×10^{-9} / -	3.9×10^{-7} / -	-
bISO-3Cz + PC-Z, 1:3	4.3	1.2×10^{-10} / -	4.6×10^{-7} / -	6.3 / -
bISO-2Cz + PC-Z, 1:3	8.0	5.5×10^{-8} / 8.4×10^{-8}	4.8×10^{-7} / 3.7×10^{-8}	2.2 / -0.8
bISO-2Cz	1.7	3.5×10^{-6} / 2.9×10^{-6}	2.1×10^{-4} / 8.0×10^{-5}	4.2 / 3/3

The glassy layer of **bISO-2Cz** derivative showed sufficient morphological stability for the XTOF measurements. Hole and electron mobility values of 2.1×10^{-4} and 8.0×10^{-5} cm^2/V/s, respectively were recorded at an electric field of 2.5×10^5 V/cm. For the molecular mixtures of **mISO-3Cz** and **bISO-3Cz** with PC-Z, it was

observed that the hole mobility was comparable with that of **bISO-2Cz** + **PC-Z** (3.9×10^{-7} and 4.6×10^{-7} cm^2/Vs, respectively) while electron transport was not detected.

4.6.6 Performance in bulk heterojunction solar cells

Bulk heterojunction-photo-voltaic devices were prepared using solutions (40 mg/ml in chlorobenzene) of **mISO-2Cz** and **bISO-2Cz** molecules as donor materials and PCBM as acceptor material. The fabricated device structures and energetic levels are shown in Fig. 4.51. To analyze the device performance, different donor/acceptor weight ratio were used (Table 4.20

Table 4.20).

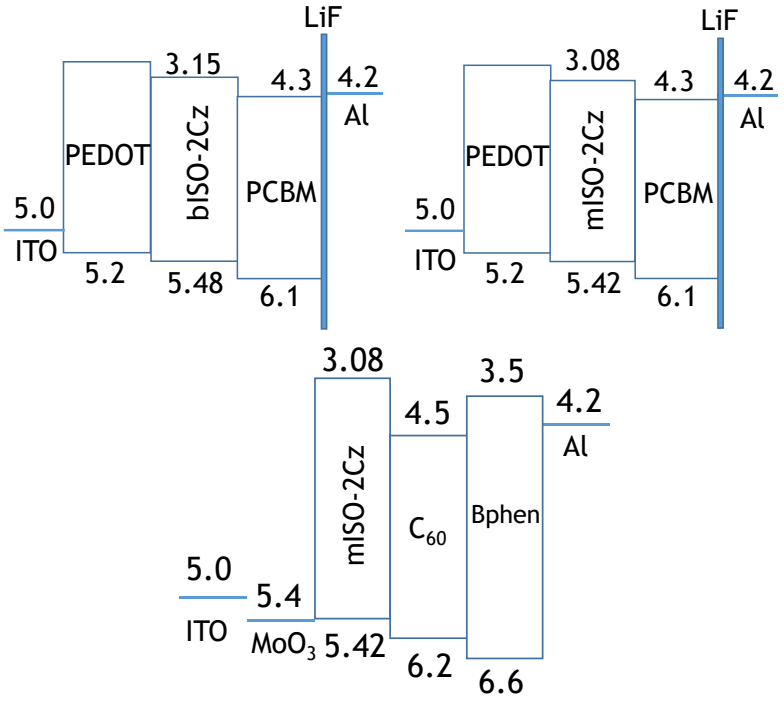

Fig. 4.51. Energetic levels of the components of organicsolar cells based on **mISO-2Cz** and **bISO-2Cz**

The J-V curves are shown in Fig. 4.52. The best performance was observed from device C, which produced an open circuit voltage (V_{OC}) of 0.74 V, a short-circuit current (J_{SC}) of 0.053 mA/cm^2, a fill factor (*FF*) of 0.31 and a power conversion efficiency (*PCE*) of 0.012 %. In addition, the planar organic photovoltaic device (G) using thermal evaporation was fabricated. The structure of the device is shown in Fig. 4.51. Compared to bulk heterojunctionsolar cells (A,B,C,D,F), the experiment showed that the PCE value of device G increased by the factor of 2.5.

Table 4.20. Performance of bulk heterojunction solar cells containing **mISO-2Cz** and **bISO-2Cz** derivatives

Device	Ratio (donor/acceptor)	V_{oc}, V	J_{sc}, mA/cm^2	*FF*	*PCE*, %
A (bISO-2Cz:PCBM)	1:1	0.62	0.028	0.37	0.0048
B (bISO-2Cz:PCBM)	1:2	0.74	0.04	0.29	0.0087
C (bISO-2Cz:PCBM)	1:3	0.74	0.053	0.31	0.0121
D (bISO-2Cz:PCBM)	1:4	0.68	0.053	0.33	0.0118
F (mISO-2Cz:PCBM)	1:1	0.64	0.022	0.30	0.0042
G (OPV (mISO-2Cz))	-	0.74	1.03	0.39	0.30

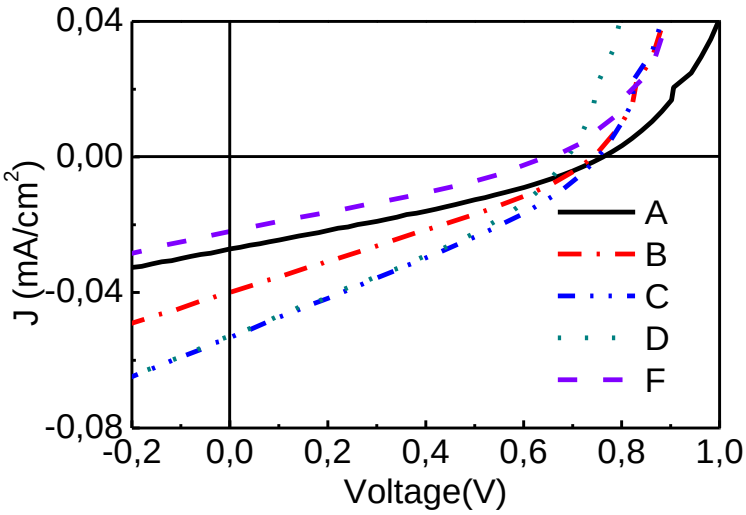

Fig. 4.52. *J*–*V* curves of photovoltaic devices containing **mISO-2Cz** and **bISO-2Cz**

In conclusion, during research a series of new derivatives with isoindigo and carbazole with the different linking topology and the different length alkyl side chains (methyl or izopenthyl) were synthesized. All the new derivatives showed relatively high thermal stability with 5 % weight loss temperatures exceeding 380 °C. The absorption spectra of the derivatives of isoindigo and carbazole cover almost all the visible spectral range. Due to more effective conjugation, isoindigo derivatives with a carbazolyl unit linked via C-3 position showed comparable spectra with respect to those of the counterparts having carbazolyl moiety linked via C-2 position. Isoindigo derivative containing a carbazole unit linked via C-2 position showed ambipolar charge-transporting properties in air with the hole mobilities reaching 2.1×10^{-4}cm$^2\cdot$V^{-1}s^{-1} and electron mobilities reaching 8.0×10^{-5} cm$^2\cdot$V^{-1}s^{-1} at

high electric fields. Due to the broad absorption spectra and effective charge transport, the carbazolyl-substituted isoindigo derivatives were employed in the organic bulk heterojunction solar cell, which exhibited a power conversion efficiency reaching 0.3 %.

5. CONCLUSIONS

1. 2,7-Dimethoxy and 3,6-dimethoxy carbazole derivatives possessing diphenylethenyl moieties were synthesized by condensation of the corresponding derivative of dimethoxycarbazole with diphenylacetaldehyde. Both of the isomers exhibit high thermal stability and form molecular glasses. Since the majority of molecules in the crystal structure of 2,7-dimethoxy isomer form *J*-aggregates, this compound showed the effect of aggregation induced emission, while 3,6-dimethoxy isomer showed the effect of aggregation-caused quenching. Both the compounds showed comparable ionization potentials of ca. 5.4 eV. The derivative based on 3,6-dimethoxycarbazole showed superior charge transporting properties relative to its 2,7-dimethoxy counterpart. The time-of-flight hole drift mobilities in its layers exceeded 10^{-3} cm^2/Vs at high electric fields.
2. An efficient method for the synthesis of carbazole based diaza[6]helicenes was developed. Electrophilic substitution reactions were performed, resulting in the formation of functionalized chiral materials. The configuration of the diaza[6]helicene diastereomers was proven by time-dependent density functional theory calculations. The new chiral carbazole based helicenes absorb radiation in UV and the blue region up to 425 nm, while the chlorinated, its precursor, showed a 30 nm red shifted spectra. According to density functionnal theory calculations, these compounds can potentially be of interest as hole-transporting p-type semiconductors.
3. N-annelated perylenes containing two differently linked carbazolyl substituents were synthesized, and their thermal, optical, photophysical and electrochemical properties were studied. The derivatives form molecular glasses with glass transition temperatures of 107-110 °C. The compounds showed high thermal stability with 5 % weight loss temperatures ranging from 400 to 457 °C. The ionization potentials of the compounds vary in range from 5.14 to 5.53 eV. The time-of-flight measurements revealed hole and electron mobility values reaching 10^{-3} cm^2/Vs. The synthesized compounds were found to be efficient green-emitting fluorophores. They were used for the preparation of emissive layers of the effective organic light emitting diodes with the brightness value exceeding 62000 cd/m^2 and external quantum efficiency reaching 4.2%.
4. Four carbazole derivatives substituted with methoxy groups at C1, C2, C3, C6, C7 and C8 positions were synthesized. It was established by X-ray crystallography that methoxy groups of 3,6- and 2,7-disubstituted and 2,3,6,7-tetrasubstituted carbazole derivatives lay in the same plane as carbazole aromatic rings, while, in the case of 1,2,3,6,7,8-hexasubstituted

carbazole, they are bent above and below the carbazole plane. Compared to standalone carbazole, all the target compounds showed a significant red-shifted fluorescence spectra, which consequently resulted in higher Stokes shift values. Compared to standalone carbazole, methoxysubstituted derivatives showed higher HOMO energy values by 0.30-0.50 eV and lower ionization potentials by 0.20-0.30 eV.

5. By the reactions of 3,6- and 2,7-dimethoxy and 2,3,6,7-tetramethoxycarbazole with 9-(2-ethylhexyl)-3,6-diiodo-9H-carbazole, three new glass forming (T_g~93-103 °C) derivatives were synthesized. The compounds with 3,6-dimethoxy and 2,3,6,7-tetramethoxycarbazole moieties showed reversible oxidation-reduction waves up to 1.0 V in the experiments of cyclic voltammetry. The ionization potentials of all the compounds vary in range between 5.20 eV and 5.44 eV. For the layer of the 3,6-dimethoxycarbazole based compound, the time-of-flight hole drift mobility reached 10^{-3} cm^2/Vs at high electric fields.
6. A series of new derivatives based on the isoindigo core linked via 6,6'-positions with two 3-carbazolyl and 2-carbazolyl units alkylated with the different alkyl chains were synthesized. The derivatives showed high thermal stability with 5 % weight loss temperatures exceeding 380 °C. The absorption spectra of isoindigo based compounds cover almost all visible spectrum. Isoindigo derivative containing two 2-carbazolyl-9-isopentyl fragments showed ambipolar charge transport in air with the hole mobilities reaching 2.1×10^{-4} $cm^2\cdot V^{-1}s^{-1}$ and electron mobilities reaching 8.0×10^{-5} $cm^2\cdot V^{-1}s^{-1}$ at high electric fields. Due to the broad absorption spectrum and effective charge transporting properties, 2-carbazolylsubstituted isoindigo compounds were employed in the organic solar cells, which exhibited a power conversion efficiency reaching 0.3 %.

6. REFERENCES

1. MORIN, J.-F., et al. Syntheses and Characterization of Electroactive and Photoactive 2,7-Carbazolenevinylene-Based Conjugated Oligomers and Polymers. *Chemistry of Materials*. 2004, 16, 4619–4626.
2. LIN, W.-C., et al. A bipolar host containing carbazole/dibenzothiophene for efficient solution-processed blue and white phosphorescent OLEDs. *Journal of Materials Chemistry C*. 2013, 1, 6835–6841.
3. HUDSON, Z. M., et al. N-Heterocyclic Carbazole-Based Hosts for Simplified Single-Layer Phosphorescent OLEDs with High Efficiencies. *Advanced Materials*. 2012, 24, 2922–2928.
4. ARBISER, J. L., et al. Carbazole Is a Naturally Occurring Inhibitor of Angiogenesis and Inflammation Isolated from Antipsoriatic Coal Tar. *Journal of Investigative Dermatology*. 2006, 126, 1396–1402.
5. TOMKEVICIENE, A., et al. Impact of Linking Topology on the Properties of Carbazole Trimers and Dimers. *The Journal of Physical Chemistry C.* 2011, 115, 4887–4897.
6 MICHINOBU, T., et al. Multicolor emission and thin film transistor properties of 1,8-diethynylcarbazole-based conjugated copolymers. *Polymer.* 2011, 52, 5756-5763.
7. WAKIM, S., et al. Charge Transport, Photovoltaic, and Thermoelectric Properties of Poly(2,7-Carbazole) and Poly(Indolo[3,2-b]Carbazole) Derivatives. *Polymer Reviews*. 2008, 48, 432–462
8. LI, Y., et al. Air-Stable n-Type Semiconductor: Core-Perfluoroalkylated Perylene Bisimides. *Organic Letters*. 2008, 10, 529–532.
9. ZHAO, Q., et al. Tetraphenylethenyl-modified perylene bisimide: aggregation-induced red emission, electrochemical properties and ordered microstructures. *Journal of Materials Chemistry*. 2012, 22, 7387–7394.
10. WANG., E., et al. 25th Anniversary Article: Isoindigo-Based Polymers and Small Molecules for Bulk Heterojunction Solar Cells and Field Effect Transistors. *Advanced Materials.* 2014, 26, 1801–1826.
11. KIM, C., et al. Synthesis, characterization, and transistor response of tetrathia-[7]-helicene precursors and derivatives. *Organic. Electronics.* 2009, 10, 1511-1520.
12. PAN, J. H., et al. Theoretical Investigation of Organic Amines as Hole Transporting Materials: Correlation to the Hammett Parameter of the Substituent, Ionization Potential, and Reorganization Energy Level. *Australian Journal of Chemistry*. 2009, 62, 483-492.
13. SAKALYTE, A., et al. Effect of Methoxy Substituents on the Properties of the Derivatives of Carbazole and Diphenylamine. *The Journal of Physical Chemistry C.*2011, 115, 4856–4862.
14. http://en.wikipedia.org/wiki/Electroluminescence
15. ROUND, H. J. A note on carborundum. *Electron. World*, 1907, 19, 309–310.
16. BERNANOSE, A., et al. A new method of light emission by certain organic compounds. *Journal de chimie physique*. 1953, 50, 64-68.

17. BERNANOSE, A., and VOUAUX P. Organic electroluminescence type of emission. *Journal de chimie physique*. 1953, 50, 261.
18. BERNANOSE, A. On the mechanism of organic electroluminescence. *Journal de chimie physique*. 1955, 52, 396-400.
19. BERNANOSE, A., and VOUAUX P. Relation between organic electroluminescence and the concentration of active products. *Journal de chimie physique*. 1955, 52, 509.
20. POPE, M., et al. Electroluminescence in organic crystals. *The Journal of Chemical Physics*. 1963, 38, 2042-2043.
21. DIGBY, W., and SCHADT, M. US Patent US3621321, Nov 16, 1971. Ref.: http://www.google.com/patents/US3621321
22. PARTRIDGE, R. US Patent US3995299, Nov 30, 1976. Ref.: http://www.google.com/patents/US3995299.
23. VINCETT, P., et al. Electrical conduction and low voltage blue electroluminescence in vacuum-deposited organic films. *Thin Solid Films.* 1982, 94, 171-183.
24. TANG, C. US Patent US4164431, Aug 14, 1979. Ref.: http://www.google.com/patents/US4164431
25. TANG, C. US Patent US4356429, Oct 26, 1982. Ref.: http://www.google.com/patents/US4356429
26. TANG, C., and VANSLYKE, S. Organic electroluminescent diodes. *Applied Physics Letters*. 1987, 51, 913-915.
27. BURROUGHES, J., et al. Light-emitting diodes based on conjugated polymers.*Nature.* 1990, 347, 539-541.
28. FRIEND, R., et al. US Patent US5247190, Sep 21, 1993. Ref.: http://www.google.com/patents/US5247190
29. BRAUN, D., and HEEGER, A. Visible light emission from semiconducting polymer diodes. *Applied Physics Letters*. 1991, 58, 1982-1984.
30. BALDO, M. A., et al. Highly efficient phosphorescent emission from organic electroluminescent devices. *Nature.* 1998, 395, 151-154.
31. ADACHI, C., et al.High-efficiency organic electrophosphorescent devices with tris(2-phenylpyridine) iridium doped into electron-transporting materials. *Applied Physics Letters*. 2000, 77, 904-906.
32. SUN, Y., et al. Management of singlet and triplet excitons for efficient white organic light-emitting devices. *Nature*. 2006, 440, 908-912.
33. REINEKE, S., et al.White organic light-emitting diodes with fluorescent tube efficiency. *Nature*. 2009, 459, 234-238.
34. https://en.wikipedia.org/?title=Iridium
35. LEE, S. Y., et al. High-efficiency organic light-emitting diodes utilizing thermally activated delayed fluorescence from triazine-based donor–acceptor hybrid molecules. *Applied Physics Letters*. 2012, 101, 093306-1-4.
36. http://en.wikipedia.org/wiki/Hair
37. LI, Z., and MENG H.. Organic Light-Emitting Materials and Devices. Taylor & Francis Group. 2007, 296-395.

38. HASSHEIDER, T., et al. Color-Tuned Electroluminescence from Columnar Liquid Crystalline Alkyl Arenecarboxylates. *Angewandte Chemie International Edition*. 2001, 40, 2060-2063.

39. HUANG, T.H., et al. Dipolar Dibenzothiophene S,S-Dioxide Derivatives Containing Diarylamine: Materials for Single-Layer Organic Light-Emitting Devices. *Advanced Materials.* 2006, 18, 602-606.

40. JUSTIN THOMAS, K. R., et al. Color Tuning in Benzo[1,2,5]thiadiazole-Based Small Molecules by Amino Conjugation/Deconjugation: Bright Red-Light-Emitting Diodes. *Advanced Functional Materials.* 2004, 14, 83-90.

41. JOU, J. H., et al. Hole-transporting-layer-free high-efficiency fluorescent blue organic light-emitting diodes. *Applied Physics Letters*. 2007, 91, 043504.

42. NAKANOTANI, H., et al. Extremely Low-Threshold Amplified Spontaneous Emission of 9,9′-Spirobifluorene Derivatives and Electroluminescence from Field-Effect Transistor Structure. *Advanced Functional Materials.* 2007, 17, 2328-2335.

43. GRISORIO, R., et al. First disubstituted dibenzothiophene-5,5-dioxide monodispersed molecular materials for efficient blue-electroluminescence. *Journal of Materials Chemistry.* 2010, 20, 1012-1018.

44. SUN, Y., and S. R. FORREST. Enhanced light out-coupling of organic light-emitting devices using embedded low-index grids.Nature Photonics. 2008, 2, 483-487.

45. MÜLLER, C. D., et al.Multi-colour organic light-emitting displays by solution processing. *Nature.* 2003, 421, 829-833.

46. SHEN, Z., et al.Three-Color, Tunable, Organic Light-Emitting Devices. *Science*. 1997, 276, 2009-2011.

47. KIDO, J., et al.Multilayer white light-emitting organic electroluminescent device.*Science*. 1995, 267, 1332-1334.

48. HEUSING, S., et al. Wet Chemical Deposited ITO Coatings on Flexible Substrates for Organic Photodiodes. *Thin Solid Films.* 2009, 518, 1164−1169.

49. ERITT, M., et al. OLED Manufacturing for Large Area Lighting Applications. *Thin Solid Films.* 2010, 518, 3042-3045.

50. STÖSSEL, M., et al. Impact of the cathode metal work function on the performance of vacuum-deposited organic light emitting-devices.*Applied Physics A*. 1999, 68, 387-390.

51. GARCIA-BELMONTE, G., et al. Capacitance-voltage characteristics of organic light-emitting diodes varying the cathode metal: Implications for interfacial states. *Physical Review B*. 2007, 75, 085316-1-8.

52. BOCHKAREV, M. N., et al. New Cathode Materials for Organic Light-Emitting Diodes: Tm:Yb and Eu:Yb. *Nanotechnologies in Russia*. 2008, 3, 470-473.

53. http://www.instruction.greenriver.edu/kmarr/chem%20162/Chem162%20Labs/Elements%20Sorted%20by%20Ionization%20energy/List%20of%20Periodic%20Table%20Elements%20Sorted%20by%20Ionization%20energy.asp

54. HUNG, L. S., et al. Enhanced electron injection in organic electroluminescence devices using an Al/LiF electrode. *Applied Physics Letters*. 1997, 70, 152-154.

55. PARKER, I. D., and H. H. KIM. Fabrication of polymer light-emitting diodes using doped silicon electrodes. *Applied Physics Letters*. 1994, 64, 1774-1776.

56. MORI, T., et al. Electronic structure of 8-hydroxyquinoline aluminum/LiF/Al interface for organic electroluminescent device studied by ultraviolet photoelectron spectroscopy. *Applied Physics Letters*. 1998, 73, 2763-2765.

57. BROWN, T. M., et al. Electronic line-up in light-emitting diodes with alkali-halide/metal cathodes. *Journal of Applied Physics*. 2003, 93, 6159-6172.

58. LEE, J., et al. *Tris*-(8-hydroxyquinoline)aluminum-based organic light-emitting devices with Al/CaF2 cathode: Performance enhancement and interface electronic structures. *Applied Physics Letters*. 2002, 80, 3123-3125.

59. KANG, S. J., et al. Enhancing the electroluminescent properties of organic light-emitting devices using a thin NaCl layer. *Applied Physics Letters*. 2002, 81, 2581-2583.

60. LEE, T.-W., et al. Polymer light-emitting devices using ionomers as an electron injecting and hole blocking layer. *Journal of Applied Physics*. 2001, 90, 2128-2134.

61. KIDO, J., and T. MATSUMOTO. Bright organic electroluminescent devices having a metal-doped electron-injecting layer. *Applied Physics Letters*. 1998, 73, 2866-2868.

62. SLYKE, S. A. V., et al. Bright organic electroluminescent devices having a metal-doped electron-injecting layer. *Applied Physics Letters*. 1996, 69, 2160-2162.

63. CUI, J., et al. Interfacial Microstructure Function in Organic Light-Emitting Diodes: Assembled Tetraaryldiamine and Copper Phthalocyanine Interlayers. *Advanced Materials*. 2002, 14, 565-569.

64. DENG, Z. B., et al. Enhanced brightness and efficiency in organic electroluminescent devices using SiO*2* buffer layers. *Applied Physics Letters*. 1999, 74, 2227–2229.

65. POON, C. O., et al. Improved performance and stability of organic light-emitting devices with silicon oxy-nitride buffer layer. *Applied Physics Letters*. 2003, 83, 1038–1040.

66. HUNG, L. S., et al. Anode modification in organic light-emitting diodes by low-frequency plasma polymerization of CHF*3*. *Applied Physics Letters*. 2001, 78, 673–675.

67. GROENENDAAL, L., et al.Poly(3,4-ethylenedioxythiophene) and Its Derivatives: Past, Present, and Future.*Advanced Materials.* 2000, 12, 481–494.

68. TAO, Y., et al. Organic host materials for phosphorescent organic light-emitting diodes.*Chemical Society Reviews.* 2011, 40, 2943–2970.

69. KUWABARA, Y., et al. Thermally stable multilared organic electroluminescent devices using novel starburst molecules, 4,4′,4″-Tri(*N*-carbazolyl)triphenylamine (TCTA) and 4,4′,4″-Tris(3-methylphenylphenylamino)triphenylamine (*m*-MTDATA), as hole-transport materials. *Advanced Materials*. 1994, 6, 677-679.

70. KIM, S. H., et al. Triplet host engineering for triplet exciton management in phosphorescent organic light-emitting diodes. *Journal of Applied Physics*. 2008, 103, 054502-1-4.

71. FANG, J., et al. Improved efficiency by a fluorescent dye in red organic light-emitting devices based on a europium complex. *Chemical Physics Letters*. 2004, 392, 11-16.

72. GOUSHI, K., et al. Triplet exciton confinement and unconfinement by adjacent hole-transport layers. *Journal of Applied Physics*. 2004, 95, 7798-7802.

73. ADAMOVICH, V. I., et al. New charge-carrier blocking materials for high efficiency OLEDs. *Organic Electronics.* 2003, 4, 77-87.

74. BALDO, M. A., and S. R. FORREST. Transient analysis of organic electrophosphorescence: I. Transient analysis of triplet energy transfer. *Physical Review B*. 2000, 62, 10958-10966.

75. KONDAKOVA, M. E., et al. High-efficiency, low-voltage phosphorescent organic light-emitting diode devices with mixed host. *Journal of Applied Physics*. 2008, 104, 094501-1-17.

76. WANG, Q., et al. Harvesting Excitons Via Two Parallel Channels for Efficient White Organic LEDs with Nearly 100% Internal Quantum Efficiency: Fabrication and Emission-Mechanism Analysis. Advanced Functional Materials. 2009, 19, 84-95.

77. XU, H., et al. Recent progress in metal–organic complexes for optoelectronic applications. *Chemical Society Reviews*. 2014, 43, 3259–3302.

78. ZHU, M., and YANG, C. Blue fluorescent emitters: design tactics and applications in organic light-emitting diodes.*Chemical Society Reviews*. 2013, 42, 4963–4976.

79. TAO, Y., et al. Thermally Activated Delayed Fluorescence Materials Towards the Breakthrough of Organoelectronics. *Advanced Materials.* 2014, 26, 7931–7958.

80. YOOK, K. S., and LEE, J. Y. Small Molecule Host Materials for Solution Processed Phosphorescent Organic Light-Emitting Diodes.*Advanced Materials*, 2014, 26, 4218–4233.

81. KLESSINGER, M., and MICHL, J. Excited States and Photochemistry of Organic Molecules, VCH, New York, 1995.

82. ADACHI, C., et al. Nearly 100% internal phosphorescence efficiency in an organic light-emitting device. *Journal of Applied Physics*. 2001, 90, 5048–5051.

83. http://www.sigmaaldrich.com/technicaldocuments/articles/materialmatters/organicsemiconductor .html

84. UDAGAWA, K., et al. Low-Driving-Voltage Blue Phosphorescent Organic Light-Emitting Devices with External Quantum Efficiency of 30%. *Advanced. Materials.* 2014, 26, 5062–5066.

85. SHIH, P.-I., et al. Novel Carbazole/Fluorene Hybrids: Host Materials for Blue Phosphorescent OLEDs. *Organic Letters*. 2006, 8, 2799–2802.

86. LI, W., et al. Novel fluorene/carbazole hybrids with steric bulk as host materials for blue organic electrophosphorescent devices. *Tetrahedron*, 2007, 63, 10161–10168.

87. HAN, W.-S., et al. Silicon-Based Blue Phosphorescence Host Materials: Structure and Photophysical Property Relationship on Methyl/Phenylsilanes Adorned with 4-(N-Carbazolyl)phenyl Groups and Optimization of Their Electroluminescence by Peripheral 4-(N-Carbazolyl)phenyl Numbers. *The Journal of Physical Chemistry C*. 2009, 113, 19686–19693.

88. BIN, J.-K., et al. New Host Material for High-Performance Blue Phosphorescent Organic Electroluminescent Devices. *Advanced Materials*. 2012, 24, 2911–2915.

89. JIANG, W., et al. Tuning of Charge Balance in Bipolar Host Materials for Highly Efficient Solution-Processed Phosphorescent Devices. *Organic Letters*. 2011, 13, 3146–3149.

90. SASABE, H., et al. 3,3′-Bicarbazole-Based Host Materials for High-Efficiency Blue Phosphorescent OLEDs with Extremely Low Driving Voltage. *Advanced Materials*. 2012, 24, 3212–3217.

91. ZHUANG, J., et al. Configuration effect of novel bipolar triazole/carbazole-based host materials on the performance of phosphorescent OLED devices. *Organic Electronics.* 2012, 13, 2210–2219.
92. DENG, L., et al. Simple bipolar host materials incorporating CN group for highly efficient blue electrophosphorescence with slow efficiency roll-off. Journal of Materials Chemistry C. 2013, 1, 8140–8145.
93. LEE, C. W., and J. Y. LEE. Above 30% External Quantum Efficiency in Blue Phosphorescent Organic Light-Emitting Diodes Using Pyrido[2,3-b]indole Derivatives as Host Materials. *Advanced Materials*. 2013, 25, 5450–5454.
94. WAGNER, D., et al. Triazine Based Bipolar Host Materials for Blue Phosphorescent OLEDs. *Chemistry of Materials*. 2013, 25, 3758–3765.
95. JOU, J.-H., et al. High-efficiency blue organic light-emitting diodes using a 3,5-di(9H-carbazol-9-yl)tetraphenylsilane host via a solution-process. *Journal of Materials Chemistry*. 2010, 20, 8411–8416.
96. LEE, C. W., et al. Synthesis and device application of hybrid host materials of carbazole and benzofuran for high efficiency solution processed blue phosphorescent organic light-emitting diodes. *Organic Electronics.* 2013, 14, 1009–1014.
97. LEE, C. W., and J. Y. LEE. High Quantum Efficiency in Solution and Vacuum Processed Blue Phosphorescent Organic Light Emitting Diodes Using a Novel Benzofuropyridine-Based Bipolar Host Material. *Advanced Materials*. 2013, 25, 596–600.
98. SU, S.-J., et al. Pyridine-Containing Bipolar Host Materials for Highly Efficient Blue Phosphorescent OLEDs. *Chemistry of Materials*. 2008, 20, 1691–1693.
99. GONG, S., et al. Solution-Processed Double-Silicon-Bridged Oxadiazole/Arylamine Hosts for High-Efficiency Blue Electrophosphorescence. *Chemistry of Materials*. 2012, 24, 3120–3127.
100. YE, S., et al. Solution-Processed Solid Solution of a Novel Carbazole Derivative for High-Performance Blue Phosphorescent Organic Light-Emitting Diodes. *Advanced Materials.* 2010, 22, 4167–4171.
101. YOOK, K. S., and J. Y. LEE. High efficiency in solution processed blue phosphorescent organic light-emitting diodes using an alcohol soluble emitting layer. *Organic Electronics.* 2011, 12, 1595–1599.
102. KIM, J. H., et al. New host materials with high triplet energy level for blue-emitting electrophosphorescent device. *Synthetic Metals*. 2007, 157, 743–750.
103. YAO, C., et al. Solution processed blue phosphorescent organic light emitting diodes using a Ge-based small molecular host. *Journal of Materials Chemistry C*. 2015, 3, 5017–5025.
104. JEON, Y. P., et al. Blue phosphorescent organic light-emitting devices based on carbazole/ thioxanthene-S,S-dioxide with a high glass transition temperature. *Journal of Materials Chemistry C.* 2015, 3, 6192–6199.
105. XIE, Y.-M., et al. Efficient blue/white phosphorescent organic light-emitting diodes based on a silicon-based host material via a direct carbon–nitrogen bond. *Journal of Materials Chemistry C.* 2015, 3, 5347–5353.
106. GONG, S., et al. Simple CBP isomers with high triplet energies for highly efficient blue electrophosphorescence. *Journal of Materials Chemistry.* 2012, 22, 2894–2899.

107. Pan, B., et al. Systematic study of TCTA-based star-shaped host materials by optimizing ratio of carbazole/diphenylphosphine oxide: achieving both low efficiency roll-off and turn-on voltage for blue PHOLEDs. *Journal of Materials Chemistry C.* 2014, 2, 7428–7435.

108. HAN, C., et al. Controllably Tuning Excited-State Energy in Ternary Hosts for Ultralow-Voltage-Driven Blue Electrophosphorescence. *Angewandte Chemie International Edition*. 2012, 51, 10104–10108.

109. DING, J., et al. Design of star-shaped molecular architectures based on carbazole and phosphine oxide moieties: towards amorphous bipolar hosts with high triplet energy for efficient blue electrophosphorescent devices. *Journal of Materials Chemistry.* 2010, 20, 8126–8133.

110. LEE, Y.,-T. et al. Solution-processed bipolar small molecular host materials for single-layer blue phosphorescent organic light-emitting diodes. *Journal of Materials Chemistry* C. 2013 2, 382–391.

111. JEON, S. O., et al. Phenylcarbazole-Based Phosphine Oxide Host Materials For High Efficiency In Deep Blue Phosphorescent Organic Light-Emitting Diodes. *Advanced Functional Materials*. 2009, 19, 3644–3649.

112. SON, H. S., et al. Correlation of the substitution position of diphenylphosphine oxide on phenylcarbazole and device performances of blue phosphorescent organic light-emitting diodes. *Journal of Materials Chemistry*. 2011, 21, 5638–5644.

113. JEON, S. O., and J. Y. LEE. Comparison of symmetric and asymmetric bipolar type high triplet energy host materials for deep blue phosphorescent organic light-emitting diodes. *Journal of Materials Chemistry.*2012, 22, 7239–7244.

114. JEON, S. O., et al. High-Efficiency Deep-Blue-Phosphorescent Organic Light-Emitting Diodes Using a Phosphine Oxide and a Phosphine Sulfide High-Triplet-Energy Host Material with Bipolar Charge-Transport Properties. *Advanced Materials.* 2010, 22, 1872–1876.

115. JEON, S. O., et al. Y. External Quantum Efficiency Above 20% in Deep Blue Phosphorescent Organic Light-Emitting Diodes. *Advanced Materials*. 2011, 23, 1436–1441.

116. MOON, B.-J., et al. Synthesis, photophysical and electro-optical properties of bis-carbazolyl methane based host material for pure-blue phosphorescent OLED. *Journal of Luminescence*. 2012, 132, 2557–2560.

117. SCHRÖGEL, P., et al. Meta-linked CBP-derivatives as host materials for a blue iridium carbene complex. *Organic Electronics*. 2011, 12, 2047–2055.

118. YANG, J. W. and LEE, J. Y. Pyridoindole modified carbazole compounds as high triplet energy host materials of imidazole derived blue triplet emitters for high quantum efficiency. *Organic Electronics*. 2015, 22, 74–80.

119. KANG, J.-W., et al. A host material containing tetraphenylsilane for phosphorescent OLEDs with high efficiency and operational stability. *Organic Electronics*. 2008, 9, 452–460.

120. JIANG, Z., et al. Diarylmethylene-bridged 4,4′-(bis(9-carbazolyl))biphenyl: morphological stable host material for highly efficient electrophosphorescence. *Journal of Materials Chemistry*. 2009, 19, 7661–7665.

121. KIM, K.-S., et al. Synthesis and electro-optical properties of carbazole derivatives with high band gap energy. *Thin Solid Films*. 2009, 518, 284–289.

122. PARK, J.-H., et al. New Bipolar Green Host Materials Containing Benzimidazole-Carbazole Moiety in Phosphorescent OLEDs. *Bulletin of the Korean Chemical Society*. 2011, 32 (3), 841-846.

123. ZHANG, T., et al. A CBP derivative as bipolar host for performance enhancement in phosphorescent organic light-emitting diodes. *Journal of Materials Chemistry* C. 2012, 1, 757–764.

124. MAZETYTE, D., et al. Carbazole- and phenylindole-based new host materials for phosphorescent organic light emitting diodes. *Optical Materials*. 2013, 35, 604–608.

125. GAO, Z., et al. High-efficiency deep blue fluorescent emitters based on phenanthro[9,10-d]imidazole substituted carbazole and their applications in organic light emitting diodes. *Organic Electronics.* 2014, 15, 2667–2676.

126. LEE, N.-J., et al. Triphenylene containing host materials with high thermal stability for green phosphorescent organic light emitting diode. *Dyes and Pigments*. 2014, 101, 221–228.

127. GE, Z., et al. Synthesis and Properties of 3,8-Bis[4-(9H-carbazol-9-yl)phenyl]-1,10-phenanthroline for Phosphorescent OLEDs. *Chemistry Letters.* 2008, 37, 262–263.

128. LI, J., et al. Solution-Processible Carbazole Dendrimers as Host Materials for Highly Efficient Phosphorescent Organic Light-Emitting Diodes. *Advanced Functional Materials.* 2013, 23, 619–628.

129. JOU, J.-H., et al. A wet and dry processable phosphorescent green dye based organic light-emitting diodes. *Dyes and Pigments*. 2015, 113, 341–350.

130. VEZZU, D. A. K., et al. Acridinone/Amine(carbazole)-Based Bipolar Molecules: Efficient Hosts for Fluorescent and Phosphorescent Emitters. *Organic Letters*. 2009, 11, 4310–4313.

131. SOH, M. S., et al. Solution processable high band gap hosts based on carbazole functionalized cyclic phosphazene cores for application in organic light-emitting diodes. *Journal of Polymer Science Part B: Polymer Physics*. 2011, 49, 531–539.

132. AIZAWA, N., et al. J. Solution-processable carbazole-based host materials for phosphorescent organic light-emitting devices. *Organic Electronics*. 2012, 13, 2235–2242.

133. GONG, W.-L., et al. Carbazole oligomers revisited: new additions at the carbazole 1- and 8-positions. *RSC Advances*. 2012, 2, 10821–10828.

134. ZENG, L., et al. A new class of non-conjugated bipolar hybrid hosts for phosphorescent organic light-emitting diodes. *Journal of Materials Chemistry*.2009, 19, 8772–8781.

135. BAN, X., et al. Systematically tuning the ΔEST and charge balance property of bipolar hosts for low operating voltage and high power efficiency solution-processed electrophosphorescent devices. *Journal of Materials Chemistry C.* 2015, 3, 5004–5016.

136. TSUZUKI, T., and S. TOKITO. Highly efficient and stable organic light-emitting diode using 4,4′-bis(N-carbazolyl)-9,9′-spirobifluorene as a thermally stable host material. *Applied Physics Letters.* 2009, 94, 033302.

137. CHANG, C.-H., et al. A dicarbazole–triazine hybrid bipolar host material for highly efficient green phosphorescent OLEDs. *Journal of Materials Chemistry*. 2012, 22, 3832–3838.

138. HUNG, W.-Y., et al. A new benzimidazole/carbazole hybrid bipolar material for highly efficient deep-blue electrofluorescence, yellow–green electrophosphorescence, and two-color-based white OLEDs. *Journal of Materials Chemistry*. 2010, 20, 10113–10119.

139. CHEN, C.-H., et al. Highly efficient orange and deep-red organic light emitting diodes with long operational lifetimes using carbazole–quinoline based bipolar host materials. *Journal of Materials Chemistry C*. 2014, 2, 6183–6191.

140. YOOK, K. S., and J. Y. LEE. Solution processed multilayer deep blue and white phosphorescent organic light-emitting diodes using an alcohol soluble bipolar host and phosphorescent dopant materials. *Journal of Materials Chemistry*. 2012, 22, 14546–14550.

141. DU, X., et al. Highly Efficient Orange and Warm White Phosphorescent OLEDs Based on a Host Material with a Carbazole–Fluorenyl Hybrid. *Chemistry – An Asian Journal*. 2014, 9, 1500–1505.

142. WU, C., et al. A new multifunctional fluorenyl carbazole hybrid for high performance deep blue fluorescence, orange phosphorescent host and fluorescence/phosphorescence white OLEDs. *Dyes and Pigments*. 2013, 97, 273–277.

143. ORSELLI, E., et al. Orange phosphorescent organic light-emitting diodes with high operational stability. *Organic Electronics*. 2012, 13, 1506–1510.

144. TAO, Y., et al. Solution-processable highly efficient yellow- and red-emitting phosphorescent organic light emitting devices from a small molecule bipolar host and iridium complexes. *Journal of Materials Chemistry*. 2008, 18, 4091–4096.

145. WANG, X., et al. High performance fluorescent and phosphorescent organic light-emitting diodes based on a charge-transfer-featured host material. *Organic Electronics*. 2015, 21, 78–85.

146. DENG, L., et al. Solution-processible small-molecular host materials for high-performance phosphorescent organic light-emitting diodes. *Dyes and Pigments*. 2014, 102, 150–158.

147. LIN, C.-H., et al. Phosphorescent OLEDs assembled using Os(II) phosphors and a bipolar host material consisting of both carbazole and dibenzophosphole oxide. *Journal of Materials Chemistry*. 2012, 22, 10684–10694.

148. LIU, Y., et al. Highly efficient single-layer organic light-emitting devices based on a bipolar pyrazine/carbazole hybrid host material. *Journal of Materials Chemistry C*. 20142, 2488–2495.

149. WANG, H., et al. Highly Efficient Orange and Red Phosphorescent Organic Light-Emitting Diodes with Low Roll-Off of Efficiency using a Novel Thermally Activated Delayed Fluorescence Material as Host. *Advanced Materials*. 2015, 27, 4041–4047.

150. KWAK, J., et al. New carbazole-based host material for low-voltage and highly efficient red phosphorescent organic light-emitting diodes *Journal of Materials Chemistry*. 2012, 22, 6351–6355.

151. JEON, J. H., et al. Thermally-stable 2,3-diphenylated benzotiophene containing host materials for red phosphorescent organic light-emitting diodes. *Dyes and Pigments*. 2014, 111, 116–123.

152. GUAN, M., et al. The host materials containing carbazole and oxadiazole fragment for red triplet emitter in organic light-emitting diodes. *Organic Electronics*. 2006, 7, 330–336.

153. SU, T.-H., et al. Highly efficient deep-red organic electrophosphorescent devices with excellent operational stability using bis(indoloquinoxalinyl) derivatives as the host materials. *Journal of Materials Chemistry* C. 2013, 1, 5084–5092.

154. GONG, W.-L., et al. Tetraphenylethene-decorated carbazoles: synthesis, aggregation-induced emission, photo-oxidation and electroluminescence. *Journal of Materials Chemistry C*. 2014, 2, 7001–7012.

155. TONG, Q.-X., et al. Highly Efficient Blue Organic Light-Emitting Device Based on a Nondoped Electroluminescent Material. *Chemistry of Materials*. 2008, 20, 6310–6312.

156. GRISORIO, R., et al. Influencing the Spectral Stability and the Electroluminescence Behavior of New Blue-Emitting Bifluorene-Based Materials by the 7,7‘-Functionalization of the Core. *Journal of Materials Chemistry C*. 2008, 112, 7005–7014.

157. KUO, W.-J., et al. Efficient and bright non-doped blue light-emitting diodes based on glassy styrylcarbazoles. *Thin Solid Films*. 2008, 516, 4145–4152.

158. LIN, S.-L., et al. Highly Efficient Carbazole-π-Dimesitylborane Bipolar Fluorophores for Nondoped Blue Organic Light-Emitting Diodes. *Advanced Materials*. 2008, 20, 3947–3952.

159. ADHIKARI, R. M., et al. Ethynylphenyl-Linked Carbazoles as a Single-Emitting Component for White Organic Light-Emitting Diodes. *Chemistry of Materials*. 2009, 21, 4638–4644.

160. TANG, S., et al. A Molecular Glass for Deep-Blue Organic Light-Emitting Diodes Comprising a 9,9′-Spirobifluorene Core and Peripheral Carbazole Groups. *Advanced Functional Materials*. 2007, 17, 2869–2877.

161. SETOGUCHI, Y., and C. Adachi. Suppression of roll-off characteristics of electroluminescence at high current densities in organic light emitting diodes by introducing reduced carrier injection barriers. *Journal of Applied Physics*. 2010, 108, 064516 1-7.

162. AGARWAL, N., et al. Tuning of HOMO levels of carbazole derivatives: New molecules for blue OLED. *Synthetic Metals*. 2011, 161, 466–473.

163. ZHOU, Y., et al. Covalent Functionalized Conjugated Dendrimers for Organic Light Emitting Diodes: Synthesis, Characterization, and the Deep Blue Electroluminescence. *Australian Journal of Chemistry*. 2011, 64, 160–165.

164. KHUNCHALEE, J., et al. Synthesis and properties of oligofluorene-thiophenes as emissive materials for organic electroluminescent devices: color-tuning from deep blue to orange. *Tetrahedron.* 2012, 68, 8416–8423.

165. LIN, Y., et al. Oligofluorene-based push–pull type functional materials for blue light-emitting diodes. *Journal of Photochemistry and Photobiology A: Chemistry*. 2012, 230, 55–64.

166. LINTON, K. E., et al. Colour tuning of blue electroluminescence using bipolar carbazole–oxadiazole molecules in single-active-layer organic light emitting devices (OLEDs). *Journal of Materials Chemistry*. 2012, 22, 11816–11825.

167. TONG, Q.-X., et al. An efficient hole-transporting blue fluorophore 3,6-dipyrenyl-9-ethylcarbazole for undoped organic light-emitting devices. *Synthetic Metals*. 2012, 162, 415–418.

168. BHALLA, V., et al. Carbazole-based linear conjugated molecules: structure–property relationships and device properties. *RSC Advances.* 2013, 3, 14722–14730.

169. CHANG, Y.-C., et al. New carbazole-substituted anthracene derivatives based non-doped blue light-emitting devices with high brightness and efficiency. *Dyes and Pigments.* 2013, 99, 577–587.

170. SHI, H., et al. A novel tetraphenylethene–carbazole type compound containing the dimesitylboron moiety: aggregation-induced emission enhancement and electroluminescence properties. *RSC Advances*. 2014 4, 19418–19421.

171. TANG, X., et al. Novel violet emitting material synthesized by stepwise chemical reactions. *Journal of Materials Chemistry C*. 2014, 2, 5019–5027.

172. WU, C.-L., et al. High efficiency non-dopant blue organic light-emitting diodes based on anthracene-based fluorophores with molecular design of charge transport and red-shifted emission proof. *Journal of Materials Chemistry C.* 2014, 2, 7188–7200 .

173. LIAN, J., et al. Efficient near ultraviolet organic light-emitting devices based on star-configured carbazole emitters. *Current Applied Physics*. 2011, 11, 295–297.

174. CHEN, C.-H., et al. Stilbene like carbazole dimer-based electroluminescent materials. *Tetrahedron*. 2006, 62, 8564–8570.

175. FISCHER, A., et al. Highly efficient multilayer organic pure blue light emitting diodes with substituted carbazoles compounds in the emitting layer. *Journal of Physics D: Applied Physics.* 2006, 39, 917.

176. USLUER, O., et al. White organic light emitting diodes based on fluorene-carbazole dendrimers. *Journal of Luminescence.* 2014, 146, 6–10

177. USLUER, O., et al. Fluorene-Carbazole Dendrimers: Synthesis, Thermal, Photophysical and Electroluminescent Device Properties. *Advanced Functional Materials.* 2010, 20, 4152–4161.

178. ALBRECHT, K., et al. Carbazole Dendrimers as Solution-Processable Thermally Activated Delayed-Fluorescence Materials. *Angewandte Chemie International Edition.* 2015, 54, 5677-5682.

179. LU, J., et al. Synthesis and Properties of Multi-Triarylamine-Substituted Carbazole-Based Dendrimers with an Oligothiophene Core for Potential Applications in Organic Solar Cells and Light-Emitting Diodes. *Chemistry of Materials*. 2006, 18, 6194–6203.

180. ENDO, A., et al. Thermally Activated Delayed Fluorescence from Sn4+–Porphyrin Complexes and Their Application to Organic Light Emitting Diodes — A Novel Mechanism for Electroluminescence.*Advanced Materials*, 2009, 21, 4802–4806.

181. UOYAMA, H. et al. Highly efficient organic light-emitting diodes from delayed fluorescence. *Nature*. 2012, 492, 234–238.

182. MASUI, K., et al. Analysis of exciton annihilation in high-efficiency sky-blue organic light-emitting diodes with thermally activated delayed fluorescence. *Organic electronics*. 2013, 14, 2721–2726.

183. HIRATA, S., et al. Highly efficient blue electroluminescence based on thermally activated delayed fluorescence. *Nature Materials*. 2015, 14, 330–336.

184. ZHANG, Q., et al. Design of Efficient Thermally Activated Delayed Fluorescence Materials for Pure Blue Organic Light Emitting Diodes. *Journal of the American Chemical Society*. 2012, 134, 14706–14709.

185. SEREVIČIUS, T., et al. Enhanced electroluminescence based on thermally activated delayed fluorescence from a carbazole–triazine derivative. *Physical Chemistry Chemical Physics*. 2013, 15, 15850–15855.

186. WU, S., et al. High-efficiency deep-blue organic light-emitting diodes based on a thermally activated delayed fluorescence emitter. *Journal of Materials Chemistry C.* 2013, 2, 421–424.

187. KIM, B. S., and J. Y. LEE. Phosphine Oxide Type Bipolar Host Material for High Quantum Efficiency in Thermally Activated Delayed Fluorescent Device. *ACS Applied Materials & Interfaces*. 2014, 6, 8396–8400.

188. LEE, S. Y., et al. Luminous Butterflies: Efficient Exciton Harvesting by Benzophenone Derivatives for Full-Color Delayed Fluorescence OLEDs. *Angewandte Chemie International Edition*. 2014, 53, 6402–6406.

189. NISHIMOTO, T., et al. A six-carbazole-decorated cyclophosphazene as a host with high triplet energy to realize efficient delayed-fluorescence OLEDs. *Materials Horizons*. 2014, 1, 264–269.

190. TAKAHASHI, T., et al. Donor–acceptor-structured 1,4-diazatriphenylene derivatives exhibiting thermally activated delayed fluorescence: design and synthesis, photophysical properties and OLED characteristics. *Science and Technology of Advanced Materials*. 2014, 15, 034202.

191. ZHANG, Q., et al. Anthraquinone-Based Intramolecular Charge-Transfer Compounds: Computational Molecular Design, Thermally Activated Delayed Fluorescence, and Highly Efficient Red Electroluminescence. *Journal of the American Chemical Society*. 2014, 136, 18070–18081.

192. WANG, H., et al. Novel Thermally Activated Delayed Fluorescence Materials–Thioxanthone Derivatives and Their Applications for Highly Efficient OLEDs. *Advanced Materials*. 2014, 26, 5198–5204.

193. KIM, B. S., and J. Y. LEE. Engineering of Mixed Host for High External Quantum Efficiency above 25% in Green Thermally Activated Delayed Fluorescence Device. *Advanced Functional Materials.* 2014, 24, 3970–3977.

194. GAJ, M. P., et al. Highly efficient Organic Light-Emitting Diodes from thermally activated delayed fluorescence using a sulfone–carbazole host material. *Organic Electronics.* 2015, 16, 109–112.

195. MACRAE, C. F., et al. Mercury CSD 2.0 - New Features for the Visualization and Investigation of Crystal Structures. *Journal of Applied Crystallography*. 2008, 41, 466-470.

196. MALINAUSKAS, T., et al.Multifunctional red phosphorescent bis-cyclometallated iridium complexes based on 2-phenyl-1,2,3-benzotriazole ligand and carbazolyl moieties.*Tetrahedron*. 2011, 67, 1852-1861.

197. Blazys, G., et al.Phenothiazinyl-containing aromatic amines as novel amorphous molecular materials for optoelectronics. *Journal of Photochemistry and Photobiology A: Chemistry*. 2005, 174, 1-6.

198. MIYAMOTO, E., et al. Ionization Potential of Organic Pigment Film by Atmospheric Photoelectron Emission Analysis. *Electrophotography*. 1989, 28, 364.

199. MONTRIMAS, E., et al. The discharge kinetics of negatively charged Se electrophotographic layers. *Lithuanian Journal of Physics.* 1966, 6, 569-578.

200. VAEZI-NEJAD, S.M.Xerographic time of flight experiment for the determination ofdrift mobility in high resistivity semiconductors. *International Journal ofElectronics*. 1987, 62, 361-384.

201. AMORIM, C. A., et al.Determination of carrier mobility in MEH-PPV thin-films by stationary and transient current techniques. *Journal of Non-Crystalline Solids*. 2012, 358, 484-491.

202. VOLYNIUK, D., et al. Highly Efficient Blue OLEDs Based on Intermolecular Triplet-Singlet Energy Transfer. *Journal of Physical Chemistry C.* 2013, 117, 22538–22544.

203. NAKA, S., et al. High electron mobility in bathophenanthroline. *Applied Physics Letters.* 2000, 76, 197-199.

204. FRISCH, M.J., et al. Gaussian 09, Revision A.02, Gaussian, Inc., Wallingford CT, 2009.

205. VALEEV, E. F., et al. Effect of Electronic Polarization on Charge-Transport Parameters in Molecular Organic Semiconductors. *Journal of the American Chemical Society.* 2006, 128, 9882–9886.

206. CHAI, J.-D., and M. HEAD-GORDON. Long-range corrected hybrid density functionals with damped atom–atom dispersion corrections. *Physical Chemistry Chemical Physics.* 2008, 10, 6615–6620.

207. Spartan'14 for Windows Version 1.1.2. 1840 Von Karman Avenue, Suite 370, Irvine, CA.

208. SCHEIN, L. B. and A. R. MCGHIE. Band-hopping mobility transition in naphthalene and deuterated naphthalene. *Physical Review B.* 1979, 20, 1631–1639.

209. BECKE, A. D. Density-Functional Exchange-Energy Approximation with Correct Asymptotic Behavior. *Physical Review A.* 1988, 38, 3098−3100.

210. LEE, C., et al. Development of the Colle-Salvetti Correlation-Energy Formula into a Functional of the Electron Density. *Physical Review B.* 1988, 37, 785−789.

211. FRANCL, M. M., et al. A Polarization-Type Basis Set for 2nd-row Elements. *The Journal of Chemical Physics.* 1982, 77, 3654−3665.

212. RUNGE, E., and E. K. U. GROSS. Density-Functional Theory for Time-Dependent Systems. *Physical Review Letters.* 1984, 52, 997−1000.

213. MIERTUS, S., et al. Electrostatic interaction of a solute with a continuum. A direct utilization of Ab initio molecular potentials for the prevision of solvent effects. *Chemical Physics.* 1981, 55, 117–129.

214. DATTA, A., et al. Electron and hole mobilities in polymorphs of benzene and naphthalene: Role of intermolecular interactions. *Journal of Chemical Physics.* 2007, 126, 144710-144710-7.

215. DOBARRO, A., et al. Synthesis of symmetric and asymmetric carbazolyl monomers and their siloxane polymers. Effect of the 2,3,6,7,9-substitution in the carbazole unit on its mesomorphic behavior. *Macromolecular Chemistry and Physics.* 1997, 198, 2563-2581.

216. FREEMAN, A. W., et al.Triphenylphosphine-Mediated Reductive Cyclization of 2-Nitrobiphenyls: A Practical and Convenient Synthesis of Carbazoles.*The Journal of Organic Chemistry*. 2005, 70, 5014-5019.

217. LI., J.C., et al.A Thiophene, Benzothiadiazole, and Carbazole-Based Copolymer: Synthesis and Characterization.*Bulletin of the Korean Chemical Society*. 2009, 30, 951-953.

218. KIKUGAWA, Y., et al.Synthesis of Carbazoles from *N*-(*N*,*N*-Diarylamino)phthalimides with Aluminum Chloride via Diarylnitrenium Ions.*The Journal of Organic Chemistry*. 2001, 66, 8612-8615.

219. JIANG, W., et al. Heteroatom-Annulated Perylenes: Practical Synthesis, Photophysical Properties, and Solid-State Packing Arrangement. *The Journal of Organic Chemistry*. 2008, 73, 7369–7372.

220. LOOKER, J. J. Mononitration of perylene. Preparation and structure proof of the 1 and 3 isomers. *The Journal of Organic Chemistry*. 1972, 37, 3379–3381.

221. TANG, W., et al. Synthesis, photophysics, theoretical modeling, and electroluminescence of novel 2,7-carbazole-based conjugated polymers with sterically hindered structures. *Journal of Polymer Science Part A: Polymer Chemistry*. 2008, 46, 7725–7738.

222. TUCKER, S. H. Iodination in the carbazole series. *Journal of the Chemical Society*. 1926, 129, 546–553.

223. REGHU, R. R., et al. Air stable electron-transporting and ambipolar bay substituted perylene bisimides. *Journal of Materials Chemistry*. 2011, 21, 7811–7819.

224. GAUTHIER, S., and J. M. J. FRECHET. Phase-Transfer Catalysis in the Ullmann Synthesis of Substituted Triphenylamines. *Synthesis*. 1987, 4, 383–385.

225. MEI, J., et al. Synthesis of Isoindigo-Based Oligothiophenes for Molecular Bulk Heterojunction Solar Cells. *Organic Letters*. 2010, 12, 660–663.

226. KRUCAITE, G., et al. 3,6-Diaryl substituted 9-alkylcarbazoles as hole transporting materials for various organic light emitting devices.*Dyes and Pigments*. 2014, 106, 1–6.

227. MÜLLEN, K., and U. SCHERF. *Organic Light-Emitting Devices*. Wiley-VCH, Heidelberg, 2005, p. 410.

228. (a) DIMITRAKOPOULOS, C. D., and P.R. L. MALENFANT.Organic Thin Film Transistors for Large Area Electronics.*Advanced Materials*. 2002, 14, 99–117. (b) REIG, M., et al. Molecular order of air-stable p-type organic thin-film transistors by tuning the extension of the π-conjugated core: the cases of indolo[3,2-*b*]carbazole and triindole semiconductors.*Journal of Materials Chemistry C*. 2015, 3, 506-513.

229. (a) PUCKYTE, G., et al. Carbazole-based molecular glasses for efficient solid-state dye-sensitized solar cells. *Journal of Power Sources*. 2013, 233, 86-92. (b) BOUDREAULT, P.-L. T., et al. Polycarbazoles for plastic electronics.*Polymer Chemistry*. 2010, 1, 127-136.

230. GUO, X., et al. Designing π-conjugated polymers for organic electronics.*Progress in Polymer Science*. 2013, 38, 1832-1908.

231. (a) MORIN, J.-F., et al. Polycarbazoles: 25 Years of Progress.*Macromolecular Rapid Communications*. 2005, 26, 761-778. (b) GRAZULEVICIUS, J. V., et al. Carbazole-

containing polymers: synthesis, properties and applications.*Progress in Polymer Science.* 2003, 28, 1297-1353.

232. ZOTTI, G., et al.Electrochemical, Conductive, and Magnetic Properties of 2,7-Carbazole-Based Conjugated Polymers. *Macromolecules*. 2002, 35, 2122-2128.
233. DIERSCHKE, F., et al. Efficient Synthesis of 2,7-Dibromocarbazoles as Components for Electroactive Materials.*Synthesis*. 2003, 16, 2470-2472.
234. WU, F.-I., et al. Novel distyrylcarbazole derivatives as hole-transporting blue emitters for electroluminescent devices. *Journal of Materials Chemistry.* 2005, 15, 4753–4760
235. WANG, T.-T., et al. Relaxation Dynamics of 2,7- and 3,6-Distyrylcarbazoles in Solutions and in Solid Films: Mechanism for Efficient Nonradiative Deactivation in the 3,6-Linked Carbazole**.** *The Journal of Physical Chemistry B.* 2005, 109, 23827-23835.
236. KERUCKAS, J., et al. Influence of methoxy groups on the properties of 1,1-bis(4-aminophenyl)cyclohexane based arylamines: experimental and theoretical approach. *Journal of Materials Chemistry.* 2012, 22, 3015–3027.
237. AZIZ, H., and Z. D. POPOVIC. Degradation Phenomena in Small-Molecule Organic Light-Emitting Devices. *Chemistry of Materials.* 2004, 16, 4522–4532.
238. LI, F., et al. Stable and Controllable Polymer/Fullerene Composite Nanofibers through Cooperative Noncovalent Interactions for Organic Photovoltaics. *Chemistry of Materials.* 2014, 26, 3747–3756.
239. LI, F., et al. Complementary Hydrogen Bonding and Block Copolymer Self-Assembly in Cooperation toward Stable Solar Cells with Tunable Morphologies. *Macromolecules.* 2013, 46, 9021–9031.
240. LI, F., et al. Nano-structuring polymer/fullerene composites through the interplay of conjugated polymer crystallization, block copolymer self-assembly and complementary hydrogen bonding interactions. *Polym. Chem.* 2015,6, 721–731.
241. QU, J., et al. Synthesis and electro-optical properties of helical polyacetylenes carrying carbazole and triphenylamine moieties. *Polymer.* 2007, 48, 4628–4636.
242. MENG, H., et al. Synthesis and characterization of a novel blue electroluminescent polymer constituted of alternating carbazole and aromatic oxadiazole units. *Physical Chemistry Chemical Physics.* 1999, 1, 3123–3127.
243. BUBNIENE, G., et al. Easily functionalizable carbazole based building blocks with extended conjugated systems for optoelectronic applications. *Tetrahedron.* 2010, 66, 3199–3206.
244. ISHIKAWA, W., et al. Polymorphism of starburst molecules: methyl-substituted derivatives of 1,3,5-tris(diphenylamino)benzene. *Journal of Physics D: Applied Physics.* 1993, 26, B94-B99.
245. YU, L., et al. Thermochemistry and Conformational Polymorphism of a Hexamorphic Crystal System. *Journal of the American Chemical Society.* 2000, 122, 585–591.
246. SONNTAG, M., and Strohriegl, P. Novel 2,7-Linked Carbazole Trimers as Model Compounds for Conjugated Carbazole Polymers. *Chemistry of Materials.* 2004,16, 4736–4742.
247. DUVANEL, G., et al. Ultrafast excited-state dynamics of a series of zwitterionic pyridinium phenoxides with increasing sterical hindering. *Photochemical & Photobiological Sciences.* 2010, 9, 908-915.

248. MORAIS, J., et al. Solvent dependence of the twisted excited state energy of tetraphenylethylene: evidence for a zwitterionic state from picosecond optical calorimetry. *The Journal of Physical Chemistry.* 1991, 95, 3885–3888.

249. MEI, J., et al. Aggregation-Induced Emission: The Whole Is More Brilliant than the Parts. *Advanced Materials.* 2014, 26, 5429–5479.

250. YANG, Y., et al. Aggregation-induced emission in BF2–hydrazone (BODIHY) complexes. *Chemical Science.* 2012, 3, 610–613.

251. WÜRTHNER, F., et al. J-Aggregates: From Serendipitous Discovery to Supramolecular Engineering of Functional Dye Materials. *Angewandte Chemie International Edition.* 2011,50, 3376–3410.

252. PLATT. J. R. Classification of Spectra of CataCondensed Hydrocarbons. *The Journal of Chemical Physics.* 1949, 17, 484-495.

253. YI, J. T., et al. Rotationally resolved S1←S0 electronic spectra of fluorene, carbazole, and dibenzofuran: Evidence for Herzberg-Teller coupling with the S2 state. *The Journal of Chemical Physics.* 2006, 124, 244302.

254. ZELENT, B., et al. Studies on the photophysical properties of some 2,7-dimethoxycarbazoles in various environments by steady state and time resolved spectroscopic methods Part 1. Synthesis, absorption and fluorescence spectra at room temperature. *Journal of Photochemistry and Photobiology A: Chemistry.* 1991,56, 165–181.

255. BREDAS, J. L., et al. Chain-length dependence of electronic and electrochemical properties of conjugated systems: polyacetylene, polyphenylene, polythiophene, and polypyrrole. *Journal of the American Chemical Society.* 1983, 105, 6555–6559.

256. AMBROSE, J.F., and R.F NELSON. Anodic Oxidation Pathways of Carbazoles. *Journal of The Electrochemical Society*. 1968, 115, 1159-1164.

257. D'ANDRADE, B. W., et al. Relationship between the ionization and oxidation potentials of molecular organic semiconductors. *Organic Electronics.* 2005, 6, 11–20.

258. STANIONYTE, R., et al. Synthesis and properties of oxetane monomers and oligomers with electro-active pendent groups. *Polymer International.* 2008, 57, 1036–1041.

259. BORSENBERGER, P.M., and D.S. WEISS. *Organic photoreceptors for xerography*. New York: Dekker; 1998. p. 768.

260. SHUAI, Z., et al. *Theory of Charge Transport in Carbon Electronic Materials*, SpingerBriefs in Molecular Science, Springer, 2012.

261. WAKAMIYA, A., et al. On-Top π-Stacking of Quasiplanar Molecules in Hole-Transporting Materials: Inducing Anisotropic Carrier Mobility in Amorphous Films. *Angewandte Chemie International Edition.* 2014, 53, 5800–5804.

262. COROPCEANU, V.,et al. Charge Transport in Organic Semiconductors. *Chemical Reviews.* 2007, 107, 926–952.

263. CHEN, W.-C., and I. CHAO. Molecular Orbital-Based Design of π-Conjugated Organic Materials with Small Internal Reorganization Energy: Generation of Nonbonding Character in Frontier Orbitals. *The Journal of Physical Chemistry C.* 2014, 118, 20176–20183.

264. DUHM, S., et al. Charge Reorganization Energy and Small Polaron Binding Energy of Rubrene Thin Films by Ultraviolet Photoelectron Spectroscopy. *Advanced Materials.* 2012, 24, 901–905.

265. SATO, N., et al. Reevaluation of electronic polarization energies in organic molecular crystals. *Chemical Physics.* 1987, 115, 269–277.

266. NORTON, J. E., and J.-L BRÉDAS. Polarization Energies in Oligoacene Semiconductor Crystals. *Journal of the American Chemical Society.* 2008, 130, 12377–12384.

267. RYNO, S. M., et al. Electronic Polarization Effects upon Charge Injection in Oligoacene Molecular Crystals: Description via a Polarizable Force Field. *The Journal of Physical Chemistry C.* 2013, 117, 13853–13860.

268. MALAGOLI, M., and J. L. BRÉDAS. Density functional theory study of the geometric structure and energetics of triphenylamine-based hole-transporting molecules. *Chemical Physics Letters.* 2000, 327, 13–17.

269. KASHA, M., et al. The exciton model in molecular spectroscopy. *Pure and Applied Chemistry.* 1965, 11,371-392.

270. GOONESEKERA, A., and S. DUCHARME. Effect of dipolar molecules on carrier mobilities in photorefractive polymers. *Journal of Applied Physics.* 1999, 85, 6506–6514.

271. DIECKMANN, A., et al. An assessment of the role of dipoles on the density-of-states function of disordered molecular solids. *The Journal of Chemical Physics.* 1993, 99, 8136–8141.

272. RAJCA, A., and M. MIYASAKA. Synthesis and Characterization of Novel Chiral Conjugated Materials *Functional Organic Materials.* 2007, 15, 547-581

273. SHEN, Y., and C.-F. CHEN. Helicenes: Synthesis and Applications. *Chemical Review.* 2011, 112, 1463–1535.

274. STARA, I. G., and I. STARY. Phenanthrenes, helicenes, and other angular acenes. *Science of Synthesis* 2010, *45b*, 885–953.

275. RAJCA, A., et al. Annelated, Chiral π-Conjugated Systems: Tetraphenylenes and Helical β-Oligothiophenes. *Synlett*. 2007, 2007, 1799–1822.

276. COLLINS, S. K., and M. P. VACHON. Unlocking the potential of thiaheterohelicenes: chemical synthesis as the key.*Organic & Biomolecular Chemistry*. 2006,4, 2518-2524.

277. URBANO, A. Recent Developments in the Synthesis of Helicene-Like Molecules. *Angewandte Chemie International Edition.* 2003, 42, 3986-3989.

278. GINGRAS, M. One hundred years of helicene chemistry. Part 1: non-stereoselective syntheses of carbohelicenes. *Chemical Society Reviews*. 2013, 42, 968–1006.

279. URBANO, A., and M. C. CARRENO. Enantioselective synthesis of helicenequinones and -bisquinones *Organic & Biomolecular Chemistry*. 2013, 11, 699-708.

280. DUMITRASCU, F., et al. Azahelicenes and other similar tri and tetracyclic helical molecules. *Arkivoc*, 2010, 1-32.

281. KASEYAMA, T., et al. Hierarchical Assembly of a Phthalhydrazide-Functionalized Helicene. *Angewandte Chemie International Edition.* 2011,50, 3684-3687.

282. VERBIEST, T., et al. A. Strong Enhancement of Nonlinear Optical Properties Through Supramolecular Chirality *Science*,1998, 282, 913-915.

283. RYBACEK, J., et al.Racemic and Optically Pure Heptahelicene-2-carboxylic Acid: Its Synthesis and Self-Assembly into Nanowire-Like Aggregates *European Journal of Organic Chemistry*. 2011, 5, 853-860.

284. ICHINOSE, W., et al. Optical Resolution of Aromatic Alcohols Using Silica Nanoparticles Grafted with Helicene. *Organic Letters*. 2012, 14, 3123-3125.

285. AN, Z., and M.YAMAGUCHI. Chiral recognition in aggregation of gold nanoparticles grafted with helicenes *Chemical Communications*. 2012, 48, 7383-7385.

286. GINGRAS, M. One hundred years of helicene chemistry. Part 3: applications and properties of carbohelicenes. *Chemical Society Reviews.* 2013, 42, 1051-1095;

287. GINGRAS, M., et al. One hundred years of helicene chemistry. Part 2: stereoselective syntheses and chiral separations of carbohelicenes. *Chemical Society Reviews.*2013, 42, 1007-1050;

288. TANAKA, K. *Transition-metal-mediated Aromatic Ring Construction*; John Wiley & Sons, 2013.

289. ALKORTA, I., et al. Distinction between homochiral and heterochiral dimers of 1-aza[n]helicenes (n = 1–7) with alkaline cations. *Tetrahedron:Asymmetry.* 2010, 21, 962-968.

290. CRITTALL, M. R., et al. Design, Synthesis, and Evaluation of a Helicenoidal DMAP Lewis Base Catalyst. *Organic Letters.* 2011, 13, 1250-1253

291. TAKENAKA, N., et al. Helical Chiral Pyridine N-Oxides: A New Family of Asymmetric Catalysts. *Angewandte Chemie International Edition*. 2008, 47, 9708-9710.

292. MURGULY, E., et al.Chiral Discrimination in Hydrogen-Bonded [7]Helicenes. *Organic Letters.* 2000, 2, 3169-3172.

293. GRAULE, S., et al. Metal−Bis(helicene) Assemblies Incorporating π-Conjugated Phosphole-Azahelicene Ligands: Impacting Chiroptical Properties by Metal Variation. *Journal of the American Chemical Society*. 2009, 131, 3183-3185.

294. CARONNA, T., et al. Approaches to the Azahelicene System: Synthesis and Spectroscopic Characterization of Some Diazapentahelicenes. *Helvetica Chimica Acta.* 2002,85, 1-8.

295. BAZZINI, C., et al. Synthesis and Characterization of Some Aza[5]helicenes *European Journal of Organic Chemistry*. 2005, 7, 1247-1257.

296. HARROWVEN, D. C., et al.Efficient Phenanthrene, Helicene, and Azahelicene Syntheses *Angewandte Chemie International Edition*. 2006, 45, 2242-2245.

297. MISEK, J., et al. A Straightforward Route to Helically Chiral N-Heteroaromatic Compounds: Practical Synthesis of Racemic 1,14-Diaza[5]helicene and Optically Pure 1- and 2-Aza[6]helicenes. *Angewandte Chemie International Edition*. 2008, 47, 3188−3191.

298. KELGTERMANS, H., et al. Synthesis of Functionalized Dioxa-aza[7]helicenes Using Palladium Catalyzed Arylations. *Organic Letters*. 2012, 14, 1500−1503.

299. SHI, L., et al. Synthesis, Structure, Properties, and Application of a Carbazole-Based Diaza[7]helicene in a Deep-Blue-Emitting OLED. *Chemistry - A European Journal.* 2012, 18, 8092-8099.

300. UPADHYAY, G. M., et al. Synthesis of carbazole derived aza[7]helicenes. *Tetrahedron Letters.* 2014, 55, 5394-5399.

301. HUA, W., et al. Deep-blue electroluminescence from nondoped and doped organic light-emitting diodes (OLEDs) based on a new monoaza[6]helicene. *RSC Advances.* 2015, 5, 75-84.

302. WAGHRAY, D., et al. Diazadithia[7]helicenes: Synthetic Exploration, Solid-State Structure, and Properties *Chemistry - A European Journal.* 2013, 19, 12077-12085.

303. BOUCHARD, J., et al. Solvatochromic Properties of 2,7-Carbazole-Based Conjugated Polymers. *Macromolecules.* 2003, 36, 4624-4630

304. GROEN, M. B., and H. Wynberg. Optical properties of some heterohelicenes. Absolute configuration. *Journal of the American Chemical Society.* 1971, 93, 2968–2974.

305. BRUHN, T., et al. SpecDis: Quantifying the Comparison of Calculated and Experimental Electronic Circular Dichroism Spectra. *Chirality.* 2013, 25, 243-249.

306. BRINGMANN, G., et al. The Assignment of Absolute Stereostructures through Quantum Chemical Circular Dichroism Calculations. *European Journal of Organic Chemistry.* 2009, 17, 2717-2727.

307. PESCITELLI, G., et al. N. Conformational aspects in the studies of organic compounds by electronic circular dichroism. *Chemical Society Reviews.* 2011, 40, 4603-4625.

308. NAKAI, Y., et al. Theoretical and Experimental Studies on Circular Dichroism of Carbo[n]helicenes. *The Journal of Physical Chemistry A.* 2012, 116, 7372-7385.

309. ANTHONY, J. E., et al. n-Type Organic Semiconductors in Organic Electronics. *Advanced Materials.* 2010, 22, 3876-3892.

310. ZHU, Y., et al. New Ambipolar Organic Semiconductors. 1. Synthesis, Single-Crystal Structures, Redox Properties, and Photophysics of Phenoxazine-Based Donor−Acceptor Molecules. *Chemistry of Materials.* 2008, 20, 4200–4211.

311. FISHER, A. L., et al. Efficient Deep-Blue Electroluminescence from an Ambipolar Fluorescent Emitter in a Single-Active-Layer Device. *Chemistry of Materials*. 2011, 23, 1640–1642.

312. WU, J., et al. Theoretical study on dithieno[3,2-b :2′,3′-d]phosphole derivatives: high-efficiency blue-emitting materials with ambipolar semiconductor behavior. *Theoretical Chemistry Accounts.* 2010, 127, 419–427.

313. DUAN, L., et al. Strategies to Design Bipolar Small Molecules for OLEDs: Donor-Acceptor Structure and Non-Donor-Acceptor Structure. *Advanced Materials.* 2011, 23, 1137–1144.

314. LIU, H., et al. Highly efficient near ultraviolet organic light-emitting diode based on a meta-linked donor–acceptor molecule. *Chemical Science.* 2015, 6, 3797–3804.

315. MCNEILL, C. R., and N. C. GREENHAM. Conjugated-Polymer Blends for Optoelectronics. *Advanced Materials.* 2009, 21, 3840–3850.

316. HUNG, W.-Y., et al. The First Tandem, All-exciplex-based WOLED. *Scientific Reports.* 2014, 4, 5161-5166.

317. ZHOU, D.-Y., et al. Host to Guest Energy Transfer Mechanism in Phosphorescent and Fluorescent Organic Light-Emitting Devices Utilizing Exciplex-Forming Hosts. *Journal of Physical Chemistry C*. 2014, 118, 24006–24012.

318. MINAEV, B., et al. Principles of Phosphorescent Organic Light Emitting Devices. *Physical Chemistry Chemical Physics.* 2014, 16, 1719–1758.

319. CHERPAK, V., et al. Efficient “Warm-White” OLEDs Based on the Phosphorescent bis-Cyclometalated iridium(III) Complex. *Journal of Physical Chemistry C*. 2014, 118, 11271−11278.

320. CHERPAK, V., et al. Mixing of Phosphorescent and Exciplex Emission in Efficient Organic Electroluminescent Devices. *ACS Applied Materials & Interfaces.* 2015, 7, 1219–1225.

321. WURTHNER, F. Perylene bisimide dyes as versatile building blocks for functional supramolecular architectures. *Chemical Communications.* 2004, 14, 1564–1579.

322. JONES, B. A., et al. Tuning Orbital Energetics in Arylene Diimide Semiconductors. Materials Design for Ambient Stability of n-Type Charge Transport. *Journal of the American Chemical Society*. 2007, 129, 15259–15278.

323. THOMAS, K. R. J., et al. Electroluminescent bipolar compounds containing quinoxaline or pyridopyrazine and triarylamine segments. *Journal of Materials Chemistry.* 2002, 12, 3516-3522.

324. BRUNNER, K., et al. Carbazole Compounds as Host Materials for Triplet Emitters in Organic Light-Emitting Diodes: Tuning the HOMO Level without Influencing the Triplet Energy in Small Molecules. *Journal of the American Chemical Society*. 2004, 126, 6035–6042.

325. GAO, Z. Q., et al. New Host Containing Bipolar Carrier Transport Moiety for High-Efficiency Electrophosphorescence at Low Voltages. *Advanced Materials.* 2009, 21, 688–692.

326. ULLMANN, F., and J. BIELECKI. Ueber Synthesen in der Biphenylreihe. *Chemische Berichte.* 1901, 34, 2174–2178.

327. LIU, X., et al. Effects of Alkyl Chain Length on the Optoelectronic Properties and Performance of Pyrrolo-Perylene Solar Cells. *ACS Applied Materials & Interfaces*. 2015, 7, 8859 −8867.

328. DJUROVICH, P.I., et al. Measurement of the lowest unoccupied molecular orbital energies of molecular organic semiconductors *Organic Electronics*. 2009, 10 (3), 515–520.

329. GRITZNER, G. Polarographic half-wave potentials of cations in nonaqueous solvents. *Pure andApplied Chemistry*. 1990, 62, 1839–1858.

7. LIST OF PUBLICATIONS ON THE SUBJECT OF THE THESIS

1. Bucinskas, A.; Waghray, D.; Bagdziunas, G.; Thomas, J.; Grazulevicius, J. V.; Dehaen, W. Synthesis, functionalization, and optical properties of chiral carbazole-based diaza[6]helicenes // Journal of organic chemistry (American Chemical Society). ISSN 0022-32632015. vol. 80, iss. 5, p. 2521-2528.

2. Bucinskas, A.; Bagdziunas, G.; Tomkeviciene, A.; Volynyuk, D.; Kostiv, N.; Gudeika, D.; Jankauskas, V.; Rutkis, M.; Grazulevicius, J. V. Structure property relationship of isomeric diphenylethenyldisubstituted dimethoxycarbazoles // RSC Advances (The Royal Society of Chemistry). 2015, vol. 5, p. 49577-49589.

3. Bučinskas, A.; Volyniuk, D.; Danyliv, Y.; Grazulevicius, J.V.; Baryshnikov, G.V.; Minaev, B.F.; Ivaniuk, K.; Cherpak, V.; Stakhira, P. N-Annelated perylenes as effective green emitters for OLED // RSC Advances (The Royal Society of Chemistry). 2015, vol 5, p. 78150-78159.

8. OTHER PUBLICATIONS

1. Garcia Amoros, J.; Bucinskas, A.; Reig, M.; Nonell, S.; Velasco, D. Fastest molecular photochromic switches based on nanosecond isomerizing benzothiazoliumazophenolic salts // Journal of materials chemistry C (The Royal Society of Chemistry). London: The Royal Society of Chemistry. ISSN20507526. 2014, vol. 2, p. 474-480.

2. Gudeika, D.; Grazulevicius, J. V.; Sini, G.; Bucinskas, A.; Jankauskas, V.; Miasojedovas, A.; Jursenas, S. New derivatives of triphenylamine and naphthalimide as ambipolar organic semiconductors: Experimental and theoretical approach// Dyes and pigments (Elsevier Science). ISSN 01437208. 2014, vol. 106, p. 58-70.

3. Higgins, S.; Torsi, L.; Whitworth, G.; Laurand, N.; Zhang, S.; Samuel, I.; Ebenhoch, B.; Wudl, F.; Frey, G.; Bučinskas, A.; Inigo, J.; Perepichka, D.; Lemmer, U.; Skabara, P.; Ottosson, H.; Bradley, D.; McCulloch, I. Photonics: generaldiscussion. // Faraday discussions (The Royal Society of Chemistry). ISSN 13645498. 2014, vol. 174, p. 235-253.

9. LIST OF PRESENTATIONS AT THE INTERNATIONAL CONFERENCES

1. A. Bucinskas, A. Tomkeviciene, G. Buika, J.V. Grazulevicius, V. Jankauskas. Synthesis and properties of dimetoxy-substituted carbazole derivatives with diphenylethenyl moieties // ELECMOL 2012: 6th International Meeting on Molecular Electronics/ December 3-7, 2012, Grenoble, France: list of posters and participants, abstract, practical information. p.129.

2. A. Bucinskas, A. Tomkeviciene, G. Buika, J.V. Grazulevicius, V. Jankauskas, D.Y. Volyniuk. New glass-forming carbazolyl-containing semiconductors// ICEPOM-9[elektroninis išteklius]: Electronic processes in organic materials // May 20-24, 2013, Lviv, Ukraine: list of oral presentations, abstract, practical information. p. 128-129.

3. A. Bucinskas, A. Tomkeviciene, J.V. Grazulevicius, V. Jankauskas, D.Y. Volyniuk, M. Rutkis. Electroactive carbazole derivatives containing diphenylethenyl and isoindigo moieties. FPi-11: 11th international symposium on functional pi-electron systems/June 2-7, 2013. Arcachon, France: list of posters and participants, practical information.

4. A. Bucinskas, A. Tomkeviciene, G. Bagdziunas, J.V. Grazulevicius. Synthesis and Studies of Methoxy Multisubstituted Derivatives of Carazole // BOS 2014[elektroninis išteklius]: 8th Biennial International Conference on Organic Synthesis / June 6-9, 2014, Vilnius, Lietuva: content, abstract, practical information. p 158.

5. A. Bucinskas, A. Tomkeviciene, J.V. Grazulevicius, D. Yu. Volyniuk, V. Jankauskas. New derivatives of carbazole as hole-transporting and ambipolar semiconductors // ELECMOL 2014: 7th International Conference on Molecular Electronics/ August 24-29, 2014, Strasbourg, France: content, abstract, practical information. p.1.

6. A. Bucinskas, A. Tomkeviciene, G. Bagdziunas, J. V. Grazulevicius, D.Volyniuk, P. Stakhira, V. Cherpak, M. Chapran and Z. Hotra. New Nannulated perylene and carbazole derivatives for OLED's // Faraday Discussion 174: Organic Photonics and Electronics /August 24-29, 2014, Glazgow, UK: content, abstract, practical information. p.10.

7. A. Bucinskas, A. Tomkevicienė, G. Bagdziunas, J. V. Grazulevicius. Effect of the number and positions of methoxy groups on the properties of carbazole and its trimers: theoretical and experimental approach. // Baltic polymer symposium 2014 : Laulasmaa, Estonia, September 24-26, 2014 / Tallinn University of Technology, Tallinn: program and abstracts: 2014. p. 39.

8. A. Bucinskas, D. Waghray, G. Bagdziunas, J. Thomas, J. V. Grazulevicius, W. Dehaen. Easy functionalized chiral carbazole based diaza[6]helicenes – a new opportunity to obtain materials for organic electronics. // ECME2015 // September 1-5, 2015, Strasburg, France.

9. A. Bucinskas, D. Volyniuk, G.V. Baryshnikov, B.F. Minaev, K. Ivaniuk, V. Cherpak, P, Stakhira and J. V. Grazulevicius. Perylene and carbazole based derivatives as glass forming molecules for organic light-emitting diodes: experimental and theoretical approach. // Baltic polymer symposium 2015 : Sigulda, Latvia, September 16-18, 2015.

10. ACKNOWLEDGEMENTS

Prof. Habil. Dr. J.V. Gražulevičius, Department of Polymer Chemistry and Technology, Kaunas University of Technology, is greatly acknowledgement for the supervision of my Doctoral research.

Prof. Dehaen, Wim, KU LEUVEN University, is thanked for the supervision of my internship spent in Belgium.

Prof. Dolores Velasco, Departament de Qu´ımica Organica, Universitat de Barcelona, is thanked for the supervision of my internship spent in Barcelona.

Dr. Aušra Tomkevičienė, Department of Polymer Chemistry and Technology, Kaunas University of Technology, is thanked for consultations and for helping in synthesis.

Dr. Gintautas Bagdziunas, Department of Polymer Chemistry and Technology, Kaunas University of Technology, is thanked for helping in DFT level calculations, interpretations and X-Ray crystallography analysis.

Dr. Laura Pečiulytė, Department of Polymer Chemistry and Technology, Kaunas University of Technology, is thanked for helping in DSC and TGA measurements.

Ina Liutvieniene, Department of Polymer Chemistry and Technology, Kaunas University of Technology, is thanked for helping in IR, UV-vis, FL measurements.

Dr. Dmytro Volyniuk Department of Polymer Chemistry and Technology, Kaunas University of Technology, is thanked for helping in the fabrication of electroluminescent devices.

Dr. V. Gaidelis and Dr. V. Jankauskas, Department of Solid State Electronics, Vilnius University, are thanked for helping in the measurements of ionisation potentials and charge carrier mobilities.

Dr. D. Waghray, KU LEUVEN University, is thanked for helping in the measurements of CD spectra and synthesis.

Prof. L. Y. Chen, National Tsing-Hua University, is thanked for helping in fabrication of photovoltaic devices.

Prof. B. F. Minaev, Bohdan Khmelnytsky National University, is thanked for theoretical calculations which were performed at the PDC supercomputers of the Royal Institute of Technology, Stockholm.

11. APPENDIX

Technological scheme for large scale application of N-annelated perylene and carbazole based materials

In Fig. I the process flow chart applicable for large scale OLED production is presented. It shows the need of an effective synthesis (less steps, high yield of the target product), less energy consumption and low cost raw materials. The price of the product increases with every additional step of synthesis needed to achieve the target product. OLED design is the second stage, which is rather similar for many materials.

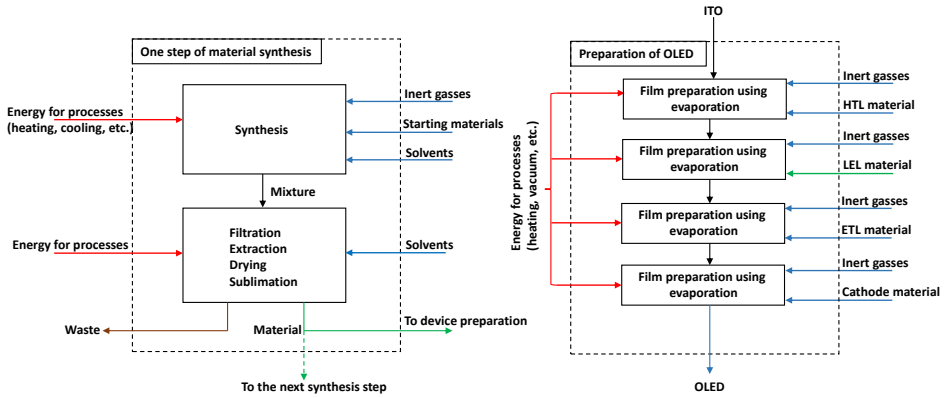

Fig. I. Process flow chart showing material one step synthesis and OLED fabrication

The search of material for large scale production starts from theoretical calculations. The next step is to design the route of an effective synthesis and the final step is the employment of the achieved material in the fabrication of OLED.

A process flow diagram of one step synthesis is presented in Fig. II. M1, M2 and M3 mixes the incoming raw materials with solvent. In the case of low material solubility, a recirculation line and heat exchanger (H-1) is used. Afterwards, the resulted solution is sent to the synthesis reactor R-1. The additives, used for reaction; such as catalysts, can be injected directly into the reactor. In all the processes, (such as dissolving, mixing and the synthesis), to avoid the reactive oxygen from the air – a nitrogen gas atmosphere is used. In addition, to avoid overpressure in the volume of all the mixers (M1, M2, M3) and the synthesis reactor (R-1), additional pipelines with grease catchers (F-1, F-2) are connected. In the case of high-pressure reactions, the nitrogen gas compressor (CO-1) can be used. After the reaction, the mixture is directed to mixer M-4, which is needed to cool-down the solution before the extraction stage. For an effective and fast extraction process - centrifugal extractor EX-1 is employed. The final step to obtain the crystals of the organic compound - the vessel for crystallization and solvent evaporation (CR-1) is used.

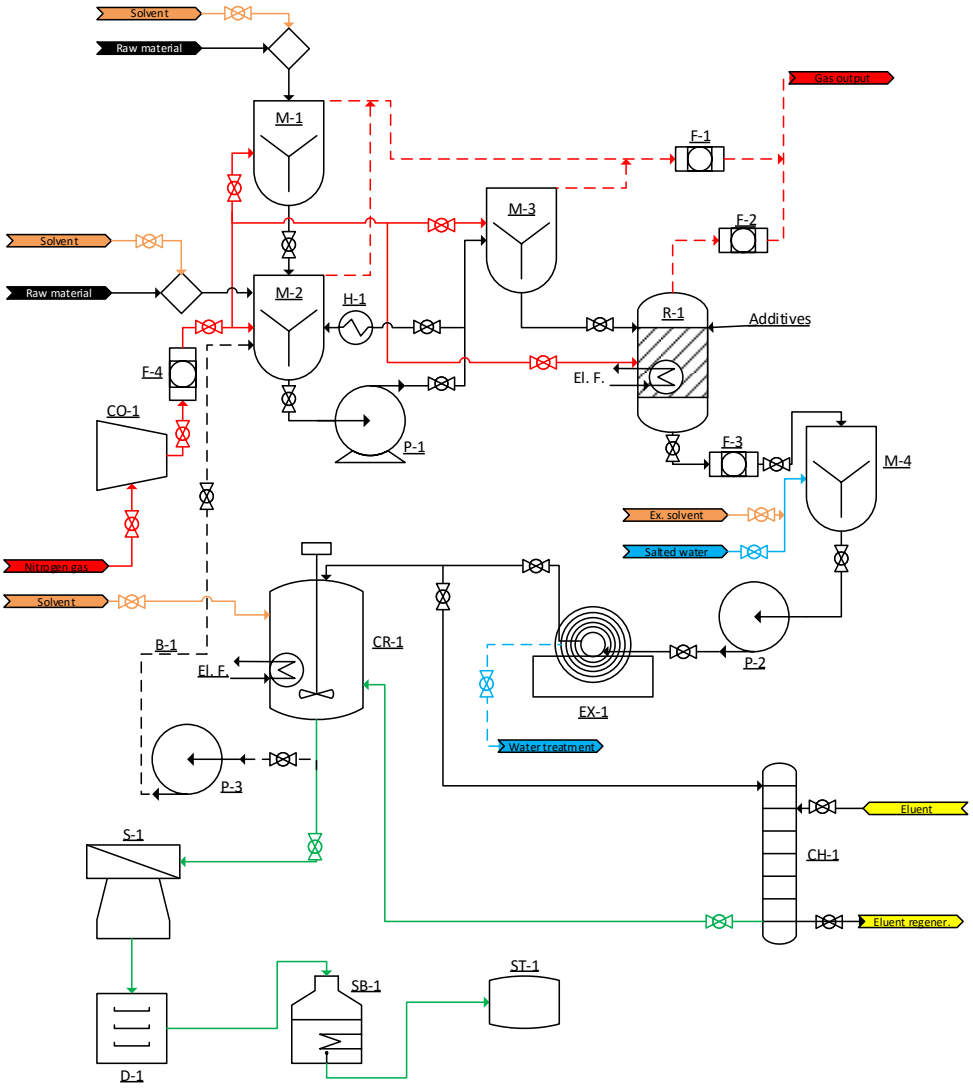

Fig. II. Process flow diagram of material synthesis. (M-1, M-2, M-3, M-4 – mixers; F-1, F-2, F-4 – grease catcher; CO-1 – nitrogen gas compressor; P-1, P-2, P-3 – solution pumps; EX-1 – centrifugal extractor; CH-1- chromatography column; R-1 – synthesis reactor with heater; CR-1 – volume for cristallization and solvent evaporation; S-1 – crystal separator; D-1 – dryer; SB-1 – volume for material sublimation; ST-1 – storage; H-1 – electrical heater; B-1 – bypassing line.)

In case of the presence of oily impurities in the crude product, which possess a high boiling point, the column for absorption chromatography (CH-1) can be attached to the purification process. In the crystal separator S-1, the obtained crystals are separated and directly sent to the dryer (D-1). Before storage (ST-1) the

sublimation process is used (SB-1) to achieve a high purity of materials needed for optoelectronic devices.

Using the presented process flow diagram (Fig. II) carbazolyl-substituted perylene derivatives (**NP-9-Cz**, **NP-3-Cz**, **NP-2-Cz**) can be synthesized. To optimize the overall synthesis, steps a, b and c (Scheme 4.6), which are used to achieve precursor **A-NP**, can be combined into a one step process employing a bypassing line B-1. Adding the next two steps (d and e or f, Scheme 4.6) a full view of the high scale three-step production of organic semiconductors **NP-9-Cz**, **NP-3-Cz**, **NP-2-Cz** is achieved, which can be used as emitters for effective fluorescent OLEDs.

SL344. 2015-11-13, 22 leidyb. apsk. l. Tiražas 12 egz. Užsakymas 435.
Išleido Kauno technologijos universitetas, K. Donelaičio g. 73, 44249 Kaunas
Spausdino leidyklos „Technologija“ spaustuvė, Studentų g. 54, 51424 Kaunas